



universität
wien

DISSERTATION

Titel der Dissertation

The mitochondrial K^+/H^+ exchanger: identification and
characterization of novel components

Verfasser

Mag.rer.nat. Markus Aleschko

angestrebter akademischer Grad

Doktor der Naturwissenschaften (Dr.rer.nat.)

Wien, 2011

Studienkennzahl lt. Studienblatt: A 091 441

Dissertationsgebiet lt. Studienblatt: Genetik - Mikrobiologie

Betreuerin: Prof. Dr. Kristina Djinovic - Carugo

“I believe in intuition and inspiration. Imagination is more important than knowledge. For knowledge is limited, whereas imagination embraces the entire world, stimulating progress, giving birth to evolution. It is, strictly speaking, a real factor in scientific research.”

Albert Einstein

For my parents

Table of contents

1.1. Summary	1
1.2. Zusammenfassung	3
2. Introduction	5
2.1. Mitochondrial morphology	5
2.2. Mitochondrial ion homeostasis and volume control.....	7
2.3. Mitochondrial cation/proton exchange	8
2.4. The molecular identity of the mitochondrial cation/proton.....	11
exchangers	
2.5. Regulation of mitochondrial K⁺/H⁺ exchange	12
2.6. Mitochondrial K⁺/H⁺ exchange involves the <i>LETMI/YOL027C</i>	13
gene family	
2.6.1. <i>YOL027C/MDM38/MKH1</i>	13
2.6.2. <i>YPR125W/MRS7/YLH47</i>	15
2.6.3. <i>LETMI</i>	15
2.6.4. <i>HCCR-1/LETMD1</i>.....	17
2.7. Mitochondrial autophagy – Mitophagy	17
3. Materials and Methods	20
3.1. Materials	20
3.1.1. Table 1: Yeast strains used in this study	20
3.1.2. Table 2: Plasmids and oligonucleotides used in this study	21
3.1.3. Media	23
3.1.4. Chemicals and antibodies	24
3.1.5. Affinity resins.....	24

3.2. Methods	25
3.2.1. Gene disruption	25
3.2.2. Chromosomal tagging and plasmid construction.....	25
3.2.3. Mitochondrial isolation	26
3.2.4. Protein precipitation and immunoblotting	26
3.2.5. Blue native electrophoresis	26
3.2.6. Chemical cross-linking.....	26
3.2.7. Protein A affinity purification.....	27
3.2.8. CBP affinity purification	27
3.2.9. CBP - protein A tandem affinity purification (TAP)	28
3.2.10. Ni-NTA affinity purification.....	28
3.2.11. Ni-NTA - CBP TAP	28
3.2.12. Strep affinity chromatography.....	29
3.2.13. Ni-NTA - Strep TAP.....	29
3.2.14. Size exclusion chromatography (SEC)	29
3.2.15. Mass spectrometry.....	30
3.2.16. Fluorescence microscopy	30
3.2.17. Potassium acetate (KOAc)-induced swelling of isolated mitochondria.....	30
3.2.18. Synthetic genetic array (SGA) analysis	31
4. Publication: ‘Novel components of an active mitochondrial	32
K⁺/H⁺ exchange’	
5. Results.....	53
5.1. Working hypothesis – Mdm38p/Mkh1p is an essential.....	53
interaction partner of the mitochondrial K⁺/H⁺ exchanger	
5.2. Mdm38p complex purification strategy	54

5.3. Tandem Affinity Purification (TAP) of chromosomally tagged.....	56
Mdm38p	
5.3.1. The HIS-TAP tag does not disturb Mdm38p function and complex.....	58
formation	
5.3.2. Chemical cross-linking of Mdm38-HIS-TAP.....	58
5.3.3. Protein A affinity purification of Mdm38-HIS-TAP.....	61
5.3.4. CBP affinity purification of Mdm38-HIS-TAP	63
5.3.5. CBP – protein A TAP of Mdm38-HIS-TAP	64
5.3.6. Ni-NTA - CBP tandem affinity purification of Mdm38-HIS-TAP	65
5.3.7. Size exclusion chromatography (SEC) of Mdm38-HIS-TAP	67
5.3.8. The Mdm38p complex is intact after SEC	69
5.4. Single–step HIS and Strep affinity purification of.....	71
chromosomally tagged Mdm38p	
5.4.1. Affinity chromatography using One-Strep-tagged Mdm38p allows	71
recovery of the high molecular weight complex	
5.4.2. Purity of single-step affinity chromatography is limited	74
5.4.3. Mass spectrometry (MS) analysis of the Mdm38-One-Strep complex	75
5.5. Ni-NTA – Strep TAP of vector expressed Mdm38p	76
5.5.1. OSH-tagged Mdm38p restores the respiratory growth defect of	77
<i>mdm38</i> Δ mutant cells	
5.5.2. The Mdm38p complex is intact after Ni-NTA – Strep TAP	78
5.5.3. Ssc1p and Erg5p co-elute with Mdm38-OSH after Ni-NTA – Strep TAP ..	80
5.6. Ergosterol and mitochondrial K⁺/H⁺ exchange	81
5.6.1. Synthetic growth defects of BY <i>mdm38</i> Δ <i>erg5</i> Δ and BY <i>mdm38</i> Δ <i>erg6</i> Δ	83
double mutant strains	
5.6.2. Aberrant mitochondrial and vacuolar morphology in the absence of.....	84
<i>MDM38</i> , <i>ERG5</i> , and <i>ERG6</i>	

5.6.3. KOAc-induced mitochondrial swelling	89
5.7. Synthetic genetic array (SGA) analysis.....	91
5.7.1. Synthetic lethal screen.....	92
5.7.2. Synthetic suppression screen.....	94
5.7.3. Double mutant strains exhibit a restored mitochondrial network	97
6. Discussion	101
6.1. Interaction partners of Mdm38p	102
6.2. Ssc1p and Erg5p co-purify with Mdm38p.....	102
6.3. Genetic interaction of <i>MDM38</i> , <i>ERG5</i> , and <i>ERG6</i>	104
6.4. Disturbed mitochondrial and vacuolar morphology upon	105
deletion of <i>MDM38</i> , <i>ERG5</i> , and <i>ERG6</i>	
6.5. Ergosterol and mitochondrial K ⁺ /H ⁺ exchange.....	106
6.6. Synthetic genetic array analysis.....	108
6.7. Is Mdm38p the mitochondrial K ⁺ /H ⁺ exchanger?.....	109
7. Abbreviations.....	111
8. References	113
9. Acknowledgements	130
10. Curriculum Vitae.....	131

1.1. Summary

Mitochondria are double membrane-bound organelles controlling several essential cellular processes like ATP production, apoptosis, ion homeostasis, volume control, and many other metabolic pathways. To fulfill these functions, mitochondria establish an inside negative membrane potential ($\Delta\psi$) across the inner membrane, which is maintained by the ejection of H^+ by redox pumps of the electron transport chain. In presence of high abundance of K^+ and other cellular cations like Na^+ and Li^+ , the inside negative $\Delta\psi$ is a strong driving force for an inwardly directed ion flux. To maintain mitochondrial ion homeostasis and osmolarity, excess cation fluxes have to be counteracted by cation/proton antiporters, as proposed half a century ago by Nobel laureate Peter Mitchell. Solid data showed that the Mdm38p/Letm1 family of single membrane spanning, inner mitochondrial membrane proteins is essential for mitochondrial K^+/H^+ exchange. Deletion of yeast *MDM38* results in a severe respiratory growth defect, mitochondrial K^+ overload, almost abolished mitochondrial K^+/H^+ exchange activities, depolarization of the mitochondrial membrane, drastic mitochondrial swelling, and fragmentation of the mitochondrial reticulum. Though a role of *MDM38* in controlling mitochondrial K^+/H^+ exchange is undoubted, the molecular identity of the exchanger *per se* still remains elusive.

In this research project we focused on the characterization of proteins involved in mitochondrial cation/proton exchange, ultimately aiming at the identification of the actual mitochondrial K^+/H^+ exchanger.

In a genome-wide screen for multicopy suppressors of the *mdm38 Δ* mutant, we identified the Mdm38p homolog Mrs7p and the unrelated Ydl183cp as strong suppressors of impaired mitochondrial K^+/H^+ exchange. Triple deletion mutants exhibited completely abolished K^+/H^+ exchange, reduced cellular viability, and autophagic degradation of defective mitochondria. Moreover, both suppressors and Mdm38p were shown to be components of high molecular weight protein complexes. Accordingly, we established a working hypothesis based on the idea of Mdm38p functioning as an auxiliary protein directly interacting with the unknown K^+/H^+ exchanger. By biochemical analyses based on affinity chromatography, we identified the putative interaction partners of Mdm38p: the essential mitochondrial chaperon Ssc1p and the ergosterol biosynthetic enzyme Erg5p. However, we failed to identify a protein with several transmembrane helices as expected features for the K^+/H^+ exchanger. Nevertheless, we provide strong evidence for a direct link between membrane sterol composition, mitochondrial ion homeostasis, membrane fusion, and cellular viability. Contrary to our initial

consideration, data presented here strongly suggest that Mdm38p itself may represent the exchanger. This would be the first known exchanger containing a single membrane spanning helix.

In a second approach, we performed a genome-wide synthetic genetic array analysis of the *mdm38Δ* mutant, and identified six suppressor mutants restoring respiratory growth and mitochondrial morphology in the double mutant. Currently we can only speculate how these suppressors, with various cellular functions in transcriptional regulation or cytoskeletal organization, may restore the growth and morphology phenotype. Based on these findings there are exciting experiments ahead.

1.2. Zusammenfassung

Mitochondrien sind von einer Doppelmembran umschlossene Organellen, die verschiedene essentielle Zellprozesse kontrollieren, wie etwa ATP-Produktion, Apoptose, Ionenhomöostase, Volumenkontrolle und viele weitere Stoffwechselwege. Um diese Funktionen zu erfüllen, erzeugen Mitochondrien ein Membranpotential ($\Delta\psi$) an der inneren Membran. Aufgrund des Ausstoßes von H^+ durch Redoxpumpen der Elektronentransportkette, wird dieses Membranpotential, welches innen negative ist, aufrecht erhalten. In Anwesenheit von hohen Mengen an K^+ und anderen zellulären Kationen wie Na^+ und Li^+ , bewirkt das innen negative $\Delta\psi$ einen starken Ioneneinstrom. Um die mitochondriale Ionenhomöostase und Osmolarität aufrecht zu erhalten, muß diesem Ionenüberschuss mittels Kationen/Protonen Austauschern entgegengewirkt werden, wie es von Nobelpreisträger Peter Mitchell vor einem halben Jahrhundert vorgeschlagen wurde. Bisherige Daten konnten eindeutig zeigen, dass die Mdm38p/Letm1 Familie - Proteine der inneren Mitochondrienmembran mit einer Transmembranhelix - für den mitochondrialen K^+/H^+ Austausch essentiell ist. Die Deletion des *MDM38* Gens in der Hefe führt zu schwerwiegendem atmungsdefekten Wachstum, mitochondrialer K^+ Überladung, fast vollständig fehlender K^+/H^+ Austausch-Aktivität, Depolarisation der Mitochondrienmembran, sowie starker Schwellung und Fragmentierung des mitochondrialen Netzwerkes. Obwohl eine tragende Funktion von *MDM38* in der Kontrolle des mitochondrialen K^+/H^+ Austausches nicht bezweifelt werden kann, ist die molekulare Identität des eigentlichen Austauschers weiterhin unbekannt.

In diesem Forschungsprojekt konzentrierten wir uns auf die Charakterisierung von Proteinen, welche im mitochondrialen Kationen/Protonen Austausch involviert sind, mit dem letztendlichen Ziel der Identifizierung des tatsächlichen mitochondrialen K^+/H^+ Austauschers. In einer genomweiten Suche nach Überexpressions-Suppressoren der *mdm38Δ* Mutante identifizierten wir Mrs7p, ein Mdm38p homologes Protein, sowie das nicht verwandte Protein Ydl183cp, als starke Suppressoren des beeinträchtigten mitochondrialen K^+/H^+ Austausches. Dreifach deletierte Mutanten besaßen keinerlei K^+/H^+ Austausch-Aktivität und zeigten reduzierte zelluläre Lebensfähigkeit sowie autophagischen Abbau defekter Mitochondrien. Desweiteren sind Mdm38p und beide Suppressoren Komponenten von hochmolekularen Proteinkomplexen. Demzufolge entwickelten wir eine Arbeitshypothese, basierend auf der Idee, dass Mdm38p als ein Hilfsprotein direkt mit dem unbekanntem K^+/H^+ Austauscher interagiert. Durch biochemische Analysen mithilfe von Affinitätschromatographie identifizierten wir mögliche Interaktionspartner von Mdm38p: das essentielle mitochondriale

Chaperonprotein Ssc1p und das Ergosterol biosynthetische Enzym Erg5p. Hingegen gelang es uns nicht ein Protein mit mehreren Transmembranhelices zu identifizieren, was einem erwarteten Merkmal eines K^+/H^+ Austauschers entsprechen würde. Nichtsdestotrotz legen unsere Resultate einen engen Zusammenhang zwischen der Membransterol-Zusammensetzung, mitochondrialer Ionenhomöostase, Membranfusion und zellulärer Lebensfähigkeit nahe. Entgegen unserer ursprünglichen Annahme, sprechen die hier gezeigten Daten stark dafür, dass Mdm38p selbst den gesuchten Austauscher darstellt. Dies wäre der erste bekannte Austauscher mit nur einer Transmembranhelix.

In einem zweiten Ansatz führten wir eine genomweite synthetisch-genetische Analyse der *mdm38Δ* Mutante durch. Dabei identifizierten wir sechs Suppressormutanten, die das atmungsabhängige Wachstum und die mitochondriale Morphologie in der Doppelmutante wiederherstellten. Momentan können wir nur darüber spekulieren wie diese Suppressoren, welche in verschiedenen zellulären Funktionen – von transkriptioneller Regulation bis zu zytoskelettaler Organisation – involviert sind, den Wachstums- und Morphologie-Phänotyp wiederherstellen. Basierend auf diesen Erkenntnissen liegen spannende Experimente vor uns.

2. Introduction

Mitochondria are double-membraned subcellular organelles that have kept part of their own genome, reflective of their endosymbiotic origin. They are present in all eukaryotic cells, except mature erythrocytes. The most prominent mitochondrial function is to supply the cell with energy in the form of ATP. The central role of mitochondria in this process is the conversion of pyruvate, the end product of glycolysis, into acetyl CoA followed by ATP synthesis *via* the citric acid cycle (also known as tricarboxylic acid cycle or Krebs cycle) and oxidative phosphorylation. Furthermore, mitochondria are critical for a series of other processes including metabolic biosynthesis, cell signaling, cell death decisions, as well as ion buffering and storing functions (Arino *et al.*, 2010; Bernardi, 1999; Butow & Avadhani, 2004; Danial & Korsmeyer, 2004; McBride *et al.*, 2006; Szabadkai & Duchon, 2008).

2.1. Mitochondrial morphology

Mitochondria are highly dynamic organelles exhibiting a complex and plastic morphology. In several species and cell types, mitochondria do not exist as individual, distinct subcellular compartments, but form networks of elongated, interconnected tubules frequently changing size and shape (Bereiter-Hahn & Voth, 1994; Egner *et al.*, 2002; Hoffmann & Avers, 1973; Yoon *et al.*, 2007). Moreover, association with microtubules and actin filaments allows movement of mitochondria along cytoskeletal tracks (Bereiter-Hahn & Voth, 1994; Ligon & Steward, 2000; Nunnari *et al.*, 1997; Romagnoli *et al.*, 2007). Several studies during recent years revealed that mitochondrial morphology and network connectivity is regulated by two opposing events, fission and fusion, which are critical for mitochondrial function (Bleazard *et al.*, 1999; Chan, 2006; Sesaki & Jensen, 1999). The fact that most fission and fusion proteins are conserved from yeast up to human (Legros *et al.*, 2002; Malka *et al.*, 2005) underscores the importance of mechanisms regulating mitochondrial integrity and functionality. Moreover, disturbances in mitochondrial fission and fusion were shown to be implicated in apoptosis by the release of cytochrome c (Karbowski & Youle, 2003; Lee *et al.*, 2004; Olichon *et al.*, 2003) and to be involved in neuromuscular and neurodegenerative diseases (Alexander *et al.*, 2000; Baloh *et al.*, 2007; Chen & Chan, 2009; Shy, 2004; Song *et al.*, 2011).

Mitochondria are bound by two membranes which differ in their lipid and protein composition (Zinser *et al.*, 1991). The outer mitochondrial membrane (OMM) contains integral membrane proteins forming beta-barrel pores called porins, also known as VDAC (voltage-dependent anion channel). Mitochondrial porins show a similar architecture as the outer membrane porins of Gram-negative bacteria and permit passive diffusion of nucleosides, sugars, ions, and other solutes up to a size of ~ 600 Da (Menze *et al.*, 2005; Nikaido & Rosenberg, 1983; Zeth & Thein, 2010). Accordingly, the OMM does not represent a barrier for the exchange of cations between the cytosol and the intermembrane space.

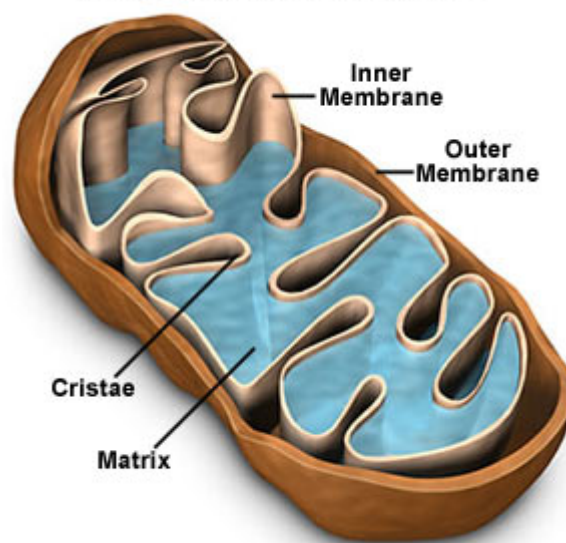


Figure 1: Schematic representation of the mitochondrial structure

Figure adapted from <http://micro.magnet.fsu.edu/>

In contrast to the OMM, the inner mitochondrial membrane (IMM) is highly folded into cristae (Figure 1), thereby dramatically increasing its surface (Garlid & Paucek, 2003). Moreover, the IMM contains high amounts of cardiolipin, a lipid typically found in bacterial plasma membranes (Schagger, 2002). Importantly, the IMM is highly impermeable to virtually all molecules and ions, which enter the mitochondrial matrix mostly *via* integral membrane transporters. This impermeability is an essential necessity for the establishment of a charge separation at the IMM, and maintaining the electrochemical gradient built by the proton pumps of the electron transport chain (Bernardi, 1999).

2.2. Mitochondrial ion homeostasis and volume control

Proton ejection together with the low passive permeability of the IMM results in the formation of a pH gradient (ΔpH) of about 0.3 units and an inside negative membrane potential ($\Delta\psi$) of approximately -180 mV (Garlid & Paucek, 2003). In combination, this proton electrochemical gradient ($\Delta\mu$), also known as proton motive force, provides the energy needed for various essential mitochondrial processes, like the import of nuclear encoded proteins, ion transport and ATP synthesis by the F_0/F_1 ATPase (Bernardi, 1999).

Although the establishment of an electrochemical gradient is indispensable for mitochondrial energy conservation, it simultaneously creates the problem of maintaining ion homeostasis and volume control. The inside negative $\Delta\psi$ highly favors matrix cation accumulation, either by transporter mediated uptake or diffusive cation influx (Garlid & Paucek, 2003). In the case of K^+ , which has a high cytosolic concentration of ~ 150 mM, the electrochemical equilibrium inside mitochondria would be reached at 150 M according to the Nernst equation (Azzone *et al.*, 1977; Bernardi, 1999). In contrast to the low permeability of the IMM to ions and protons, it is highly permeable to water (Garlid & Paucek, 2003). Thus, changes of mitochondrial cation concentration caused by net uptake or loss of K^+ , which moves together with water, subsequently lead to osmotic swelling or shrinkage of the organelle (Bernardi, 1999). Facing the high intracellular concentration of K^+ and Na^+ , fluxes of these osmotically active cations have to be tightly regulated to maintain mitochondrial osmolarity and to avoid rupture of the organelle due to excessive swelling. Accordingly, already in 1961 Peter Mitchell postulated the existence of cation/proton antiporters that permit the electroneutral extrusion of cations out of the matrix, driven by the electrochemical proton gradient (Mitchell, 1961; Mitchell, 1966).

On the one hand, a direct demonstration of electroneutral cation/proton exchange was complicated by the existence of additional transport systems for cations and protons in the IMM. On the other hand, researchers took advantage of the use of ionophores and their substrate specific transport properties. Moreover, determination of cation transport based on changed light scattering of isolated mitochondria upon volume change (passive swelling) turned out to be a valuable tool for various transport assays (Azzone *et al.*, 1976; Blondin *et al.*, 1969).

2.3. Mitochondrial cation/proton exchange

Initial experiments to clarify the existence of mitochondrial cation/proton exchange systems were performed with isolated, non-respiring mammalian mitochondria in presence of isotonic potassium acetate (KOAc) and sodium acetate (NaOAc) media (Mitchell & Moyle, 1969). Due to the high permeability of the IMM to water and also to the protonated form of acetic acid (HAc), exchangers were expected to catalyze matrix accumulation of K^+ or Na^+ in exchange for H^+ and to cause mitochondrial swelling, which can be followed by decreased absorbance (Azzone *et al.*, 1976; Bernardi, 1999; Blondin *et al.*, 1969). Interestingly, mitochondria treated with NaOAc exhibited fast swelling, whereas incubation in KOAc resulted only in marginal swelling. Addition of the exogenous electroneutral K^+/H^+ exchanger nigericin, which specifically acts on the IMM (Kovac *et al.*, 1982a), caused fast swelling in KOAc-based medium (Figure 2). In contrast, yeast mitochondria were found to swell in presence of both KOAc and NaOAc, suggesting that mammalian mitochondria possess an active Na^+/H^+ exchanger and additionally a latent or inactive K^+/H^+ exchange system, whereas yeast is supposed to have only an unspecific mitochondrial cation/proton exchanger (Cockrell, 1973; Douglas & Cockrell, 1974; Nakashima & Garlid, 1982; Welihinda *et al.*, 1993).

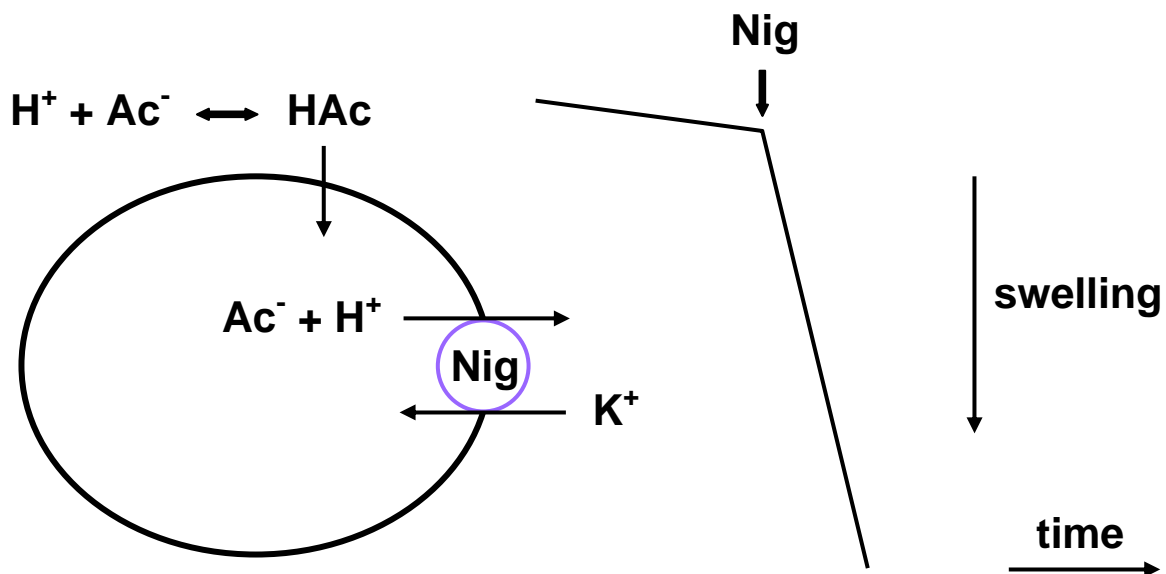


Figure 2: Nigericin (Nig)-induced K^+ fluxes in acetate medium

The electroneutral K^+/H^+ exchanger nigericin causes fast swelling of non-respiring mitochondria. K^+ uptake is followed by rapid diffusion of acetic acid (HAc), resulting in KOAc accumulation and swelling due to water influx. The mitochondrial volume increase can be followed by decreased light scattering. Figure adapted from (Bernardi, 1999).

Importantly, mitochondrial swelling only occurs if K^+ and H^+ fluxes are coupled. Addition of either the protonophore carbonyl cyanide *p*-trifluoromethoxyphenylhydrazone (FCCP) or the K^+ -specific ionophore valinomycin alone does not cause swelling, as charge compensation is inhibited due to the low permeability of the IMM to K^+ and H^+ . Only upon addition of both ionophores fast swelling takes place (Figure 3), similar to nigericin-treated mitochondria (Azzone *et al.*, 1976; Bernardi, 1999; Douglas & Cockrell, 1974; Mitchell & Moyle, 1969).

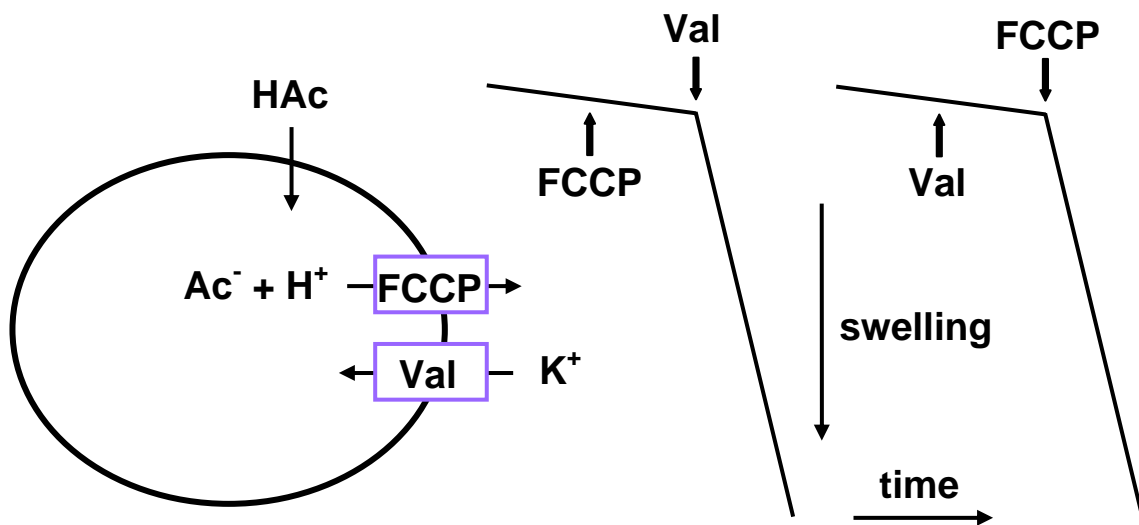


Figure 3: Passive swelling is dependent on coupled K^+ and H^+ fluxes

Addition of the protonophore FCCP or the K^+ ionophore valinomycin (Val) alone does not cause swelling of deenergized mitochondria due to the low permeability of the IMM to ions. Fast swelling is only observed after addition of both ionophores which causes a process of electroneutral K^+/H^+ exchange, resulting in net uptake of KOAc. Figure adapted from (Bernardi, 1999).

Principally, swelling experiments proved successful to confirm the presence of mitochondrial cation/proton exchange systems. However, in contrast to the Na^+/H^+ exchanger, existence of the K^+/H^+ exchanger was questioned due to its low activity. Subsequent studies revealed that the K^+/H^+ exchanger has to be activated by depletion of the mitochondrial matrix for divalent cations. Treatment of mitochondria with the $Me^{2+}/2H^+$ exchanger A-23187 (Reed & Lardy, 1972) and EDTA highly increased KOAc-induced mitochondrial swelling. Initially, this finding suggested a direct contribution of A-23187 to K^+ transport, but additional studies showed that activation of K^+/H^+ exchange was likely caused by extrusion of matrix Mg^{2+} (Azzone *et al.*, 1978; Dordick *et al.*, 1980; Duszynski & Wojtczak, 1977).

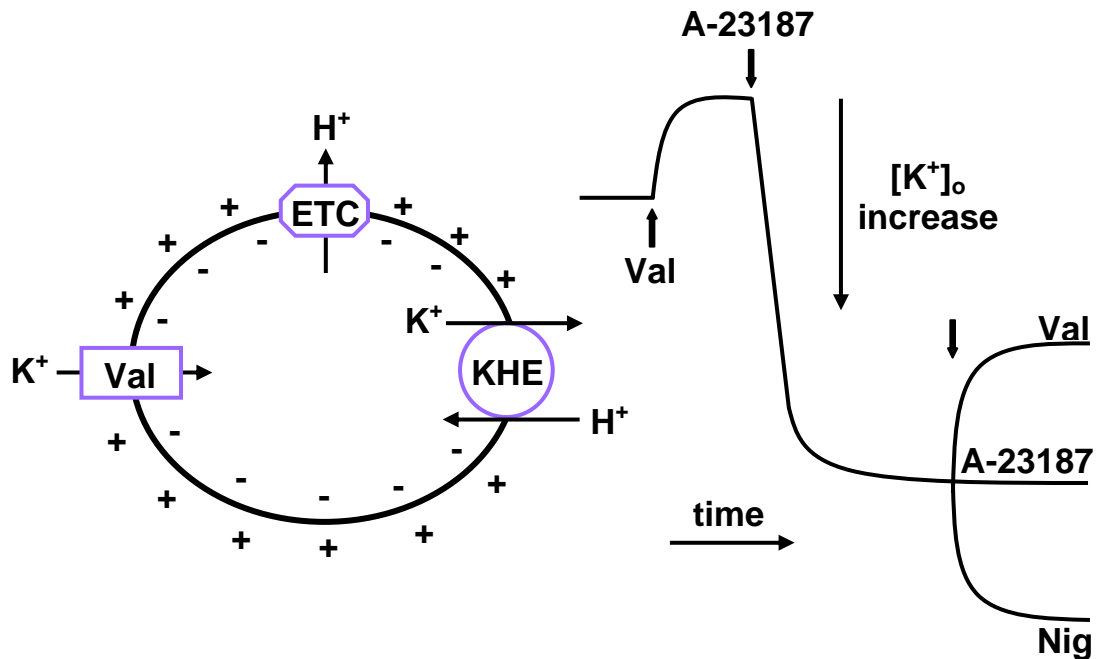


Figure 4: Mitochondrial K⁺/H⁺ exchange is electroneutral and activated by matrix Me²⁺ depletion

Under low K⁺ conditions, valinomycin treatment of energized mitochondria causes K⁺ influx driven by the inside negative $\Delta\psi$. The outside K⁺ concentration ($[K^+]_o$) decreases to a new steady-state. Addition of A-23187 activates the K⁺/H⁺ exchanger (KHE), causing K⁺ efflux until a new steady-state establishes that cannot be changed by further addition of A-23187. In contrast, subsequent treatment with valinomycin or nigericin causes K⁺ influx and efflux, respectively. ETC, electron transport chain; Figure adapted from (Bernardi, 1999; Dordick *et al.*, 1980).

Anyway, these experiments could not answer the question if K⁺ and H⁺ fluxes were mediated by the proposed electroneutral K⁺/H⁺ exchanger or by coupled uniport processes as shown in Figure 2 and 3, respectively. This was finally accomplished by a swelling experiment using energized mitochondria (Figure 4). Addition of valinomycin under conditions of low K⁺ leads to K⁺ accumulation, driven by the inside negative $\Delta\psi$, until outside K⁺ has reached a new steady-state concentration. Treatment with A-23187 causes net K⁺ efflux until a new steady-state is reached, which is reflective of K⁺ influx upon valinomycin treatment and K⁺ efflux driven by the activated K⁺/H⁺ exchanger. This steady-state cannot be disturbed by subsequent addition of A-23187, suggesting that A-23187 does not transport K⁺. In contrast, further K⁺ efflux and uptake is provoked by nigericin and valinomycin treatment, respectively. Together, these findings clearly show that A-23187 activated an endogenous, electroneutral K⁺/H⁺ exchanger facilitating K⁺ extrusion against the K⁺ electrochemical gradient (Bernardi, 1999; Dordick *et al.*, 1980; Shi *et al.*, 1980).

2.4. The molecular identity of the mitochondrial cation/proton exchangers

Today it is generally accepted that mammalian mitochondria possess two distinct cation/proton exchange systems (Nakashima & Garlid, 1982), a Na⁺ (Li⁺)-specific Na⁺/H⁺ antiporter (Mitchell & Moyle, 1969) that does not transport K⁺, Rb⁺ or Cs⁺, and an unspecific cation/proton exchanger transporting all alkali cations (Na⁺, K⁺, Li⁺, Rb⁺ and Cs⁺). Considering the high cytosolic concentration of K⁺, this unspecific antiporter primarily exchanges K⁺ for H⁺ and therefore is designated as a K⁺/H⁺ antiporter (Garlid & Paucek, 2003). Although the transport properties of both systems have been extensively studied, the molecular identity of the respective proteins is still unclear.

Studies aiming at the identification of the exchanger proteins were highly supported by the use of pharmacological inhibitors. The Na⁺/H⁺ exchanger was found to be reversibly inhibited by amiloride analogs (Brierley *et al.*, 1989). In contrast, the K⁺/H⁺ exchanger is reversibly inhibited by amphiphilic amines (e.g. quinine, propranolol) and irreversibly inhibited by dicyclohexylcarbodiimide (DCCD) after matrix Mg²⁺ depletion (Beavis & Garlid, 1990; Brierley *et al.*, 1994). Although DCCD, a carboxylic group interacting compound, cannot be considered a K⁺/H⁺ exchanger-specific inhibitor, binding of radiolabeled DCCD enabled purification of an 82 kDa protein from mammalian mitochondria (DiResta *et al.*, 1986; Martin *et al.*, 1984). When reconstituted into liposomes, this protein exhibited transport properties expected for the K⁺/H⁺ exchanger and was inhibited with quinine and DCCD (Li *et al.*, 1990). However, identification of the corresponding gene encoding this protein failed.

Results on the molecular nature of the mammalian mitochondrial Na⁺/H⁺ exchanger are still controversial and their interpretation is complicated by the presence of various protein isoforms and cell type-specific expression patterns. Initially, Na⁺/H⁺ exchange activity was attributed to a partially purified and liposome reconstituted 59 kDa protein (Garlid *et al.*, 1991). Later, human Nhe6 was reported to function as the Na⁺-specific mitochondrial Na⁺/H⁺ exchanger (Nass *et al.*, 1997; Numata *et al.*, 1998). However, subsequent studies showed that Nhe6 rather represents an endosomal Na⁺/H⁺ exchanger (Brett *et al.*, 2002; Ohgaki *et al.*, 2010). Finally, mammalian Nha2, which shows sequence homology to the *Escherichia coli* Na⁺/H⁺ exchanger NhaA (Brett *et al.*, 2005a), was characterized as a Na⁺/H⁺ exchanger exhibiting subcellular localization at the plasma membrane, mitochondria, late endosomes, and lysosomes, dependent on the cell type investigated (Battaglino *et al.*, 2008; Fuster *et al.*, 2008; Hofstetter *et al.*, 2010; Xiang *et al.*, 2007). Clearly, further studies will be needed to

unequivocally elucidate the identity of the mammalian Na^+ -specific mitochondrial Na^+/H^+ exchanger.

As mentioned above, swelling experiments suggest that yeast mitochondria possess only an unspecific mitochondrial cation/proton exchanger, transporting all alkali metal cations (Welihinda *et al.*, 1993), whose identity still remains to be determined. Surprisingly, mitochondrial Na^+/H^+ exchange was initially assigned to Nhx1p, which shows sequence homology to human Nhe6. Yeast cells deleted for *NHX1* exhibited abolished uptake of $^{22}\text{Na}^+$ from acetate medium (Numata *et al.*, 1998). Besides Na^+ , Nhx1p is supposed to mediate the transport of Rb^+ , K^+ and Li^+ (Brett *et al.*, 2005a; Kinclova-Zimmermannova *et al.*, 2004; Nass *et al.*, 1997; Quintero *et al.*, 2000). However, several studies confirmed that Nhx1p localized to the membranes of late endosomes, similarly to human Nhe6, and not to mitochondria (Bowers *et al.*, 2000; Brett *et al.*, 2005b; Nass & Rao, 1998).

2.5. Regulation of mitochondrial K^+/H^+ exchange

An active mitochondrial K^+/H^+ exchanger, constitutively mediating cation efflux driven by the proton electrochemical gradient, causes the problem of membrane potential dissipation. Therefore, it is rather conceivable that the exchanger is regulated. Supported by the finding that depletion of divalent cations in the mitochondrial matrix upon treatment with A-23187 induced K^+ efflux, Garlid proposed the ‘ Mg^{2+} Carrier Break Hypothesis’ (Dordick *et al.*, 1980; Garlid, 1980; Shi *et al.*, 1980). Accordingly, matrix Mg^{2+} , whose concentration is relatively stable, would function as a concentration-dependent and reversible inhibitor of the K^+/H^+ exchanger. Water influx following cation K^+ uptake increases the matrix volume, thereby reducing the inhibitor concentration by dilution. Furthermore, electroneutral K^+ efflux would be induced by anions capable of forming complexes with divalent cations, like citrate and phosphate (Garlid, 1980). Thus, increased matrix anion content, caused by net uptake of salts, would complex Mg^{2+} and in concert with matrix swelling release the K^+/H^+ exchanger from Mg^{2+} inhibition and thereby activate K^+ efflux (Garlid, 1980; Garlid & Paucek, 2003).

Although it has been clearly shown that the K^+/H^+ exchanger is inhibited by Mg^{2+} (Beavis & Garlid, 1990; DiResta *et al.*, 1986; Froschauer *et al.*, 2005; Nakashima *et al.*, 1982), the role of Mg^{2+} in the Carrier Break Hypothesis as a matrix volume sensor has been questioned. Changed matrix Mg^{2+} concentration following different swelling conditions was determined by direct measurement using the Mg^{2+} -sensitive fluorescent dye mag-fura-2. The low reduction of the matrix Mg^{2+} concentration was suggested to be incompatible with a function

of Mg^{2+} in volume control and regulation of the K^+/H^+ exchanger (Jung & Brierley, 1999). Additionally, the authors showed that the K^+/H^+ exchanger is also inhibited by matrix Ca^{2+} and considered different regulatory mechanisms. Changes in the matrix protein concentration may affect kinases or phosphatases that regulate the exchanger (Minton *et al.*, 1992). Alternatively, mechanical signals evoked by a stronger contact of the IMM and OMM upon swelling may be involved in regulation (Hoffmann & Dunham, 1995; Jung & Brierley, 1999). Finally, the K^+/H^+ exchanger is allosterically inhibited by matrix protons. As a result, activity of the exchanger increases with alkaline pH (Beavis & Garlid, 1990; Brierley *et al.*, 1991; Garlid & Paucek, 2003; Nakashima & Garlid, 1982).

2.6. Mitochondrial K^+/H^+ exchange involves the *LETM1/YOL027C* gene family

Recent studies characterized the first known proteins involved in mitochondrial K^+/H^+ exchange and volume control, namely yeast Mdm38p/Mkh1p and Mrs7p as well as their human homolog Letm1. They are members of a new family of evolutionary conserved eukaryotic proteins. They are encoded in the nucleus and localize to the mitochondrial inner membrane. These proteins exhibit an overall sequence homology of ~ 40%, highly conserved in the region of the predicted single transmembrane helix (Frazier *et al.*, 2006; Nowikovsky *et al.*, 2004; Zotova *et al.*, 2010). All three proteins are supposed to contain C-terminal coiled coils, whereas Letm1 is predicted to additionally contain two EF-hand Ca^{2+} -binding domains (Endele *et al.*, 1999).

2.6.1. *YOL027C/MDM38/MKH1*

Yeast *YOL027C/MDM38/MKH1* encodes a ~ 65 kDa protein originally identified to be involved in maintenance of mitochondrial morphology (Dimmer *et al.*, 2002). Moreover, *MDM38* was shown to be a multicopy suppressor of cells deleted for the yeast IMM Mg^{2+} transporter *MRS2* (Kolisek *et al.*, 2003; Nowikovsky *et al.*, 2004; Waldherr *et al.*, 1993), and deletion of both genes resulted in synthetic lethality on non-fermentable carbon sources and loss of mitochondrial DNA (Nowikovsky *et al.*, 2004). Mutants deleted for *MDM38* exhibit a severe growth defect on non-fermentable carbon sources and contain a highly fragmented mitochondrial reticulum. Involvement of *MDM38* in mitochondrial ion homeostasis was initially suggested by the finding that *mdm38* Δ mitochondria appeared to be heavily swollen,

devoid of the cristae structures, displayed severely reduced $\Delta\psi$, and increased K^+ accumulation (Nowikovsky *et al.*, 2004; Nowikovsky *et al.*, 2007). These features are consistent with defective mitochondrial K^+/H^+ exchange previously described (Garlid & Paucek, 2003). Remarkably, addition of the K^+/H^+ ionophore nigericin restored all mitochondrial functions and respiratory growth of *mdm38Δ* cells, suggesting a direct role of Mdm38p in mitochondrial K^+/H^+ exchange (Nowikovsky *et al.*, 2004; Nowikovsky *et al.*, 2007).

Mitochondria lacking Mdm38p are refractory to KOAc-induced swelling and are already swollen prior the measurement. Thus, direct measurement of ion fluxes was performed with submitochondrial particles (SMPs) with entrapped K^+ - and H^+ -sensitive fluorescent dyes potassium-binding benzofuran isophthalate (PBFI) and 2,7-bis(carboxyethyl)-5,6-carboxyfluorescein (BCECF), respectively. Electroneutral exchange of K^+ , Na^+ , and Li^+ for H^+ , driven by their concentration gradients and sensitive to DCCD, quinine and Mg^{2+} , was observed in wild-type SMPs in accordance with the transport properties expected for the unspecific K^+/H^+ exchanger. In contrast, electroneutral cation/ H^+ exchange in SMPs prepared from *mdm38Δ* mitochondria was almost completely abolished but could be restored by addition of nigericin (Froschauer *et al.*, 2005).

Interestingly, disturbed K^+ homeostasis in *mdm38Δ* cells resulted not only in mitochondrial dysfunction and fragmentation but also influenced vacuolar morphology. Vacuoles exhibited membrane indentations and close association with swollen mitochondria (Nowikovsky *et al.*, 2007), followed by vacuolar uptake and mitophagy, the autophagic degradation of damaged mitochondria (Goldman *et al.*, 2010; Lemasters, 2005; Priault *et al.*, 2005).

Despite the unambiguous evidence for a direct contribution of Mdm38p to mitochondrial K^+/H^+ exchange, additional functions of this protein were recently proposed. Mdm38p was reported to be associated with mitochondrial ribosomes and newly synthesized mitochondrial proteins. Mitochondria of *mdm38Δ* cells exhibited reduced amounts of respiratory chain complexes III and IV and several mitochondrial encoded proteins. Accordingly, Mdm38p was suggested to be involved in mitochondrial protein export and regulation of mitochondrial translation (Bauerschmitt *et al.*, 2010; Frazier *et al.*, 2006).

Reduced levels of mitochondrial encoded proteins upon deletion of *MDM38* were confirmed in our laboratory. Importantly, addition of nigericin completely restored the protein levels. Moreover, doxycycline-induced shut-off of *MDM38* revealed that the amounts of mitochondrially translated proteins remained unchanged for more than 25 h after reduction of Mdm38p below the level of detection (Nowikovsky *et al.*, 2007). On the contrary, loss of K^+/H^+ exchange, reduction of $\Delta\psi$, as well as swelling and fragmentation of the mitochondrial

reticulum were shown to be immediate events upon deletion of *MDM38*. These findings strongly suggest that the changed pattern of mitochondrial encoded proteins is secondary to the loss of K^+/H^+ exchange (Nowikovsky *et al.*, 2007).

2.6.2. *YPR125W/MRS7/YLH47*

The second member of the protein family present in yeast is *YPR125W (MRS7/YLH47)*. It is a homolog of *MDM38* and was identified as a multicopy suppressor of *mrs2* Δ mutant cells (Waldherr *et al.*, 1993). Deletion of *MRS7* causes only a marginal growth defect on non-fermentable carbon sources but does not influence the mitochondrial morphology (personal observations). However, multicopy expression of *MRS7* restores K^+/H^+ exchange and mitochondrial dysfunctions of *mdm38* Δ mutant cells, suggesting functional homology of both proteins (Nowikovsky *et al.*, 2004; Zotova *et al.*, 2010). Similar to Mdm38p, Mrs7p was found to interact with mitochondrial ribosomal proteins. Moreover, Mrs7p was reported to copurify with protein A-tagged Mdm38p and *vice versa* (Frazier *et al.*, 2006).

2.6.3. *LETMI*

Letm1 (leucine zipper-EF-hand containing transmembrane protein 1) is the ~ 83 kDa human homolog of Mdm38p and Mrs7p and has been implicated in the hereditary Wolf-Hirschhorn syndrome (WHS), which is caused by hemizygous deletion of several genes located on the distal short arm of chromosome 4 (4p16.3) (Zollino *et al.*, 2003). WHS is characterized by a series of neuromuscular symptoms, including severe growth and mental retardation, loss of muscular tone, congenital heart defects, hypertelorism, microcephaly, speech problems and epilepsy (Bergemann *et al.*, 2005). Interestingly, seizures, which represent the most life-threatening consequence of the full WHS phenotype, were found to be invariably associated with deletion of *LETMI*. The extent of the chromosomal deletion directly influences the combinations and severity of the clinical hallmarks observed in different patients (Endele *et al.*, 1999; Schlickum *et al.*, 2004).

Consequences of knock-down of *LETMI* appeared to be in accordance with phenotypic effects resulting from deletion of yeast *MDM38*. Reduced levels of Letm1 in mammalian cells caused mitochondrial swelling and fragmentation independent of Drp1, the mitochondrial fission factor, as well as caspase-independent necrotic cell death (Dimmer *et al.*, 2008). Mitochondrial respiration, respiratory chain assembly, and the membrane potential appeared

unaffected, likely due to maintenance of these functions by the action of residual Letm1. Importantly, mitochondrial morphology was restored by nigericin (Dimmer *et al.*, 2008) and overexpression of *LETMI* in human and *C. elegans* cells resulted in condensed mitochondrial matrices, swollen cristae, and reduced membrane potential (Hasegawa & van der Blik, 2007), suggesting involvement of Letm1 in mitochondrial K^+ and volume homeostasis. Similar to mammalian cells, *LETMI* knock-down in *C. elegans* and *D. melanogaster* caused mitochondrial swelling, followed by mitophagy observed in *D. melanogaster* S2 cells. Moreover, Letm1 was shown to be essential for normal larval development and neuronal function of *C. elegans* and *D. melanogaster* (Hasegawa & van der Blik, 2007; McQuibban *et al.*, 2010). Most importantly, human and fly *LETMI* encode functional homologs of yeast *MDM38*, restoring respiratory growth and K^+/H^+ exchange activity of *mdm38* Δ mutant cells (Froschauer *et al.*, 2005; McQuibban *et al.*, 2010; Nowikovsky *et al.*, 2004; Zotova *et al.*, 2010).

The presence of coiled coils in all K^+/H^+ exchange family members points to possible homo- or hetero-oligomerization of these proteins. Indeed, Letm1 was shown to self-interact and to be part of several high molecular weight protein complexes of unknown composition (Dimmer *et al.*, 2008; Hasegawa & van der Blik, 2007). Furthermore, Letm1 was reported to interact with the mitochondrial ribosomal protein Mrpl36 (Piao *et al.*, 2009) and the mitochondrial AAA-ATPase Bcs1L, which was shown to influence Letm1 complex formation (Tamai *et al.*, 2008). Possible involvement of Letm1 in seizures of WHS patients was supported by the presence of EF-hand Ca^{2+} -binding domains (Endele *et al.*, 1999), as disturbed Ca^{2+} homeostasis often correlates with neurodegenerative disorders (Biessels & Gispen, 1996; Burgess *et al.*, 1997; Lim *et al.*, 2008). However, the Letm1 EF-hands exhibit low affinity for divalent cations, suggesting that they may bind matrix Mg^{2+} , which inhibits the K^+/H^+ exchanger, rather than Ca^{2+} (Endele *et al.*, 1999; Nakashima *et al.*, 1982).

Very recently, Jiang *et al.* performed a genome-wide *Drosophila* RNAi screen to identify genes involved in mitochondrial Ca^{2+} transport. Knock-down of *LETMI* caused reduced mitochondrial Ca^{2+} uptake and functional assays performed with liposome reconstituted human Letm1 led the authors to the conclusion that Letm1 represents a mitochondrial Ca^{2+}/H^+ exchanger mediating electrogenic, Ruthenium Red sensitive Ca^{2+} uptake into mitochondria at nanomolar cytosolic Ca^{2+} concentrations (Jiang *et al.*, 2009). These findings are in contrast to the conclusive data that indicate involvement of Letm1 in K^+/H^+ exchange and challenge current concepts on mitochondrial Ca^{2+} transport. In view of our own and previous results, we critically discuss the report of Jiang *et al.* in our recent publication (Zotova *et al.*, 2010) and this thesis.

2.6.4. *HCCR-1/LETMD1*

Sequence alignments revealed that *LETMI* has a human homolog. *HCCR-1* (human cervical cancer oncogene 1)/*LETMD1* (Letm1 domain containing 1) encodes a mitochondrial protein containing a domain homologous to Letm1, reaching from position 75 to 346 (Cho *et al.*, 2007; Zotova *et al.*, 2010). *HCCR-1* was reported to be overexpressed in various human cancers, including leukemia, lymphoma, and carcinomas of the breast, kidney, ovary, stomach, colon, and uterine cervix, and to function as a negative regulator of the p53 tumor suppressor (Ko *et al.*, 2003). Moreover, mice transgenic for *HCCR-1* developed breast cancers and metastasis (Ko *et al.*, 2004), and uncontrolled expression of *HCCR-1* was suggested to trigger tumorigenesis by mitochondrial dysfunction resulting in suppression of UVC- and staurosporine-induced apoptosis (Cho *et al.*, 2007). Recently, *HCCR-1* was also found to induce epithelial-to-mesenchymal transition (EMT) and mesenchymal-to-epithelial transition (MET) in human and mouse, respectively and expression of *HCCR-1* was detected during embryonic kidney development. Thus, *HCCR-1* was proposed to be a regulatory factor of epithelia or mesenchyme morphogenesis during cancer development (Ha *et al.*, 2010).

2.7. Mitochondrial autophagy - Mitophagy

Autophagy refers to the process of degradation of cellular components, such as cytosol, protein aggregates and organelles. It is induced under stress conditions like nutrient limitation, but is also required for cellular growth and development. Furthermore it is involved in pathogen elimination and serves the function of a quality control mechanism by the selective removal of damaged organelles (Abeliovich & Klionsky, 2001; Gutierrez *et al.*, 2004; Huang & Klionsky, 2002).

Cytosolic cargo degraded by autophagy is either engulfed by the so called isolation membrane, a double-membrane structure forming the autophagosome, which then fuses with a vacuole/lysosome (Macroautophagy), or the components are directly taken up by lysosomal/vacuolar pinocytosis (Microautophagy) (Nakatogawa *et al.*, 2009; Yang & Klionsky, 2010). Accordingly, mitophagy denotes the selective degradation of mitochondria by autophagy (Figure 5) (Goldman *et al.*, 2010; Lemasters, 2005; Youle & Narendra, 2011). Mitochondria may be removed due to adjustment to changing metabolic conditions and requirements or as a consequence of dysfunction of the organelle. Interestingly, elimination of yeast mitochondria preferentially occurs by micromitophagy, whereas in higher eukaryotes

macromitophagy seems to be predominant (Tolkovsky, 2009). Importantly, in yeast and mammalian cells mitophagy follows mitochondrial fission (Nowikovsky *et al.*, 2007; Twig *et al.*, 2008). Also reduced mitochondrial membrane potential ($\Delta\psi$) seems to trigger mitophagy, although it is not essential (Tolkovsky, 2009).

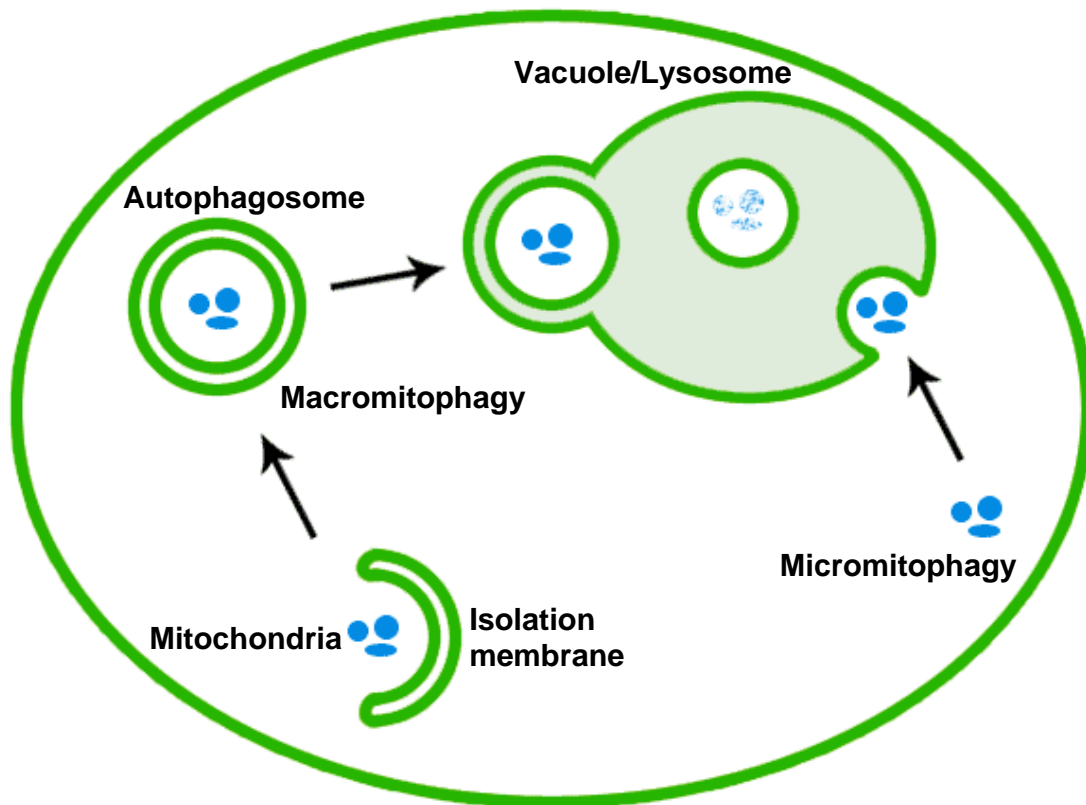


Figure 5: Schematic representation of mitochondrial autophagy

Mitochondria are either directly taken up by vacuolar/lysosomal pinocytosis (Micromitophagy) or engulfed by the autophagosome, which subsequently fuses with the vacuole/lysosome (Macromitophagy). Figure adapted from <http://en.wikipedia.org/wiki/File:Macro-micro-autophagy.gif>

Knowledge about the molecular mechanisms regulating mitophagy in yeast and mammalian cells is still scarce. However, new data are emerging. In yeast, several proteins are known to participate in mitophagy. The OMM protein Uth1p and the mitochondrial type 2C protein phosphatase (PP2C) Aup1p were shown to be required for mitophagy upon nutrient changes (Kissova *et al.*, 2004) and in stationary phase (Tal *et al.*, 2007), respectively. Furthermore, genome wide screens identified several genes involved in mitochondrial degradation (Kanki *et al.*, 2010) and the OMM protein Atg32p was shown to be required for selective mitophagy (Kanki *et al.*, 2009; Okamoto *et al.*, 2009). Mitochondria are believed to be directed to an autophagosome by interaction of Atg32p with Atg11p, which itself binds to autophagosome-

associated Atg8p (Okamoto *et al.*, 2009). Alternatively, Atg32p-bound Atg11p may recruit mitochondria to the vacuole where micromitophagic uptake occurs (Kanki *et al.*, 2009; Youle & Narendra, 2011).

In mammalian cells, also functional mitochondria are removed during developmental processes. The OMM protein NIP3-like protein X (NIX) was reported to be required for mitophagy during the maturation of reticulocytes to red blood cells. NIX directly interacts with the autophagosome-associated mammalian Atg8p homolog LC3 and GABA receptor-associated protein (GABARAP), a LC3 homolog (Novak *et al.*, 2009; Schwarten *et al.*, 2009). Also the UNC51-like kinase 1 (Ulk1) and Atg7 are involved in this process (Kundu *et al.*, 2008; Zhang *et al.*, 2009). Damaged mammalian mitochondria are removed by a mitophagy pathway that is linked to Parkinson's disease. When mitochondria lose $\Delta\psi$, the PINK1 (PTEN-induced putative kinase protein 1) kinase accumulates on the OMM and recruits the cytosolic E3 ubiquitin ligase parkin which ubiquitylates OMM proteins, like mitofusins (Gegg *et al.*, 2010; Narendra *et al.*, 2010; Vives-Bauza *et al.*, 2010). As mitofusins mediate mitochondrial fusion (Legros *et al.*, 2002), their degradation may promote mitochondrial fragmentation and mitophagy (Tanaka *et al.*, 2010). Several mutations in parkin impaired mitophagy in Parkinson's disease patients (Lee *et al.*, 2010) and PINK1 mutations caused defective parkin recruitment and parkin-induced mitophagy (Geisler *et al.*, 2010; Youle & Narendra, 2011). Additionally, increased mitophagy is suspected to be involved in Alzheimer's disease (Moreira *et al.*, 2007; Santos *et al.*, 2010).

Recently, disruption of the mitochondrial K^+/H^+ exchange system was shown to trigger mitophagy in yeast cells (Nowikovsky *et al.*, 2007; Zotova *et al.*, 2010) and in *Drosophila melanogaster* after knock-down of *LETMI* (McQuibban *et al.*, 2010). Moreover, developmental lethality in *LETMI*-depleted *Drosophila* larvae was proposed to be the result of deregulated mitophagy (McQuibban *et al.*, 2010). Taken together, these findings contribute to the elucidation of the regulatory mechanisms of mitophagy and the causes of neurodegenerative diseases.

3. Materials and Methods

3.1. Materials

3.1.1. Table 1: Yeast strains used in this study

Strain	Genotype	Source
BY4741	<i>MAT a; his3Δ1; leu2Δ0; met15Δ0; ura3Δ0</i>	Euroscarf
BY <i>mdm38</i> Δ	<i>MAT a; his3Δ1; leu2Δ0; met15Δ0; ura3Δ0; mdm38::HIS5</i>	this study
BYdeletion strains	<i>MAT a; his3Δ1; leu2Δ0; met15Δ0; ura3Δ0; orf::KANMX4</i>	Euroscarf
BY7092	<i>MAT α; can1:: STE2pr-HIS5; lyp1Δ; his3Δ1; leu2Δ0; ura3Δ0; met15Δ0; LYS2</i>	Boone C.
BY7092 <i>mdm38</i> Δ	<i>MAT α; can1:: STE2pr-HIS5; lyp1Δ; his3Δ1; leu2Δ0; ura3Δ0; met15Δ0; LYS2; mdm38::URA3</i>	this study
BY <i>mdm38</i> Δ <i>erg5</i> Δ	<i>MAT a; can1:: STE2pr-HIS5; lyp1Δ; his3Δ1; leu2Δ0; ura3Δ0; met15Δ0; LYS2; mdm38::URA3; erg5::KANMX4</i>	this study
BY <i>mdm38</i> Δ <i>erg6</i> Δ	<i>MAT a; can1:: STE2pr-HIS5; lyp1Δ; his3Δ1; leu2Δ0; ura3Δ0; met15Δ0; LYS2; mdm38::URA3; erg6::KANMX4</i>	this study
BY <i>mdm38</i> Δ <i>ygr026w</i> Δ	<i>MAT a; can1:: STE2pr-HIS5; lyp1Δ; his3Δ1; leu2Δ0; ura3Δ0; met15Δ0; LYS2; mdm38::URA3; ygr026w::KANMX4</i>	this study
BY <i>mdm38</i> Δ <i>ldb16</i> Δ	<i>MAT a; can1:: STE2pr-HIS5; lyp1Δ; his3Δ1; leu2Δ0; ura3Δ0; met15Δ0; LYS2; mdm38::URA3; ldb16::KANMX4</i>	this study
BY <i>mdm38</i> Δ <i>hof1</i> Δ	<i>MAT a; can1:: STE2pr-HIS5; lyp1Δ; his3Δ1; leu2Δ0; ura3Δ0; met15Δ0; LYS2; mdm38::URA3; hof1::KANMX4</i>	this study
BY <i>mdm38</i> Δ <i>rxt2</i> Δ	<i>MAT a; can1:: STE2pr-HIS5; lyp1Δ; his3Δ1; leu2Δ0; ura3Δ0; met15Δ0; LYS2; mdm38::URA3; rxt2::KANMX4</i>	this study
BY <i>mdm38</i> Δ <i>rtf1</i> Δ	<i>MAT a; can1:: STE2pr-HIS5; lyp1Δ; his3Δ1; leu2Δ0; ura3Δ0; met15Δ0; LYS2; mdm38::URA3; rtf1::KANMX4</i>	this study
BY <i>mdm38</i> Δ <i>ssn8</i> Δ	<i>MAT a; can1:: STE2pr-HIS5; lyp1Δ; his3Δ1; leu2Δ0; ura3Δ0; met15Δ0; LYS2; mdm38::URA3; ssn8::KANMX4</i>	this study
BY <i>mdm38</i> Δ <i>ctk1</i> Δ	<i>MAT a; can1:: STE2pr-HIS5; lyp1Δ; his3Δ1; leu2Δ0; ura3Δ0; met15Δ0; LYS2; mdm38::URA3; ctk1::KANMX4</i>	this study

Materials and Methods

DBY747	<i>MAT a his3-Δ1; leu2-3,-112; trp1-289; ura3-52</i>	ATCC 204659
DBY <i>mdm38Δ</i>	<i>MAT a his3-Δ1; leu2-3,-112;</i> <i>trp1-289; ura3-52; mdm38::HIS3</i>	(Nowikovskiy <i>et al.</i> , 2004)
DBY <i>mrs2Δ</i>	<i>MAT a his3-Δ1; leu2-3,-112;</i> <i>trp1-289; ura3-52; mrs2::HIS3</i>	(Wiesenberger <i>et al.</i> , 1992)
DBY-MDM38-HIS-TAP ^a	<i>MAT a his3-Δ1; leu2-3,-112; trp1-289; ura3-52;</i> <i>MDM38-HIS-TAP-TRP1</i>	this study
DBY-MDM38-HIS	<i>MAT a his3-Δ1; leu2-3,-112; trp1-289; ura3-52;</i> <i>MDM38-HIS-TRP1</i>	this study
DBY-MDM38-Strep	<i>MAT a his3-Δ1; leu2-3,-112; trp1-289; ura3-52;</i> <i>MDM38-Strep-TRP1</i>	this study
DBY-MDM38-OS ^b	<i>MAT a his3-Δ1; leu2-3,-112; trp1-289; ura3-52;</i> <i>MDM38-One-Strep-TRP1</i>	this study

^a TAP, tandem affinity purification

^b OS, One-Strep

3.1.2. Table 2: Plasmids and oligonucleotides used in this study

Plasmid	Source
YCplac22	(Gietz & Sugino, 1988)
YCp22-MDM38-OSH ^c	this study
YCp22-MRS2-OSH	this study
pBS1479	(Rigaut <i>et al.</i> , 1999)
pBS1479-OS	this study
pYX142-mtGFP ^d	(Westermann & Neupert, 2000)
pSG634	(Partridge <i>et al.</i> , 1991)
pUG72	(Gueldener <i>et al.</i> , 2002)

Oligonucleotide	Sequence
<i>MDM38-Del-fw</i>	5' - CTA TCT CTA TCA CTA CAG ATA ATA TAC TAA TAT GTT GAA TTT CGC ATC CTG ACG CTG CAG GTC GAC - 3'

<i>MDM38-Del-rev</i>	5'- TAG TTT TTT TCT TAG GCT TTG ATC TAA TAT CAA TCT TTC TTA ATG ACA TAG GCC ACT AGT GGA TCT G - 3'
<i>MDM38-HIS-TAP-fw</i>	5' - TAC CTC CCA TTC CGG CCG ATC AAG CTG CGA AGA CTT TTG TCA TTA AGA AAG ATC ATC ACC ATC ACC ATC ACT CCA TGG AAA AGA GAA G - 3'
<i>MDM38-HIS-TAP-rev</i>	5'-CCT GAT GTA CTC ACA TTT CCA TCT GGT GAG GAT GGA GGT GGA GAC GTC GTA GAC ATG GAA CCC TGT TTA CGA CTC ACT ATA GGG -3'
<i>MDM38-HIS-fw</i>	5'- TTC CGG CCG ATC AAG CTG CGA AGA CTT TTG TCA TTA AGA AAG ATC ATC ACC ATC ACC ATC ACT GAT CCA TGG AAA AGA GAA G -3'
<i>MDM38-Strep-fw</i>	5'CAT TCC GGC CGA TCA AGC TGC GAA GAC TTT TGT CAT TAA GAA AGA TTG GAG CCA CCC GCA GTT CGA AAA ATG ATC CAT GGA AAA GAG AAG -3'
OS tag	5' - GGA TCC GAG AAT TTG TAT TTT CAG GGT TGG AGC CAC CCG CAG TTC GAG AAA GGT GGA GGT TCC GGA GGT GGA TCG GGA GGT AGC GCT TGG AGC CAC CCG CAG TTC GAA AAA TAA TGA GAA TTC CTG CAG GGA TCC - 3'
OSH tag	5' - CTG CAG GAG AAT TTG TAT TTT CAG GGT TGG AGC CAC CCG CAG TTC GAG AAA GGT GGA GGT TCC GGA GGT GGA TCG GGA GGT AGC GCT TGG AGC CAC CCG CAG TTC GAA AAA AGA GGC TCC CAT CAC CAT CAC CAT CAC TAA TGA GGA TCC GCG GCC GC - 3'
<i>MDM38-OS-fw</i>	5' - CAT TCC GGC CGA TCA AGC TGC GAA GAC TTT TGT CAT TAA GAA AGA TGA GAA TTT GTA TTT TCA GG - 3'
<i>MDM38-OSH-fw</i>	5' - CGG GAT CCA ACG ATC ACC AAA GCA TTA GCA ACC - 3'
<i>MDM38-OSH-rev</i>	5'- ATA GTC GAC TCA GTG ATG GTG ATG GTG ATG CGA TCC TCT TTT TTC GAA CTG CGG GTG GCT CCA AGC -3'
<i>MRS2-OSH-fw</i>	5'- TAG AGC TCG ATC GAC CAG CAG CTT GTA TAC C - 3'
<i>MRS2-OSH-rev</i>	5'- TAA GTC GAC ATT TTT CTT GTC TTC TAT CAA CC - 3'

^c OSH, One-Strep-HIS

^d mtGFP, mitochondrial matrix-targeted GFP

3.1.3. Media

YPD

1% yeast extract, 2% peptone, 2% dextrose;

YPD was supplemented with 15 µg/ml valinomycin (Sigma-Aldrich) when indicated.

YPG

1% yeast extract, 2% peptone, 3% glycerol;

YPG was supplemented with 7.5 µg/ml valinomycin (Sigma-Aldrich) when indicated.

YPdG

1% yeast extract, 2% peptone, 0.1% dextrose, 3% glycerol;

YPEG

1% yeast extract, 2% peptone, 3% ethanol, 3% glycerol;

Enriched sporulation medium

Per liter: 10g potassium acetate, 1g yeast extract, 0.5g glucose, 0.1g amino acids supplement mixture, 50 mg G418;

Amino acids supplement mixture:

3g adenine	2g uracil	2g inositol	0.2g para-amino benzoic acid
2g alanine	2g arginine	2g asparagines	2g aspartic acid
2g cysteine	2g glutamic acid	2g glutamine	2g glycine
2g histidine	2g isoleucine	10g leucine	2g lysine
2g methionine	2g phenylalanine	2g proline	2g serine
2g threonine	2g tryptophan	2g tyrosine	2g valine

Synthetic minimal medium

0.67% yeast nitrogen base including ammonium sulfate, 2% glucose, or 2% galactose, or 2% galactose and 1% raffinose, and amino acids as required;

When G418 (200µg/ml final concentration) was added, monosodium glutamic acid (1g/l, Sigma-Aldrich) was used as a nitrogen source instead of ammonium sulfate, which impedes the function of G418. 10 mM 3-Amino-1,2,4-triazole (3-AT, Sigma-Aldrich) was supplemented when appropriate.

3.1.4. Chemicals and antibodies

FM4-64	(Molecular Probes)
Disuccinimidyl suberate (DSS)	(Thermo Fisher Scientific)
Triton X-100	(Sigma-Aldrich)
Complete mini protease inhibitor mixture	(Roche Applied Science)
Monosodium glutamic acid	(Sigma-Aldrich)
Amino-1,2,4-triazole (3-AT)	(Sigma-Aldrich)
Anti-His antibody	(Quiagen)
Anti-Strep antibody	(Quiagen)
Anti-protein A (PAP) antibody	(Sigma-Aldrich)
Anti-calmodulin binding peptide (CBP) antibody	(Immunology Consultants Laboratory)
HRP-conjugated goat anti-mouse IgG	(Promega)
HRP-conjugated goat anti-rabbit IgG	(Promega)

3.1.5. Affinity resins

IgG Sepharose 6 fast flow	(GE Healthcare)
Calmodulin affinity resin	(Stratagene)
Ni-NTA Superflow resin	(Qiagen)
Strep-Tactin Superflow	(Qiagen)

3.2. Methods

3.2.1. Gene disruption

The haploid deletion strains *BYmdm38Δ* and *BY7092mdm38Δ* were constructed according to the one step gene replacement protocol (Wach *et al.*, 1994). Parental strains BY4741 and BY7092 were deleted for the *MDM38* ORF by homologous recombination with a *HIS5* disruption cassette PCR-amplified from plasmid pSG634 and a *URA3* cassette PCR-amplified from plasmid pUG72, respectively. For both gene disruptions the primers *MDM38-Del-fw* and *MDM38-Del-rev* (Table 1) were used. All double mutants were obtained by crossing of strain *BY7092mdm38Δ* with single mutants of the Euroscarf deletion strain library and sporulation of the diploids.

3.2.2. Chromosomal tagging and plasmid construction

All chromosomally integrated affinity tags were C-terminally fused to *MDM38* by homologous recombination in strain DBY747. The HIS-TAP tag was PCR-amplified together with the *TRP1* selection marker from plasmid pBS1479 using the primer pair *MDM38-HIS-TAP-fw* and *MDM38-HIS-TAP-rev* (Table 2). To fuse the 6xHIS and the Strep tag in-frame with *MDM38*, the respective forward primers *MDM38-HIS-fw* and *MDM38-Strep-fw* were used. The reverse primer *MDM38-HIS-TAP-rev* served to PCR-amplify cassettes for both tags containing the *TRP1* selection marker from plasmid pBS1479. Chromosomal integration of the One-strep (OS) tag was performed as described previously (Zotova *et al.*, 2010). Briefly, the synthesized OS sequence was cloned into BamHI-linearized plasmid pBS1479 (pBS1479-OS) and PCR-amplified together with the *TRP1* marker using the primer pair *MDM38-OS-fw* and *MDM38-HIS-TAP-rev*. All chromosomal integrations were verified by analytical PCR.

Plasmid-based One-Strep-HIS (OSH)-tagged *MDM38* was created by addition of the 6xHIS tag to OS-tagged *MDM38* by PCR-amplification from chromosomal DNA of strain DBY-*MDM38-OS* using the primer pair *MDM38-OSH-fw* and *MDM38-OSH-rev*. The resulting PCR product, including the endogenous promoter of *MDM38*, was cloned into the BamHI/SalI-linearized centromeric plasmid YCplac22, thereby creating the construct YCp22-*MDM38-OSH*. As a control, the OSH tag was also fused to *MRS2*, which encodes an IMM Mg²⁺ channel (Kolisek *et al.*, 2003). The complete OSH tag was synthesized (Eurofins MWG

GmbH) and cloned into PstI/NotI-linearized YCplac22. The *MRS2* ORF including its endogenous promoter was PCR-amplified and cloned into SacI/SalI-linearized YCplac22 containing the OSH tag, thereby creating the construct YCp22-*MRS2*-OSH.

3.2.3. Mitochondrial isolation

Yeast strains were grown overnight in YPD medium and harvested at early stationary phase. Mitochondria were isolated as described previously (Zinser & Daum, 1995) and resuspended in breaking buffer (250 mM Sucrose, 10 mM Tris-HCl pH 7.4). The average yield of crude mitochondria isolated from DBY strains was about 400 mg/12 liters of culture (~ 120 g cells). Isolation from BY strains resulted in a yield of only ~ 20% compared to DBY strains. Mitochondria were either processed immediately or stored at -80°C until use.

3.2.4. Protein precipitation and immunoblotting

Proteins were precipitated with TCA (12% final concentration) for 15 min on ice. Subsequent washings of the precipitate were performed using 90% acetone. Protein extracts were dissolved by boiling in SDS-loading buffer, separated on a 12% SDS-polyacrylamide gel, transferred to a PVDF membrane, and immunodetected. Immunoblotting was performed in TBS-Tween plus 2.5% dry milk with the desired antibodies. The proteins were visualized by using the SuperSignal West Pico system (Pierce, Rockford, Illinois).

3.2.5. Blue native electrophoresis

Protein samples were supplemented with a 0.25 volume of sample buffer (500 mM aminocaproic acid, 5% Serva blue G) and analyzed on a 5-18% linear polyacrylamide gradient gel as described elsewhere (Schagger *et al.*, 1994). Proteins were transferred to a PVDF membrane followed by immunodetection with the desired antibodies.

3.2.6. Chemical cross-linking

Mitochondrial extracts (50-90 µg total protein) were supplemented with breaking buffer (BB, 0.6M Sorbitol, 20 mM Tris-HCl, pH 7.4) and the amine-reactive cross-linker disuccinimidyl suberate (DSS) at increasing concentrations (0.1-0.5 mM) in a total reaction volume of

100 μ l. Probes were incubated on ice (30 - 45 min) and the reaction was quenched by adding 5 μ l of 100 mM N-ethylmaleimic acid (10 min on ice). Cross-linking was performed in presence of protease inhibitor mixture. Samples were TCA precipitated, supplemented with SDS-loading buffer, heated (5 min, 65°C), and subjected to SDS-PAGE followed by immunodetection against the 6xHIS epitope of HIS-TAP-tagged Mdm38p.

3.2.7. Protein A affinity purification

Protein A affinity purification was performed according to (Puig *et al.*, 2001). Mitochondria isolated from strain DBY-*MDM38*-HIS-TAP (~ 200 mg total protein) were solubilized in IPP150 buffer (10 mM Tris-HCl pH 8.0, 150 mM NaCl) containing 1.2% Triton X-100 (TX-100) for 30 min on ice. The suspension was subjected to a clarifying spin (30 min at 45.000 g) to get rid of insoluble debris. About 1 ml of IgG Sepharose beads were equilibrated with IPP150 buffer and transferred to a 10 ml Poly-Prep Chromatography Column (Bio-Rad). The mitochondrial extract was added to the beads and incubated under rotation for 2 h at 4°C. Unbound material was removed by gravity flow and the beads were washed with two column volumes of IPP150 buffer containing 0.8% TX-100 and one volume of TEV cleavage buffer (10 mM Tris-HCl pH 8.0, 150 mM NaCl, 0.8% TX-100, 0.5 mM EDTA, 1 mM DTT). Cleavage was performed in presence of 50 units AcTEV protease (Invitrogen) for 2 h at 16°C. Residual bound proteins were eluted with 0.1 M glycine buffer, pH 3. To increase cleavage efficiency, 100 units of TEV protease were used for 2 h at 28°C and the TX-100 concentration of the TEV cleavage buffer was reduced to 0.1%. Eluted proteins, flow through and wash fractions were TCA precipitated, subjected to SDS-PAGE, and immunodetected with an antibody directed against CBP.

3.2.8. CBP affinity purification

Mitochondria isolated from strain DBY-*MDM38*-HIS-TAP (~ 200 mg total protein) were solubilized in IPP150 calmodulin binding buffer (10 mM β -mercaptoethanol, 10 mM Tris-HCl pH 8.0, 150 mM NaCl, 1 mM magnesium acetate, 1 mM imidazole, 2 mM CaCl₂, 1.2% TX-100) and the clarified protein extracts were incubated with ~ 1 ml equilibrated calmodulin affinity resin in a Poly-Prep Chromatography Column in presence 0.8% TX-100 for 2 h at 4°C. After washing with two column volumes of binding buffer, proteins were eluted in 5 fractions of 200 μ l IPP150 elution buffer (10 mM β -mercaptoethanol, 10 mM Tris-HCl pH

8.0, 150 mM NaCl, 1 mM magnesium acetate, 1 mM imidazole, 2-4 mM EGTA, 0.8% TX-100). Residual bound proteins were eluted with 0.1 M glycine buffer, pH 3. Eluted proteins were TCA precipitated, subjected to SDS-PAGE and immunodetected with an antibody directed against CBP.

3.2.9. CBP - protein A tandem affinity purification (TAP)

CBP affinity purification was performed exactly as described above. All IPP150 elution fractions were combined (~ 1 ml), supplemented with 4 ml of IPP150 buffer (10 mM Tris-HCl pH 8.0, 150 mM NaCl, 0.8% TX-100) containing ~ 1 ml of IgG Sepharose beads and protease inhibitor mixture. Protein A affinity purification was performed as described above and bound proteins were eluted with 0.1 M glycine buffer, pH 3. Flow through, wash fractions and eluted proteins were TCA precipitated, subjected to SDS-PAGE and immunodetected with an anti-CBP antibody.

3.2.10. Ni-NTA affinity purification

Ni-NTA affinity purification was exactly performed as described elsewhere (Zotova *et al.*, 2010).

3.2.11. Ni-NTA - CBP TAP

Ni-NTA affinity purification was performed as previously described (Zotova *et al.*, 2010). Elution fractions were combined and supplemented with 4 elution volumes of modified calmodulin binding buffer (10 mM β -mercaptoethanol, 10 mM Tris-HCl pH 7.8, 50 mM NaCl, 1 mM magnesium acetate, 2 mM CaCl₂, 0.6% TX-100) containing ~ 1 ml equilibrated calmodulin affinity resin in a Poly-Prep Chromatography Column. CBP affinity purification was performed as described above and bound proteins were eluted with modified elution buffer (10 mM β -mercaptoethanol, 10 mM Tris-HCl pH 7.8, 50 mM NaCl, 1 mM magnesium acetate, 4 mM EGTA, 0.6% TX-100). In the reverse order, elution fractions after CBP purification were supplemented with 4 elution volumes of Ni-NTA Hi 50 binding buffer (10 mM Tris-HCl, pH 7.8, 50 mM NaCl, 20 mM imidazole, 0.6% TX-100) containing ~ 0.5 ml Ni-NTA Superflow resin and Ni-NTA affinity purification was performed. All steps were done in presence of protease inhibitor mixture. Elution fractions were directly used for Blue

native electrophoresis followed by immunodetection with antibodies directed against the 6xHIS epitope or protein A.

3.2.12. Strep affinity chromatography

Strep affinity chromatography was exactly performed as described elsewhere (Zotova *et al.*, 2010).

3.2.13. Ni-NTA - Strep TAP

Mitochondria containing OSH-tagged Mdm38p or Mrs2p (~ 800 mg total protein) were used. Ni-NTA affinity purification was exactly performed as previously described (Zotova *et al.*, 2010). Elution fractions were combined and supplemented with 4 elution volumes of Strep 50 binding buffer (100 mM Tris-HCl, pH 7.8, 50mM NaCl, 0.6% TX-100) containing ~ 0.5 ml Strep-Tactin Superflow resin. Strep affinity chromatography was exactly performed as described elsewhere (Zotova *et al.*, 2010). In the reverse order, elution fractions after Strep affinity chromatography were supplemented with 4 elution volumes of Hi 50 binding buffer and Ni-NTA affinity purification was performed. All steps were done in presence of protease inhibitor mixture. Elution fractions were either directly used for Blue native electrophoresis followed by immunodetection with antibodies directed against the Strep epitope, or eluted proteins were TCA precipitated, separated by SDS-PAGE, and detected by Coomassie staining.

Control experiments for all affinity purifications described were performed with mitochondria isolated from untagged wild-type cells or strains carrying empty plasmids.

3.2.14. Size exclusion chromatography (SEC)

Crude mitochondria isolated from strain DBY-*MDM38*-HIS-TAP (~ 500 mg total protein) were solubilized as described for Ni-NTA affinity purification (Zotova *et al.*, 2010) and the suspension was subjected to a clarifying spin (30 min at 45.000 g). To mimic the elution conditions after Ni-NTA affinity chromatography, the supernatant was supplemented with 200 mM imidazole and the TX-100 concentration was reduced to 0.6% by dilution with Ni-NTA elution buffer. Solubilized proteins were subjected to SEC using a 26/60 Superdex 200 column (Amersham) and the elution volume was collected in 1.5 ml fractions.

3.2.15. Mass spectrometry

Protein samples cut out from Blue native polyacrylamide gels were analyzed at our in-house mass spectrometry facility (Max F. Perutz Laboratories, Vienna, Austria), using a LTQ Orbitrap Velos ETD mass spectrometer (Thermo Fisher Scientific) and Scaffold 3 software (Proteome Software, Inc., Portland, OR) for protein identification. Coomassie stained samples cut out from SDS-polyacrylamide gels were analyzed at the BSRC mass spectrometry and proteomics facility (University of St. Andrews, United Kingdom), using a 4800 MALDI TOF/TOF mass spectrometer (Applied Biosystems) and Mascot software (Perkins *et al.*, 1999).

3.2.16. Fluorescence microscopy

Yeast cells were grown to early logarithmic phase in synthetic minimal medium containing galactose, glucose, or galactose and raffinose as carbon sources. Mitochondrial morphology was visualized by expression of mitochondrial matrix-targeted GFP from plasmid pYX142-mtGFP (Westermann & Neupert, 2000). Vacuoles were stained with FM4-64 (10 μ M final concentration). Shown are representative fluorescence microscopy images of living cells without fixation, as well as respective differential interference contrast (DIC) images to observe cell morphology. Images were captured with equivalent exposures using a Zeiss Axioplan 2 fluorescence microscope with an AxioCam MRc5 CCD camera using AxioVision 4.8.1 software (Carl Zeiss, Oberkochen, Germany). Grayscale images were processed with Photoshop CS3 (Adobe, San Jose, CA).

3.2.17. Potassium acetate (KOAc)-induced swelling of isolated mitochondria

The light scattering method was used to measure the mitochondrial K⁺/H⁺ exchange activity. Swelling of isolated mitochondria was recorded with a Hitachi U-2000 spectrophotometer as previously described (Nowikovsky *et al.*, 2004). Briefly, mitochondria were prepared from BY4741 wild-type, *mdm38* Δ , *erg5* Δ , *erg6* Δ , *mdm38* Δ *erg5* Δ , and *mdm38* Δ *erg6* Δ mutant cells, resuspended in 0.6 M sorbitol buffer pH 7.4 to a final protein concentration of 10 mg/ml. Mitochondria were incubated 5 min with antimycin A (5 μ M) prior to measurement to block the respiratory chain. To deplete mitochondria of endogenous Mg²⁺, the 4-bromo-calcium ionophore A-23187 (0.5 μ M) and EDTA (10 mM) were added prior to KOAc treatment. After

addition of mitochondria to swelling buffer (55 mM KOAc, 5 mM TES, 0.1 mM EGTA, and 0.1 mM EDTA) in cuvettes, swelling of mitochondria was measured as a decrease of OD_{540} immediately thereafter. To inhibit swelling, the K^+/H^+ exchange inhibitor quinine (200 μ M) was added to A-23187/EDTA-treated mitochondria prior to measurement.

3.2.18. Synthetic genetic array (SGA) analysis

SGA analysis was developed as an efficient approach for the systematic construction of double mutants and the analysis of functional relationships between genes and pathways (Tong *et al.*, 2001; Tong & Boone, 2006). By robotic colony manipulation a query mutation is crossed to a non-essential deletion mutant library and the haploid double mutant progeny is obtained by sporulation of the resulting diploid strains.

The *MAT α* query strain BY7092 was deleted for *MDM38* by homologous recombination with a *URA3* cassette PCR-amplified from plasmid pUG72 (see also chapter 3.2.1.). Importantly, strain BY7092 carries the reporter *STE2pr-HIS5* which is only expressed in *MAT α* cells and allows growth on medium lacking histidine. Using a Singer RoToR HDA bench top robot, the BY7092*mdm38* Δ strain was crossed to the ordered Euroscarf deletion library of \sim 4900 haploid mutant strains (*MAT α* ; *xxx* Δ ::*KANMX4*; 96 (12x8) strains per plate). Each of these strains was deleted for one non-essential gene using the dominant selectable marker *KANMX4* (Winzeler *et al.*, 1999), which confers resistance to geneticin (G418). Heterozygous diploid strains were selected by pinning of crossed cells to synthetic minimal medium lacking uracil and containing 200 μ g/ml G418 (SD – URA + GEN). To induce sporulation, diploid cells were transferred to solid enriched sporulation medium (see also chapter 3.1.3.) and incubated for 10-12 days at room temperature. To select for haploid double mutant progeny, spores were pinned to synthetic minimal medium lacking uracil and histidine and containing G418 (SD - URA - HIS + GEN). This medium allows for selective germination of *MAT α* haploid double mutant meiotic progeny, as these cells express the *STE2pr-HIS5* reporter. To increase stringency of *STE2pr-HIS5* reporter expression and haploid double mutant selection, SD - URA - HIS + GEN plates were supplemented with 10 mM 3-Amino-1,2,4-triazole (3-AT), a competitive inhibitor of the *HIS5* gene product. To confirm correctness of the double mutant progeny and marker segregation, random tetrad dissection was performed using the Singer MSM system 300 micromanipulator.

4. Publication

Novel components of an active mitochondrial K^+/H^+ exchange

Ludmila Zotova, Markus Aleschko, Gerhard Sponder, Roland Baumgartner,
Siegfried Reipert, Monika Prinz, Rudolf J. Schweyen, and Karin Nowikovsky

Novel Components of an Active Mitochondrial K^+/H^+ Exchange^{*[5]}

Received for publication, August 27, 2009, and in revised form, February 26, 2010. Published, JBC Papers in Press, March 2, 2010, DOI 10.1074/jbc.M109.059956

Ludmila Zotova^{†1}, Markus Aleschko^{†1}, Gerhard Sponder^{‡2}, Roland Baumgartner[‡], Siegfried Reipert[§], Monika Prinz[‡], Rudolf J. Schweyen^{†‡}, and Karin Nowikovsky^{†3}

From the Departments of [†]Microbiology, Immunobiology, and Genetics and [§]Molecular Cell Biology, Max F. Perutz Laboratories, Vienna University, A-1030 Vienna, Austria

Defects of the mitochondrial K^+/H^+ exchanger (KHE) result in increased matrix K^+ content, swelling, and autophagic decay of the organelle. We have previously identified the yeast Mdm38 and its human homologue LETM1, the candidate gene for seizures in Wolf-Hirschhorn syndrome, as essential components of the KHE. In a genome-wide screen for multicopy suppressors of the *pet⁻* (reduced growth on nonfermentable substrate) phenotype of *mdm38Δ* mutants, we now characterized the mitochondrial carriers PIC2 and MRS3 as moderate suppressors and MRS7 and YDL183c as strong suppressors. Like Mdm38p, Mrs7p and Ydl183cp are mitochondrial inner membrane proteins and constituents of ~500-kDa protein complexes. Triple mutant strains (*mdm38Δ mrs7Δ ydl183cΔ*) exhibit a remarkably stronger *pet⁻* phenotype than *mdm38Δ* and a general growth reduction. They totally lack KHE activity, show a dramatic drop of mitochondrial membrane potential, and heavy fragmentation of mitochondria and vacuoles. Nigericin, an ionophore with KHE activity, fully restores growth of the triple mutant, indicating that loss of KHE activity is the underlying cause of its phenotype. Mdm38p or overexpression of Mrs7p, Ydl183cp, or LETM1 in the triple mutant rescues growth and KHE activity. A LETM1 human homologue, HCCR-1/LETMD1, described as an oncogene, partially suppresses the yeast triple mutant phenotype. Based on these results, we propose that Ydl183p and the Mdm38p homologues Mrs7p, LETM1, and HCCR-1 are involved in the formation of an active KHE system.

The high, inside negative membrane potential ($\Delta\psi$) of mitochondria favors uptake of cations through the inner mitochondrial membrane. Potassium is an osmotically active ion and the most abundant cation in the cytosol and in the mitochondrial

matrix. The uncontrolled influx of K^+ into mitochondria causes an increase of osmotic pressure of the organelles and their swelling. The presence of K^+/H^+ exchangers in mitochondria which, driven by the inside-directed pH gradient, extrude excess K^+ from mitochondria was already postulated in the 1960s by Mitchell (1). Although the KHE⁴ has been studied extensively by physiological methods, its molecular identity remained obscure. Recently, our studies identified Mdm38/LETM1 as major players of this extrusion system (2–4).

Phenotypic analyses of *mdm38Δ* are consistent with the loss of KHE activity (4). These included increased matrix K^+ content, swelling, and fragmentation of mitochondria, reduced mitochondrial $\Delta\psi$, as well as reduced growth of cells on nonfermentable substrate. Further tests involving submitochondrial inner membrane particles (SMPs) confirmed the near total lack of KHE activity (2). Addition of the synthetic KHE nigericin to *mdm38Δ* cells restored all mitochondrial functions, including growth on nonfermentable substrates, $\Delta\psi$, morphology, and KHE activity (4, 5). This result strongly supported the conclusion that Mdm38 acts as an essential regulator or subunit of the mitochondrial KHE, because it is unlikely that a protein with only one transmembrane domain like Mdm38 forms the KHE itself.

Mdm38p is conserved in all eukaryotic organisms. The human homologue, LETM1, has been implicated in the Wolf-Hirschhorn syndrome (6). The yeast *Saccharomyces cerevisiae* encodes a homologue, YPR125w. YPR125w had initially been identified as a multicopy suppressor of mutants lacking the mitochondrial Mg^{2+} transporter MRS2 and was named MRS7 (7). YPR125w/MRS7, also named YLH47 for yeast LETM1 homologue of 47 kDa (6), encodes a protein located in mitochondria (4, 8). Although disruption of MRS7 has a weak phenotype, its overexpression restores growth of *mdm38Δ* strains, showing a functional homology to Mdm38p (4). The human genome also encodes a second member of the Mdm38/LETM1 family, named HCCR-1 or LETMD1, which was found to be overexpressed in various human cancer cells (9).

Here, we characterize the role of four yeast multicopy suppressors of *mdm38Δ* as well as of LETM1 and HCCR-1 with

* This work was supported by the Austrian Science Fund (to R. J. S.) and SYSMO (to R. J. S. and K. N.).

[5] The on-line version of this article (available at <http://www.jbc.org>) contains supplemental Figs. 1–4 and an additional reference.

This paper is dedicated to the memory of Rudolf Schweyen, who tragically passed away during the writing of this manuscript.

[†] Deceased February 15, 2009.

¹ Both authors contributed equally to this work.

² To whom correspondence may be addressed: Dept. of Microbiology, Immunobiology and Genetics, Max F. Perutz Laboratories, Vienna University, Dr. Bohr Gasse 9, A-1030 Wien, Austria. Tel.: 43-1-4277-54619; Fax: 43-1-4277-9546; E-mail: gerhard.sponder@univie.ac.at.

³ To whom correspondence may be addressed: Dept. of Microbiology, Immunobiology and Genetics, Max F. Perutz Laboratories, Vienna University, Dr. Bohr Gasse 9, A-1030 Wien, Austria. Tel.: 43-1-4277-54619; Fax: 43-1-4277-9546; E-mail: karin.nowikovsky@univie.ac.at.

⁴ The abbreviations used are: KHE, K^+/H^+ exchanger; SMP, submitochondrial particle; FM4-64, N-(3-triethylammoniumpropyl)-4-(6-(4-(diethylamino)phenyl)hexatrienyl)pyridinium dibromide; GFP, green fluorescent protein; HA, hemagglutinin; CoIP, coimmunoprecipitation; ORF, open reading frame; Ni-NTA, nickel-nitrilotriacetic acid; GFP, green fluorescent protein; BCECF, 2',7'-bis(carboxyethyl)-5,6-carboxyfluorescein; BN, Blue Native; YFP, yellow fluorescent protein; PBFI, potassium-binding benzofuran isophthalate.

Novel Players in Mitochondrial KHE

respect to their potential to restore K^+/H^+ exchange activity. We find that like Mdm38p, Mrs7p and Ydl183cp are part of a large mitochondrial KHE protein complex. We discuss its putative composition and analyze the additive effects resulting from the triple deletion of *MDM38*, *MRS7*, and *YDL183c*.

EXPERIMENTAL PROCEDURES

Yeast Strains and Growth Media—The *S. cerevisiae* strains W303 (ATCC accession number 2012239) and DBY747 (ATCC accession number 204659) were used as wild type. W303 *mdm38::HIS3* termed *mdm38Δ* was described previously (4). W303 cells were grown in YPD (yeast extract, bacto peptone, 2% dextrose), YPG (2% glycerol) or YPGal (yeast extract, bacto peptone, 2% galactose) media as indicated. YPG plates were supplemented with 2 μ M nigericin when indicated. Synthetic minimal media (S-Gal, synthetic medium containing 2% galactose, or SD, synthetic medium with 2% dextrose, 2% glucose) were supplemented with amino acids and bases when appropriate.

Genomically tagged versions of *MDM38* and *MRS7* were constructed by homologous recombination. The TAP tag and the selection marker *TRP1*-KL were amplified by PCR from the vector pBS1479 (10). The following primers were used to create a C-terminally tagged version of *MDM38* with His₆ and the TAP tag consisting of two immunoglobulin binding domains of protein A and the calmodulin-binding peptide: *MDM38HisTAPfw*, 5'-TACCTCCCATTCCGGCCGATCAAGCTGCGAAGACTTTTGTCA-TTAAGAAAGATCATCACCATCACCATCACTCCATGGA-AAAGAGAAG-3'; *MDM38HisTAPrev*, 5'-CCTGATGTACTCACATTTCCATCTGGTGAGGATGGAGGTGGAGACGTCGTAGACATGGAACCCTGTTTACGACTCACTA-TAGGG-3'. For tagging *MRS7* with His₆ and TAP tag, the following primers were used: *MRS7HisTAPfw*, 5'-AACCGCATGACACCAAGCCTATCGGAGAAGCCGCTGCCATCAAAGAGAAGCATCACCATCACCATCACTCCATGGAAAAGAGAAG-3'; *MRS7HisTAPrev*, 5'-TAGACACTCTATTCTTTGAGTAATTTTGGAGGGAGAGCAGCAATG-ATTAACACTACGACTCACTATAGGG-3'.

To create chromosomal, C-terminally His₆-tagged versions of *MDM38* and *MRS7*, the following forward primers were used: *MDM38Hisfw*, 5'-TTCCGGCCGATCAAGCTGCGAAGACTTTTGTCA-TTAAGAAAGATCATCACCATCACCATCACTGATCCATGGAAAAGAGAAG-3'; *MRS7Hisfw*, 5'-CGCATGACACCAAGCCTATCGGAGAAGCCGCTGCCATCAAAGA-GAAGCATCACCATCACCATCACTAATCCATGGAAAAGAGAAG-3'. *MDM38HisTAPrev* and *MRS7HisTAPrev* served as reverse primers, respectively. To create chromosomal, C-terminally One-StrEP (11)-tagged versions of *MDM38* and *MRS7*, the One-StrEP sequence (based on the plasmid pEXPR-IBA103, IBA BioTAGnology) was synthesized (Eurofins MWG GmbH) and cloned into the BamHI-linearized pBS1479 plasmid. Chromosomal integration was performed using the forward primers: *MDM38OneStrEPfw*, 5'-CATTCCGGCCGATCAAGCTGCGAAGACTTTTGTCA-TTAAGAAAGATGAGAATTTGTATT-TTCAGG-3', and *MRS7OneStrEPfw* 5'-GCATGACACCAA-GCCTATCGGAGAAGCCGCTGCCATCAAAGAGAAGG-

AGAATTTGTATTTTCAGG-3'. *MDM38HisTAPrev* and *MRS7HisTAPrev* served as reverse primers, respectively.

Multicopy Suppressor Screen—The *mdm38Δ* mutant strain was transformed with 1 μ g of genomic library (constructed in YEp181, a 2- μ m plasmid marked with *LEU2*, gift of Juraj Gregan and Kim Nasmith, IMP, Vienna, Austria). Transformants growing on SD-leu plates were replica-plated on YPG plates and incubated at 37 °C. Three hundred ninety six positive putative candidates were selected and classified into strong or weak suppressors. To confirm that the suppression was plasmid-borne, the plasmids were recovered, amplified in *Escherichia coli*, used for retransformation of W303 *mdm38Δ*, and tested for growth on YPG plates at 37 °C. Confirmed plasmids were then analyzed by restriction digestion patterns to eliminate self-complementation, and the inserts of selected plasmids were sequenced by VBC-Biotech Services GmbH. The suppressor plasmids contained multiple ORFs. Individual ORFs were subcloned and tested for their ability to suppress the growth phenotype. The individual plasmids containing *PIC2*, *MRS3*, *MRS7*, or *YDL183c* were used in all experiments if not otherwise indicated.

Gene Deletions—Deletion of the genes was performed according to the one-step replacement protocol (12). The *MRS7* ORF was disrupted from the start to the stop codon by replacement with the *KANMX4* disruption cassette, which was amplified with the primers 5'-TAGGTTTCGAGTAAAGAAA-ATTTTCATAAAGAAATCAACAAGACACACGTACGCTGCAGCTCGAC-3' and 5'-GCGGAGAGTGTATCGTGCGG-TTTAATGGGCCAGGTGAAAACCTGGGATCGATGAATTCGAGCTCG-3'. To delete *YDL183c* in W303, the whole ORF was replaced with a *URA3* disruption cassette flanked by loxP sites, using the primers 5'-CATCGATAGAATCATTATTCACAATACCAAACTT-3' and 5'-CTCAGGAATACCTGTATGTATATTTACATGAGATA-3'. Following verification of the correct gene replacement using analytical PCR (12), the selection marker was removed with the CRE recombinase containing vector pSH63 (13). *YDL183c* deletion in DBY747 was performed by replacement with the *LEU2* disruption cassette, using the primers 5'-TCACAATACCAAACTTTCATCCGGTGTATTTTAGATTAAGCGTACGCTGCAGGTCGAC-3' and 5'-ACCTGTTATGTATATTTACATGAGATAGTGGA-CAATCTACATAGGCCACTAGTGGATCTG-3'. Double and triple deletion strains were obtained in W303 by crossing and sporulation of the diploids or in DBY747 by stepwise disruptions.

Plasmid Constructs—To provide *MRS7*, *MDM38*, and *YDL183c* with a C-terminal GFP tag, the entire respective ORFs were cloned into the centromeric vector pUG35 (14). *MRS7* coding sequence was amplified by PCR from YEp351-*MRS7* plasmid (7) with the 5' primer 5'-ACAAGAATTCATGCTGAAATACAGGTC-3' and the 3' primer 5'-ACATGTCGACCTTCTCTTTGATGGC-3' (EcoRI and SalI sites are underlined) and cloned into the EcoRI/SalI sites of the plasmid pUG35 carrying the methionine promoter. To clone *YDL183c* into the pUG35 plasmid, the entire ORF sequence was amplified by PCR from W303 genomic DNA by use of 5' primer 5'-CGGGATCCATGATACGTTCAATATTTATAACCGC-3' and 3' primer 5'-GCGTCGACAATTTTGTTTTTCTCTT-

GAGATTTTCG-3' introducing the underlined BamHI and Sall restriction sites. The amplified fragment was cloned into the BamHI- and Sall-linearized pUG35 plasmid. A C-terminally GFP-tagged version of the entire ORF *MDM38* was obtained by cloning *MDM38* in pUG35 by use of the forward primer 5'-TAATATGGATCCATGTTGAATTCGCATCAAGAGCG-3' and the reverse primer 5'-AATATCTATCGATCTTAATGACAAAAGTCTTCGC-3' (BamHI and ClaI sites underlined).

To express *YDL183c* from its own promoter and in fusion with the triple HA epitope at the C-terminal end, the entire ORF and its flanking region, including 217 nucleotides upstream of the ATG, were amplified from W303 genomic DNA with the primers 5'-CTTGAGCTCGGATGGATGGACTTGACGGC-3' and 5'-GCGTCGACCAATTTGTTTTTCTCTTGAGATTTCC-3' and inserted in the SacI/Sall sites of the YCp33-HA vector. The vectors YCp33-*MDM38*-HA and Yep351-*MDM38*-HA expressing Mdm38p under the control of its native promoter and pVTU103-LETM1-HA expressing the human LETM1 from the *ADH* promoter were described previously (4). To express HCCR-1 in yeast, the entire ORF was amplified from MGC IRAT human (Invitrogen 6009854) with the forward primer 5'-AACGGGATCCCGGATGGCGCTCTCCAGGGTGTG-3' and the reverse primer 5'-CATGCTCGAGTTCAGTGGTGGTGGTGGTGGTGGCGCCTTGCCCAAGGTAGT-3' digested with BamHI and XhoI and inserted in the pVTU103 vector.

Isolation and Subfractionation of Mitochondria—Yeast mitochondria used for ion-flux measurements were isolated from cells growing overnight to stationary phase. For all other experiments, cells were grown to $A_{600} = 1$. Mitochondrial isolation and mitoplast preparation were done as described previously (15). Protein extraction with sodium carbonate was performed according to Ref. 16 followed by protein precipitation with trichloroacetic acid and Western blotting analysis. Proteinase K protection experiments were performed as described previously (17). Resuspended mitoplasts were incubated in the presence or absence of proteinase K as indicated for 20 min, and the proteinase K reaction was inactivated with 1 μ M phenylmethylsulfonyl fluoride, and the proteins were trichloroacetic acid-precipitated. 50 μ g of protein were loaded in each lane of a 12.5% SDS-PAGE, transferred onto polyvinylidene difluoride membrane, and immunoblotted in Tris-buffered saline/Tween plus 2.5% dry milk with the antibodies against the following: HA (laboratory stock; hexokinase-1 (Biotrend); F₁ β , Tim44, and Yme1 (generous gifts of Gottfried Schatz, Hans van der Spek, and Tom Fox, respectively). The proteins were visualized by use of the SuperSignal™ West Pico system (Pierce).

Blue Native PAGE—Proteins of isolated mitochondria were solubilized as indicated with 1.2% *n*-dodecyl-*D*-maltoside or Triton X-100, and after a clarifying spin, 200 μ g of proteins (25 μ l) per lane were separated by BN-PAGE according to Ref. 18 on 5–18% polyacrylamide gradient gels. Following electrophoresis, wet blotting to polyvinylidene difluoride membrane was performed for 1 h at 100 V. Protein complexes were detected by immune decoration. The calibration standards (Amersham Biosciences) used in the BN-PAGE were bovine thyroglobulin (669 kDa), horse spleen apoferritin (440 kDa), bovine

liver catalase (232 kDa), bovine heart lactate dehydrogenase (140 kDa), and bovine serum albumin monomer (67 kDa).

Affinity Chromatography—180 mg of isolated mitochondria were used for standard protein purification. Isolated mitochondria were adjusted to a concentration of 20 mg/ml. For affinity chromatography using Ni-NTA Superflow resin (Qiagen), mitochondria were solubilized with 1.2% Triton X-100 on ice for 30 min in Hi 50 buffer (10 mM Tris-HCl, pH 7.8, 50 mM NaCl, 20 mM imidazole, protease inhibitor mixture (Complete Mini, Roche Applied Science)). After centrifugation at $43,000 \times g$ for 30 min (4 °C) to remove nonsolubilized mitochondrial debris, the Triton concentration of the supernatant was reduced to 1% by addition of Hi 50 buffer. Ni-NTA Superflow resin (Qiagen) was washed two times with 10 ml of Hi 50 buffer containing 1% Triton X-100. The clarified supernatant was incubated with the resin for 30 min under gentle shaking and loaded on a Poly-Prep chromatography column (Bio-Rad). The column was washed twice with 15 ml of Hi 50 Wash buffer 1 (0.8% Triton X-100, 20 mM imidazole) and twice with 15 ml of Hi 50 Wash buffer 2 (0.6% Triton X-100, 30 mM imidazole). Finally, bound proteins were eluted with Hi 50 Elution buffer (10 mM Tris-HCl, pH 7.8, 50 mM NaCl, 200 mM imidazole, 0.6% Triton X-100 and, unless otherwise stated, complete protease inhibitor mixture).

For streptavidin affinity chromatography using Strep-Tactin Superflow (Qiagen), mitochondria were solubilized with 1.2% Triton X-100 in Strep 50 buffer (100 mM Tris-HCl, pH 7.8, 50 mM NaCl, protease inhibitor mixture). All other steps were performed as described for the Ni-NTA chromatography except that Strep-Tactin Superflow (Qiagen) was used as affinity resin, and bound proteins were eluted with Strep 50 buffer with a final concentration of 2.5 mM *D*-desthiobiotin.

All purification steps were performed at 4 °C. Control experiments were performed for each affinity chromatography with untagged or untransformed DBY747 wild-type or *mdm38* Δ strains. Two-dimensional gel electrophoresis was performed as described previously (19). Anti-His antibody was purchased from Qiagen, and anti-Mdm38 was generously provided by P. Rehling.

Coimmunoprecipitation (CoIP)—UltraLink immobilized protein A, covalently bound to HA antiserum with the cross-linker, was kindly provided by A. Pichler. Isolated mitochondria (2 mg of protein) expressing YEp-*MDM38*-HA (70 kDa) and either pUG-*MDM38*-GFP (92 kDa), *YDL183*-GFP (64 kDa), or *AIF*-GFP (68 kDa) were solubilized for 30 min in RIPA buffer (50 mM Tris, pH 7.4, 150 mM NaCl, 1% Nonidet P-40, 0.5% sodium deoxycholate, 0.1% SDS containing 1.2% *n*-dodecyl-*D*-maltoside (Sigma)) and protease inhibitor mixture (complete Mini, Roche Applied Science) plus 1 mM phenylmethylsulfonyl fluoride and, after a clarifying spin, incubated under rotation for 1 h with 10 μ l of the HA-coupled beads, washed four times in RIPA buffer, and eluted in Laemmli buffer. Proteins were separated on 12.5% SDS-PAGE, transferred, and analyzed by immunoblotting with GFP (Roche Applied Science) and HA (laboratory stock) antibodies.

Measurements of the Mitochondrial Membrane Potential—The membrane potential of isolated mitochondria was recorded in an LS 55 fluorescence spectrometer (PerkinElmer Life Sciences) by monitoring the fluorescence of 5,5',6,6'-tetrachloro-1,1,3,3'-tetraethylbenzimidazolylcarbocyanine iodide

Novel Players in Mitochondrial KHE

(Molecular Probes) according to Ref. 20. Measurements were carried out in breaking buffer (0.6 M sorbitol, 10 mM Tris-HCl, pH 7.4). For calibration, aliquots of the same preparation were hyperpolarized with 1 μ M nigericin (Sigma) and depolarized with 1 μ M carbonyl cyanide *p*-trifluoromethoxyphenylhydrazone (Sigma) in breaking buffer. The reading after addition of nigericin was set as 100% and that after carbonyl cyanide *p*-trifluoromethoxyphenylhydrazone as 0%. The values were linearized, and the relative membrane potential was calculated using $y = kx + d$.

K⁺/H⁺ Exchange Measurements in SMPs—Preparations of SMPs and loading with the K^+ - and H^+ -sensitive fluorescent dyes potassium-binding benzofuran isophthalate (PBFI) and BCECF (both Invitrogen) were made as described previously (2). SMPs were treated with 1 μ M antimycin A and 1 μ M oligomycin prior to measurements. To determine the kinetics of K^+ and H^+ transport across the membrane, 150 mM KCl was added to the SMPs. When indicated, incubation of SMPs with 10 μ M nigericin (Sigma) was done at room temperature for 5 min before the measurements. All measurements were repeated at least three times with different preparations of SMPs.

Confocal Microscopy—The plasmids pHS72 (TOM72-YFP) (21) and pYX232-mtGFP (22) were gifts from H. Sesaki and B. Westermann, respectively, and served to label mitochondria. Alternatively, mitochondria were labeled with Mitotracker Red (100 nM). Vacuoles were stained with FM4-64 in a final concentration of 10 μ M (Molecular Probes). Microscopy settings were used as described previously (5).

Electron Microscopy—Cells were harvested at logarithmic growth phase ($A_{600} = 1$). Cryofixation, freeze substitution, thin sectioning, and image acquisition were performed as described previously (5).

RESULTS

PIC2, MRS3, MRS7, and a Novel Gene YDL183c Act as Multicopy Suppressors of *mdm38* Δ —Absence of Mdm38p in yeast cells (*mdm38* Δ mutants) results in reduced growth on nonfermentable substrate (*pet⁻* phenotype) (4). According to our previous data, the antibiotic nigericin, a KHE ionophore, acts as a multivalent suppressor of the *mdm38* Δ deletion phenotype. It restores cell growth on nonfermentable substrate, KHE activity, and $\Delta\psi$ and reverts matrix swelling and fragmentation of mitochondria (5).

To identify proteins substituting similarly for the function of MDM38, we have screened a yeast genomic library and selected suppressor genes that, being overexpressed, restored growth of *mdm38* Δ on nonfermentable substrate (Fig. 1). Among the suppressors, we found three previously described genes, *PIC2*, *MRS3*, and *MRS7*, encoding mitochondrial proteins. *PIC2* and *MRS3* encode mitochondrial carrier proteins involved in P_i transport and Fe^{2+} accumulation, respectively (23, 24). *MRS7* encodes a functional homologue of Mdm38p, located in the inner membrane of mitochondria, with a weak deletion phenotype depending on the strain (7, 8). Additionally, we found one not yet characterized gene, *YDL183c*.

Up-regulation of *Pic2*, *Mrs3*, *Mrs7*, *Ydl183c*, or Human LETM1 Increases the Mitochondrial Membrane Potential of *mdm38* Δ — $\Delta\psi$ was found to be moderately reduced in *ydl183c* Δ or *mrs7* Δ and substantially impaired in *mdm38* Δ

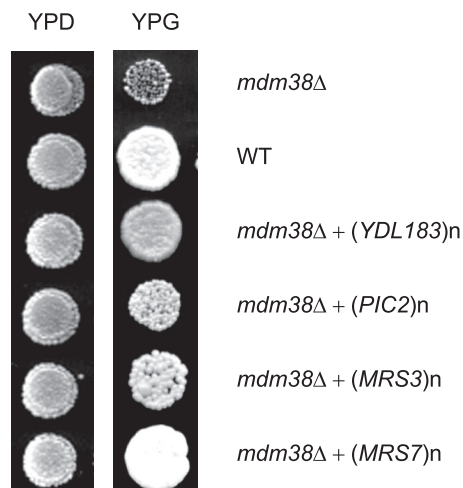


FIGURE 1. Multicopy suppressors and their growth effects on *mdm38* Δ . Effects of *YDL183c*, *PIC2*, *MRS3*, and *MRS7* on the nonfermentative growth of *mdm38* Δ cells are shown. W303 *mdm38* Δ mutant cells containing an empty vector or a vector overexpressing *YDL183c*, *PIC2*, *MRS3*, or *MRS7* and wild-type (WT) cells were spotted onto YPD or YPG plates and grown at 28 °C for 3 or 5 days, respectively.

mitochondria. Having determined that overexpression of *Pic2p*, *Mrs3p*, *Mrs7p*, and *Ydl183cp* rescued the nonfermentative cellular growth of *mdm38* Δ , we asked whether this positive growth effect also correlated with a rise of the mitochondrial $\Delta\psi$ of the *mdm38* Δ mutant. Although $\Delta\psi$ was slightly increased upon overexpression of *Pic2p* and more significantly upon overexpression of *Mrs3p* in *mdm38* Δ , overexpression of *Mrs7p* and *Ydl183cp* in the mutant restored $\Delta\psi$ close to the wild-type levels (Table 1).

Mitochondrial Morphology Is Restored upon Overexpression of the Suppressor Genes in *mdm38* Δ —Next, we investigated whether high copy expression of the suppressor genes reversed the fragmentation of *mdm38* Δ mitochondria. For this purpose, *mdm38* Δ cells expressing a GFP targeted to the mitochondrial matrix and a vector with or without the suppressor genes were observed under the confocal microscope. Mitochondria from *mdm38* Δ cells transformed with the empty vector appeared fragmented into large unconnected spheres (Fig. 2*a*). Compared with wild-type cells, *mdm38* Δ cells displayed wild-type-like elongated tubular mitochondria in only about 3% of the population. Mutant *mdm38* Δ cells overexpressing *PIC2* exhibited a heterogeneous mixture of spherical and tubular mitochondria, indicating a partial reversion of the phenotype (Fig. 2*c*). Overexpression of *MRS3*, *YDL183c*, or *MRS7* resulted in a tubular mitochondrial network (Fig. 2, *d–f*, respectively, and Table 2) similar to that displayed by wild-type cells (Fig. 2*b*). The percentage of elongated tubular mitochondria was shifted to almost 80% upon overexpression of *Pic2* and to about 95% when *Mrs3*, *Mrs7*, or *Ydl183c* was overexpressed (Table 2).

YDL183c Is a Strong Suppressor for Mitochondrial KHE Activity in *mdm38* Δ —Because swelling, depolarization, and fragmentation of *mdm38* Δ mitochondria result from loss of mitochondrial KHE activity and mitochondrial K^+ overload (5), we next asked whether overexpression of the suppressor genes restored the mitochondrial defects by modulating the KHE activity.

TABLE 1

Relative $\Delta\psi$ of *mdm38Δ* (Δ) and *mdm38Δ mrs7Δ ydl183cΔ* ($\Delta\Delta\Delta$) mutants in function of the overexpressed suppressor genes

The relative $\Delta\psi$ of mitochondria are expressed in % relatively to hyperpolarization of the probe with nigericin. ND, no data.

Strains	Vectors						
	Empty	<i>PIC2</i>	<i>MRS3</i>	<i>MRS7</i>	<i>YDL183</i>	<i>MDM38</i>	LETM1
Δ	48	62 ± 3.4	85 ± 2.7	98 ± 3	92 ± 6	95 ± 6	ND
$\Delta\Delta\Delta$	17 ± 2	ND	ND	89 ± 3.3	78.6 ± 3.3	62.3 ± 3.4	82.3 ± 5.2

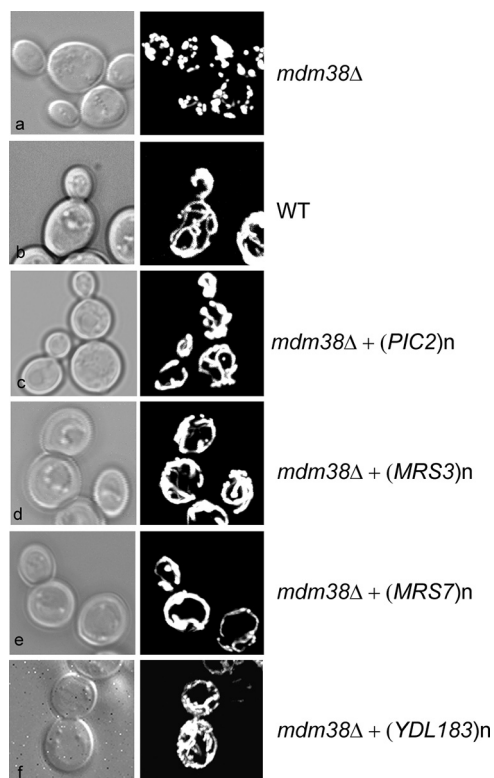


FIGURE 2. Mitochondrial morphology in function of overexpression of the proteins Pic2, Mrs3, Mrs7, or Ydl183c in W303 *mdm38Δ* mutant cells. Mitochondrial morphology of cells cotransformed with a mitochondrial matrix targeted GFP (pYX232-mtGFP) and the vector without (a) or with the following suppressor genes: *PIC2* (c), *MRS3* (d), *YDL183c* (f), and *MRS7* (e) were compared with wild-type (WT) cells (b). Cells were grown in galactose-containing medium and analyzed by differential interference contrast (Nomarski) and confocal fluorescence microscopy.

TABLE 2

Mitochondrial morphology of W303 *mdm38Δ* cells in function of the overexpressed suppressor gene

Strains were grown overnight, and mitochondrial morphology was visualized by detection of the expression of the mitochondrial targeted matrix GFP under fluorescence microscopy. Cells were counted with hidden identity.

Strain	Total cells	% cells with fragmented mitochondria
Wild type	602	2.6 ± 1.6
<i>mdm38Δ</i>	680	89.0 ± 5.8
<i>mdm38Δ</i> + (<i>MRS7</i>) <i>n</i>	1660	7.3 ± 2.6
<i>mdm38Δ</i> + (<i>PIC2</i>) <i>n</i>	870	20.3 ± 4
<i>mdm38Δ</i> + (<i>MRS3</i>) <i>n</i>	1126	10.6 ± 6.3
<i>mdm38Δ</i> + (<i>YDL183c</i>) <i>n</i>	1040	7.7 ± 3.8

We have developed a method to measure the KHE activity across the mitochondrial inner membrane using SMPs with entrapped K^+ - and H^+ -sensitive fluorescent dyes PBFI and BCECF (2). This approach allows controlling internal and external ion milieu at will and recording of both proton and potassium fluxes. As shown previously and here in Fig. 3,

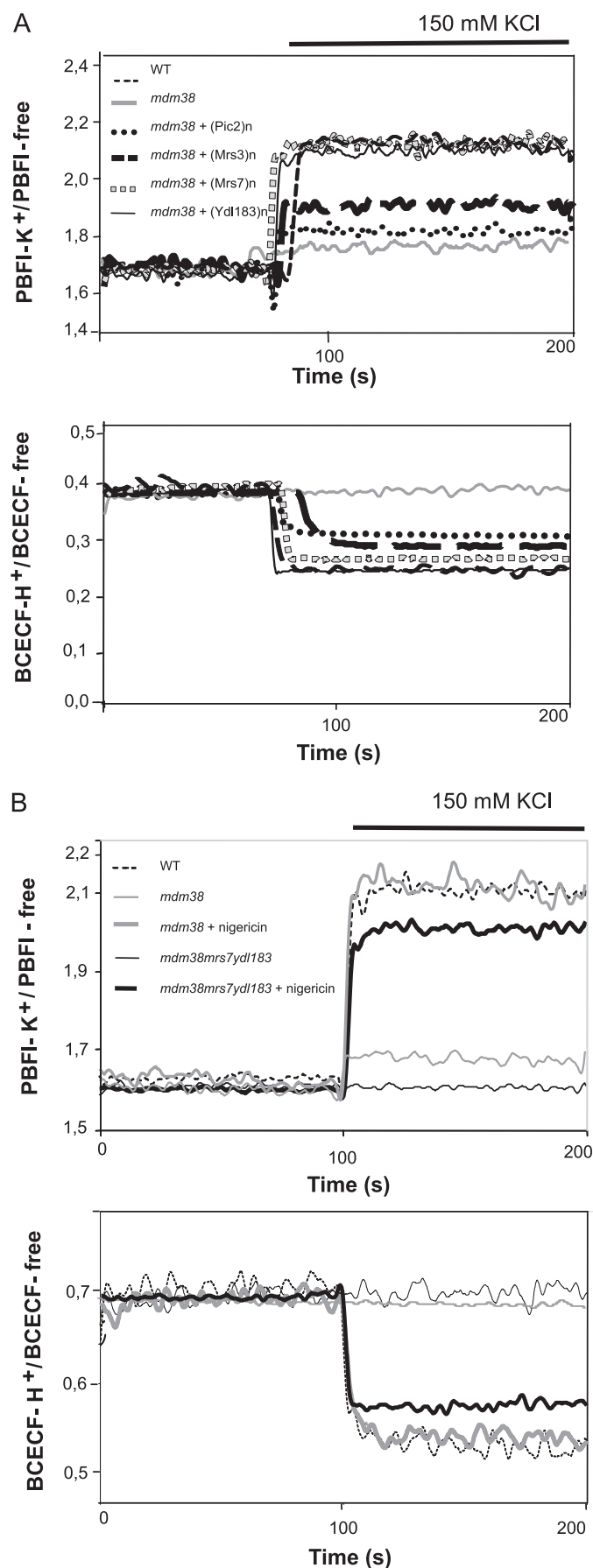
SMPs prepared from wild-type mitochondria exhibited rapid, reciprocal translocation of K^+ and H^+ driven by concentration gradients of either. In contrast, SMPs from *mdm38Δ* failed to exhibit changes in $[H^+]$, and those in $[K^+]$ were drastically reduced. Nigericin restored K^+ and H^+ translocation in mutant SMPs to the wild-type level (Fig. 3B) (3).

SMPs were then prepared from *mdm38Δ* mitochondria overexpressing the respective suppressors (Fig. 3A). Overexpression of the phosphate carrier Pic2p showed a mild increase in K^+ fluxes and a stronger increase in H^+ fluxes (Fig. 3A, round dotted line). Interestingly, when K_2HPO_4 was used as K^+ salt instead of KCl, K^+ fluxes were not significantly re-established, whereas H^+ fluxes reached wild-type levels (data not shown), which are consistent with the role of Pic2 as PO_4^-/H^+ transporter (23). Overexpression of Mrs3p poorly restored the K^+ and H^+ fluxes (Fig. 3A, black broken line). However, overexpression of Ydl183cp restored the K^+ and H^+ exchange activity to a wild-type level, as did overexpression of Mrs7p, the yeast Mdm38p homologue (Fig. 3A, black solid line and gray square dotted line, respectively) or addition of nigericin. These results confirmed that, in contrast to Pic2p or Mrs3p, Ydl183cp, like Mrs7p, can fully substitute for Mdm38p in providing mitochondria with KHE activity.

Ydl183cp Is an Integral Mitochondrial Protein—*YDL183c* encodes a protein of 320 amino acids with a molecular mass of about 37 kDa. The computer programs DAS and TMPRED (available on line) predict one transmembrane domain (196–212 amino acids) and a potential N-terminal mitochondrial targeting sequence. Homologues are found in fungi and in some green plants like *Arabidopsis thaliana* (At1g53760 accession number Q6NQN0). These proteins share one conserved putative transmembrane domain rich in proline residues (Fig. 4A). Except for the presence of a proline-rich putative transmembrane domain, there was no obvious sequence similarity between Ydl183cp and proteins of the Mdm38p/LETM1 family.

To determine the cellular localization of Ydl183c, cells expressing the fusion protein Ydl183c-GFP from the *MET* promoter encoded on the centromeric plasmid pUG35 were stained with Mito Tracker Red. Fluorescence confocal microscopy revealed the colocalization of GFP and red fluorescence, indicating the mitochondrial localization of Ydl183-GFP (Fig. 4B). To confirm these data, biochemical studies were performed with cells expressing the low copy vector encoding Ydl183cp from its own promoter and C-terminally tagged with the triple hemagglutinin (HA) epitope. Cell fractionation and immunoblotting showed Ydl183c-HA protein to cofractionate with a mitochondrial protein (Porin1, Por1p), whereas the cytosolic protein hexokinase 1 (Hxk1p) was detected in the post-mitochondrial fraction, excluding the possibility of cross-

Novel Players in Mitochondrial KHE



contamination of cytoplasmic and mitochondrial fractions (Fig. 4C, panel a). Fractionation of mitochondria into pellet and supernatant upon alkaline sodium carbonate treatment released the membrane-associated β subunit of the F1-ATPase (F1 β) almost entirely into the supernatant, whereas the membrane protein Por1p was retained in the pellet fraction containing integral proteins. Ydl183c-HA was found in the membrane pellet (Fig. 4C, panel b, lane P). However, in contrast to Por1p, Ydl183c-HA was also partially found in the soluble fraction (Fig. 4C, panel b, lane SN). These results indicated that Ydl183cp is inserted into one of the mitochondrial membranes where it can be partly released by alkaline treatment.

For further determination of the topology of Ydl183cp, intact mitochondria were first treated with or without proteinase K. Ydl183cp was not degraded upon addition of proteinase K (data not shown). Mitoplasts were prepared by osmotic swelling and rupture of the mitochondria. Mitoplasts containing the inner membrane were treated with proteinase K (Fig. 4C, panel c). To control the intactness of mitoplasts, the topology of known proteins was also tested. Tim44p, a matrix-sided protein of the inner membrane, remained protected from proteinase K, indicating that the mitoplasts were intact. In contrast, Yme1p, an inner mitochondrial membrane protein partially exposed to the outside of mitoplasts, was accessible to proteinase K indicating that the outer membrane was disrupted. The C-terminally tagged Ydl183cp was resistant to 40 μ g/ml proteinase K, whereas it became accessible to higher proteinase K concentrations. Proteinase K at 120 μ g/ml degraded most of Ydl183-HA without generating proteolytic C-terminal fragments. When mitoplast were lysed with Triton X-100 and then treated with proteinase K, the protein was entirely degraded. Altogether, although alkaline extraction released some of the protein, these results qualify Ydl183p as an integral protein of the inner mitochondrial membrane, with a C_{out} (facing the intermembrane space) topology. Degradation of Ydl183c-HA occurred only in presence of high concentrations of proteinase K as compared with Yme1, either because it is shielded by other proteins or Ydl183cp is intrinsically more resistant to proteinase K.

Synthetic Growth Effect of Triple Disruptions of MDM38, MRS7, and YDL183c—The W303 and DBY *ydl183c* Δ disruptant strain showed reduced growth on nonfermentable carbon sources (YPG) at high temperature (37 °C) (data not shown). Reduced growth on nonfermentable substrate was also reported by Volckaert *et al.* (25) for a FY *ydl183c* Δ mutant at 30 °C and 37 °C. The double disruptants *ydl183c* Δ *mrs7* Δ exhibited a mild growth reduction on nonfermentable sub-

FIGURE 3. KHE activity of *mdm38* Δ SMPs in the function of the suppressors *Pic2*, *Mrs3*, *Mrs7*, and *Ydl183c*. Submitochondrial inner membrane particles were prepared from wild-type and *mdm38* Δ mutant cells with entrapped K^+ -sensitive PBFI or H^+ -sensitive BCECF. Ratios of K^+ -bound or H^+ -bound to -unbound dyes were recorded at 25 °C at resting conditions and upon the addition of 150 mM KCl. **A**, shown are the effects on K^+ and H^+ fluxes in SMPs upon overexpression of the suppressor genes in W303 *mdm38* Δ . SMPs were prepared from mitochondria of wild type (WT) (black thin dashed line) or mutant *mdm38* Δ cells carrying the empty plasmid (gray solid) or the suppressor plasmid containing the genes *PIC2* (black dotted line), *MRS3* (black bold dashed line), *MRS7* (gray square dotted line), or *YDL183c* (black solid line). **B**, increase of $[K^+]$ and $[H^+]$, observed in SMPs from DBY wild-type (black dashed line), single mutant *mdm38* (gray dashed line), or triple mutant *mdm38* *mrs7* *ydl183c* Δ (black thin solid line) in the absence of nigericin or *mdm38* (gray bold solid line) and *mdm38* *mrs7* *ydl183c* Δ (black bold solid line) in the presence of nigericin.

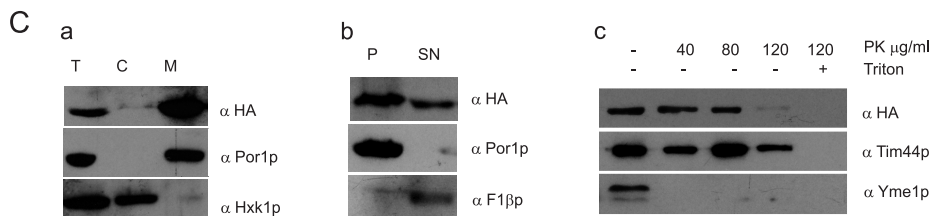
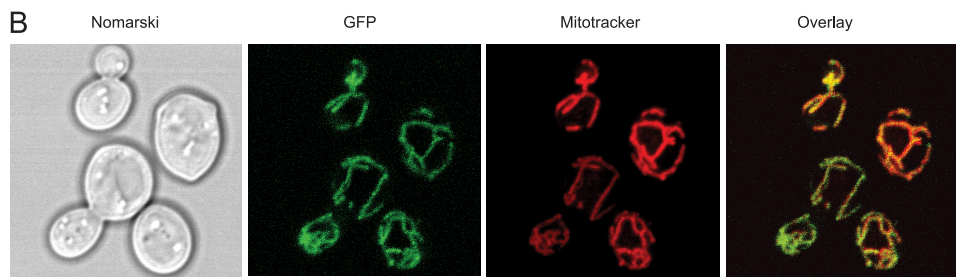
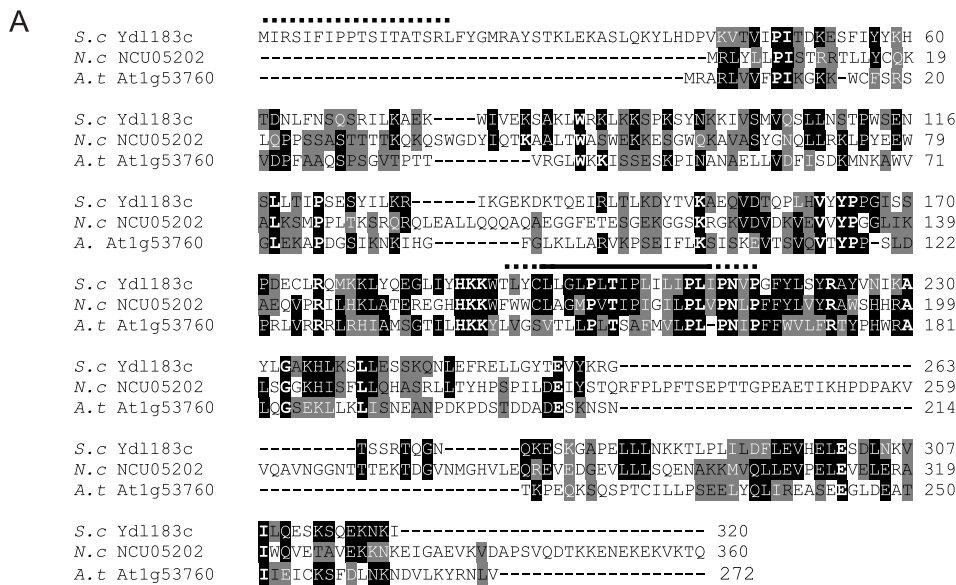


FIGURE 4. Ydl183cp is a component of the mitochondrial inner membrane. *A*, Ydl183cp is a member of a novel protein family. Homologous proteins were identified by a BLAST search. A sequence alignment (ClustalW) of Ydl183cp and its homologues in *A. thaliana* (*A.t.*) and *Neurospora crassa* (*N.c.*) is shown here. Identical amino acids are highlighted in *black* and similar amino acids in *gray*. The putative potential N-terminal mitochondrial targeting sequence is marked with a *dotted bar* and the putative transmembrane domain with a *solid bar*. *B*, localization of the Ydl183c-GFP fusion protein analyzed under confocal microscopy. W303 cells expressing C-terminally GFP-tagged *YDL183c* gene were grown to log phase in galactose containing medium at 28 °C. Mitochondria are labeled with MitoTracker red chloromethyl-X-rosamine. *C*, subcellular and submitochondrial localization of Ydl183cp. *Panel a*, W303 cells expressing the Ydl183c-HA fusion protein (YcP-*YDL183c*-HA, 42 kDa) were grown to log phase in galactose-containing medium. Protoplasts were homogenized and separated into total cell (T), mitochondrial (M), and post-mitochondrial (C) fractions. Equal amounts of protein of subcellular fractions were subjected to SDS-PAGE, and immunodetection with antisera against the HA tag, Hxk1p and Por1p, was performed. *Panel b*, crude mitochondria (2 mg of protein) were treated with 0.1 M Na₂CO₃ and fractionated by centrifugation at 100,000 × *g* into pellet (P) and supernatant (SN). Both fractions (100 μg of protein/lane) were subjected to SDS-PAGE and immunoblotted with antisera against HA, Por1p, and F₁β. *Panel c*, mitoplasts prepared by osmotic shock were separated into supernatant containing the inter-membrane space and pellet. Mitoplasts were aliquoted in equal amounts and incubated with or without proteinase K as indicated. Samples were analyzed by SDS-PAGE and immunoblotted with antisera against the HA tag and against mitochondrial proteins of the inner membrane Tim44p and Yme1p.

strate at 16 and 28 °C (data not shown). Double disruptants *mdm38Δ mrs7Δ* in W303 or DBY747 essentially showed the same phenotype as the single mutant *mdm38Δ* at 28 or 35.5 °C, whereas a slight growth improvement was detected on YPG at 16 °C (Fig. 5A). Growth of *mdm38Δ ydl183cΔ* double mutants was reduced on YPG at 16 °C (Fig. 5A). Importantly, the triple deletion mutant *mdm38Δ mrs7Δ ydl183cΔ* resulted in syn-

thetic phenotypes. Growth on non-fermentable substrates was virtually absent, and the DBY747 triple mutant strain also displayed a significant growth reduction on YPD plates at 28 and 35.5 °C (Fig. 5, A and B), consistent with a serious disturbance in mitochondrial function(s) essential for cell viability.

Growth of the triple mutant on YPD and YPG was largely restored upon expression of *MDM38* or overexpression of either *MRS7*, *YDL183c*, or human LETM1 (Fig. 5B). In comparison, overexpression of *PIC2* in the triple mutant resulted in no growth improvement, and overexpression of *MRS3* rescued the nonfermentable growth of the triple mutant only at 37 °C but not at 16 °C (data not shown).

Addition of nigericin, an electro-neutral KHE ionophore, efficiently restored growth of the triple mutant *mdm38Δ mrs7Δ ydl183cΔ* on glycerol at 16 and 28 °C (Fig. 5C). This finding is important because it suggests that the growth defects on fermentable and nonfermentable substrates were essentially due to a lack of KHE activity.

Given the strong homology of the yeast proteins Mrs7 and Mdm38, we searched for human homologous proteins of LETM1. A BLAST search of the human protein data base revealed a protein containing a LETM1 domain and named LETMD1 or HCCR-1. The sequence alignment of Mrs7, Mdm38, LETM1, and HCCR-1 shows the conserved domains as highlighted (Fig. 6A). The recent work of Kim and co-workers (9, 26) showed that HCCR-1 was overexpressed in various human cancers and might function as a negative regulator of the p53 tumor suppressor. Having shown that overexpression of LETM1 from the *ADH* promoter restored growth of the triple mutant, we tested the suppression capacity of HCCR-1 expressed under the same promoter. Overexpression of HCCR-1 restored fermentative growth of the triple mutant to wild-type levels at 28 and 37 °C and nonfermentative growth on YPG at 28 °C (Fig. 6B). However, growth was only poorly increased on YPG at 16 °C and not at all at 37 °C (data not shown). As described previously, HCCR-1 was charac-

Novel Players in Mitochondrial KHE

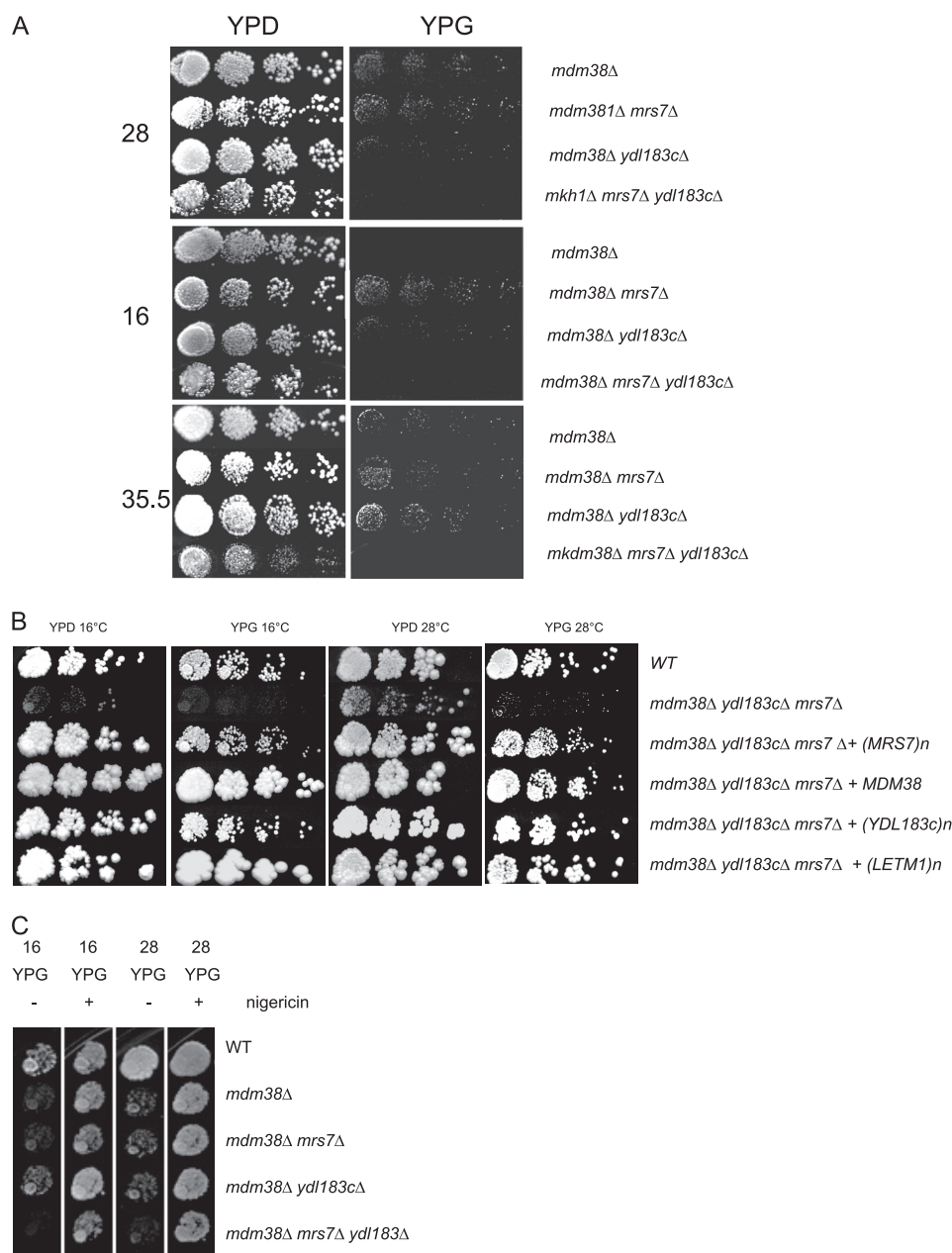


FIGURE 5. Deletion growth phenotypes. *A*, serial dilutions of DBY. *mdm38Δ*, *mdm38Δ mrs7Δ*, *mdm38Δ ydl183cΔ*, and *mdm38Δ mrs7Δ ydl183cΔ* mutants were spotted onto YDP and YPG and incubated at the indicated temperatures. Growth on 28, 35.5, and 16 °C was observed after 3, 5, and 8 days, respectively. *B*, DBY wild-type (WT) and *mdm38Δ mrs7Δ ydl183cΔ* triple mutant cells expressing an empty control vector (pUG35) or YCp33-*MDM38*-HA, pUG35-*MRS7*-GFP, pUG35-*YDL183c*-GFP, or pVT-U-*LETM1*-HA. Serial dilutions were spotted onto YPD and YPG plates and incubated for 10 days at 16 °C or 3 or 5 days at 28 and 37 °C on YDP or YPG, respectively. *C*, effect of nigericin on the nonfermentative growth of DBY747 *mdm38Δ* single, *mdm38Δ mrs7Δ*, *mdm38Δ ydl183cΔ* double, and *mdm38Δ mrs7Δ ydl183cΔ* triple mutant cells. Serial dilutions of the wild-type and mutant cells were spotted onto YPD and YPG plates containing (+) or not (–) 2 μM nigericin and incubated 10 days at 16 °C and 5 days at 28 °C.

terized as a mitochondrial protein (26). We verified its subcellular localization when heterologously expressed in yeast. Cell fractionation of wild-type (data not shown) and *mdm38Δ mrs7Δ ydl183cΔ* triple mutant cells expressing HCCR-1-His and Western blotting analysis revealed that HCCR-1 was detected as a protein of 35 kDa in the total and mitochondrial fractions (Fig. 6C). Por1p was also recovered in total and mitochondrial fractions and Hxk1p in total and cytoplasmic fractions. Accordingly, in yeast HCCR-1-His

was exclusively found in mitochondria, although in significantly less abundant amounts than Por1p (Fig. 6C).

Severe Loss of the Mitochondrial Membrane Potential in the Absence of *Mrs7p*, *Ydl183cp*, and *Mdm38p*—Most importantly, the mitochondrial $\Delta\psi$ was dramatically reduced in the triple mutant *mdm38Δ mrs7Δ ydl183cΔ* (Table 1). We tested if overexpression of the individual suppressors also restored the mitochondrial $\Delta\psi$ in the triple mutant *mdm38Δ mrs7Δ ydl183cΔ*. We found that expression of *Mdm38p* and overexpression of *Mrs7p* or *Ydl183cp* restored the reduced $\Delta\psi$ of the triple mutant to a reasonable level (Table 1), a result comparable with that observed after overexpression of human LETM1. These findings suggest that cellular growth and increase of mitochondrial $\Delta\psi$ are mechanistically linked.

Dramatic Changes of Organelle Morphology in *mdm38Δ mrs7Δ ydl183cΔ* Cells—In addition to growth impairment and profound depolarization, the triple deletion mutant *mdm38Δ mrs7Δ ydl183cΔ* differed most strikingly from the *mdm38Δ* single deletion mutant in its organellar morphology. Confocal microscopic analysis of triple mutant cells expressing the mitochondrial matrix-targeted GFP showed that mitochondria appeared fragmented in spherical units, were less numerous than in the single *mdm38Δ* mutant, and were somewhat clumped together. Furthermore, costaining of cells with the specific vacuole dye FM4-64 consistently showed a multiple lobed morphology of the vacuoles (Fig. 7A). To look into the structure of the organelles at higher resolution, electron microscopy was performed. Remarkably, numerous

vesicles were visible in each section, all looking almost alike in size and electron density. The recognition of single or double vesicle-surrounding membranes was the only morphological criterion to discriminate between mitochondrial and vacuolar vesicles. Yet a distinction of the organelles was not always possible (Fig. 7B, panels *a* and *b*, right panels). Surprisingly, a large number of cells showed vesicular mitochondria containing undefined material suggesting either internalized membranes or paracrystalline structures (Fig. 7B, panel *b*, right panel). Most

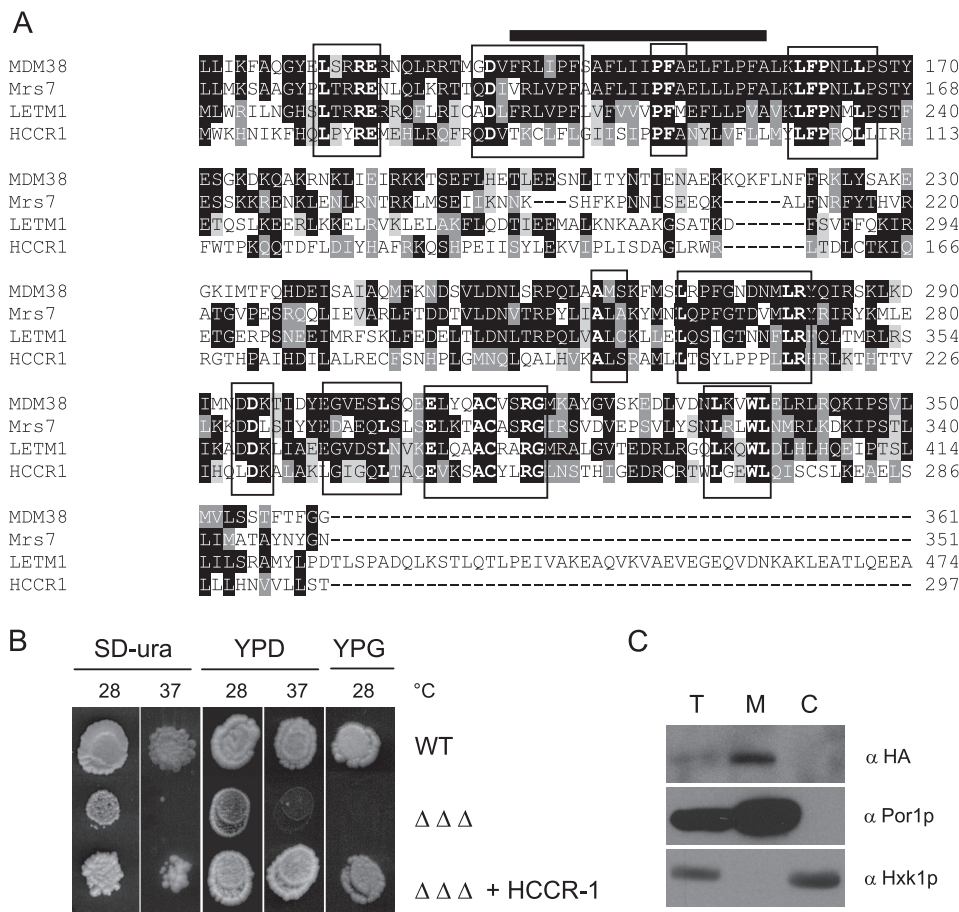


FIGURE 6. Suppression effect of human HCCR-1. *A*, sequence alignments of Mdm38, Mrs7, Letm1, and HCCR-1. ClustalW alignments of the amino acid sequences over the homologous regions are shown. Identities are highlighted in black and similarities in gray. Amino acid residues identical over all four sequences are in boldface and boxed. Bar is over the transmembrane domain. *B*, growth effect of HCCR-1 expression in yeast triple *mdm38* Δ *mrs7* Δ *ydl183c* Δ mutants ($\Delta\Delta\Delta$). Wild-type (WT) and triple mutant cells expressing pVTU103 with or without HCCR-1 were spotted onto SD-ura, YPD, and YPG plates and grown at the indicated temperatures for 6, 3, and 6 days, respectively. *C*, subcellular localization of HCCR-1 in yeast. Yeast triple *mdm38* Δ *mrs7* Δ *ydl183c* Δ mutants ($\Delta\Delta\Delta$) expressing HCCR-1 were fractionated into total (T), mitochondrial (M), and post-mitochondrial (C) fractions, and Western blotting was performed.

importantly, wild-type-like morphology of the cells was restored upon addition of nigericin (Fig. 7B, panel c) with reversion of mitochondria from swollen, fragmented, and electron-transparent to condensed, elongated, and electron-dense organelles. This key finding links the morphological phenotype of the triple mutant to a defect of K⁺ homeostasis, which can be compensated by nigericin.

For better discrimination of the origin of the visualized organelles, we used a mitochondrial YFP targeted to the outer membrane (pHS72) and the vacuolar stain FM4-64. Confocal microscopy showed stained wild-type mitochondria and vacuoles as clearly distinct organelles (Fig. 7C, panels a–d). In contrast, triple mutant cells exhibited widely overlapping fluorescence of FM4-64 (vacuoles) and YFP directed to the outer mitochondrial membrane (Fig. 7C, panels e–h), indicative of the colocalization of both organelle markers that occurs in mitophagy (27).

Mitochondrial KHE Is Totally Absent in the Triple Deletion Strain *mdm38* Δ *mrs7* Δ *ydl183c* Δ —Remarkably, SMPs from the triple mutant *mdm38* Δ *mrs7* Δ *ydl183c* Δ failed to exhibit H⁺ fluxes, and most importantly, residual K⁺ fluxes observed

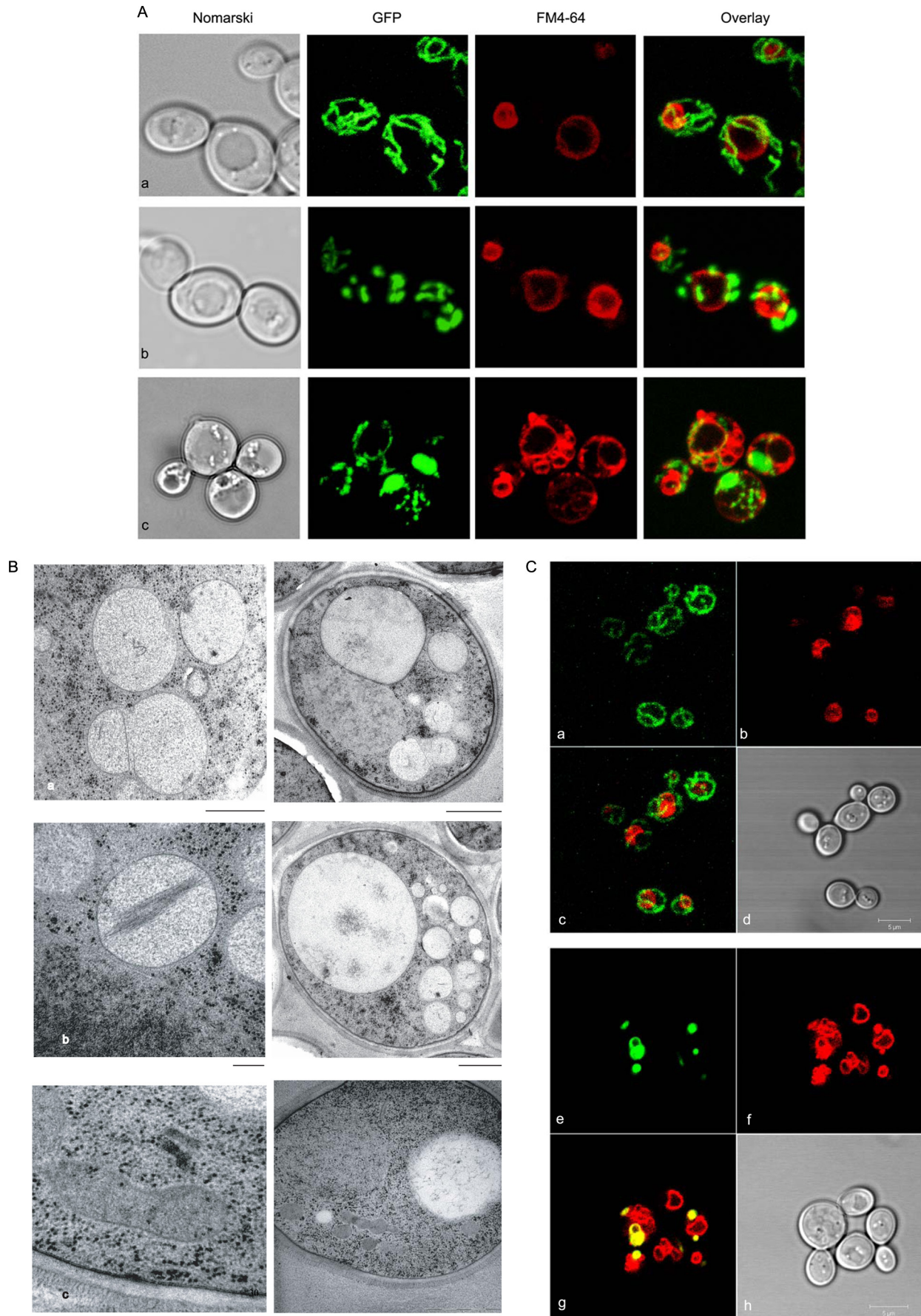
in the *mdm38* Δ single mutant SMPs were fully eliminated in the triple mutant (Fig. 3B). However, KHE was fully active in *ydl183c* Δ and moderately reduced in *mrs7* Δ (data not shown). Consistent with data reported above on cell growth and $\Delta\psi$, disruption of all three genes had additive effects on the KHE activity. However, preincubation of the *mdm38* Δ *mrs7* Δ *ydl183c* Δ SMPs with nigericin led to the activation of the K⁺ and H⁺ transport across the SMPs membrane, although not to full wild-type levels (Fig. 3B).

K⁺ and H⁺ flux measurements carried out in triple mutant SMPs revealed efficient restoration of activities by Mdm38p expressed from a single copy vector, whereas its homologue Mrs7p required expression from a multicopy vector (Fig. 8, B, black solid line, and A, black square dotted line, respectively). Overexpression of Ydl183cp also restored some of the K⁺/H⁺ fluxes in the triple mutant but not fully (Fig. 8A, black broken line). Finally, overexpression of the human homologue of Mdm38p, LETM1 in the triple mutant strains, restored most of the KHE activity (Fig. 8B, gray solid line).

Ydl183cp, Mrs7p, and Mdm38p Form High Molecular Weight Complexes—The genetic data presented here support the notion that

Mdm38, Mrs7, and Ydl183c proteins are functionally equivalent in contributing to the formation of an active KHE. All three proteins are single-pass transmembrane proteins and thus are unlikely to form an exchanger without self-association or without association with other yet unidentified proteins (homo- or hetero-oligomerization, respectively). To address the question of whether the proteins were part of high molecular weight complexes, we first performed chemical cross-linking. We used crude mitochondria expressing Mdm38p or Ydl183cp in cross-linking experiments using disuccinimidyl suberate at increasing concentrations. Based on the electrophoretic mobility of the cross-linked products, our data confirmed that Mdm38p and Ydl183cp were part of large protein complexes (supplemental material). To improve the molecular weight size resolution of the complexes, we performed BN-gel electrophoresis followed by immunodetection. Mitochondria were isolated from DBY wild-type strains expressing chromosomally tagged Mdm38-His or Mrs7-His or extra-chromosomal Ydl183-GFP from the pUG vector. Isolated mitochondria were solubilized with mild detergents and separated on nondenaturing gels prior to Western blotting and immunodetection. Probing with

Novel Players in Mitochondrial KHE



the anti-His antibody revealed that Mdm38-His (~67 kDa) migrated at ~500, <232, and <140 kDa (Fig. 9A, left panel). Of note, Mdm38-His was detected in protein complexes of the same molecular weights irrespective of the presence of Mrs7p or Ydl183cp (data not shown). Furthermore, Mrs7-His (53 kDa) appeared in three bands around ~500 kDa and an additional band of >232 kDa (Fig. 9B, lane 1). BN-PAGE analysis of solubilized mitochondria expressing Ydl183-GFP yielded a product of an apparent molecular mass of about 67 kDa, which corresponds to its molecular weight as GFP-tagged monomer and to additional bands of <232 kDa, representing YDL183GFP-containing complexes. However, in the background of a mutant *mdm38Δ* strain, Ydl183-GFP partly shifted to a major band of ~500 kDa (Fig. 9C).

Next, we affinity-purified the chromosomally His-tagged Mdm38p and Mrs7p. The proteins were bound to the resin and eluted from the column prior to analysis on BN-PAGE. Surprisingly, despite changing the experimental conditions such as the incubation times with the Ni-NTA beads or using different detergents or NaCl concentrations, the eluted Mdm38-His exclusively appeared as a single band of a molecular mass slightly smaller than 232 kDa (Fig. 9A, middle panel). This was an unexpected result. To find out if the protein complex of ~500 kDa containing the His-tagged Mdm38p as detected on BN prior affinity purification had become inaccessible to the column possibly because it was hidden by additional proteins of the larger complex, we decided to affinity-purify Mdm38 fused to the One-STrEP tag. This tag containing a linker region makes the tagged component of a protein complex more accessible to the column. In fact, using the chromosomal One-STrEP-tagged version of *MDM38*, the purified Mdm38p was recovered within high molecular complexes ranging between ~500 and < 600 kDa in addition to the complex of <232 kDa (Fig. 9A, right panel).

Affinity chromatography of solubilized mitochondria chromosomally expressing Mrs7-His followed by BN-PAGE recovered Mrs7-His within three complexes of <140, >232, and between 440 and 669 kDa as seen in Fig. 9B, left panel, lane 2. Similar results were obtained using Mrs7OneStrep instead of Mrs7His (Fig. 9, right panel). In the next step, we solubilized mitochondria from chromosomally Mrs7-His-tagged cells coexpressing either YCp-Mdm38-HA or YCp-Ydl183-HA. Mitochondrial expression of Mdm38-HA and Ydl183c-HA was confirmed by Western blotting (data not shown). Affinity purification followed by BN-PAGE and Western blotting analyses, including immunodetection with anti-His and HA antibodies, was performed. Although the anti-His antibody recognized Mrs7-His, neither Mdm38-HA nor Ydl183-HA was detectable when the eluted fractions were probed with the anti-HA anti-

body, excluding a direct interaction of Mrs7-His and Mdm38-HA or Mrs7-His and Ydl183-HA (Fig. 10, A and C, respectively). Second dimension SDS-PAGE confirmed that Mdm38-HA was not part of the Mrs7-His complex (Fig. 10B, right panel). Taken together, our experiments did not suggest any direct interaction between Mdm38-HA and Mrs7-His.

These results are in contrast to data reported previously by Frazier *et al.* (8), indicating a direct interaction of a protein A-tagged Mdm38 with numerous other mitochondrial proteins, including Mrs7p. In fact, when we used a strain expressing the Mrs7 protein C-terminally tagged with a His fused to protein A (Mrs7-His-TAP), we found that Mdm38 coeluted with Mrs7-His-TAP in the ~232-kDa complex (Fig. 11, B and C). However, a direct interaction between Mrs7-His-TAP and Ydl183c was not detectable (Fig. 10C). We asked whether the tags affected the suppression of the mutant phenotype. Mrs7-His or Mrs7-His-TAP was introduced into the *mdm38Δ* mutant, and nonfermentative growth was tested. We found that *mdm38Δ* cells expressing Mrs7-His-TAP did not grow as well as Mrs7-His or wild-type cells (Fig. 11D). Thus, these data altogether suggest that Mrs7p and Mdm38p are not interacting directly.

We used CoIP to ask whether Mdm38 homo- or hetero-oligomerizes with Ydl183cp. Mdm38 self-oligomerization was confirmed by CoIP experiments performed on *mdm38Δ* cells coexpressing Mdm38-HA (72 kDa) and Mdm38-GFP (92 kDa). Although Mdm38-HA was successfully bound to HA-coated protein A beads, only Mdm38-GFP was pulled down, and Ydl183c-GFP did not copurify in the protein A-bound fractions like Aif-GFP serving as negative control (Fig. 12).

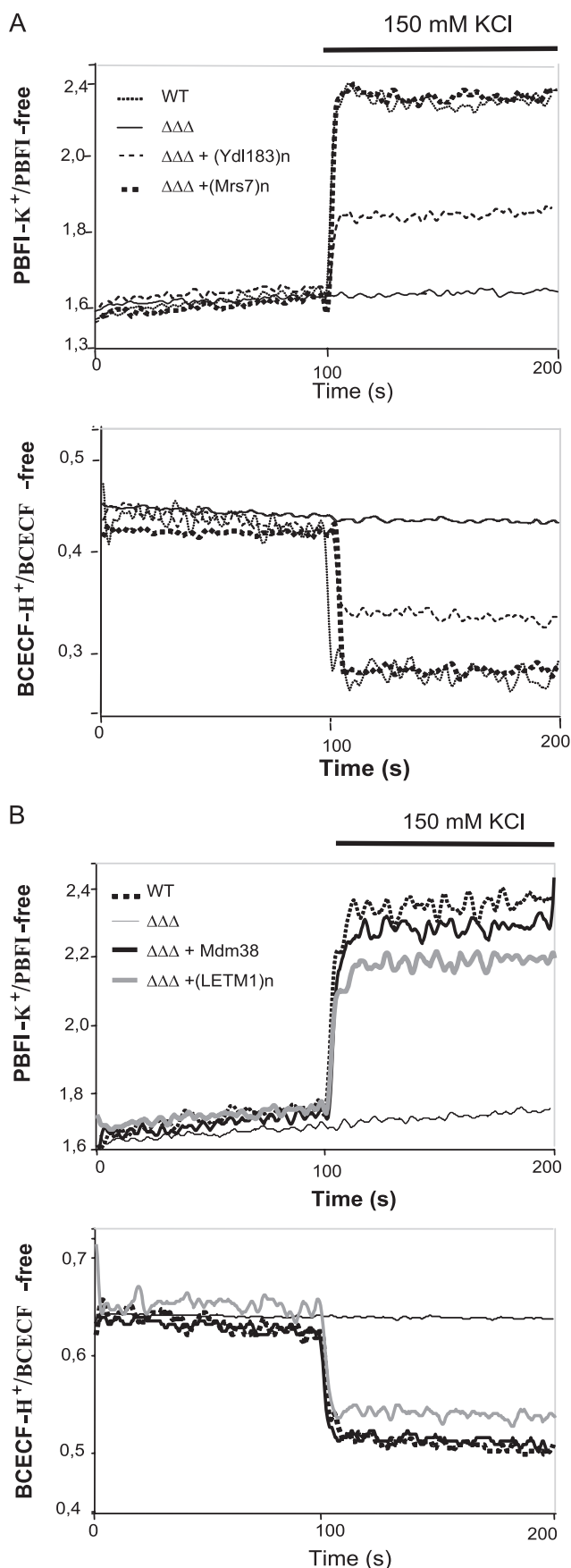
DISCUSSION

We previously characterized Mdm38p as a mitochondrial protein essential for KHE activity (2, 4). Because this protein has only one transmembrane domain, it appears unlikely to be solely responsible for the KHE process. To explore the possible existence of additional proteins involved in KHE, we carried out a genome-wide suppressor screen.

We identified the mitochondrial carriers Pic2p and Mrs3p as weak suppressors. Their overexpression rescued the growth defect of *mdm38Δ*. We showed that mitochondrial morphology of *mdm38Δ* was restored to wild-type upon overexpression of *PIC2* and *MRS3*. However, in *mdm38Δ* SMPs, KHE was not seen after overexpression of Pic2p and was only marginally restored by Mrs3p. Because overexpression of Pic2p, a P_i carrier, had no effect on mitochondrial K⁺ fluxes in *mdm38Δ* mitochondria and resulted in a marginal increase of the mitochondrial Δψ, we hypothesize that a contribution to Δψ above a threshold is sufficient to heal the growth and morphology phe-

FIGURE 7. Mitochondrial and vacuolar morphology in absence of Mdm38p, Mrs7p, and Ydl183cp. Cells were grown to logarithmic phase in galactose (A and B)- or galactose- and raffinose (C)-containing medium. Shown are representative fluorescent and electron microscopy images. A, confocal microscopy analysis of W303 wild-type cells (a), isogenic *mdm38Δ* (b) and isogenic *mdm38Δ mrs7Δ ydl183cΔ* triple mutant cells (c) expressing the mitochondrial matrix targeted GFP. Vacuoles were stained with FM4-64. B, electron micrographs of *mdm38Δ mrs7Δ ydl183cΔ* cells. Panels a and b show the organellar ultrastructure of the triple mutant grown as described above. Whole cells are shown in right panels. The cells display mitochondria with aberrant morphologies (details showing mitochondria are in the left panels). Panel c shows the organellar ultrastructure of cells from the same culture to which nigericin (2 nM) has been added for the last growth generation. Right panel, whole cells; left panel, mitochondrion after nigericin treatment. Bar, 200 nm (left panels) and 1 μm (right panels). C, confocal microscopy analysis of wild-type cells (panels a–d) and *mdm38Δ mrs7Δ ydl183cΔ* cells (panels e–h) expressing the mitochondrial targeted YFP (panels a and e) to the outer membrane (pH572). Vacuoles are indicated by FM4-64 (panels b and f). Merged fluorescence is shown in panels c and g. The yellow fluorescence detected indicates the colocalization of mitochondria and vacuoles. Differential interference contrast microscopy of wild-type (panel d) and *mdm38Δ mrs7Δ ydl183cΔ* (panel h) cells is shown.

Novel Players in Mitochondrial KHE



notype. Alternatively, Pic2p might act indirectly by modulating proton fluxes or mitochondrial pH. Overexpression of Mrs3p, a Fe²⁺ carrier, increased the mitochondrial $\Delta\psi$ and moderately the KHE. Deletion of *MRS3* had no effect on KHE, and *mrs3* Δ *mdm38* Δ mutants remained without synthetic phenotype,⁵ excluding a role of Mrs3p as the KHE. These findings suggest an indirect role of Mrs3p on the KHE activity. In fact, several ions have been stated to play a direct or indirect role in mitochondrial K⁺ homeostasis (28–31).

The suppressor screen also identified two additional genes, *MRS7* and the novel gene *YDL183c* encoding an unknown protein, which were found to restore both growth and KHE activity of *mdm38* Δ mutant cells. Although Mdm38p and Mrs7p are phylogenetically related, Ydl183cp is likely not related to them. Each of these proteins contains a single transmembrane domain and appears to be part of a high molecular weight protein complex. They are functionally redundant in establishing a functional KHE in mitochondria.

In contrast to Mdm38p, absence of either Mrs7p or Ydl183cp alone or in combination did not seriously affect the growth of yeast cells. Yet the triple mutant *mdm38* Δ *mrs7* Δ *ydl183c* Δ had a dramatically stronger negative growth phenotype than the single *mdm38* Δ mutant or double mutants. This mutant completely failed to grow on respiratory substrates and exhibited a strain- and temperature-dependent reduced growth on fermentable substrates. This synthetic phenotype of the triple mutant indicates the following: (i) all three proteins are functionally expressed in yeast; (ii) loss of all three proteins dramatically impairs mitochondrial volume homeostasis through a disturbance that can be rescued by nigericin; and (iii) impaired volume homeostasis causes mitochondrial dysfunction affecting cell vitality as indicated by the reduction in growth on fermentable substrates.

Overexpression of Mrs7p or Ydl183cp fully compensated the growth defects of the *mdm38* Δ single and the *mdm38* Δ *mrs7* Δ *ydl183c* Δ triple disruptant. Accordingly, either protein could fully substitute for Mdm38p when expressed at high abundance. Addition of the exogenous KHE nigericin equally compensated for the growth defect of *mdm38* Δ single as well as for the even stronger growth defects of the triple mutant. This finding supports the conclusion that the triple mutant growth phenotype is essentially due to a lack of KHE activity.

This important point was proved by a direct test for KHE activity on inner membrane SMPs, a system that entirely avoids any interference of osmotically swollen mutant mitochondria.

⁵ G. Wiesenberger and K. Nowikovsky, unpublished data.

FIGURE 8. KHE activity of *mdm38* Δ *mrs7* Δ *ydl183c* Δ SMPs. [K⁺]-driven changes of [K⁺], and [H⁺], in submitochondrial inner-membrane particles prepared from wild-type and *mdm38* Δ *mrs7* Δ *ydl183c* Δ mutant cells with entrapped K⁺-sensitive PBFI or H⁺-sensitive BCECF were recorded as described in Fig. 3. *A*, effect of overexpression of Mrs7p (black square dotted line) or Ydl183cp (black thin dashed line) on [K⁺]-driven changes of [K⁺], and [H⁺], in DBY triple mutant *mdm38* Δ *mrs7* Δ *ydl183c* Δ SMPs (black solid line) in comparison with wild-type SMPs (black dotted line). *B*, effect of Mdm38p (expressed from YCp33, bold black solid line) or LETM1 (expressed from pVTU- (bold gray solid line) on [K⁺]-driven changes of [K⁺], and [H⁺], in DBY *mdm38* Δ *mrs7* Δ *ydl183c* Δ SMPs (black thin solid line) in comparison with wild-type SMPs (bold square dotted line).

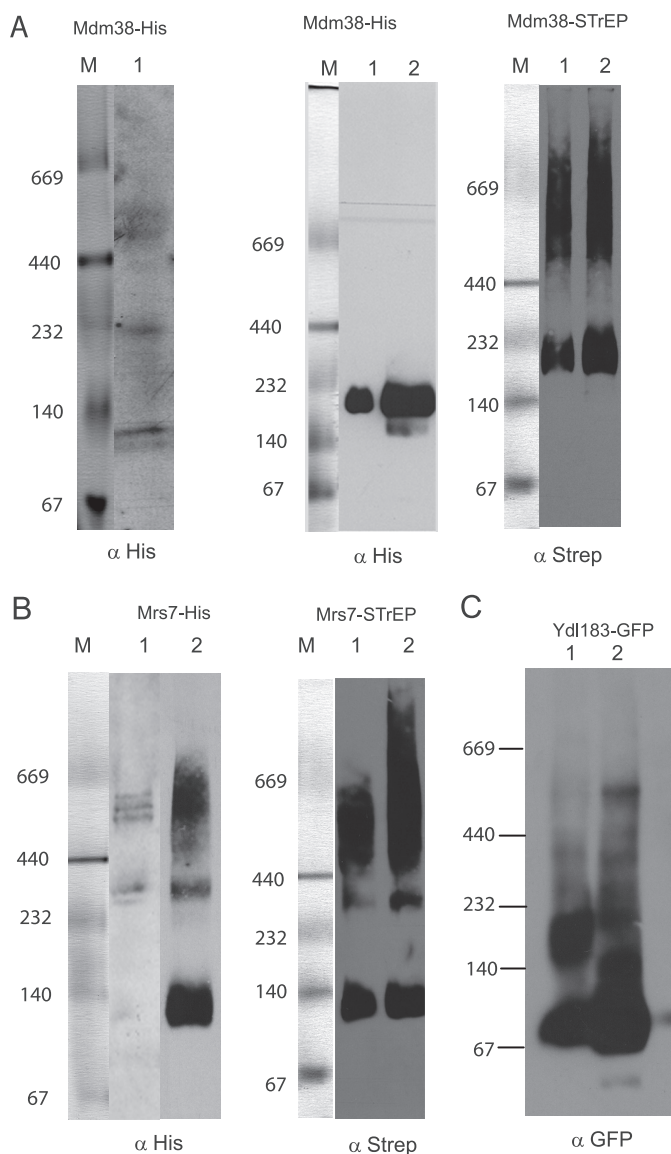


FIGURE 9. Mdm38p, Mrs7p, and Ydl183cp are part of a high molecular weight complex. *A*, DBY chromosomally Mdm38-His-tagged mitochondria were solubilized with 1.2% Triton X-100. *Left panel*, one part of the preparation was immediately separated on BN-PAGE. The anti-His antibody recognized three protein complexes of ~500, <232, and <40 kDa. *Middle panel*, other part of the same preparation was used for a further step involving nickel-affinity chromatography. Mdm38-His was recovered as part of a complex of <232 and >440 kDa. *M*, marker. *B*, DBY mitochondria expressing the chromosomally His-tagged Mrs7 were solubilized as in *A* and analyzed by BN-PAGE (*left panel, lane 1*), and parallel fractions were used for further isolation of a Mrs7-His complex by affinity chromatography (*left panel, lane 2*). Solubilized mitochondrial proteins and elution fractions from the affinity purification were separated on the same BN gel, transferred to a common membrane for Western blotting, and probed with an antiserum against His. DBY mitochondria expressing the chromosomal Mrs7-STrEP were solubilized, affinity-purified, and recovered in complexes of <140, >232, and >440 kDa. *C*, mitochondria expressing pUG-YDL183c-GFP in different backgrounds as follows: wild-type (*lane 1*) or *mdm38* Δ (*lane 2*) were solubilized with 1.2% *n*-dodecyl β -*D*-maltoside. Equal amounts of proteins were separated on BN-PAGE and immunoblotted with an antibody against GFP.

A comparison between single and triple mutants clearly revealed that the single *mdm38* Δ mutant retained a minor KHE activity, whereas the triple mutant totally lacked this activity. Thus, single and triple mutants most likely differ only in the

degree to which they have lost KHE activity. These data correlate well with the reduction in growth of the single and triple mutants. However, mild reduction in KHE activity detected in single mutants *mrs7* Δ and *ydl183c* Δ indicates that expression of Mrs7p and/or Ydl183p is necessary for full KHE activity in wild-type cells. Yet the physiological effects of *mrs7* Δ or *ydl183c* Δ mutations are too weak to result in reduced growth of mutant cells. In assays performed on the single *mdm38* Δ mutant, overexpression of Ydl183cp or Mrs7 could equally restore transmembrane K^+/H^+ fluxes, like Mdm38p or LETM1. However, in the triple mutant *mdm38* Δ *mrs7* Δ *ydl183c* Δ , Ydl183cp restored the mitochondrial KHE to a lesser extent than Mdm38p Mrs7p, or LETM1, most likely resulting from a less abundant expression of Ydl183c as compared with Mdm38 or Mrs7 (shown in [supplemental Fig. S4](#)). Taken together, these results indicate that Mdm38p, Mrs7p, and Ydl183cp are functionally redundant, but only Mdm38p is essential.

Mitochondrial depolarization in the mutants and its rescue by expression of either Mdm38p or Mrs7p or Ydl183cp correlated with loss and recovery of KHE activity, respectively, and with cell growth that was mildly affected on YPG when $\Delta\psi$ fell below 60% of wild-type values and increasingly more with lower values. The lowest $\Delta\psi$ values observed in the triple mutant also affected growth on fermentable substrate, indicating that essential functions of mitochondria, possibly protein import, were affected. The loss of $\Delta\psi$ in mitochondria of the disruptants may be a direct consequence of the absence of H^+ fluxes into the mitochondria in exchange for the efflux of K^+ rather than an additional effect resulting from the K^+ accumulation and swelling of mitochondria.

Total loss of KHE activity of the triple mutant was accompanied by more dramatic changes in organelle morphology than in the single *mdm38* Δ mutant. Both mitochondria and vacuoles appeared to be heavily fragmented and were shown to frequently colocalize, suggesting intense mitophagy. Notably, hyperosmotic stress has been reported to result in significant changes of the vacuole morphology of wild-type cells. In fact, the one to three large vacuoles usually present in wild-type cells underwent fragmentation to numerous smaller multilobe vacuoles (32). Interestingly, treatment of triple mutant cells with the K^+/H^+ ionophore nigericin efficiently reversed swelling and restored a near normal mitochondrial network. As this involves the mitochondrial fusion (33, 34), we assume that proteins regulating the fusion activity are not affected by the absence of Mdm38, Mrs7, and Ydl183c. Vacuolar fragmentation was efficiently reverted together with re-establishing mitochondrial KHE activity by nigericin (data not shown). This raises the question of how the loss of KHE and swelling of mitochondria cause fragmentation of the vacuole. In sum, this study provides strong evidence for a role of all three proteins in contributing to an active mitochondrial KHE.

A genome-wide screen in *Drosophila* S2 cells recently identified LETM1 as strongly affecting mitochondrial Ca^{2+} and H^+ homeostasis. Absence of LETM1 resulted in reduced mitochondrial Ca^{2+} uptake *in situ*, a finding that led the authors to conclude that Letm1 is the mitochondrial Ca^{2+}/H^+ antiporter (35). This conclusion is puzzling, because down-regulation of the mitochondrial Ca^{2+}/H^+ exchanger would rather have been expected to result in decreased Ca^{2+} efflux and therefore in increased mito-

Novel Players in Mitochondrial KHE

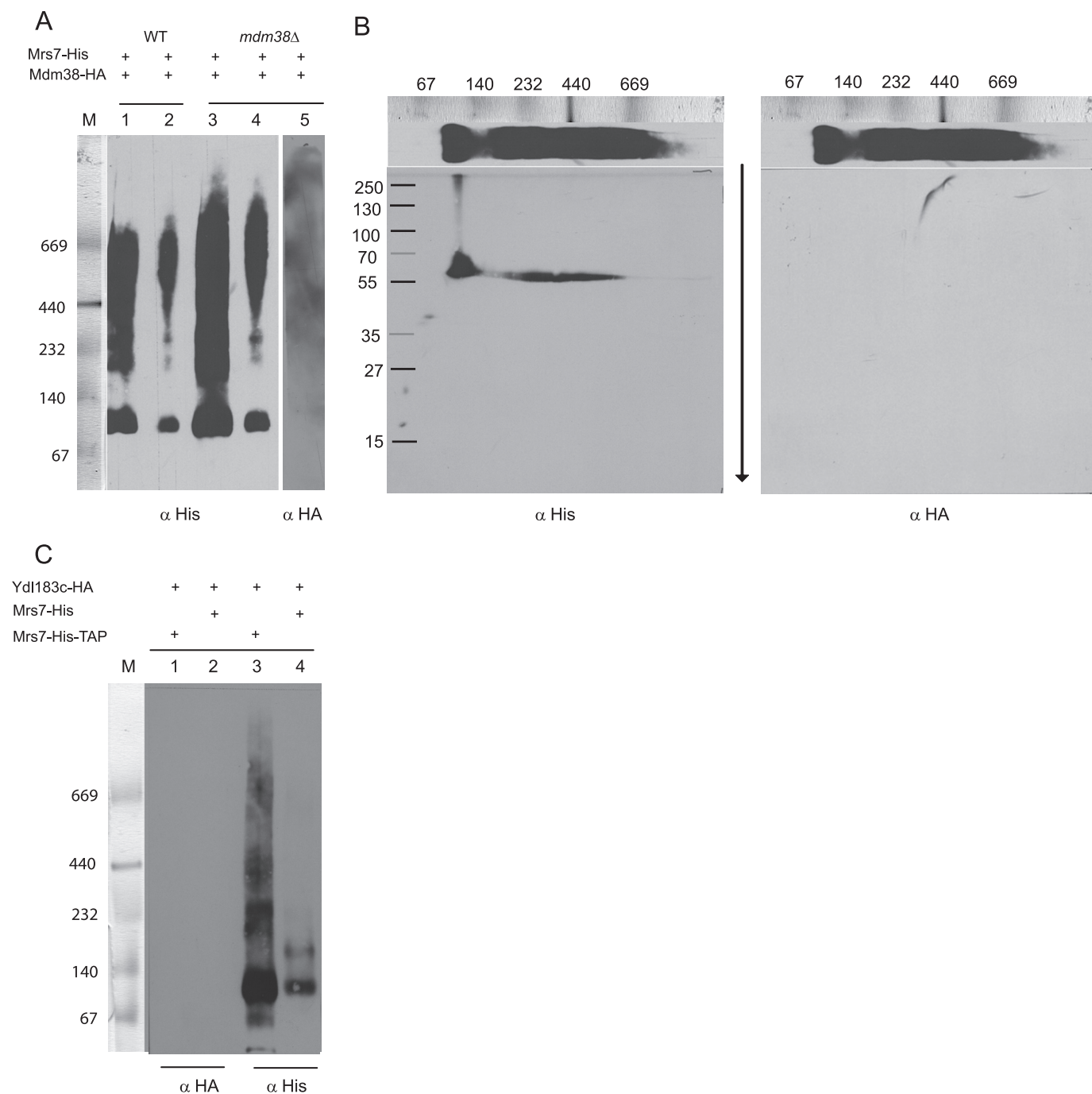


FIGURE 10. Interaction of Mrs7-His with Mdm38-HA and YDL183c-HA. *A*, affinity chromatography and preparative BN-PAGE of solubilized mitochondria coexpressing chromosomally His-tagged Mrs7 and extra-chromosomal YCp-Mdm38-HA in different backgrounds as follows: wild-type (WT) (lanes 1 and 2) and *mdm38Δ* (lanes 3–5). 120 μ l (lanes 1, 3, and 5) and 60 μ l (lanes 2 and 4) of the eluted fractions were applied to the same gel. Lanes 1–4 were probed with an antibody against His. Lane 5 served for the additional immunodetection with an antibody against HA. *M*, marker. *B*, second dimension SDS-PAGE of lane 3. *Left panel*, the antibody against His recognizes a product of ~55 kDa corresponding to Mrs7-His. The signal is in perfect agreement with the signals of the first dimension (BN-PAGE). *Right panel*, immunodetection with anti-HA antibody of the same blot after mild stripping. *C*, affinity chromatography and BN-PAGE of solubilized mitochondria coexpressing chromosomally His-tagged Mrs7 (lanes 1 and 3) or His-TAP-tagged Mrs7 (lanes 2 and 4) and extra-chromosomal Ydl183c-HA (lanes 1–4). Lanes 1 and 2 and lanes 3 and 4 were probed with antibodies against HA and His, respectively.

chondrial Ca^{2+} accumulation, because mitochondrial cation/ H^{+} antiporters protect cells from mitochondrial cation overload by mediating cation *efflux* from energized mitochondria (1). Jiang *et al.* (35) also found that reconstitution of LETM1 in liposomes catalyzed Ruthenium red-sensitive Ca^{2+} / H^{+} exchange, which raises further questions since decades of work on mitochondria indicate

that Ca^{2+} / H^{+} exchange is insensitive to Ruthenium red (36). Previous evidence that LETM1 is essential for mitochondrial K^{+} / H^{+} exchange is compelling (4, 5, 37), and the present study demonstrated that LETM1 fully restores mitochondrial KHE activity of the yeast triple mutant *mdm38Δ mrs7Δ ydl183c* like the exogenous *bona fide* KHE nigericin. We believe that further studies will

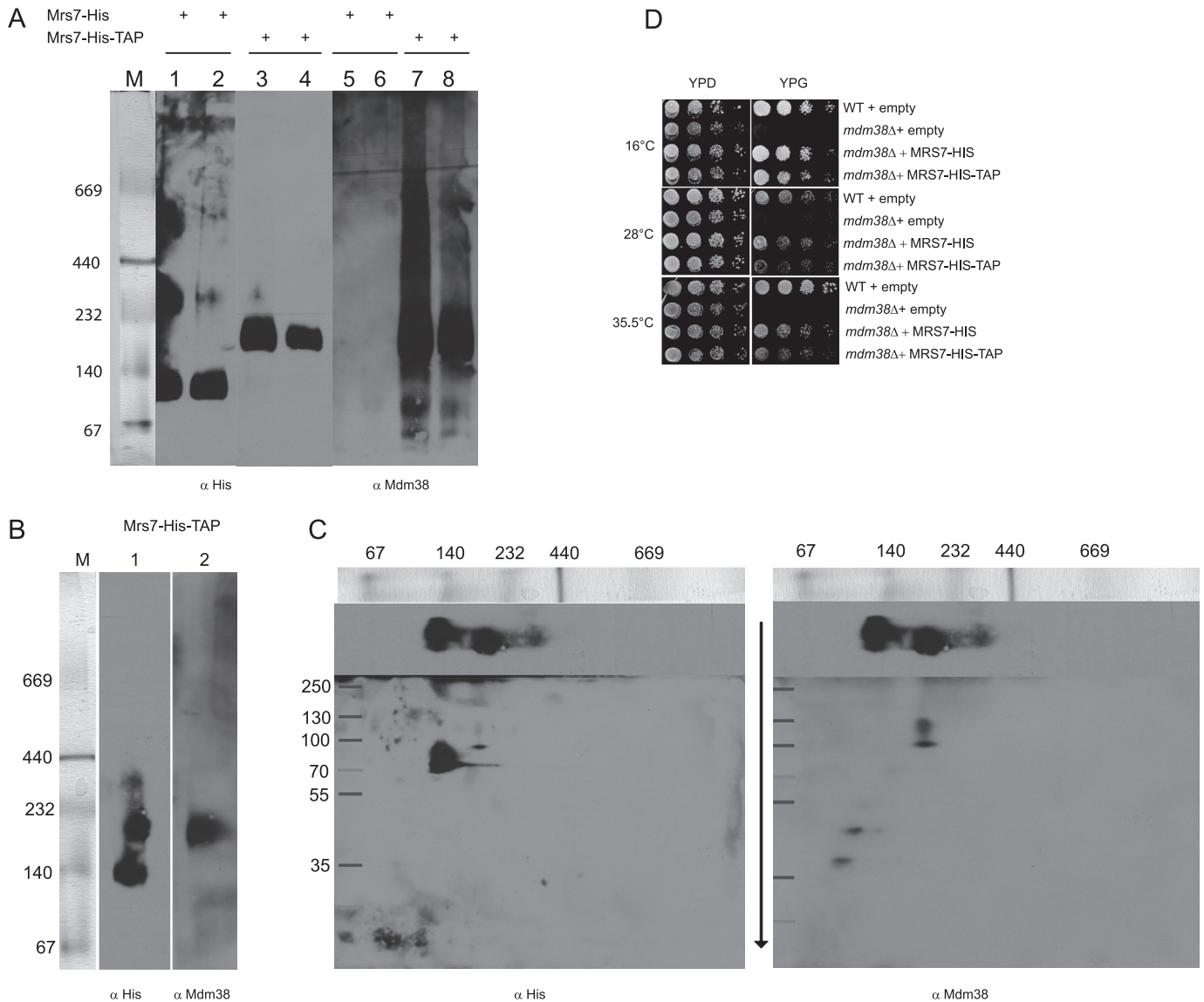


FIGURE 11. Interaction of Mdm38p with Mrs7-His and Mrs7-His-TAP. *A*, affinity chromatography and BN-PAGE of solubilized DBY mitochondria expressing either chromosomally His-tagged or His-TAP-tagged Mrs7. Eluted fractions 1–2 containing Mrs7-His were applied on lanes 1 and 2 and 5 and 6 and eluted fractions 1–2 containing Mrs7-His-TAP on lanes 3 and 4 and 7 and 8. BN-PAGE was performed and followed by immunostaining with an antibody against His (lanes 1–4) and Mdm38p (lanes 5–8). *M*, marker. *B*, preparative affinity chromatography and BN-PAGE of DBY mitochondria expressing chromosomally Mrs7-His-TAP prior to second dimension SDS-PAGE. The membrane was first incubated with an anti-His primary antibody (lane 1). Thereafter, the blot was mildly stripped and reincubated with an antibody against Mdm38p (lane 2). *C*, second dimension SDS-PAGE. *Left panel*, the blot was probed with the anti His antibody. *Right panel*, same blot probed with the anti Mdm38p antibody after mild stripping of the membrane. *D*, suppression effect of Mrs7-His and Mrs7-His-TAP in *mdm38Δ*. DBY wild type (*WT*) with YEp112 empty and *mdm38Δ* with YEp112 empty, MRS7-His, or MRS7-His-TAP were grown overnight. Serial dilutions were spotted onto YPD and YPG plates and incubated at the indicated temperatures.

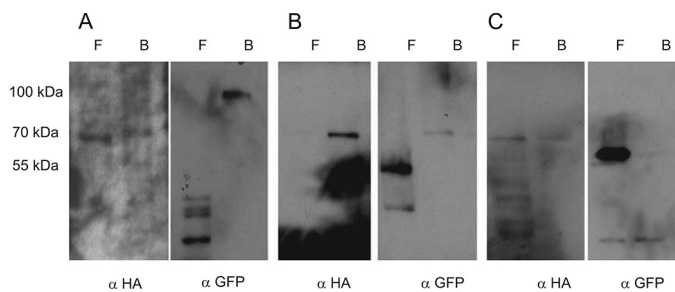


FIGURE 12. CoIP of isolated *mdm38Δ* mitochondria coexpressing YEP-MDM38-HA (72 kDa) and pUG-MDM38-GFP (92 kDa) (A), YDL183-GFP (65 kDa) (B), or AIF-GFP (68 kDa) (C). *F*, flow-through fraction; *B*, HA-coated protein A-bound fraction.

be needed to clarify whether the highly conserved LETM1 proteins exert different cation-specific functions in different eukaryotic organisms or rather disturbances of mitochondrial K^+ homeostasis can secondarily affect mitochondrial cation transport. Relevant to this discussion, we have shown that yeast mitochondria depleted of Mdm38p display a considerably reduced influx of Mg^{2+} and Ca^{2+} resulting from decreased mitochondrial $\Delta\psi$ (4).

Human LETM1 has previously been shown to be part of a complex of about 550 kDa by CoIP of GFP- and HA-tagged isomers (38). Rehling and co-workers (8) reported an interaction of Mdm38-protein A with various proteins, including numerous mitochondrial ribosomal proteins and Mrs7p. In our hands, hetero-oligomerization of Mrs7p with Mdm38p was not

Novel Players in Mitochondrial KHE

detected unless Mrs7p was fused to a tag, including protein A and calmodulin-binding protein.

We have shown that the Mdm38p, Mrs7p, and Ydl183cp form oligomers. Data provided here confirmed that Mdm38p self-dimerizes in mitochondria. However, it may hetero-oligomerize also with a yet unknown protein as suggested by BN and affinity chromatography data. Mdm38p appeared as part of high molecular complexes of ~140, 232, and 500 kDa. Ydl183cp appeared as part of protein complexes with variable molecular sizes depending on the presence or absence of Mdm38p. Remarkably, in the absence of Mdm38p, Ydl183-GFP appeared as part of a complex of ~500 kDa. In any case, a direct interaction between Ydl183cp and Mdm38p was not found according to the CoIP experiments performed in this work. Furthermore, Mrs7 was shown to be part of several protein complexes, including a complex of ~500 kDa, independently of the presence or absence of Mdm38p. Thus, data presented here exclude a direct interaction between Mrs7p and Mdm38p or Ydl183cp. Altogether, the three proteins may act as cofactors interacting with a so far unidentified KHE, which in their absence would be completely inactive. This would be reminiscent of what has been observed for plasma membrane cation exchangers, where the exchanger is regulated by essential cofactors (39, 40). We propose that either Mdm38p or Mrs7p or Ydl183cp bind to a yet unknown protein or protein complex to activate the KHE activity. Although the composition of the 500-kDa complex and the molecular mechanisms through which Mdm38p, Mrs7p, and Ydl183cp modulate KHE activity remain to be elucidated, this study has identified intriguing new players that are amenable to further genetic analysis.

Finally, we included here for the first time a human gene, *HCCR-1*, which has been shown to play a role in cancer development (34). Furthermore, *HCCR-1* shows sequence homologies to *LETM1*. We suggest a related role of *HCCR1* to *LETM1*. Discrepancies in the quality as suppressor might result from its weak expression in yeast. Further studies will be required to test the direct role of *HCCR-1* in the KHE.

Acknowledgments—We thank Kristina Djinovic for constructive discussions; Andrea Pichler for experimental advice; Paolo Bernardi for critical reading of the manuscript and supportive discussions; and Mirjana Iliev for expert technical assistance. We are indebted to Juraj Gregan for generously providing the yeast genomic library; Benedikt Westermann and Hiromi Sesaki for sharing the YFP and GFP vectors; and to Peter Rehling, Gottfried Schatz, Tom D. Fox, and Hans van der Spek for the antisera against Mdm38, F1 β , Yme1, and Tim44, respectively.

REFERENCES

- Mitchell, P. (1966) *Biol. Rev. Camb. Philos. Soc.* **41**, 445–502
- Froschauer, E., Nowikovsky, K., and Schweyen, R. J. (2005) *Biochim. Biophys. Acta* **1711**, 41–48
- McQuibban, A. G., Joza, N., Megighian, A., Scorzeto, M., Zanini, D., Reipert, S., Richter, C., Schweyen, R. J., and Nowikovsky, K. (2010) *Hum. Mol. Genet.* **19**, 987–1000
- Nowikovsky, K., Froschauer, E. M., Zsurka, G., Samaj, J., Reipert, S., Kolisek, M., Wiesenberger, G., and Schweyen, R. J. (2004) *J. Biol. Chem.* **279**, 30307–30315
- Nowikovsky, K., Reipert, S., Devenish, R. J., and Schweyen, R. J. (2007) *Cell Death Differ.* **14**, 1647–1656
- Zollino, M., Lecce, R., Fischetto, R., Murdolo, M., Faravelli, F., Selicorni, A., Buttè, C., Memo, L., Capovilla, G., and Neri, G. (2003) *Am. J. Hum. Genet.* **72**, 590–597
- Waldherr, M., Ragnini, A., Jank, B., Tepy, R., Wiesenberger, G., and Schweyen, R. J. (1993) *Curr. Genet.* **24**, 301–306
- Frazier, A. E., Taylor, R. D., Mick, D. U., Warscheid, B., Stoepel, N., Meyer, H. E., Ryan, M. T., Guiard, B., and Rehling, P. (2006) *J. Cell Biol.* **172**, 553–564
- Cho, G. W., Shin, S. M., Namkoong, H., Kim, H. K., Ha, S. A., Hur, S. Y., Kim, T. E., Chai, Y. G., and Kim, J. W. (2006) *Gene* **384**, 18–26
- Rigaut, G., Shevchenko, A., Rutz, B., Wilm, M., Mann, M., and Séraphin, B. (1999) *Nat. Biotechnol.* **17**, 1030–1032
- Junttila, M. R., Saarinen, S., Schmidt, T., Kast, J., and Westermarck, J. (2005) *Proteomics* **5**, 1199–1203
- Wach, A., Brachat, A., Pöhlmann, R., and Philippsen, P. (1994) *Yeast* **10**, 1793–1808
- Thorpe, H. M., and Smith, M. C. (1998) *Proc. Natl. Acad. Sci. U.S.A.* **95**, 5505–5510
- Cormack, B. P., Bertram, G., Egerton, M., Gow, N. A., Falkow, S., and Brown, A. J. (1997) *Microbiology* **143**, 303–311
- Zinser, E., and Daum, G. (1995) *Yeast* **11**, 493–536
- Fujiki, Y., Hubbard, A. L., Fowler, S., and Lazarow, P. B. (1982) *J. Cell Biol.* **93**, 97–102
- Daum, G., Gasser, S. M., and Schatz, G. (1982) *J. Biol. Chem.* **257**, 13075–13080
- Schägger, H., and von Jagow, G. (1991) *Anal. Biochem.* **199**, 223–231
- Schamel, W. W. (2008) *Curr. Protoc. Cell Biol.* **6**, Unit 6.10.1–6.10.21
- Nowikovsky, K., Devenish, R. J., Froschauer, E., and Schweyen, R. J. (2009) *Methods Enzymol.* **457**, 305–317
- Sesaki, H., Southard, S. M., Yaffe, M. P., and Jensen, R. E. (2003) *Mol. Biol. Cell* **14**, 2342–2356
- Westermann, B., and Neupert, W. (2000) *Yeast* **16**, 1421–1427
- Hamel, P., Saint-Georges, Y., de Pinto, B., Lachacinski, N., Altamura, N., and Dujardin, G. (2004) *Mol. Microbiol.* **51**, 307–317
- Mühlenhoff, U., Stadler, J. A., Richhardt, N., Seubert, A., Eickhorst, T., Schweyen, R. J., Lill, R., and Wiesenberger, G. (2003) *J. Biol. Chem.* **278**, 40612–40620
- Volckaert, G., Voet, M., Van der Schueren, J., Robben, J., Vanstreels, E., and Vander Stappen, J. (2003) *Yeast* **20**, 79–88
- Ha, S. A., Shin, S. M., Lee, Y. J., Kim, S., Kim, H. K., Namkoong, H., Lee, H., Lee, Y. S., Cho, Y. S., Park, Y. G., Jeon, H. M., Oh, C., and Kim, J. W. (2008) *Int. J. Cancer* **122**, 501–508
- Kissová, I., Salin, B., Schaeffer, J., Bhatia, S., Manon, S., and Camougrand, N. (2007) *Autophagy* **3**, 329–336
- Cortés, P., Castrejón, V., Sampedro, J. G., and Uribe, S. (2000) *Biochim. Biophys. Acta* **1456**, 67–76
- Lee, W. K., Spielmann, M., Bork, U., and Thévenod, F. (2005) *Am. J. Physiol. Cell Physiol.* **289**, C656–C664
- Rasheed, B. K., Diwan, J. J., and Sanadi, D. R. (1984) *Eur. J. Biochem.* **144**, 643–647
- Wojtczak, L., Nikitina, E. R., Czyz, A., and Skulskii, I. A. (1996) *Biochem. Biophys. Res. Commun.* **223**, 468–473
- Bonangelino, C. J., Nau, J. J., Duex, J. E., Brinkman, M., Wurmser, A. E., Gary, J. D., Emr, S. D., and Weisman, L. S. (2002) *J. Cell Biol.* **156**, 1015–1028
- Okamoto, K., and Shaw, J. M. (2005) *Annu. Rev. Genet.* **39**, 503–536
- Zhang, Y., and Chan, D. C. (2007) *FEBS Lett.* **581**, 2168–2173
- Jiang, D., Zhao, L., and Clapham, D. E. (2009) *Science* **326**, 144–147
- Bernardi, P. (1999) *Physiol. Rev.* **79**, 1127–1155
- Dimmer, K. S., Navoni, F., Casarin, A., Trevisson, E., Ende, S., Winterpacht, A., Salvati, L., and Scorrano, L. (2008) *Hum. Mol. Genet.* **17**, 201–214
- Hasegawa, A., and van der Blik, A. M. (2007) *Hum. Mol. Genet.* **16**, 2061–2071
- Pang, T., Su, X., Wakabayashi, S., and Shigekawa, M. (2001) *J. Biol. Chem.* **276**, 17367–17372
- Weinman, E. J., Cunningham, R., Wade, J. B., and Shenolikar, S. (2005) *J. Physiol.* **567**, 27–32

Supplemental Data

Fig 1

Left: Cross-linking of the Mdm38-His containing sub-complexes. W303 *mdm38Δ* cells were transformed with pYES-MDM38-His and grown to log phase. Mitochondria were isolated in presence of protease inhibitors and treated with DSS (Disuccinimidyl suberate) in increasing concentration as indicated, separated on SDS PAGE and immunoblotted with a His antibody. Asterisk indicates the monomers, white arrowheads the dimmers, black arrowheads a possible dimer-complex containing an unknown protein of approximately 35 kDa.

Right: Chemical cross-linking experiments were performed as above. After addition of the cross-linker, the samples (100 μg protein) were incubated on ice for 30', thereafter trichloroacetic acid (TCA) precipitated, resolved in 20 μl of the loading dye (5 μl NuPage® LDS Sample Buffer 4x, 2 μl NuPage® Reducing Agent 10x and deionized water) according to the manual of the kit. The lanes were loaded with 10 μl of the solution and the gel was run for 1 hour at 150 V using the buffers provided with the kit. After running the gel was wet blotted in a standard tank blot apparatus. The membrane was then subjected to standard western blotting using primary α-HIS antibody. White arrowhead point to a complex also present without crosslinker possibly resulting from disulfide bridges.

Fig 2

W303 strain co-expressing Mdm38-Myc and Ydl183-GFP. Cross-linked mitochondrial protein extractions were separated on a SDS PAGE and immunodecorated first with the antiserum recognizing the Myc-tag and after membrane stripping with the antiserum to GFP. Black arrowheads point to the high molecular weight complex.

Fig 3

Since the cross-link products possibly correlate with the size of homodimers or trimers of Mdm38p we investigated whether Mdm38p interacts *in vivo* with itself. For this purpose a split-YFP system was used and Mdm38p was expressed in frame with the first 1-173 nt or the last 155-238 nt of YFP. The complementation of YFP in cells transformed with both constructs was visualized under confocal

microscopy. Cells carrying both vectors exhibited YFP fluorescence, indicative of the intramolecular complementation of the YFP molecule. Mitotracker Ros staining of the cells showed the mitochondrial localization of the Mdm38 homodimers.

Material, methods and reference to Figure 3

MDM38 was cloned in frame with YFP 1-173 or YFP 155-238, by amplification of the entire ORF without stop codon using the primers 5' TAATATGAGCTCATGTTGAATTCGCATCAAGAGCG3' and 5' ATATGTCGACATCTTTCTTAATGACAAAAGTCTTCG3' introducing the underlined *SacI* and *SalI* restriction sites and inserting the digested fragments into the *SacI-SalI* digested plasmids pSCMF-143 and pSCMF-144 (1) (both kindly provided by Michael Frohman). For cloning into the yeast low-copy vector pUG35, the fragment containing *MDM38* in frame with YFP1-173 was amplified with primers 5' GATACAATTCTATTACCCCATCCATACTCTAGAACTAGTGGATCATGTTGAATTCGCATCAAGAGC3' and 5' GGCGTGAATGTAAGCGTGACATAACTAATTACATGACTCGACCAGTACTGCGCCAGTTCCTTTTCAGAGC3'. To clone the fragment containing *MDM38* in frame with YFP 155-238 into the vector pUG23, the latter described forward primer and the minus primer 5' GGCGTGAATGTAAGCGTGACATAACTAATTACATGACTCGACCAGTACTTGTA were used. These amplified *MDM38*-YFP1-173 and *MDM38*-YFP155-238 versions were *in vivo* ligated in W303 wild-type cells of opposite mating type into the *XbaI-HpaI* digested pUG35 and the *HincII* digested pUG23 vectors, respectively. The haploid transformants were tested for self-fluorescence prior crossing.

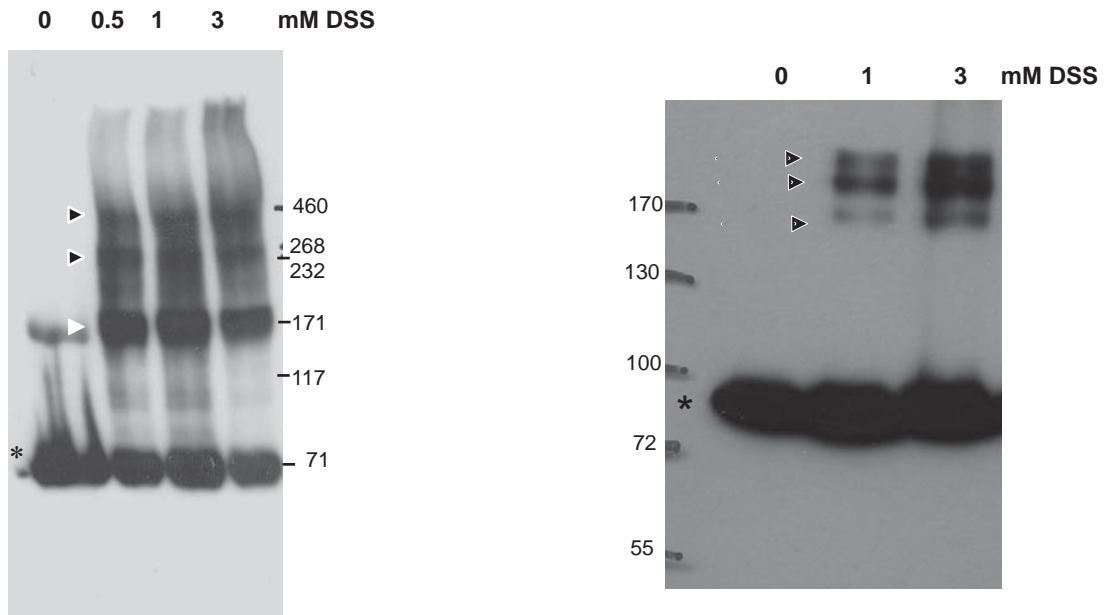
Fig 4

To compare the protein expression levels of Mdm38, Mrs7 and Ydl183 expressed from different promoters and plasmids, whole cells expressing the indicated tagged proteins were grown overnight to same OD. Same amount of cells were TCA precipitated. Same protein concentrations were applied on SDS PAGE and immunoblotted as indicated. Left blot was exposed 30 seconds, right blot 3 minutes.

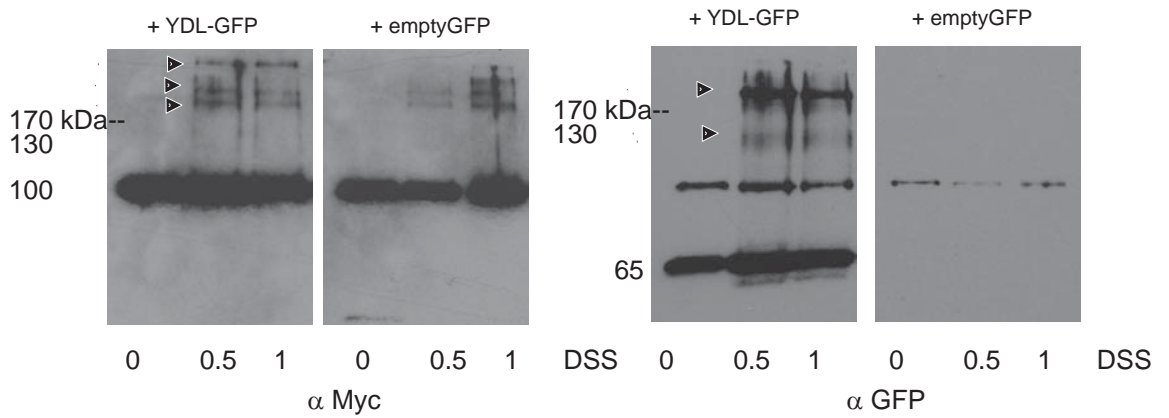
1. Choi, S. Y., Huang, P., Jenkins, G. M., Chan, D. C., Schiller, J., and Frohman, M. A. (2006) *Nat Cell Biol* **8**, 1255-1262

Supplemental Fig 1

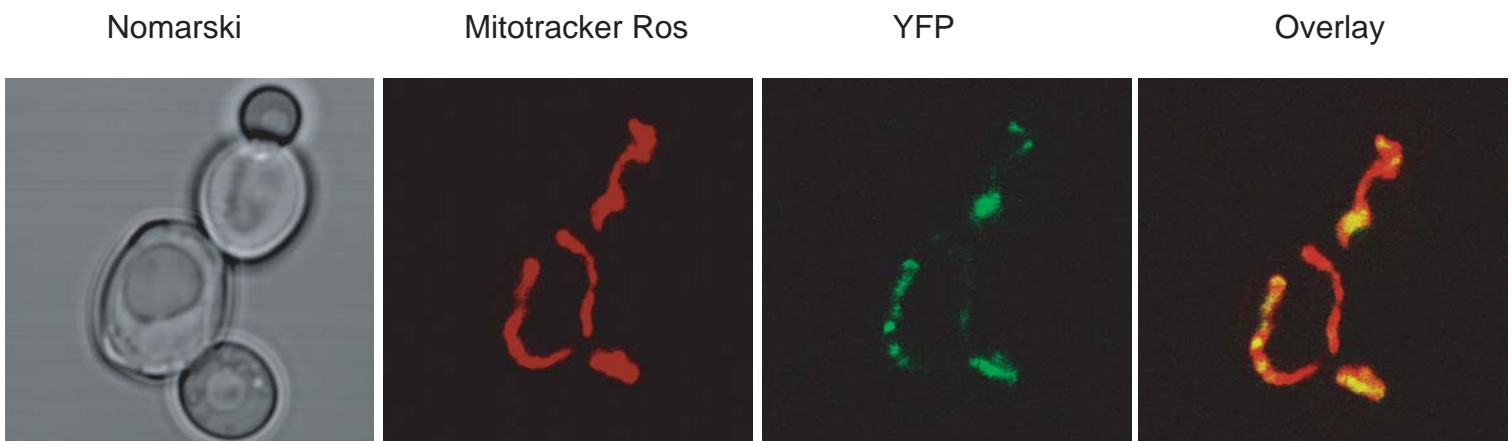
Supplemental Material can be found at:
<http://www.jbc.org/content/suppl/2010/03/02/M109.059956.DC1.html>



Supplemental Fig 2

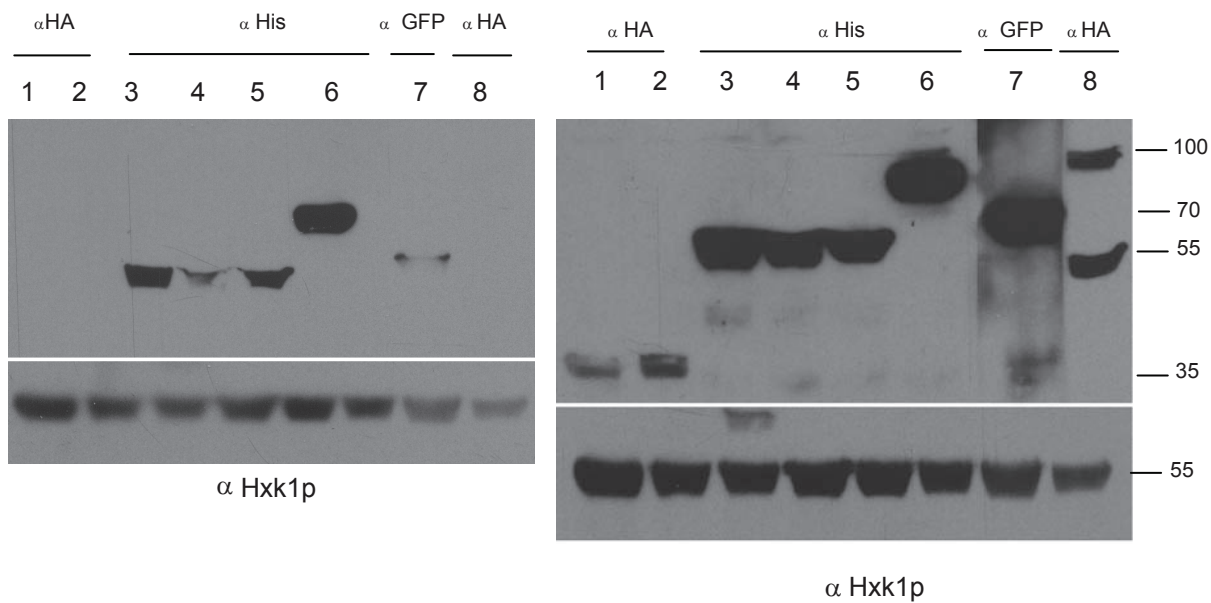


Supplemental Fig 3



Supplemental Fig 4

Supplemental Material can be found at:
<http://www.jbc.org/content/suppl/2010/03/02/M109.059956.DC1.html>



- 1 YCp22-Ydl183-HA
- 2 YEp 112Ydl183-HA
- 3 Mrs7-His (chromosomal)
- 4 YCp22Mrs7-His
- 5 YEp112Mrs7-His
- 6 Mdm38-His (chromosomal)
- 7 pUG35-Ydl183-GFP
- 8 YCp22 Mdm38-HA

5. Results

5.1. Working hypothesis – Mdm38p/Mkh1p is an essential interaction partner of the mitochondrial K^+/H^+ exchanger

Very recently, we showed that Mdm38p is capable to homo-dimerize and was found to be part of protein complexes of ~ 200 and ~ 550 kDa (Zotova *et al.*, 2010). Similarly, human Letm1 was shown to self-interact and to form protein complexes of a molecular weight of ~ 300 and between 500 and 600 kDa (Dimmer *et al.*, 2008; Hasegawa & van der Blik, 2007; Tamai *et al.*, 2008). These data suggest that Mdm38p forms the high molecular weight complex either by homo-oligomerization or by association with other yet unidentified proteins. According to the *Saccharomyces* Genome Database (SGD) (<http://genome-www.stanford.edu/Saccharomyces/>), all so far described yeast cation exchange proteins, as well as members of the mammalian Na^+/H^+ exchange family (Yun *et al.*, 1995), are predicted to contain eight to twelve transmembrane spanning helices. Furthermore, homo-dimerization of yeast and mammalian Na^+/H^+ antiporters was shown to be crucial for their function (Fafournoux *et al.*, 1994; Hisamitsu *et al.*, 2006; Mitsui *et al.*, 2005). Since Mdm38p/Letm1 have only one transmembrane helix and show no appreciable homology to any known cation exchanger, formation of the K^+/H^+ exchanger by homo-oligomerization of these proteins would represent a new family of cation/proton exchangers.

However, the more realistic hypothesis suggests that Mdm38p/Letm1 proteins act as auxiliary components of the so far unidentified K^+/H^+ exchanger (Figure 6). This would be in accordance with previous evidence that the plasma membrane Na^+/H^+ exchangers are regulated by essential interaction partners (Lehoux *et al.*, 2001; Pang *et al.*, 2001; Weinman *et al.*, 2005).

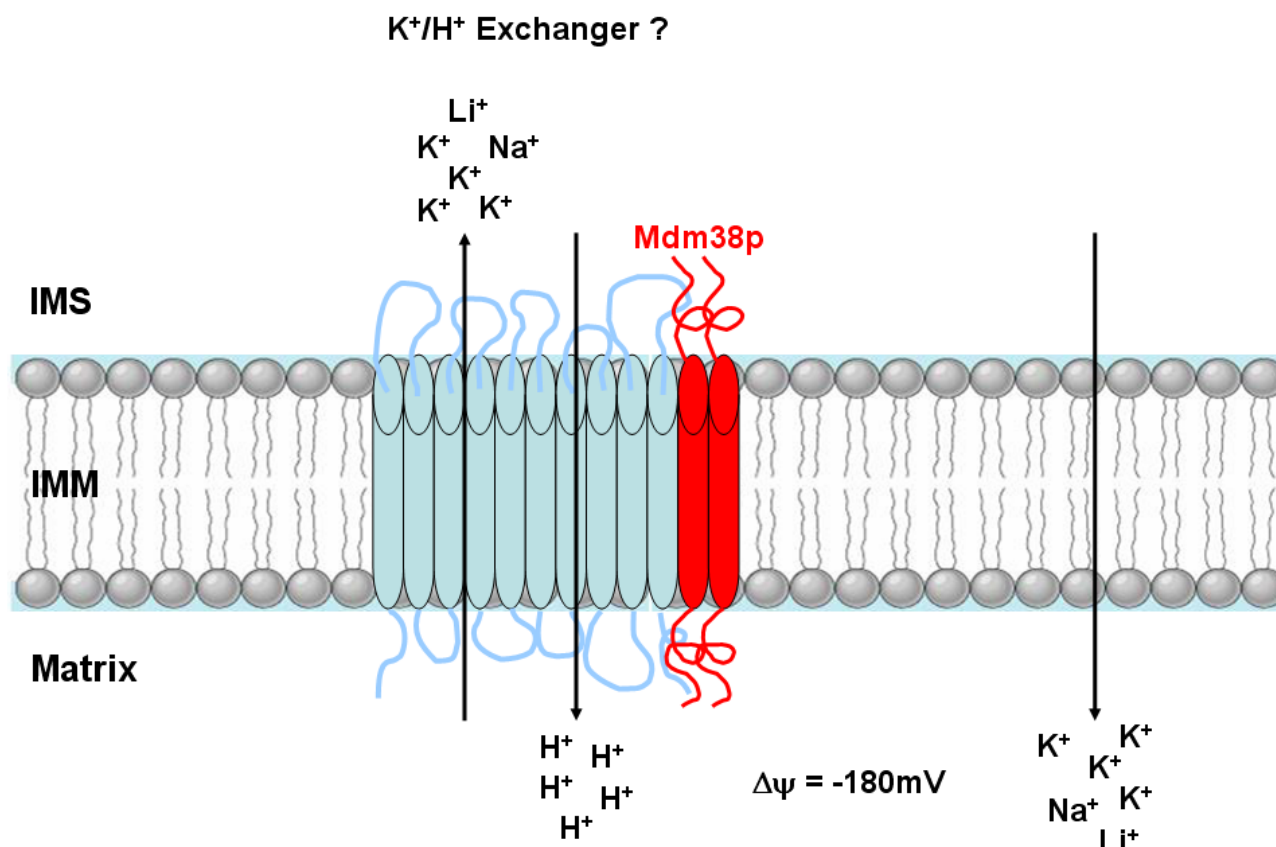


Figure 6: Schematic representation of our working hypothesis

The inside negative membrane potential ($\Delta\psi$) is the driving force for the influx of cations into the mitochondrial matrix. This influx is compensated by an electroneutral exchange process of cations against protons, driven by the yet unknown K^+/H^+ exchanger. Mdm38p is an essential factor of this exchange process. It is also part of a ~ 550 kDa protein complex, possibly in a dimeric conformation (Zotova *et al.*, 2010). We propose that Mdm38p directly interacts with the K^+/H^+ exchanger, thereby forming the protein complex. By affinity chromatography of tagged variants of Mdm38p we will try to co-purify the exchanger and other putatively interacting proteins. IMS, intermembrane space; IMM, inner mitochondrial membrane.

5.2. Mdm38p complex purification strategy

Based on our working hypothesis of Mdm38p being an essential regulatory protein directly interacting with the mitochondrial K^+/H^+ exchanger, we decided to purify the Mdm38p complex by affinity chromatography, aiming at co-purifying the K^+/H^+ exchanger. The purification strategy is schematically explained in Figure 7. Experiments were performed with chromosomally tagged or low-copy (centromeric) plasmid encoded variants of *MDM38* to

assure physiological protein levels, thus avoiding the negative dominant effects of *MDM38* overexpression (our data) and reducing the risk of identifying false-positive protein-protein interactions.

Identification of Mdm38p complex partners

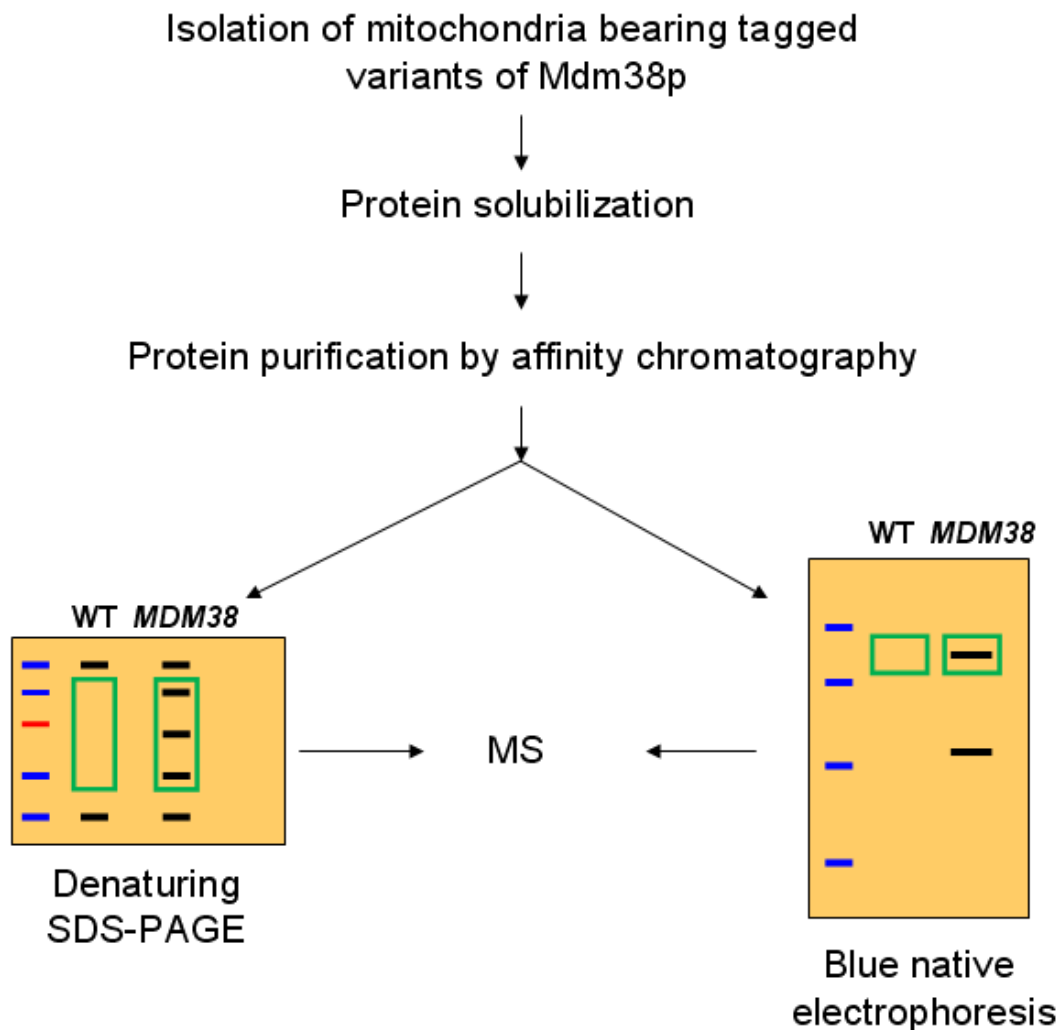


Figure 7: Flow chart of Mdm38p purification strategy

Whole mitochondria from yeast strains expressing different versions of tagged *MDM38* are prepared. The Mdm38p complex residing in the inner mitochondrial membrane is solubilized using different detergents. Subsequent purification steps of the Mdm38p complex are performed by affinity chromatography. Purified proteins are then applied either to denaturing SDS-PAGE or Blue native electrophoresis, thereby preserving the protein complex composition. Proteins are detected by Western blotting and Coomassie staining. Interesting protein bands not appearing in the control fractions are subjected to mass spectrometry (MS) for identification.

5.3. Tandem Affinity Purification (TAP) of chromosomally tagged Mdm38p

In search of a method fulfilling our requirements for rapid purification of a protein complex composed of proteins expressed at their natural level, we decided to use the protein A – CBP (calmodulin binding peptide) TAP method.

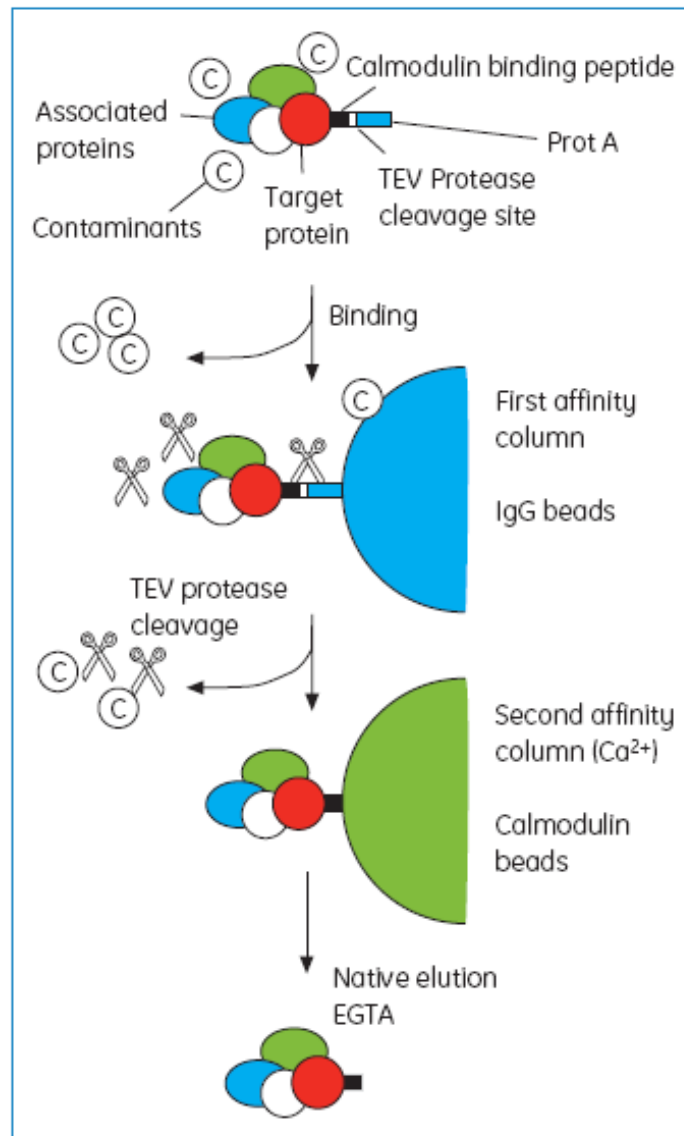


Figure 8: Schematic overview of the protein A – CBP TAP method

TAP-tagged proteins solubilized from mitochondrial membranes are purified in two steps together with interacting complex partners. Elution of proteins by TEV protease cleavage in the first step and EGTA in the second step allows native purification of protein complexes. In principle, the method can also be performed in the reverse order. TEV, Tobacco Etch Virus; Figure copyright: Elsevier Global Rights Dep.

This affinity purification strategy (Figure 8) was developed as a general procedure for protein complex purification (Puig *et al.*, 2001). Since Mdm38p contains an N-terminal mitochondrial targeting sequence, the affinity tag had to be fused C-terminally to the protein. The detailed tagging procedure is described in the Materials and Methods section. To allow for an additional purification step or to replace one of the TAP steps if necessary, we introduced a 6xHIS tag between Mdm38p and the TAP tag (Figure 9A).

A



B

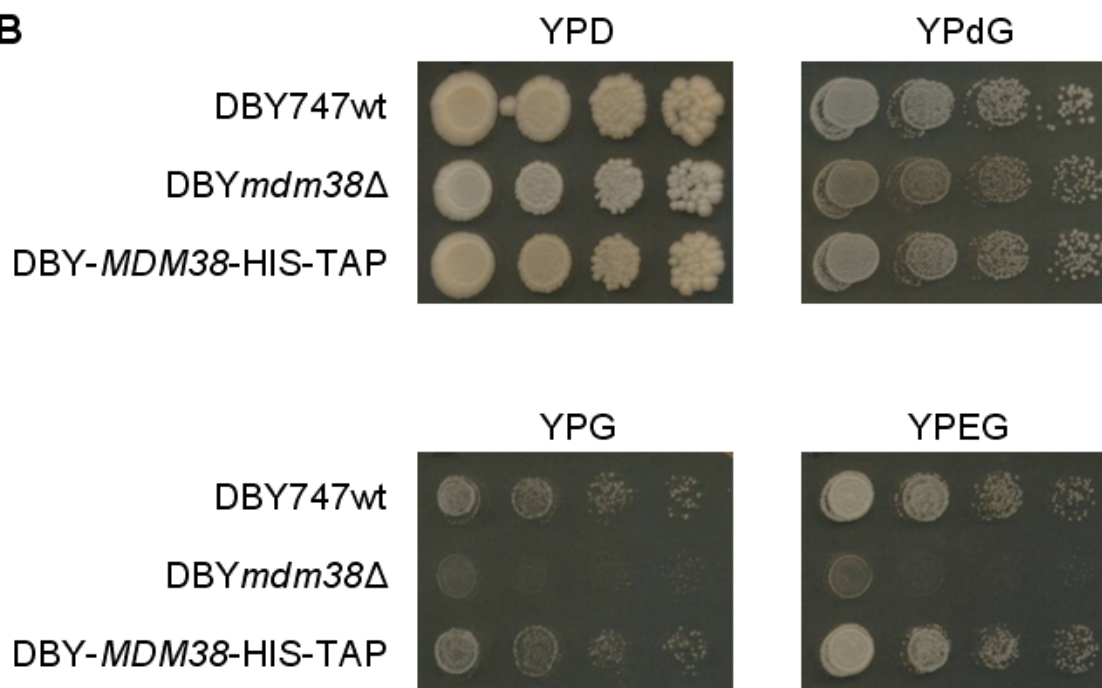


Figure 9: Growth phenotype of yeast strain DBY747 bearing HIS-TAP-tagged *MDM38*

A. Schematic representation of chromosomally HIS-TAP-tagged *MDM38*. The affinity tag was introduced C-terminally in-frame with the *MDM38* ORF by homologous recombination of PCR fragments amplified from plasmid pBS1479 (see Materials and Methods).

B. Overnight cultures of yeast strains DBY747wt, DBY*mdm38*Δ and DBY-*MDM38*-HIS-TAP grown in YPD were adjusted to $OD_{600} = 1$. Ten-fold serial dilutions were incubated at 28°C for three days on YPD plates and for four days on YPdG, YPG, and YPEG plates.

5.3.1. The HIS-TAP tag does not disturb Mdm38p function and complex formation

One limitation of affinity purification could be the affinity tag itself. Fusion of the tag to the protein of interest may interfere with protein folding and function or sterically hinder protein-protein interactions. Given the size of the HIS-TAP tag (~ 22 kDa), we first had to evaluate possible negative effects on Mdm38p function.

Therefore, serial dilutions of wild-type strain DBY747, the isogenic mutant strain DBY*mdm38* Δ , and cells bearing chromosomally HIS-TAP-tagged *MDM38* (DBY-*MDM38*-HIS-TAP) were spotted on fermentable (YPD) and non-fermentable media (YPG, YPdG, and YPEG) and incubated at 28°C (Figure 9B). DBY-*MDM38*-HIS-TAP exhibited the same growth on YPD and YPG as the wild-type, whereas DBY*mdm38* Δ showed a severe growth defect on non fermentable substrates, as expected, thus indicating that the HIS-TAP tag did not interfere with the correct function of Mdm38p.

Next, we had to confirm the presence of the Mdm38p complex in the strain DBY-*MDM38*-HIS-TAP before affinity purification. For this purpose we isolated whole mitochondria bearing Mdm38-HIS-TAP. Proteins were solubilized using 1.2% TX-100 and separated by Blue native electrophoresis on a 5-18% polyacrylamide gradient gel immediately thereafter. After transfer to a PVDF membrane, the antibody directed against the 6xHIS epitope recognized Mdm38p as part of a complex between 440 and 669 kDa (Figure 10), indicative of a normal complex formation in presence of Mdm38-HIS-TAP.

5.3.2. Chemical cross-linking of Mdm38-HIS-TAP

Although we intended to purify the complex under native conditions to keep the Mdm38p complex intact, we sought to stabilize the complex and to avoid loss of possible binding partners by chemical cross-linking. We reasoned that cross-linking would also allow us to purify the complex under denaturing conditions. Among several reagents tested, only amine-reactive disuccinimidyl suberate (DSS) showed significant cross-linking of Mdm38p. DSS is based on N-hydroxysuccinimide ester (NHS ester) and allows irreversible conjugation of primary amines.

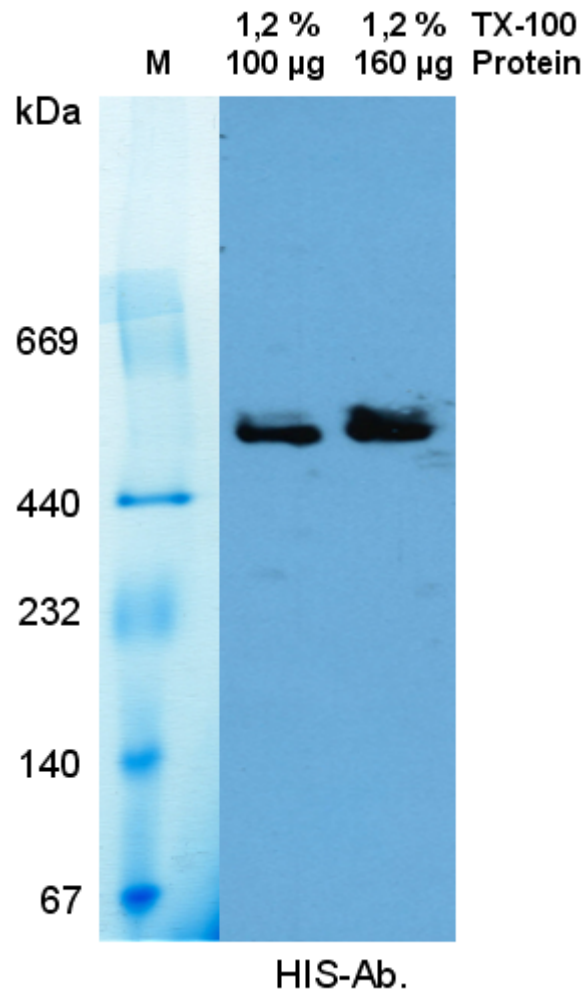


Figure 10: Blue native electrophoresis of the Mdm38p high molecular weight complex

Whole mitochondria isolated from strain DBY747 expressing chromosomally HIS-TAP-tagged *MDM38* were solubilized using 1.2% TX-100 and indicated protein amounts were loaded and separated on a native 5-18% polyacrylamide gradient gel. Proteins were transferred to a PVDF membrane and Mdm38p was detected in a ~ 550 kDa complex by immunodetection of the 6xHIS epitope. M, protein marker.

First cross-linking experiments were performed with whole mitochondria isolated from strain DBY747 expressing chromosomally HIS-TAP-tagged *MDM38*. Mitochondria were supplemented with increasing concentrations of DSS in presence of breaking buffer at indicated protein concentrations (Figure 11A).

Samples were precipitated using trichloroacetic acid (TCA), applied to SDS-PAGE and analyzed by immunodetection of Mdm38-HIS-TAP with an antibody directed against 6xHIS.

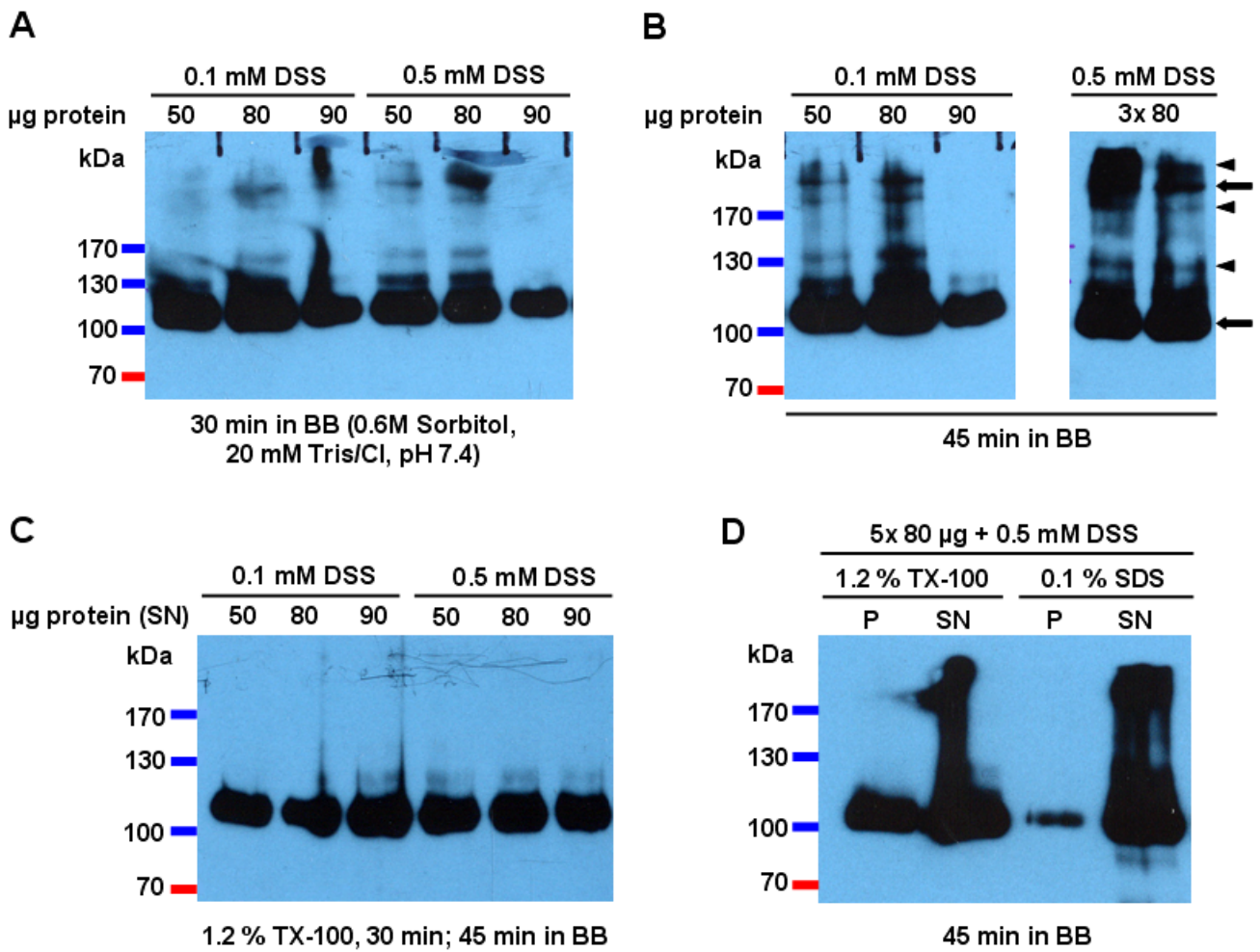


Figure 11: Chemical cross-linking of Mdm38p

A. Mitochondria were isolated from strain DBY747 expressing chromosomally HIS-TAP-tagged *MDM38* in presence of protease inhibitors and treated with amine-reactive disuccinimidyl suberate (DSS) in breaking buffer (BB) for 30 min on ice at indicated concentrations. Proteins were trichloroacetic acid (TCA) precipitated, separated by SDS-PAGE, and immunodetected with an antibody directed against the 6xHIS epitope.

B. Chemical cross-linking experiments were performed as described above, with the exception that after addition of DSS the samples were incubated on ice for 45 min and three individual samples were combined after TCA precipitation (*right panel*) prior to SDS-PAGE and Western blotting. Mdm38-HIS-TAP was detected in its monomeric and putative dimeric conformation (*black arrows*; bottom and top, respectively) and as part of undefined cross-link products (*black arrowheads*).

C. Mitochondria were solubilized with 1.2% TX-100 for 30 min on ice and centrifuged prior to DSS treatment of the supernatant (SN).

D. Mitochondrial samples (80µg) were supplemented with DSS and TX-100 or SDS at the same time and incubated on ice for 45 min. Thereafter, samples were centrifuged, five pellet (P) and supernatant (SN) fractions were TCA precipitated, combined and analyzed by SDS-PAGE and immunodetection of the 6xHIS epitope.

Best results were obtained with 80 μ g protein treated with 0.5 mM DSS, although cross-linking was rather inefficient under these conditions. Therefore we increased incubation times to 45 min which considerably increased yield of cross-linked proteins (Figure 11B). Mdm38-HIS-TAP was detected in its monomeric and apparently dimeric conformation (*black arrows*; bottom and top, respectively), as well as part of undefined intermediate and higher order cross-link products (*black arrowheads*), suggesting the presence of additional proteins in the complex.

To reduce possible contaminations and false-positive interactions caused by cross-linking of whole mitochondria, we tried to cross-link Mdm38-HIS-TAP after solubilization using 1.2% TX-100. Unfortunately, all our attempts failed (Figure 11C). Also variation of buffer conditions, cross-linking reagents and concentrations did not prove successful (data not shown). When DSS and detergents (TX-100 or SDS) were added to mitochondria at the same time cross-linking principally worked, but Western blot signals appeared as smears rather than individual bands (Figure 11D), making evaluation of cross-linking difficult. Therefore we decided to purify the Mdm38-HIS-TAP complex after cross-linking whole mitochondria.

Initial cross-link experiments were typically performed in small reaction volumes (100 μ l). Since we planned to use 200 mg of crude mitochondria for purifications, we tried to increase cross-link reaction volumes. Unexpectedly, cross-linking failed when the volumes exceeded 0.5 ml, although DSS to protein ratios were kept constant. Due to these experimental limitations we performed affinity purification of the Mdm38p complex without prior cross-linking.

5.3.3. Protein A affinity purification of Mdm38-HIS-TAP

Before starting protein A – CBP TAP, we first optimized the individual TAP steps and determined their purification efficiency. After solubilization of mitochondria isolated from strain DBY-*MDM38*-HIS-TAP with 1.2% TX-100, protein extracts were incubated with IgG Sepharose beads and incubated for 2 h at 4°C. Unbound proteins were eluted by gravity flow and beads were washed with two column volumes of solubilization buffer. Bound proteins were eluted by TEV protease cleavage performed at 16°C in presence of 0.8% TX-100. To elute residual bound proteins, beads were treated with 0.1 M glycine buffer, pH 3 (see Materials and Methods for details).

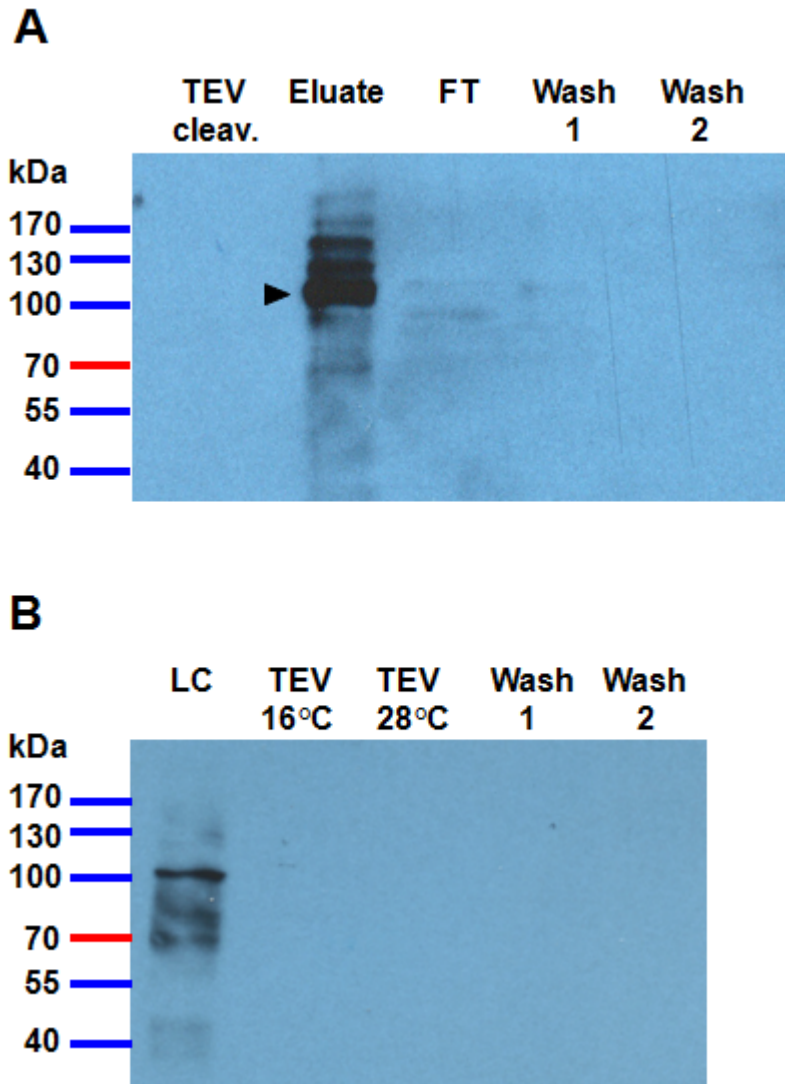


Figure 12: Protein A is not cleavable by TEV protease from HIS-TAP-tagged Mdm38p

A. Protein A affinity chromatography was performed with mitochondria from strain DBY747 expressing chromosomally HIS-TAP-tagged *MDM38*, solubilized with 1.2% TX-100 (see Materials and Methods). After binding of Mdm38-HIS-TAP to IgG beads and washing steps (Wash 1 and 2), TEV protease cleavage was performed in presence of 0.8% TX-100 at 16°C to elute proteins (TEV cleav.). Residual bound proteins were eluted with 0.1 M glycine buffer, pH 3 (Eluate). Fractions of each purification step were TCA precipitated, subjected to SDS-PAGE, and immunodetected with an antibody directed against CBP. Mdm38p is marked by a *black arrowhead*. TEV cleavage failed, since Mdm38p was not detected in lane 1. FT, flow-through; CBP, calmodulin binding peptide.

B. Protein A affinity chromatography was performed as described in A, with the difference that the TX-100 concentration was stepwise reduced to a final concentration of 0.1% during TEV cleavage, which was performed at 16°C and 28°C. Again, TEV cleavage failed under all tested conditions. LC, loading control.

Equal amounts of each fraction were TCA precipitated, subjected to SDS-PAGE and immunodetected with an antibody directed against the calmodulin binding peptide (Figure 12A). Surprisingly, Mdm38p could not be detected in the TEV cleavage fraction (lane 1). Binding to IgG beads was successful, as the flow through and washing fractions contained only marginal amounts of Mdm38-HIS-TAP. Since Mdm38p was only eluted after glycine treatment (*black arrowhead*), TEV cleavage obviously failed under these conditions. Further increasing TEV protease concentration did not improve cleavage (data not shown). Additional bands visible above the Mdm38-HIS-TAP monomer in lane 2 may result from bound IgG molecules.

To determine if TX-100 interfered with TEV cleavage efficiency, we reduced the TX-100 concentration during the washing steps to 0.1%. Cleavage was also performed at 28°C to increase the protease activity (Figure 12B). Unfortunately, TEV cleavage failed under all tested conditions, suggesting inaccessibility of the TEV cleavage site.

5.3.4. CBP affinity purification of Mdm38-HIS-TAP

Solubilized protein extracts of mitochondria isolated from strain *DBY-MDM38-HIS-TAP* were incubated with calmodulin affinity resin in presence of 2 mM calcium for 2 h at 4°C. After washing, bound proteins were eluted with elution buffer containing EGTA. Residual bound proteins were eluted with 0.1 M glycine buffer, pH 3. Equal amounts of each elution fraction were TCA precipitated, subjected to SDS-PAGE and immunodetected with an antibody directed against CBP. In presence of 2 mM EGTA elution was rather inefficient, given by detection of Mdm38-HIS-TAP in several elution fractions (Figure 13, *left panel*). Elution with 4 mM EGTA resulted in a markedly higher protein concentration within early elution fractions, although some protein still remained bound to the calmodulin beads (Glycine lane, *right panel*).

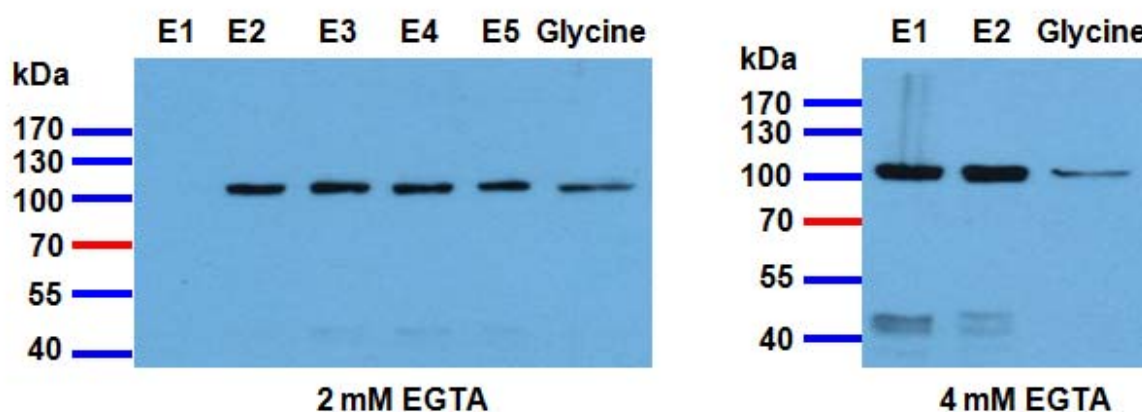


Figure 13: CBP affinity chromatography of HIS-TAP-tagged Mdm38p

Mitochondria isolated from strain DBY747 expressing chromosomally HIS-TAP-tagged *MDM38* were solubilized using 1.2% TX-100. After binding to calmodulin beads and washing steps, bound proteins were eluted with elution buffer containing 2 mM EGTA (*left panel*). To concentrate purified proteins in the elution fractions, EGTA concentration was increased to 4 mM (*right panel*). Residual bound proteins were eluted with 0.1 M glycine buffer, pH 3 (Glycine). Individual elution fractions (E) were TCA precipitated, subjected to SDS-PAGE, and immunoblotted with an anti-CBP antibody.

5.3.5. CBP – protein A TAP of Mdm38-HIS-TAP

Since elution of Mdm38p upon TEV protease cleavage was not possible, we performed TAP in the reverse order. CBP - protein A TAP was accomplished according to the individual purification steps described before. After CBP purification, proteins were eluted in presence of 4 mM EGTA and the first three elution fractions were used for subsequent protein A affinity chromatography. Thereafter proteins were eluted with glycine buffer, allowing only denaturing SDS-PAGE for protein detection. Eluted proteins were TCA precipitated, Western blotted and Mdm38-HIS-TAP was successfully immunodetected with an antibody directed against CBP (Figure 14). However, the protein concentration was too low to be detected by Coomassie staining (data not shown). This may result from protein loss during binding and washing steps and from incomplete elution. Furthermore, purification under these conditions is problematic, since the presence of the Mdm38p complex after CBP – protein A TAP cannot be verified by Blue native electrophoresis.

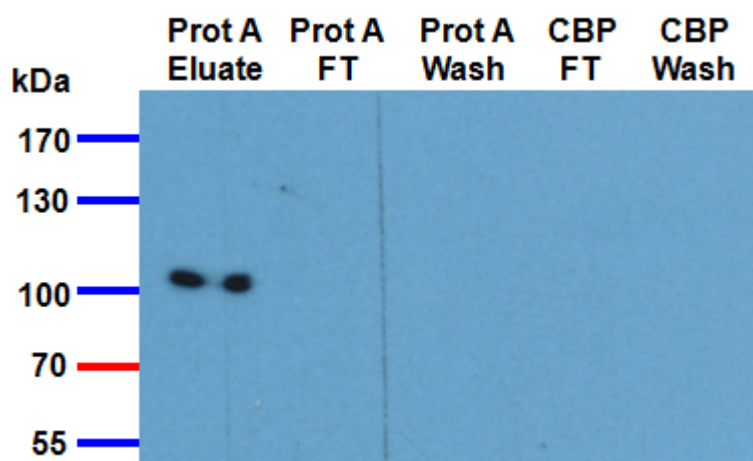


Figure 14: CBP – protein A TAP of Mdm38-HIS-TAP

DBY747 mitochondria expressing chromosomally HIS-TAP-tagged *MDM38* were subjected to TAP. Since the protein A tag could not be removed by TEV protease cleavage (Fig. 7), tandem purification was performed in the reverse order. After solubilization using 1.2% TX-100, CBP purification and EGTA elution of bound proteins was carried out and the collected fractions were applied to IgG chromatography. Purified proteins were eluted with 0.1 M glycine buffer, pH 3 (ProtA Eluate). Individual fractions were TCA precipitated, subjected to SDS-PAGE, and immunoblotted with an antibody against CBP. FT, flow-through.

5.3.6. Ni-NTA - CBP tandem affinity purification of Mdm38-HIS-TAP

To overcome the limitations of CBP - protein A TAP, we replaced the protein A step by Ni-NTA affinity chromatography using the present 6xHIS tag. We initially tested the individual purification steps for their protein binding capacity. For CBP affinity chromatography mitochondria isolated from strain DBY-*MDM38*-HIS-TAP were treated as described in chapter 5.3.4. For Ni-NTA affinity chromatography solubilized protein extracts were incubated with Ni-NTA Superflow resin for 30 min at 4°C. After washing, proteins were eluted in presence of 200 mM imidazole (see Materials and Methods for details).

To verify the presence of the Mdm38p complex after elution, we performed Blue native electrophoresis. Equal amounts of the first three elution fractions were loaded on a native 5-18% polyacrylamide gradient gel. Proteins were transferred to a PVDF membrane and Mdm38-HIS-TAP was detected by immunoblotting with antibodies either directed against the 6xHIS or the protein A epitope (Figure 15, *left and right panel*, respectively).

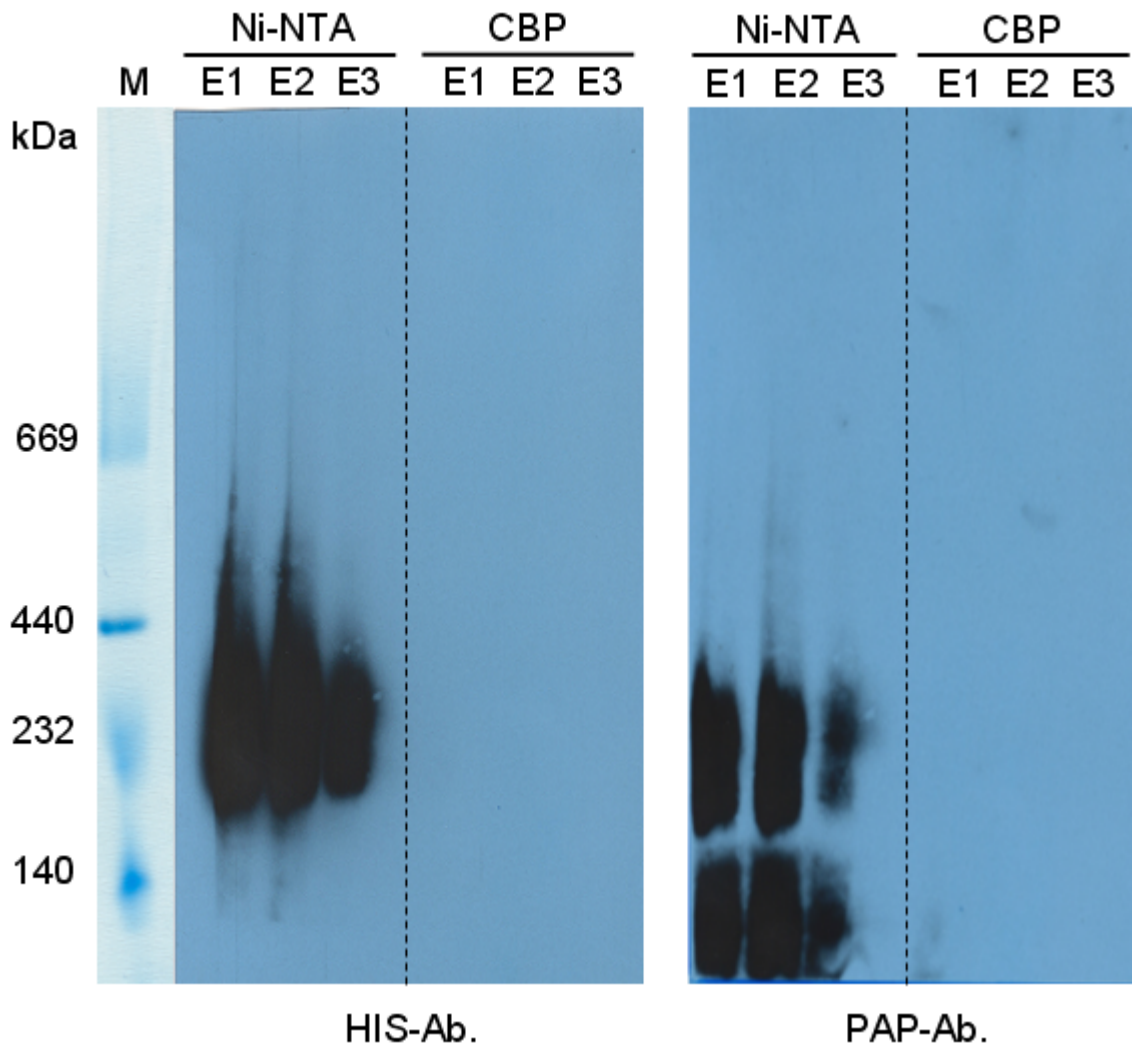


Figure 15: Ni-NTA - CBP affinity chromatography of HIS-TAP-tagged Mdm38p

Mitochondria from strain DBY747 expressing chromosomally HIS-TAP-tagged *MDM38* were isolated. Proteins were solubilized using 1.2% TX-100 and subjected to Ni-NTA or CBP affinity chromatography under native conditions (see Materials and Methods). After purification, elution fractions (E1-E3) were separated by Blue native electrophoresis, transferred to a PVDF membrane, and immunodetected with an antibody directed against the 6xHIS epitope (*left panel*) and protein A (PAP-Ab., *right panel*). Both antibodies detected Mdm38p as part of a complex of ~230 kDa, whereas the protein A antibody additionally recognized Mdm38p below 140 kDa. Ni-NTA, nickel-nitrilotriacetic acid; M, protein marker.

Mdm38-HIS-TAP was not detected in any of the elution fractions obtained from CBP affinity chromatography. In contrast, Ni-NTA purification recovered Mdm38-HIS-TAP as part of two protein complexes, suggesting a much higher protein binding capacity of the Ni-NTA Superflow resin compared to calmodulin beads. Interestingly, the anti-HIS antibody recognized a complex of ~ 230 kDa corresponding to the putative Mdm38-HIS-TAP dimer (*left panel*), whereas the anti-protein A antibody detected an additional complex below 140 kDa, likely representing the Mdm38-HIS-TAP monomer (*right panel*), although hetero-oligomerization with additional proteins can not be excluded. Resolution of the Western blot signals did not allow a clear evaluation if the ~ 230 kDa complex consisted of two individual complexes larger and smaller than 230 kDa. The fact that the anti-HIS antibody did not recognize the complex below 140 kDa strongly suggests that the HIS epitope of the Mdm38-HIS-TAP monomer is not accessible. However, neither antibody recognized the ~ 550 kDa Mdm38p complex detected prior to affinity chromatography (Figure 10). Similar results were obtained after TAP in the order Ni-NTA followed by CBP purification, whereas TAP in the reverse order completely failed to recover Mdm38-HIS-TAP (data not shown). Despite changing buffer conditions including detergent concentration and ionic strength or incubation time with the beads, the ~ 550 kDa complex remained undetectable after Ni-NTA - CBP tandem purification.

These findings may either result from dissociation of the complex during the purification procedure or inaccessibility of Mdm38-HIS-TAP, possibly caused by steric hindrance due to association of additional proteins, or by special folding and orientation of Mdm38p within the ~ 550 kDa complex.

5.3.7. Size exclusion chromatography (SEC) of Mdm38-HIS-TAP

To determine the stability of the ~ 550 kDa Mdm38p complex, we performed SEC of crude mitochondrial extracts containing Mdm38-HIS-TAP. SEC was developed to separate molecules in solution based on their size (Lathe & Ruthven, 1955). The methodological principle is shown in Figure 16.

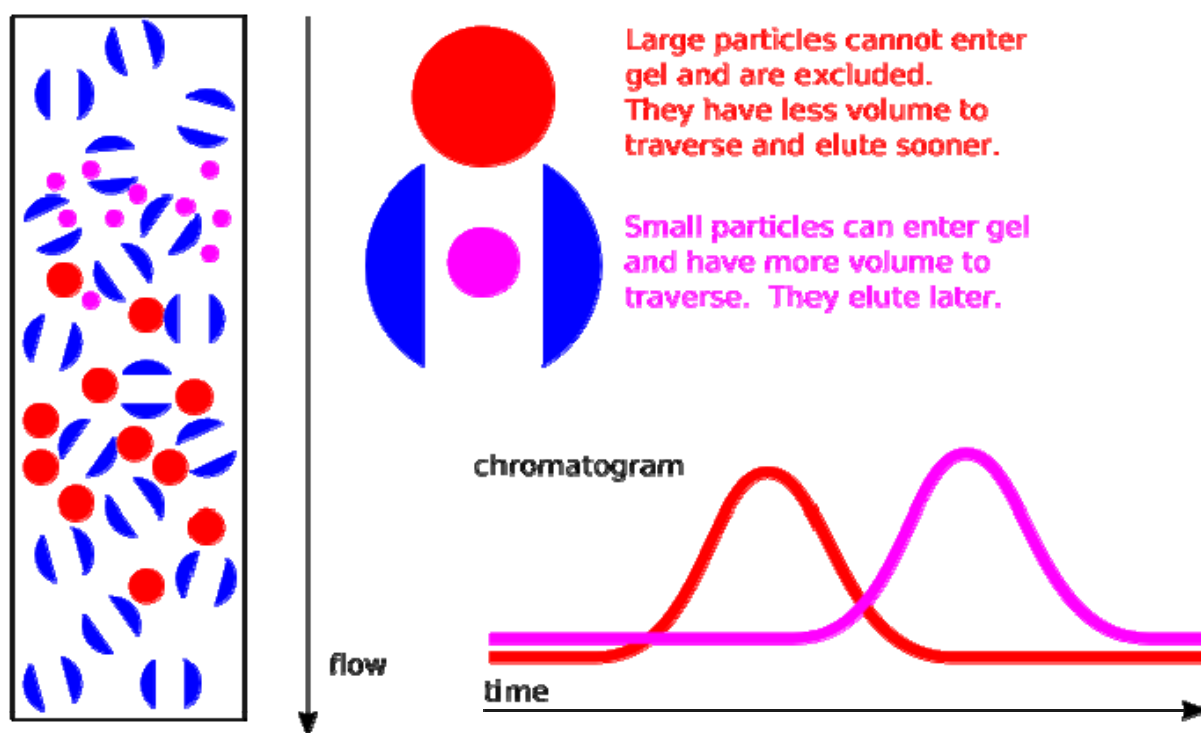


Figure 16: Size exclusion chromatography (SEC)

Schematic representation of the protein separation principle of SEC. Figure adapted from <http://en.wikipedia.org>.

Crude mitochondria isolated from strain *DBY-MDM38-HIS-TAP* were solubilized with 1.2% TX-100. To mimic the elution conditions after Ni-NTA affinity chromatography, the protein extract was supplemented with 200 mM imidazole and the TX-100 concentration was reduced to 0.6% by dilution with elution buffer (see Materials and Methods for details). Thereafter the protein solution was subjected to SEC using a 26/60 Superdex 200 column (Amersham).

The elution profile showed that the main protein part eluted in two broad peaks, indicated as pool 1 and 2 in Figure 17. The intact Mdm38p complex was expected to be collected in subfraction Fr1 of pool 1, corresponding to a molecular weight between ~ 500 and ~ 650 kDa.

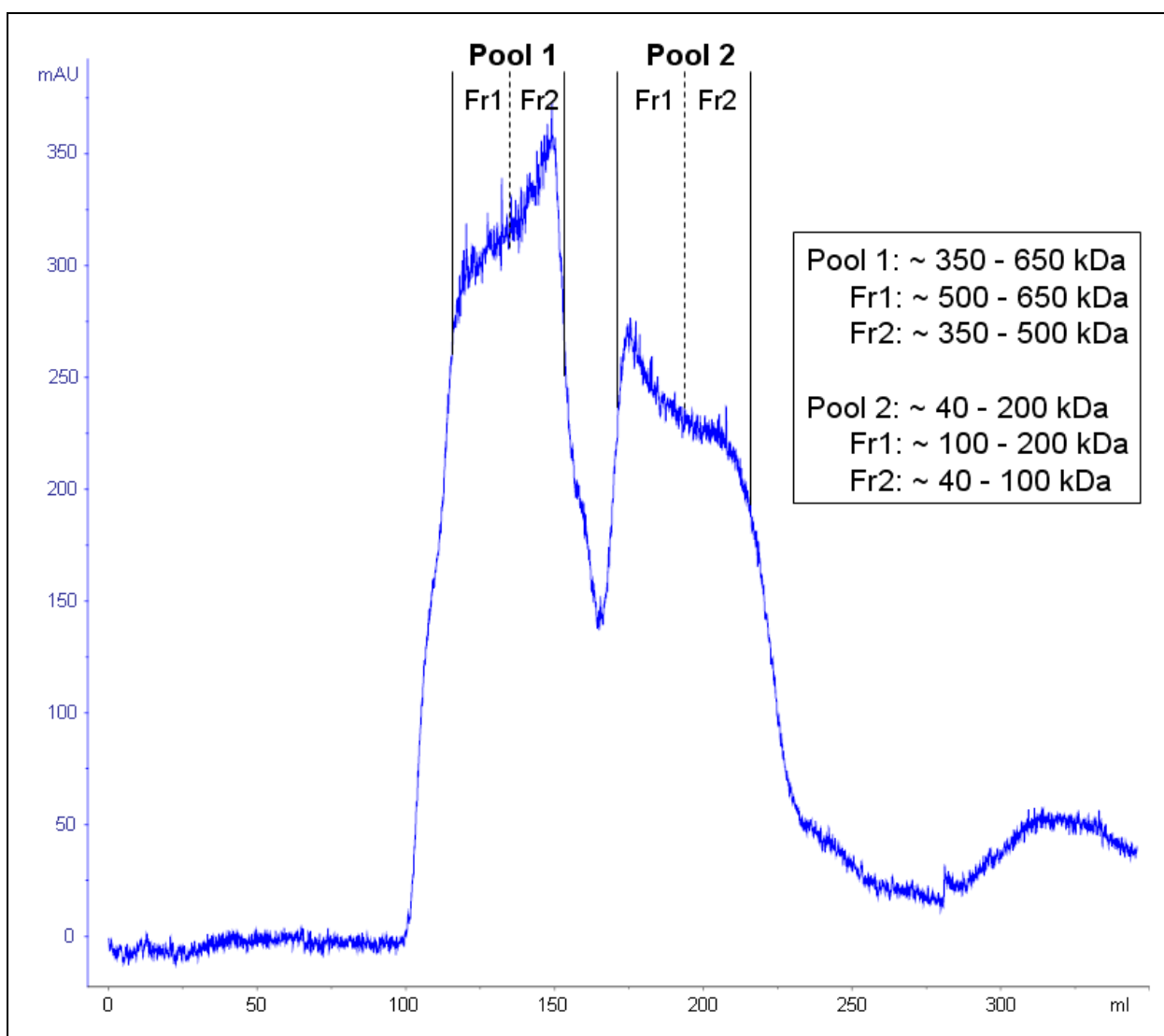


Figure 17: SEC chromatogram of crude mitochondrial extract containing Mdm38-HIS-TAP

DBY747 mitochondria expressing chromosomally HIS-TAP-tagged *MDM38* were solubilized using 1.2% TX-100. Afterwards the supernatant was adjusted to conditions mimicking elution after Ni-NTA purification and loaded on a 26/60 Superdex 200 column. Most proteins eluted in two broad peaks, designated as pool 1 and 2 and subdivided into fractions Fr1 and Fr2. The indicated legend on the right refers to the molecular weight range of each pool and subfraction. mAU, milliampere units.

5.3.8. The Mdm38p complex is intact after SEC

To determine which pool contained most of Mdm38-HIS-TAP, we used equal amounts of both pools for Ni-NTA affinity purification. The first four elution fractions of each pool were TCA precipitated and subjected to SDS-PAGE. Mdm38-HIS-TAP was detected by

immunoblotting with an antibody directed against the 6xHIS epitope. The predominant part of Mdm38p was detected in pool 1 (Figure 18A, *black arrowheads*). Additional bands represent Mdm38p degradation caused by precipitation as well as some unspecific signals.

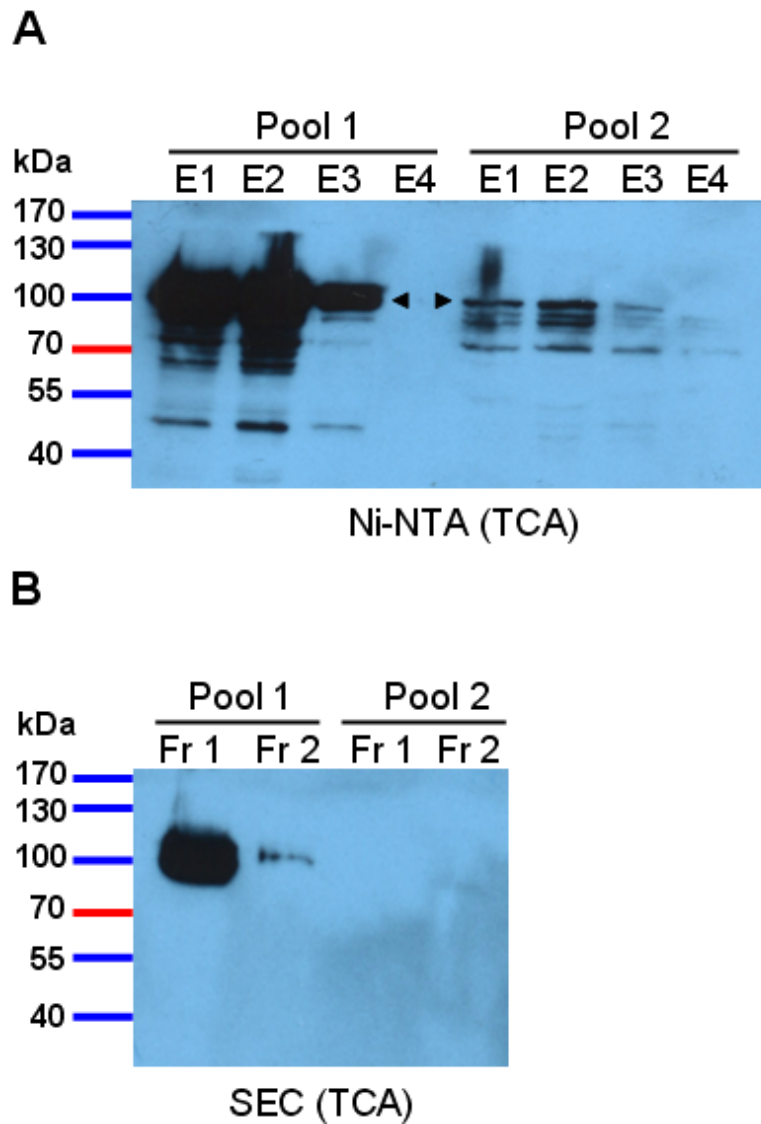


Figure 18: The Mdm38p high molecular weight complex is intact after SEC

A. After SEC, equal amounts of pool 1 and 2 were used for Ni-NTA affinity chromatography. Elution fractions (E1-E4) were TCA precipitated, subjected to SDS-PAGE and probed with an antibody against 6xHIS. The major part of HIS-TAP-tagged Mdm38p was detected in pool 1 (Mdm38-HIS-TAP is indicated by *black arrowheads*).

B. Directly after SEC, equal amounts of elution fractions (Fr 1 and 2) of pool 1 and 2 were TCA precipitated, subjected to SDS-PAGE, and immunodetected against 6xHIS. The major part of HIS-TAP-tagged Mdm38p was detected in elution fraction Fr 1 of pool 1, representing the subfraction containing proteins of a molecular weight between ~ 500 and ~ 650 kDa.

Due to the high protein concentration of Mdm38-HIS-TAP present in the elution fractions, we also TCA precipitated equal amounts of the subfractions of both pools directly after SEC and performed Western blots as described before. Results clearly show that most of Mdm38p was eluted in subfraction Fr 1 of pool 1 (Figure 18B). Although we can not exclude dissociation of the Mdm38p complex during Blue native electrophoresis, these results suggest that the ~ 550 kDa complex was intact after affinity purification.

5.4. Single-step HIS and Strep affinity purification of chromosomally tagged Mdm38p

Based on these results we concluded: (i) Ni-NTA affinity chromatography was by far the most efficient method for purification of Mdm38p; (ii) the ~ 550 kDa Mdm38p complex is most likely stable enough to endure the purification procedure; and (iii) the nature of the affinity tag seems to be important for accessibility and detection of Mdm38p. We decided to optimize the Ni-NTA purification and also performed Strep affinity chromatography to reduce contamination by endogenous proteins, since the 6xHIS sequence, in contrast to the Strep sequence, naturally occurs within some yeast proteins. Finally, we tested the One-Strep tag, a novel affinity tag especially developed for purification of not easily accessible protein complexes (Junttila *et al.*, 2005).

5.4.1. Affinity chromatography using One-Strep-tagged Mdm38p allows recovery of the high molecular weight complex

Since the 6xHIS epitope of the HIS-TAP-tagged Mdm38p monomer was not accessible to the anti-HIS antibody after Blue native electrophoresis (Figure 15), we speculated that this may be due to the localization of the HIS tag between Mdm38p and the bulky TAP tag. To avoid possible steric hindrance of the HIS tag, we created a strain bearing a C-terminal fusion of 6xHIS with *MDM38*. Additionally, we also chromosomally fused the eight-residue Strep tag and the so called One-Strep tag, which is composed of two Strep tags separated by a flexible linker region (Figure 19). This latter tag should enhance binding affinity and purification yield of the fusion protein due to the tandem arrangement of two Strep tags. Furthermore, the linker region increases accessibility of the tagged component of a protein complex to the affinity resin (Junttila *et al.*, 2005). The tagging procedure is described in detail in the Materials and Methods section.

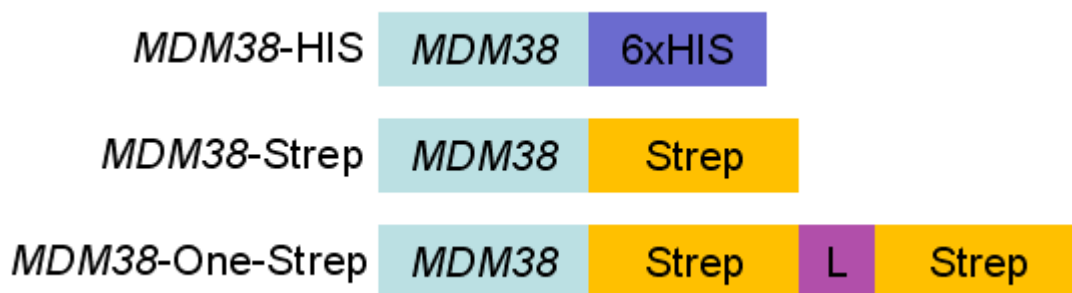


Figure 19: PCR-based genomic tagging of *MDM38*

Schematic representation of chromosomally HIS-, Strep-, and One-Strep-tagged *MDM38*. Affinity tags were introduced C-terminally in-frame with the *MDM38* ORF into strain DBY747 by homologous recombination of PCR fragments amplified from plasmid pBS1479 (see Materials and Methods). L, linker.

DBY747 mitochondria expressing chromosomally HIS-, Strep- or One-Strep-tagged *MDM38* were solubilized with 1.2% TX-100. Extracts containing Mdm38-HIS were subjected to Ni-NTA affinity chromatography as described in chapter 5.3.6. for HIS-TAP-tagged Mdm38p. Strep- and One-Strep-tagged Mdm38p was purified by Strep affinity chromatography under identical conditions. Solubilized extracts were incubated with Strep-Tactin Superflow for 30 min at 4°C and purified proteins were eluted in presence of 2.5 mM D-desthiobiotin (see Materials and Methods for details).

The first two elution fractions were used for Blue native electrophoresis and after transfer to a PVDF membrane Mdm38p was detected by probing with antibodies directed against the 6xHIS or the Strep epitopes (Figure 20). Interestingly, Mdm38-HIS was detected as part of a complex larger than 140 and smaller than 232 kDa corresponding to a putative Mdm38-HIS dimer (*left panel*), suggesting that simple removal of the TAP tag did not increase accessibility of the ~ 550 kDa complex.

Purification of Mdm38-Strep resulted in recovery of Mdm38p in a complex of similar size as shown for Mdm38-HIS. Only a minor part was detected as a complex of unknown composition slightly below 140 kDa (*middle panel*).

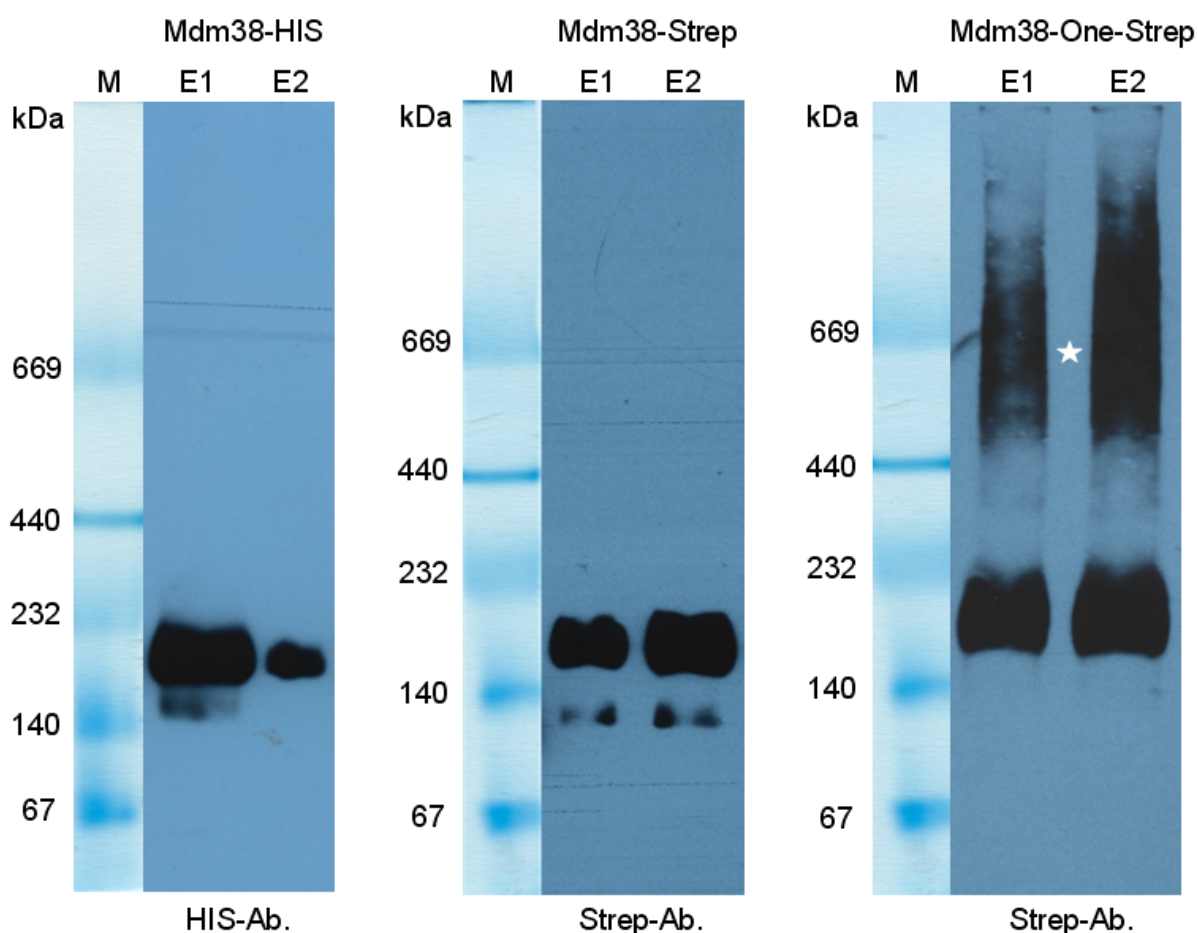


Figure 20: Affinity chromatography using One-Strep-tagged Mdm38p

Mitochondria isolated from strain DBY747 expressing chromosomally HIS-, Strep-, or One-Strep-tagged *MDM38* were solubilized using 1.2% TX-100. The supernatant containing HIS-tagged Mdm38p was subjected to Ni-NTA affinity chromatography. Strep- and One-Strep-tagged Mdm38p was subjected to Strep affinity purification under identical conditions. After purification, elution fractions (E1-E2) were separated by Blue native electrophoresis on a native 5-18% polyacrylamide gradient gel, transferred to a PVDF membrane and immunoblotted against the 6xHIS epitope (*left panel*) and the Strep epitopes (*middle and right panel*). HIS-, Strep-, and One-Strep-tagged Mdm38p was detected between 140 and 232 kDa, only Mdm38-One-Strep was additionally recovered as part of a complex between 440 and 669 kDa (*white asterisk, right panel*).

Finally, also One-Strep-tagged Mdm38p was detected between 140 and 232 kDa (*right panel*), but most importantly, only Mdm38-One-Strep was additionally recovered as part of a complex with a molecular weight between 440 and 669 kDa (indicated by *white asterisk*). These experiments showed that the One-Strep tag was crucial for successful purification of the high molecular weight complex. Since monomeric Mdm38p was not detected in either case, independently of the fused tag, most of Mdm38p seems to be incorporated in higher order complexes under physiological conditions.

5.4.2. Purity of single-step affinity chromatography is limited

Since the One-Strep tag was principally designed to purify proteins in a single step, we determined the efficiency and yield of the Mdm38-One-Strep purification.

Mitochondria of strains *DBY-MDM38-OS* and *DBY747wt* were isolated and Strep affinity purification was performed exactly as described above. The first two elution fractions were combined, TCA precipitated, and subjected to SDS-PAGE. Proteins were visualized by Coomassie staining and Mdm38-One-Strep was detected by probing with an antibody directed against the Strep epitope (Figure 21, *left and right panel*, respectively).

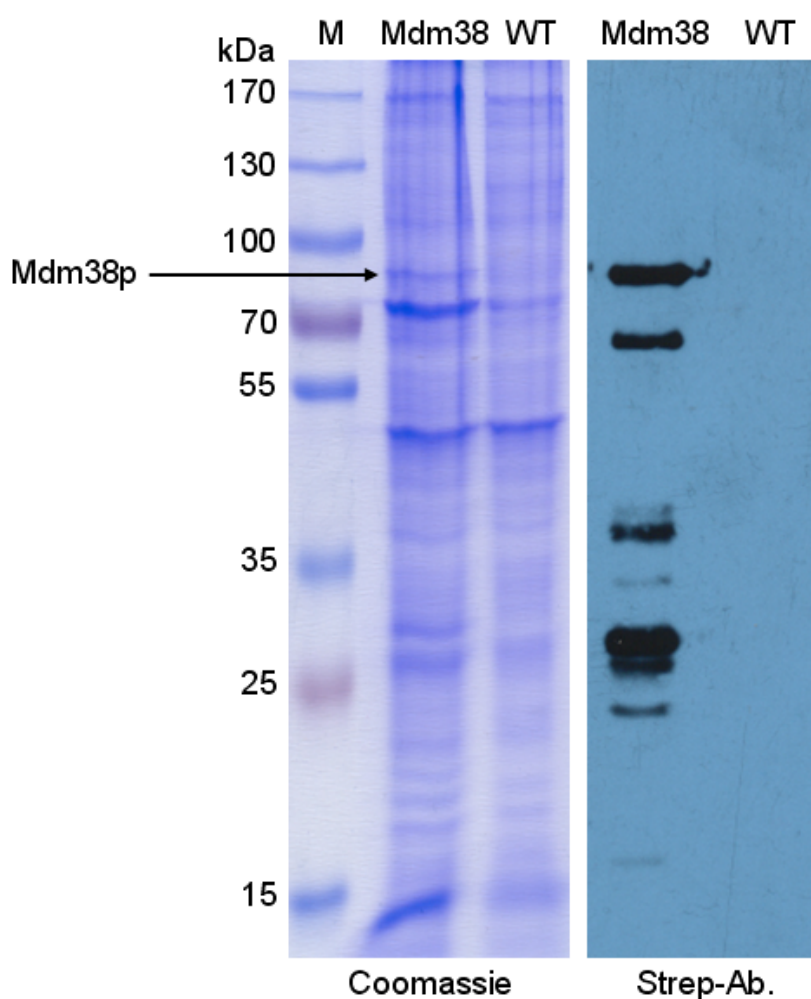


Figure 21: TCA precipitation of Mdm38-One-Strep elution fractions

After Strep affinity purification of One-Strep-tagged Mdm38p, elution fractions containing the highest amount of the Mdm38p protein complex were combined, TCA precipitated and subjected to SDS-PAGE (Mdm38). To assess purification efficiency and purity, wild-type mitochondria were processed identically (WT). Proteins were detected by Coomassie staining and immunodetection with an antibody directed against the Strep epitope. *Black arrow* indicates full length Mdm38-One-Strep.

Western blot signals point to a strong degradation of Mdm38p, possibly caused by TCA precipitation. Nevertheless, enrichment of Mdm38-One-Strep was efficient enough to be visualized by Coomassie staining (*black arrow* indicates full length Mdm38-One-Strep). However, the single-step purification was obviously not capable to remove most of the contaminating proteins, as many protein bands present in the Mdm38 elution fraction also appeared in the wild-type control fraction (Figure 21, *left panel*).

The mass spectrometry analysis of the Coomassie band representing full length Mdm38-One-Strep confirmed this observation, as besides Mdm38p dozens of proteins were detected within the sample (data not shown). Therefore, we decided to analyze the ~ 550 kDa Mdm38p complex directly from the Blue native gel, as electrophoresis itself acts as a second purification step.

5.4.3. Mass spectrometry (MS) analysis of the Mdm38-One-Strep complex

Strep affinity chromatography and Blue native electrophoresis of DBY747 mitochondria expressing One-Strep-tagged *MDM38* and of wild-type mitochondria was performed exactly as described in chapter 5.4.1. The presence of the ~ 550 kDa complex after purification was confirmed by immunodetection (data not shown). A gel piece containing the Mdm38-One-Strep complex was cut out from the Blue native gel based on Western blot signals. A control sample was also cut out at the same position in the wild-type lane (as schematically shown in Figure 7).

The gel pieces were analyzed by MS and protein hits of both samples were compared. In total, 55 and 86 proteins were detected in the Mdm38p complex and wild-type sample, respectively. Besides Mdm38p, six other proteins were only detected in the Mdm38p complex sample (see Table 3) and 48 proteins were present in both gel pieces.

Of those 48 proteins, 18 were components of ribosomal subunits. Therefore, the three ribosomal proteins detected in the Mdm38p complex sample likely represent contaminations. The other proteins identified are Ygr026wp, Ssc1p, and Erg5p. Ygr026wp is an uncharacterized protein localized to the cell periphery (Huh *et al.*, 2003). Ssc1p is an essential mitochondrial Hsp70 family ATPase, involved in protein import across the inner mitochondrial membrane and in protein folding in the mitochondrial matrix (Kang *et al.*, 1990; Liu *et al.*, 2001). Finally, Erg5p is a cytochrome P450 enzyme facilitating the penultimate step in ergosterol biosynthesis (Kelly *et al.*, 1995; Skaggs *et al.*, 1996).

Facing the relatively high number of proteins present after single-step purification, we decided to employ TAP, using a combination of Ni-NTA and Strep affinity chromatography, to increase the purity of our preparations and to confirm our preliminary results.

Table 3: Proteins identified by MS analysis of the Mdm38-One-Strep protein complex

The table contains the seven genes encoding the proteins only present in the Mdm38-One-Strep sample and not in the wild-type control sample. The score in the table represents the Mascot score of the sequenced peptides. The right column gives a brief description of the protein's function according to the *Saccharomyces* Genome Database (SGD) (<http://genome-www.stanford.edu/Saccharomyces/>).

Systematic Name	Standard Name	Molecular weight (kDa)	Score	Description
<i>YOL027C</i>	<i>MDM38</i>	65	352	Mitochondrial inner membrane protein, required for K ⁺ /H ⁺ exchange; human ortholog Letm1 implicated in Wolf-Hirschhorn syndrome
<i>YMR015C</i>	<i>ERG5</i>	61.3	108	C-22 sterol desaturase, a cytochrome P450 enzyme that catalyzes the formation of the C-22(23) double bond in the sterol side chain in ergosterol biosynthesis
<i>YJR045C</i>	<i>SSC1</i>	70.6	68	Hsp70 family ATPase, constituent of the import motor component of the Translocase of the Inner Mitochondrial membrane (TIM23 complex); involved in protein translocation and folding; subunit of Scel endonuclease
<i>YGR026W</i>	<i>YGR026W</i>	33.2	119	Uncharacterized
<i>YHR203C</i>	<i>RPS4B</i>	29.4	59	Protein component of the small (40S) ribosomal subunit; identical to Rps4Ap and has similarity to rat S4 ribosomal protein
<i>YOR369C</i>	<i>RPS12</i>	15.5	77	Protein component of the small (40S) ribosomal subunit; has similarity to rat ribosomal protein S12
<i>YBR191W</i>	<i>RPL21A</i>	18.2	68	Protein component of the large (60S) ribosomal subunit, nearly identical to Rpl21Bp and has similarity to rat L21 ribosomal protein

5.5. Ni-NTA – Strep TAP of vector expressed Mdm38p

For Ni-NTA – Strep TAP of Mdm38p we created a vector construct expressing One-Strep-HIS (OSH)-tagged *MDM38*. For this purpose we C-terminally fused the 6xHIS tag to One-Strep-tagged *MDM38* by PCR amplification from chromosomal DNA of strain DBY-*MDM38*-OS. The PCR product was then cloned into the centromeric plasmid YCplac22 (see Materials and Methods for details). A schematic representation of the vector construct is shown in Figure 22A.

5.5.1. OSH-tagged Mdm38p restores the respiratory growth defect of *mdm38Δ* mutant cells

To test for correct function of OSH-tagged Mdm38p, the ability to complement the respiratory growth defect of *mdm38Δ* mutant cells was investigated. Therefore, serial dilutions of wild-type strain DBY747 and the isogenic mutant strain DBY*mdm38Δ* bearing the empty plasmid YCplac22 or expressing OSH-tagged *MDM38* (YCp22-*MDM38*-OSH) were spotted on fermentable (YPD) and non-fermentable media (YPG, YPdG, and YPEG) and incubated at 28°C (Figure 22B).

A



B

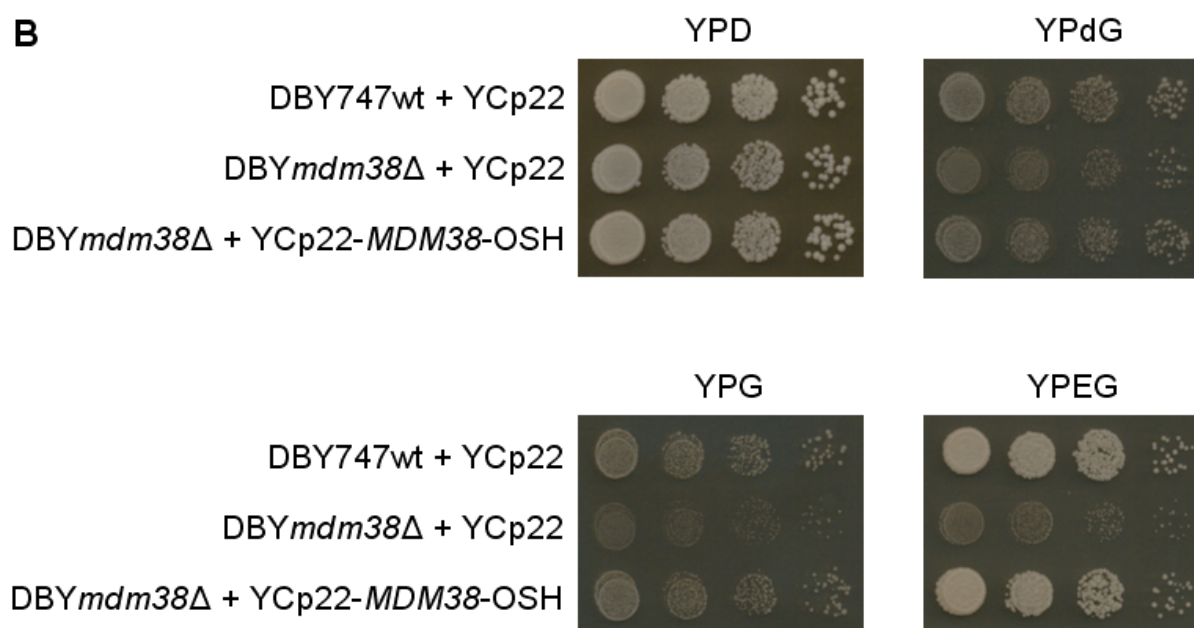


Figure 22: Ni-NTA - Strep TAP construct

A. OSH-tagged *MDM38* was PCR-amplified from chromosomal DNA of strain DBY747 bearing One-Strep-tagged *MDM38* (DBY-*MDM38*-OS) and cloned into the centromeric plasmid YCplac22 (see Materials and Methods for details). OSH, One-Strep-HIS.

B. Overnight cultures of yeast strains DBY747wt and DBY*mdm38Δ* carrying the empty YCplac22 vector or expressing OSH-tagged *MDM38* (YCp22-*MDM38*-OSH) were adjusted to $OD_{600} = 1$, ten-fold serial dilutions were incubated at 28°C for two days on YPD plates and for four days on YPdG, YPG, and YPEG plates. Reduced growth of the *mdm38Δ* mutant strain on non-fermentable media was completely restored upon expression of OSH-tagged *MDM38*.

In contrast to the respiratory deficient mutant strain *DBYmdm38Δ* carrying the empty plasmid, expression of OSH-tagged Mdm38p completely restored growth on non-fermentable media, suggesting normal function of tagged Mdm38p.

5.5.2. The Mdm38p complex is intact after Ni-NTA – Strep TAP

For Ni-NTA – Strep TAP mitochondria were isolated from strains *DBY747wt* carrying the empty *YCplac22* plasmid and *DBYmdm38Δ* expressing OSH-tagged *MDM38* from plasmid *YCp22-MDM38-OSH*. Mitochondria were treated exactly as described for single-step purifications. In order to optimize the purification efficiency, solubilized protein extracts were first subjected to Ni-NTA affinity chromatography and then to Strep affinity chromatography, as well as *vice versa* (see Materials and Methods for details).

To verify the presence of the Mdm38p complex after TAP, eluted proteins were subjected to Blue native electrophoresis and immunodetected with an antibody directed against the Strep epitope (Figure 23). Interestingly, the Mdm38 protein yield and migration varied and correlated with the order of purification steps. In fact, Mdm38-OSH was exclusively detected as part of a high molecular weight complex ranging between 440 and 669 kDa, in addition to the smaller complex with a molecular weight between 140 and 232 kDa, when Ni-NTA preceded the Strep purification. The opposite order of purification steps yielded less Mdm38p and resulted in recovery of only the smaller Mdm38p complex ranging between 140 and 232 kDa (Figure 23). Thus, detection of the Mdm38p complex likely failed because of protein loss during Strep purification, caused by the lower protein binding capacity of Strep-Tactin Superflow as compared to Ni-NTA Superflow resin. However, although the majority of Mdm38p was recovered as part of the smaller complex, Ni-NTA – Strep TAP allowed for purification of the intact ~ 550 kDa Mdm38p complex.

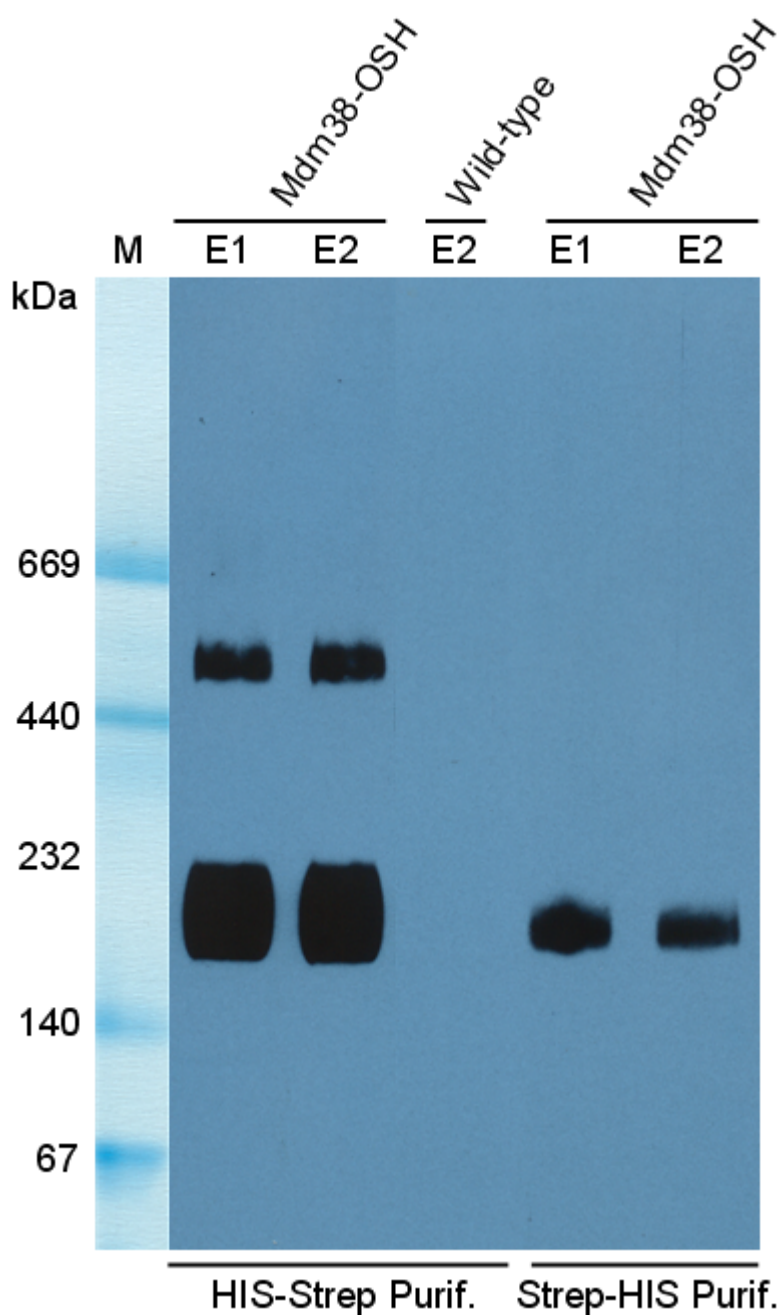


Figure 23: TAP of OSH-tagged Mdm38p

Mitochondria isolated from strains DBY747wt and DBY $mdm38\Delta$ expressing OSH-tagged *MDM38* from plasmid YCp22-*MDM38*-OSH were solubilized using 1.2% TX-100. The clarified supernatants were first subjected to Ni-NTA affinity chromatography and then to Strep affinity chromatography (HIS-Strep Purif.) or *vice versa* (Strep-HIS Purif.). Elution fractions (E1-E2) were separated by Blue native electrophoresis on a 5-18% polyacrylamide gradient gel, transferred to a PVDF membrane, and probed with an antibody directed against the Strep epitope. Only after HIS-Strep affinity chromatography Mdm38-OSH was recovered as part of a complex between 440 and 669 kDa.

5.5.3. Ssc1p and Erg5p co-elute with Mdm38-OSH after Ni-NTA – Strep TAP

To confirm the co-purification of the proteins detected by MS analysis of the Mdm38p complex directly from the Blue Native gel (chapter 5.4.3., Table 3), we repeated TAP in the order Ni-NTA followed by Strep purification exactly as described above. To compare the purity of the preparation with single-step purification (see Figure 21), the first two elution fractions were TCA precipitated, separated by SDS-PAGE, and the gel was stained with Coomassie Brilliant Blue. As controls, DBY747 wild-type mitochondria carrying the empty YCplac22 plasmid and mitochondria isolated from strain DBY*mrs2* Δ expressing OSH-tagged *MRS2* from plasmid YCp22-*MRS2*-OSH were processed identically (Figure 24). Mrs2p, which is a mitochondrial inner membrane Mg²⁺ channel, was used to identify possible mitochondria-specific contaminations remaining after purification.

The protein band patterns of all purifications were compared. Bands present in all three lanes were judged as contaminating proteins. Surprisingly, the Mrs2-OSH and wild-type patterns were identical, only the protein amounts differed in some cases (e.g. bands between 40 and 55 kDa). Mrs2p-OSH (~ 64 kDa) was also not detectable by Coomassie staining, probably because of suboptimal purification conditions for Mrs2p. More importantly, only four protein bands were solely found in the Mdm38-OSH lane (indicated by *black arrows*). These were cut out and analyzed by MS. As expected, the uppermost band was identified as Mdm38p and the lowest band turned out to be a degradation product of Mdm38p, similar to what we observed after single-step Strep purification of Mdm38-One-Strep (Figure 21).

The two protein bands in between were identified as Ssc1p and Erg5p, thereby confirming our first MS results (Table 3). The other four proteins previously detected by MS, Ygr026wp, Rps4Bp, Rps12p, and Rpl21Ap, were not found after TAP, suggesting that they indeed were contaminations or their interaction with Mdm38p was too weak to endure the second purification step.

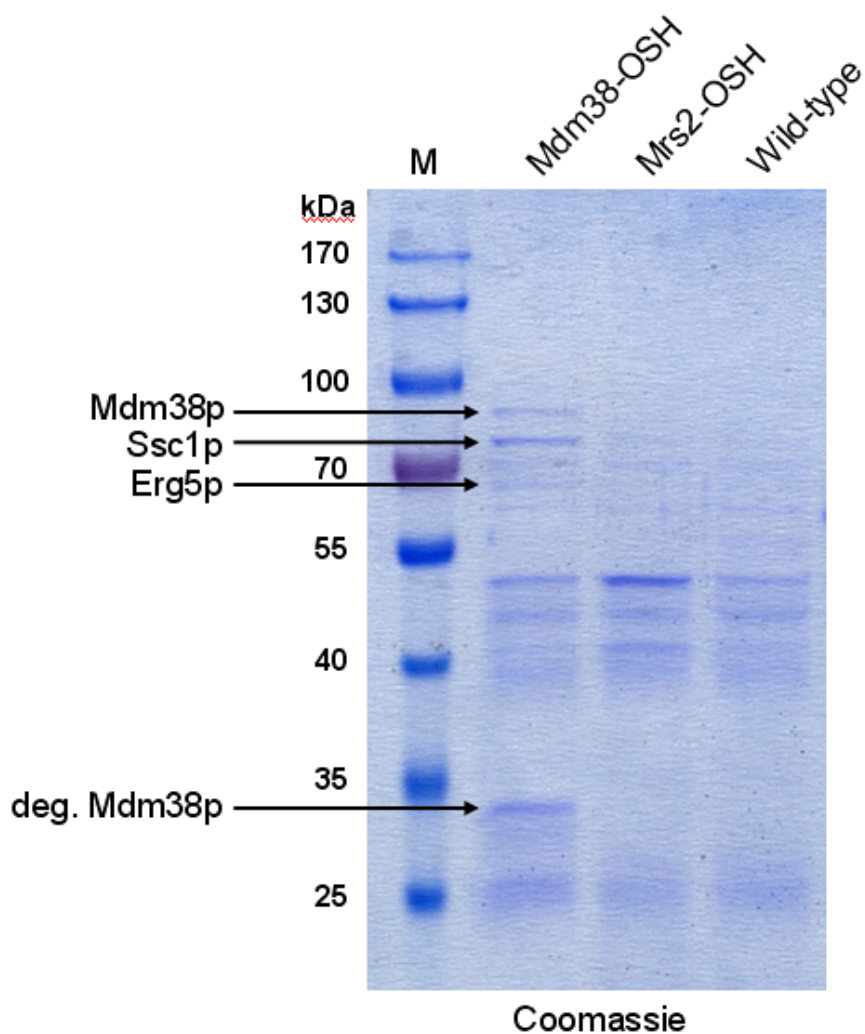


Figure 24: Ssc1p and Erg5p co-elute with Mdm38-OSH after Ni-NTA - Strep TAP

Ni-NTA - Strep TAP was performed with DBY747wt mitochondria and mitochondria isolated from strains DBY $mdm38\Delta$ and DBY $mrs2\Delta$ expressing OSH-tagged *MDM38* or *MRS2* from plasmid YCplac22, respectively. The first two elution fractions were combined, TCA precipitated, separated by SDS-PAGE, and proteins were detected by Coomassie staining. Four protein bands only present in the Mdm38-OSH lane but not in the control lanes were cut out and analyzed by MS (indicated by *black arrows*). deg., degraded.

5.6. Ergosterol and mitochondrial K^+/H^+ exchange

Previously, in a genome-wide screen aiming at identifying mutants which are resistant or highly sensitive to the K^+ ionophore valinomycin, we obtained a series of ergosterol genes, suggesting a role in the control of cellular K^+ (Aleschko M., manuscript in preparation). We therefore decided to focus on the ergosterol genes and to investigate their potential connection to Mdm38p and mitochondrial K^+/H^+ exchange.

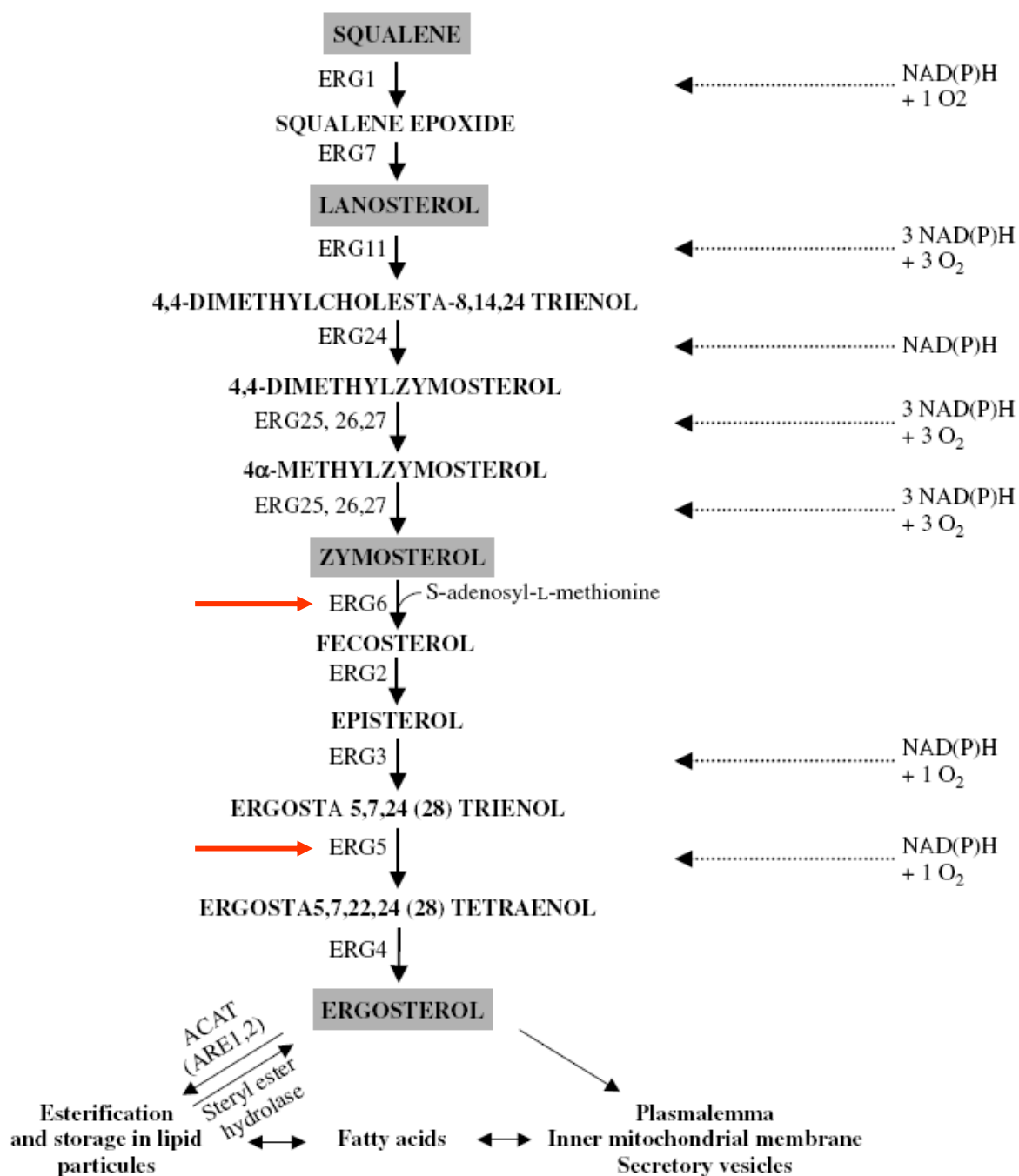


Figure 25: Ergosterol synthesis pathway

Flow chart of the oxygen-dependent steps of ergosterol synthesis in *S. cerevisiae*. Red arrows point to the steps involving *ERG5* and *ERG6*. On the right, oxygen (and NADPH) stoichiometries of the reactions catalyzed are indicated. ACAT (ARE1,2), acyl-CoA sterol acyl transferases. Figure adapted from (Rosenfeld & Beauvoit, 2003).

5.6.1. Synthetic growth defects of *BYmdm38Δerg5Δ* and *BYmdm38Δerg6Δ* double mutant strains

Figure 25 gives an overview of the post-squalene pathway of ergosterol biosynthesis. The highest amounts of ergosterol are found in the plasma membrane, secretory vesicles, and lipid particles, where it is stored. In addition it is also present in lower amounts in other cellular compartments, like the vacuolar membrane or the inner mitochondrial membrane (Zinser *et al.*, 1991; Zinser *et al.*, 1993).

We first investigated the phenotypic effects of *erg5Δ* single mutant and *mdm38Δerg5Δ* double mutant cells to depict whether the double deletion would have a synthetic phenotype, caused by a genetic interaction where two mutations in combination result in significantly enhanced defects than either alone (Guarente, 1993). Since we had also found *erg6Δ* in our valinomycin screen, we tested the synthetic phenotypes of *erg6Δ* and *mdm38Δ* and monitored the growth of all strains in presence of valinomycin. Of note, Erg6p was found to be associated with mitochondrial membranes (Bailey & Parks, 1975; Zahedi *et al.*, 2006) and is involved in maintenance of mitochondrial morphology (Dimmer *et al.*, 2002). The synthesis steps involving Erg5p and Erg6p are indicated in Figure 25 (*red arrows*).

To monitor the cellular growth, serial dilutions of the wild-type and mutant strains were spotted onto YPD, YPG, and YPEG plates with or without valinomycin, a K⁺ ionophore specifically facilitating transmitochondrial K⁺ influx (Kovac *et al.*, 1982a). On glucose medium the wild-type and single mutant strains showed normal growth, whereas addition of 15 μg/ml valinomycin only affected growth of *mdm38Δ* cells, as already shown (Nowikovskiy K., PhD thesis, 2004). In contrast, both double mutant strains exhibited a synthetic growth defect even without valinomycin, and in presence of the ionophore growth was almost completely blocked (Figure 26A).

On non-fermentable carbon sources (YPG, YPEG) wild-type and *erg5Δ* cells showed comparable growth, whereas *mdm38Δ* and *erg6Δ* cells exhibited a clear growth defect. However, growth of both double mutant strains was completely inhibited even without valinomycin. In line with our findings (Aleschko M., in preparation), in presence of 7.5 μg/ml valinomycin the *erg6Δ* mutant exhibited resistance to the ionophore and it was the only strain still able to grow (Figure 26B). Additionally, we investigated the growth phenotype of the *ygr026wΔ* mutant and tested synthetic effects of the double mutant *mdm38Δygr026wΔ*. However, growth of *ygr026wΔ* and *mdm38Δygr026wΔ* cells was similar to the wild-type and the *mdm38Δ* mutant, respectively (data not shown).

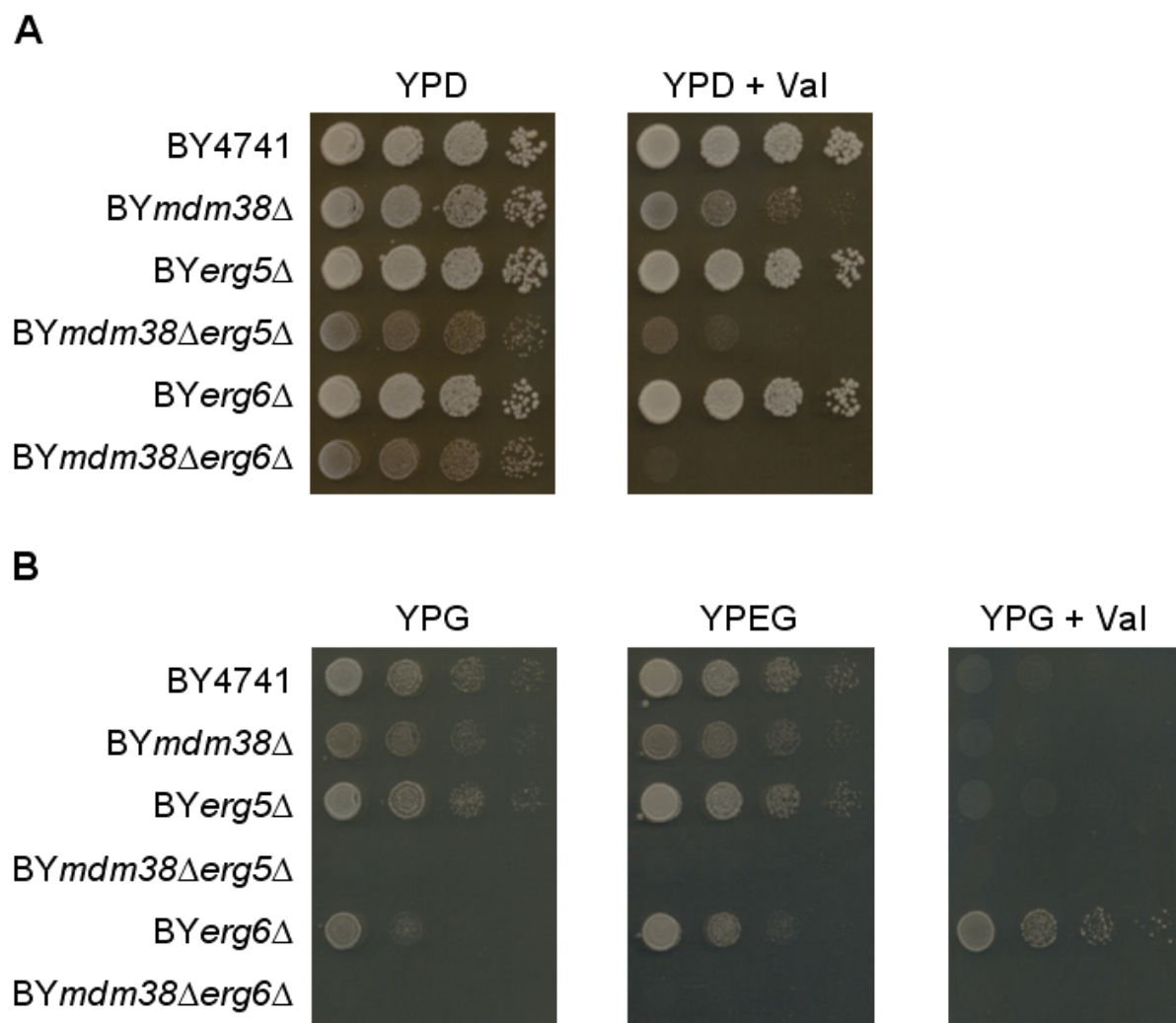


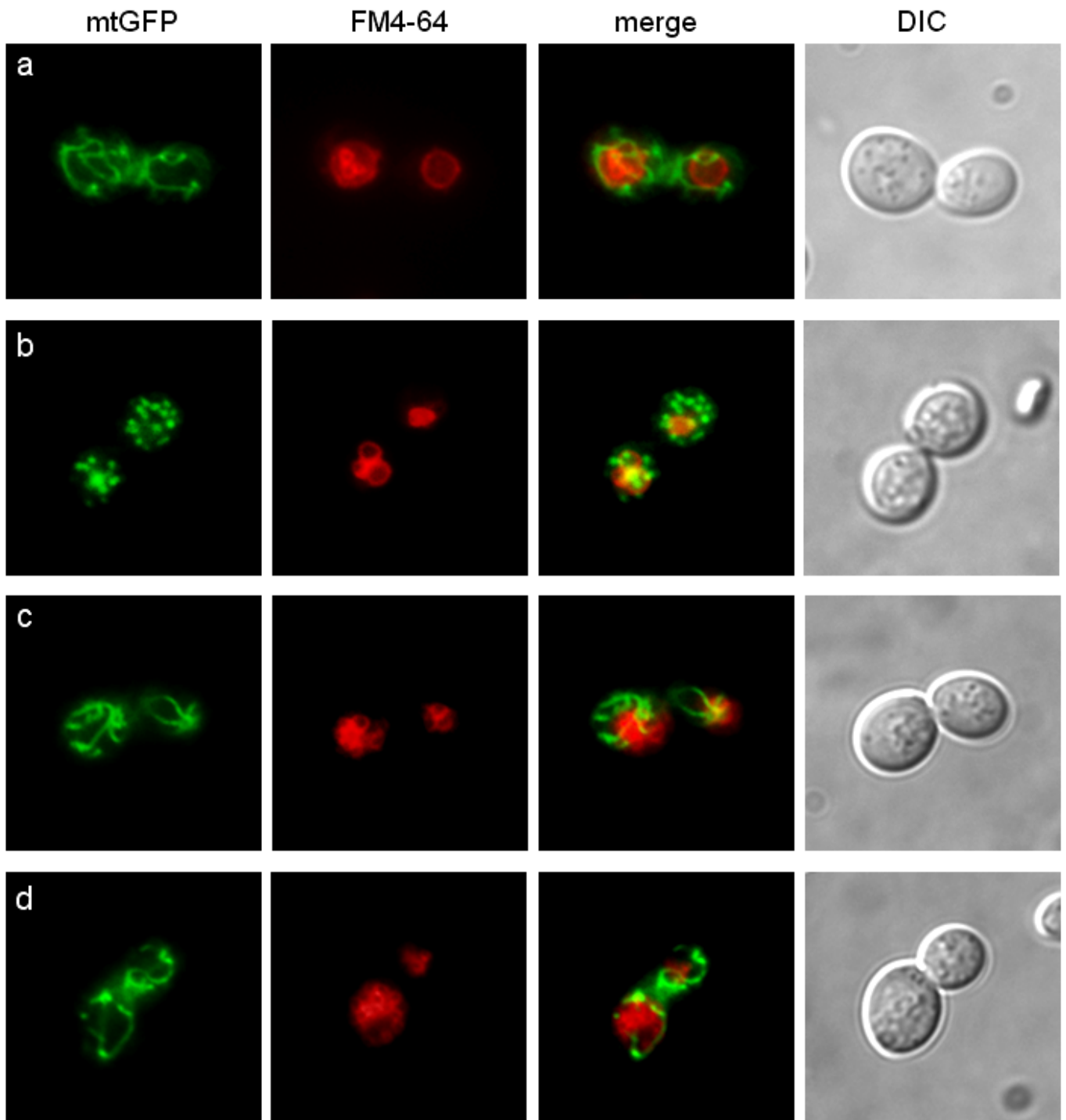
Figure 26: Synthetic growth defect observed upon deletion of *ERG5* and *ERG6* in combination with the *mdm38*Δ mutant strain.

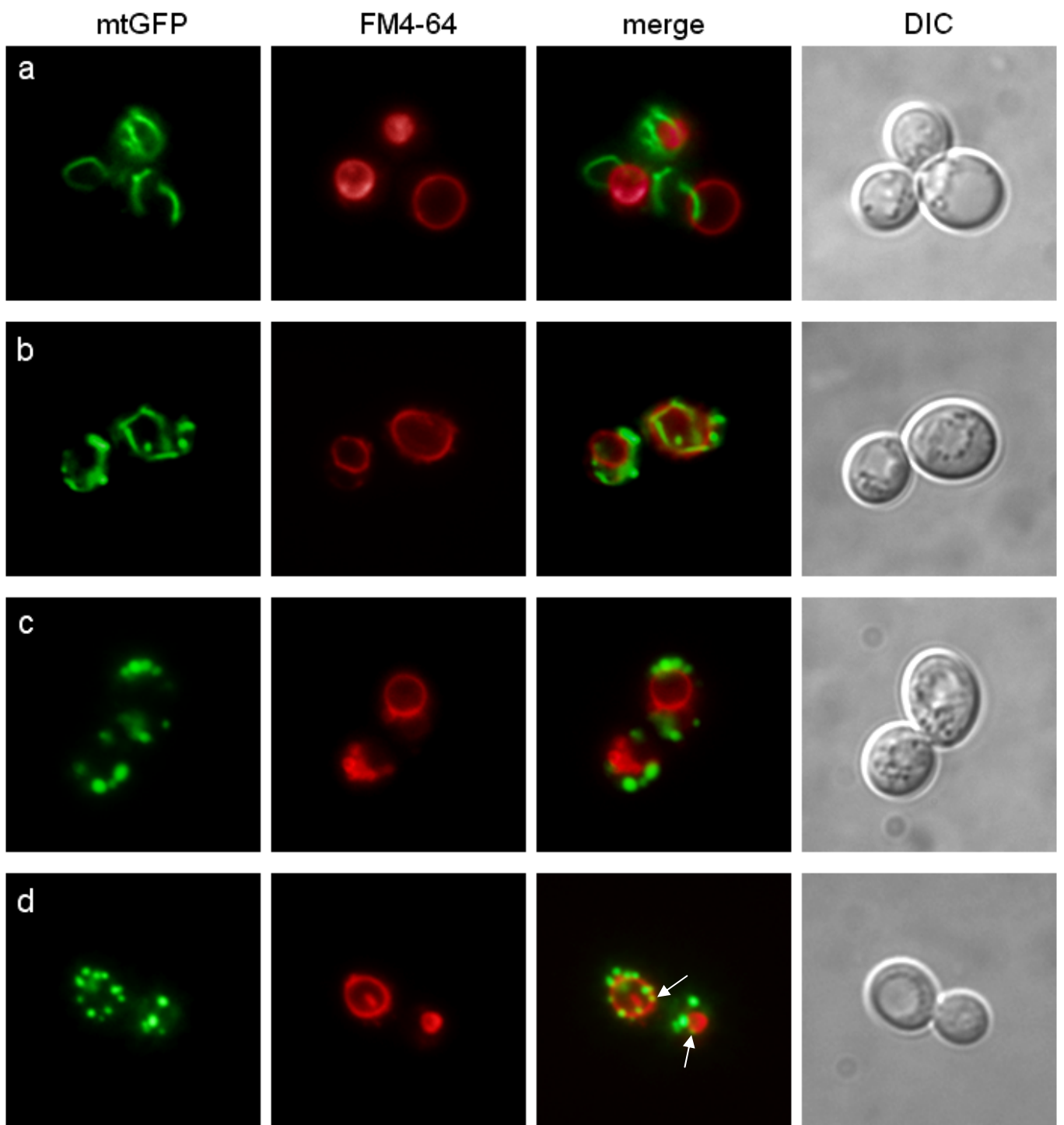
Ten-fold serial dilutions of wild-type strain BY4741, isogenic mutants *mdm38*Δ, *erg5*Δ, *erg6*Δ, and double mutants *mdm38*Δ*erg5*Δ and *mdm38*Δ*erg6*Δ were incubated at 28°C for two days on YPD and three days on YPD supplemented with 15 μg/ml valinomycin (YPD + Val, *panel A*), for three days on YPG and YPEG plates (*panel B*), and for six days on YPG plates supplemented with 7.5 μg/ml valinomycin (YPG + Val, *panel B*).

5.6.2. Aberrant mitochondrial and vacuolar morphology in the absence of *MDM38*, *ERG5*, and *ERG6*

Considering the respiratory growth deficiency and the pronounced sensitivity to valinomycin, especially of the double mutant strains, we monitored the mitochondrial and vacuolar morphology of the single and double mutants under fluorescence microscopy. Organellar morphology was visualized by labeling mitochondria with GFP (pYX142-mtGFP (Westermann & Neupert, 2000)) and co-staining of vacuoles with FM4-64.

When grown in synthetic minimal medium containing galactose, wild-type and *erg5* Δ cells displayed a branched tubular mitochondrial network (Figure 27A, *panel a* and *c*, respectively). In contrast, mitochondria of the *mdm38* Δ mutant appeared as fragmented, spherical units and cells of strain *erg6* Δ displayed an intact mitochondrial reticulum, somewhat less branched (Figure 27A, *panel b* and *d*, respectively).

A

B

C

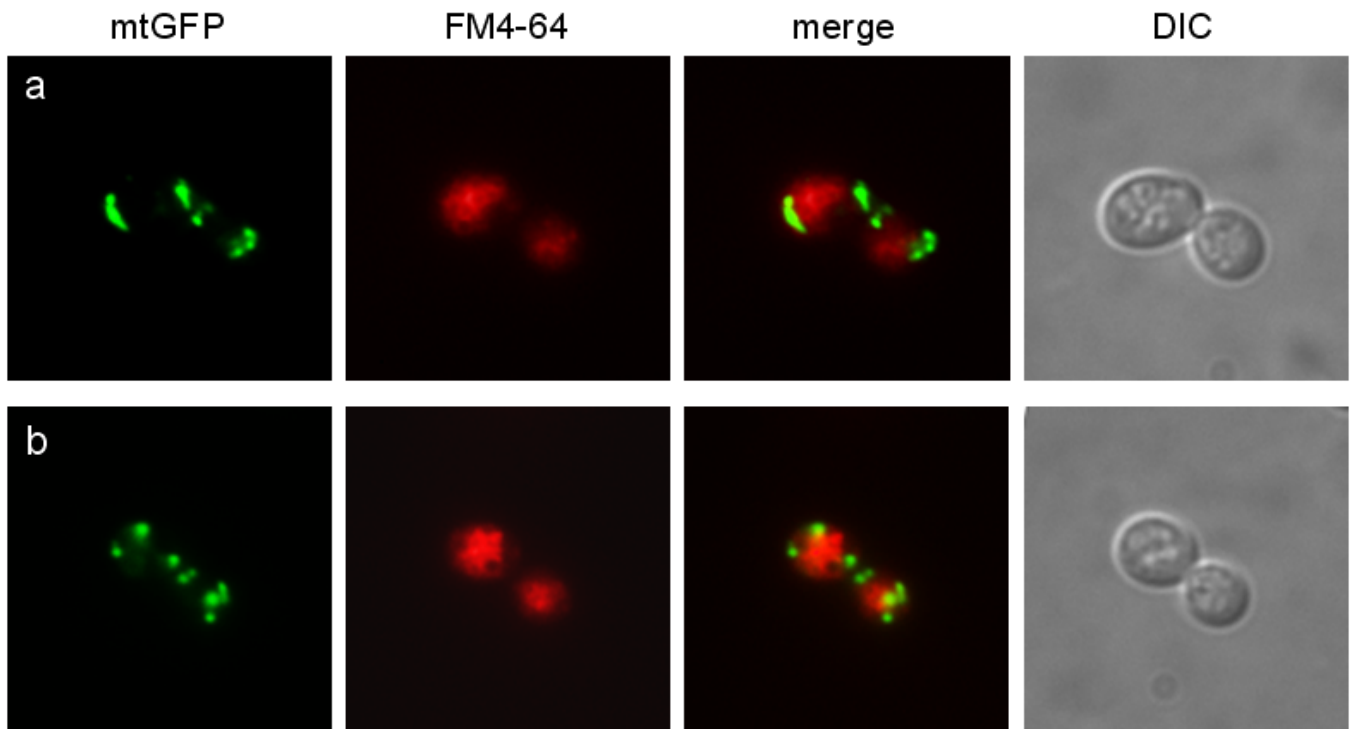


Figure 27: Mitochondrial and vacuolar morphology in absence of *MDM38*, *ERG5*, and *ERG6*

Cells were grown in synthetic minimal medium containing galactose (A), glucose (B), or galactose and raffinose (C) as carbon sources. Mitochondrial morphology was visualized by expression of mitochondrial matrix-targeted GFP from plasmid pYX142-mtGFP (Westermann & Neupert, 2000). Vacuoles were stained with FM4-64. Shown are representative fluorescence microscopy images of live cells and respective DIC images.

A. Microscopical analysis of wild-type strain BY4741 (a) and isogenic mutants *mdm38* Δ (b), *erg5* Δ (c), and *erg6* Δ (d).

B. Microscopical analysis of wild-type strain BY4741 (a) and isogenic mutants *mdm38* Δ (b), *mdm38* Δ *erg5* Δ (c), and *mdm38* Δ *erg6* Δ (d). *White arrows* indicate association of mitochondria and vacuoles (*panel d*).

C. Microscopical analysis of double mutant strains *mdm38* Δ *erg5* Δ (a), and *mdm38* Δ *erg6* Δ (b). DIC, differential interference contrast.

The vacuolar morphology of wild-type and *mdm38* Δ cells appeared normal, characterized by one to three individual vacuoles present per cell (Figure 27A, *panel a* and *b*, respectively). In contrast, *erg5* Δ and *erg6* Δ cells exhibited highly fragmented vacuoles (Figure 27A, *panel c* and *d*, respectively), which is consistent with previous reports (Jones *et al.*, 2010; Kato & Wickner, 2001). Since *mdm38* Δ *erg5* Δ and *mdm38* Δ *erg6* Δ double mutants were lethal on non-

fermentable carbon sources and exhibited reduced growth even on rich medium (YPD), we analyzed the organellar morphology of these cells grown in presence of glucose.

Vacuoles and mitochondria of wild-type cells appeared normal, although network branching of mitochondria was less pronounced (Figure 27B, *panel a*), likely caused by the medium, as glucose is known to repress mitochondrial biogenesis and protein synthesis (Ulery *et al.*, 1994; Visser *et al.*, 1995). Vacuoles of the *mdm38* Δ mutant showed wild-type morphology and the mitochondrial reticulum appeared partly fragmented (Figure 27B, *panel b*).

Interestingly, vacuoles of the *mdm38* $\Delta*erg6* Δ double mutant also exhibited normal morphology (Figure 27B, *panel c*) and vacuoles of strain *mdm38* $\Delta*erg5* Δ were only partly fragmented (Figure 27B, *panel d*), confirming an influence of the carbon source on the organellar morphology. Importantly, mitochondria of both double mutants appeared fragmented in spherical units and their colocalization with vacuolar membranes was frequently observed (Figure 27B, *panel d*, *white arrows*).$$

These observations somehow resemble the morphology we observed in the triple mutant strain *mdm38* $\Delta*mrs7* Δ *ydd183c* Δ , which showed similar organellar abnormalities (see (Zotova *et al.*, 2010) figure 7). Moreover, the *mdm38* $\Delta*mrs7* Δ *ydd183c* Δ triple mutant cells grown in presence of galactose exhibited strong colocalization of mitochondrial and vacuolar markers, indicative of mitophagy, the autophagic degradation of mitochondria inside vacuoles (Lemasters, 2005; Tolkovsky, 2009; Youle & Narendra, 2011).$$

To enable growth of the *mdm38* $\Delta*erg5* Δ and *mdm38* $\Delta*erg6* Δ double mutant strains in presence of galactose, the synthetic minimal medium was supplemented with the fermentable sugar raffinose, which does not repress mitochondrial respiration.$$

Double mutant vacuoles and mitochondria appeared completely fragmented and mitochondrial spheres were even less numerous as compared to double mutant cells grown in glucose medium (Figure 22C, *panel a* and *b*). However, none of the double mutant strains showed any colocalization of mitochondrial and vacuolar markers, suggesting that mitophagy was not ongoing.

Based on co-purification of Erg5p with Mdm38p and strong evidence for a genetic interaction of the proteins as described above, we investigated if the ~ 550 kDa Mdm38p complex retained its size in the *erg5* Δ mutant. Therefore, we expressed OSH-tagged *MDM38* from plasmid YCp22-*MDM38*-OSH in strains BY*mdm38* Δ and BY*erg5* Δ , isolated mitochondria and performed Ni-NTA - Strep TAP, as the Mdm38p complex was not detectable after Blue native electrophoresis of solubilized whole mitochondria (data not shown). Unfortunately, we failed to detect the high molecular weight complex and only recovered the smaller complex ranging between 140 and 232 kDa for both strains (data not shown). This was likely caused

by the lower quality and small amount of mitochondria isolated from the BY strains (~ 20% compared to DBY, see Materials and Methods). Thus, for future studies an *erg5Δ* mutant should be generated in the DBY background to answer this question.

5.6.3. KOAc-induced mitochondrial swelling

Treatment of mitochondria with hypoosmotic potassium acetate (KOAc) results in rapid swelling of the organelle, reflective of K^+/H^+ exchange activity across the inner mitochondrial membrane (Bernardi, 1999; Garlid *et al.*, 1986; Welihinda *et al.*, 1993). Incubation of non-respiring mitochondria in KOAc causes rapid uptake of the protonated form of acetic acid (HAc). Deprotonation of HAc in the mitochondrial matrix activates the K^+/H^+ exchange system. This results in the net accumulation of potassium acetate, water uptake, and swelling of the organelle, which can be observed as a decrease in light absorbance of mitochondrial suspensions at 540 nm (Bernardi, 1999; Garlid *et al.*, 1986; Garlid & Paucek, 2003).

Prior to measurement, proton pumping by the respiratory chain was blocked by addition of the Complex III inhibitor antimycin A and mitochondria were depleted of endogenous Mg^{2+} , a known inhibitor of the K^+/H^+ exchanger (Garlid, 1980), by addition of the divalent cation ionophore A-23187 and EDTA.

BY4741 wild-type as well as *erg5Δ* mitochondria showed rapid swelling upon addition of KOAc (Figure 28A). In contrast, *mdm38Δ* mutant mitochondria exhibited severely reduced swelling compared to wild-type mitochondria, consistent with previous findings (Nowikovskiy *et al.*, 2004). As expected, *mdm38Δerg5Δ* and *mdm38Δerg6Δ* double mutant mitochondria completely failed to swell. Surprisingly, *erg6Δ* mitochondria exhibited only marginal swelling, suggesting disturbed K^+/H^+ exchange activity or otherwise abnormal membrane behaviour. Absence of mitochondrial K^+/H^+ exchange causes swelling of the organelle prior to its isolation, as demonstrated by the reduced absorbance levels at resting conditions (Figure 28A and B). However, this was not the case for *erg6Δ* mitochondria, which also did not appear swollen under fluorescence microscopy (see figure 27A, panel D), suggesting that impaired K^+/H^+ exchange was not the cause of absent swelling of *erg6Δ* mitochondria. In presence of quinine, a known inhibitor of the K^+/H^+ exchanger (Brierley *et al.*, 1984) mitochondria became refractory to swelling, indicating that the monitored swelling was caused by the K^+/H^+ exchange activity (Figure 28B).

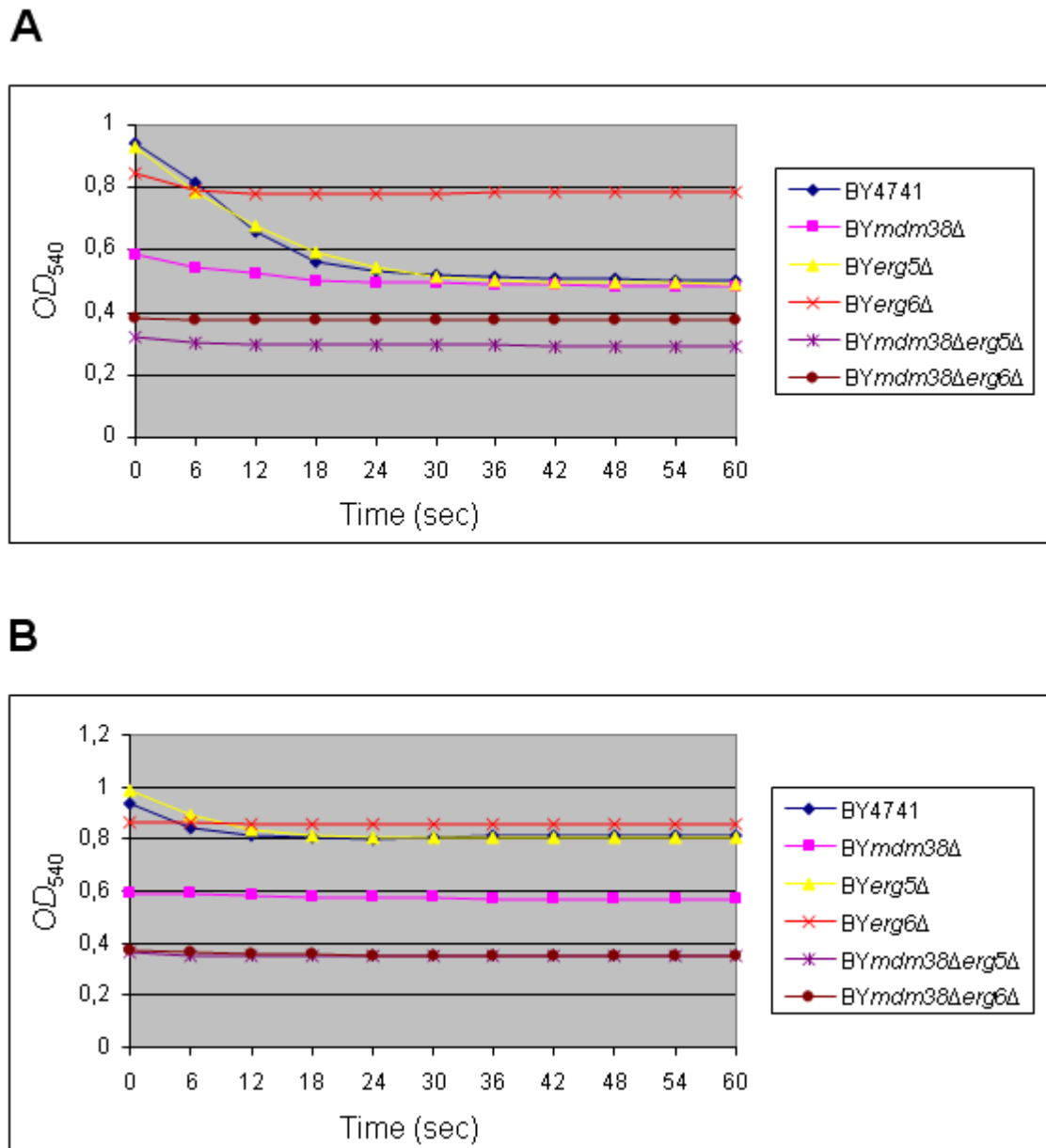


Figure 28: KOAc-induced swelling of mitochondria

Mitochondria were prepared from BY4741 wild-type, *mdm38Δ*, *erg5Δ*, *erg6Δ*, *mdm38Δerg5Δ*, and *mdm38Δerg6Δ* mutant cells, resuspended in 0.6 M sorbitol buffer, and incubated with antimycin A prior to measurement to block proton pumping. To deplete mitochondria of endogenous Mg^{2+} , the 4-bromo-calcium ionophore A-23187 and EDTA were added prior to KOAc treatment. After addition of mitochondria to the swelling buffer in cuvettes, swelling of mitochondria was measured as a decrease of OD_{540} immediately thereafter (*panel A*). To confirm that the observed swelling was caused by the K^+/H^+ exchange activity, the K^+/H^+ exchange inhibitor quinine was added to A-23187/EDTA-treated mitochondria prior to measurement (*panel B*).

5.7. Synthetic genetic array (SGA) analysis

SGA analysis was developed as an efficient approach for the systematic construction of double mutants (Tong *et al.*, 2001; Tong & Boone, 2006).

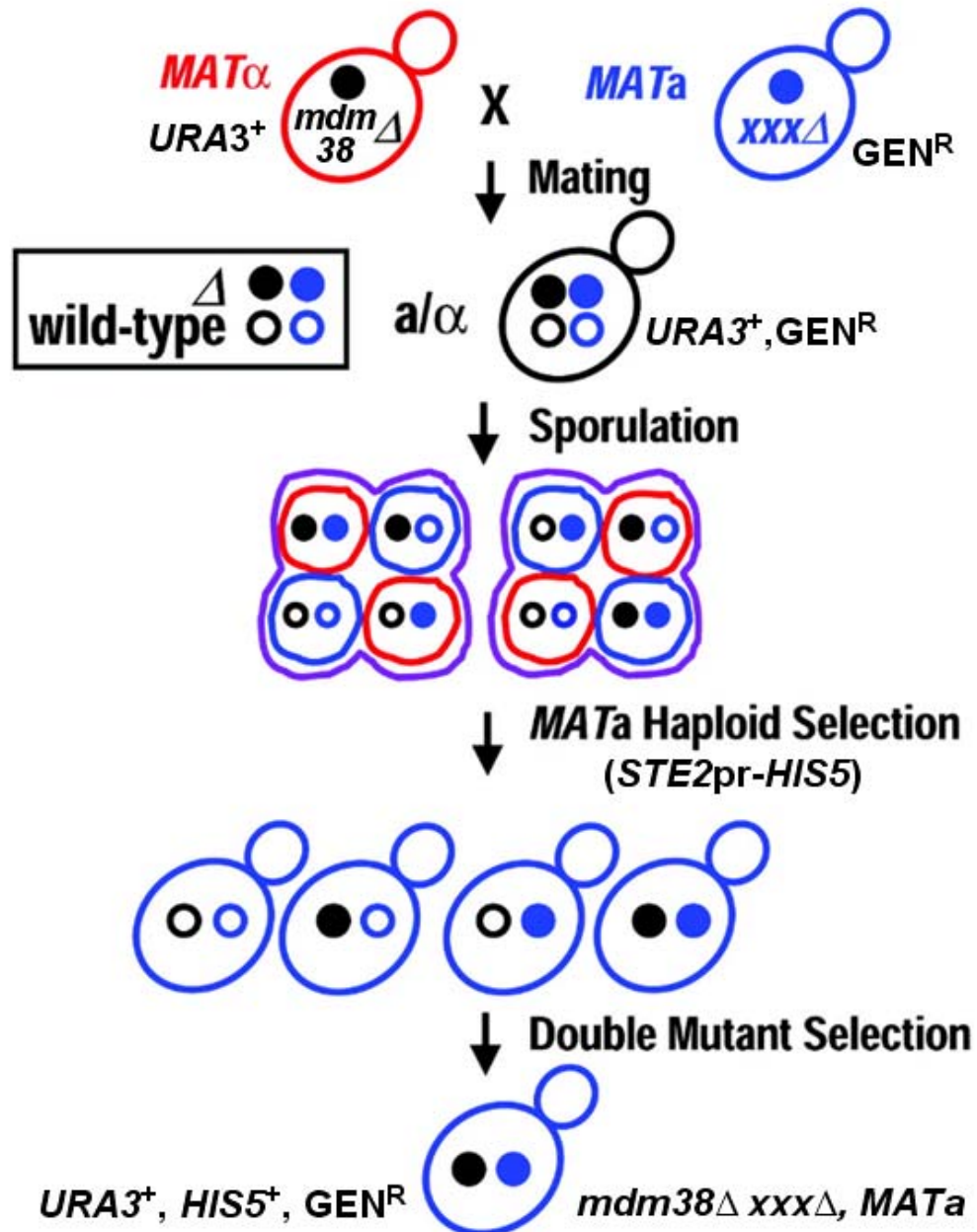


Figure 29: Synthetic genetic array (SGA) analysis

Schematic representation of the steps involved in SGA analysis. A query deletion mutant ($mdm38\Delta$) is systematically crossed to a non-essential deletion mutant library ($xxx\Delta$, ~ 4900 strains) by robotic colony manipulation. The resulting diploids are then sporulated and the haploid double mutant progeny is obtained by a series of selection platings (see Materials and Methods for details). Double mutant colonies are screened visually for aberrant growth. Figure adapted from (Tong *et al.*, 2001).

By robotic colony manipulation a query mutant strain is crossed to the Euroscarf non-essential deletion mutant library (Winzeler *et al.*, 1999). Figure 29 gives an overview of the individual steps involved in double mutant construction (see also Materials and Methods for a detailed description).

By using this genetic approach, which permits the revelation of functional relationships between genes and pathways, we aimed at the identification of synthetic lethal and synthetic suppressive interactions of the *mdm38* Δ mutant strain.

5.7.1. Synthetic lethal screen

Synthetic lethality occurs when the combination of two mutations, neither by itself lethal, leads to inviable double mutant meiotic progeny (Guarente, 1993; Novick *et al.*, 1989). Synthetic lethal genetic interactions have been extensively studied to identify genes involved in related functions or compensatory pathways (Boone *et al.*, 2007; Mani *et al.*, 2008).

We first deleted *MDM38* in the haploid *MATa* starting strain BY7092 by homologous recombination with a *URA3* disruption cassette. The resulting BY7092*mdm38* Δ mutant was crossed to the ordered array of geneticin resistant deletion mutants of the opposite mating type, *MATa*. For an easy selection of the double mutant meiotic progeny after sporulation of the resulting diploids, the BY7092*mdm38* Δ strain carries the *STE2pr-HIS5* reporter, which is only expressed in haploid *MATa* cells (Daniel *et al.*, 2006; Tong *et al.*, 2001). This permits selection of *MATa* haploid double mutants on minimal medium lacking uracil and histidine and containing geneticin (SD - URA - HIS + GEN). Moreover, this avoids contamination with diploid cells accidentally carried over by robotic colony plating or resulting from conjugation of meiotic progeny, as these cells are not viable on media lacking histidine. The growth rate of the haploid double mutant strains is monitored by visual observation or image analysis of colony size.

After screening of the *mdm38* Δ mutant against ~ 4900 viable deletion strains, we scored 57 potential synthetic lethal interactions. In order to exclude that the lethality was caused by impaired mating or sporulation and to confirm that the haploid double mutants were inviable, we first had to determine the mating and sporulation efficiency. Unfortunately, 33 diploids of the 57 candidates did not sporulate and the residual 24 mutant strains failed to conjugate with BY7092*mdm38* Δ , as they turned out to be already diploid within the library. Furthermore, expression of the *STE2pr-HIS5* reporter seemed to not be tightly controlled: when the BY7092*mdm38* Δ query mutant is crossed to the *mdm38* Δ mutant within the deletion strain library, homozygous diploid *mdm38* Δ cells are obtained but haploid double mutants cannot

form. Accordingly, these diploid cells should fail to grow on double mutant selective SD - URA - HIS + GEN plates. However, we observed growth of these cells, indicative of leaky *HIS5* expression in diploid cells carried over during robotic colony plating.

Table 4: 3-Amino-1,2,4-triazole (3-AT) – sensitive mutant strains

List of 28 genes causing lethality to 10 mM 3-AT when deleted in combination with the *mdm38Δ* mutant strain. References for these genes can be found at YPD (www.proteome.com/) or the *Saccharomyces* Genome Database (SGD) (<http://genome-www.stanford.edu/Saccharomyces/>).

Systematic Name	Standard Name
YAL047C	SPC72
YBR081C	SPT7
YBR133C	HSL7
YBR200W	BEM1
YCL032W	STE50
YDR069C	DOA4
YDR264C	AKR1
YFR010W	UBP6
YGL038C	OCH1
YGL070C	RPB9
YGR155W	CYS4
YGR204W	ADE3
YGR252W	GCN5
YHL011C	PRS3
YHR025W	THR1
YHR183W	GND1
YJL088W	ARG3
YKL213C	DOA1
YLL043W	FPS1
YLR337C	VRP1
YLR370C	ARC18
YLR399C	BDF1
YML116W	ATR1
YMR263W	SAP30
YNL059C	ARP5
YNL229C	URE2
YOL115W	PAP2
YPL129W	TAF14

Thus, the leaky expression of the reporter could possibly be the reason, why we did not detect synthetic lethal interactions (Singh *et al.*, 2009). To increase stringency of the *HIS5* reporter expression and haploid double mutant selection, we repeated the screen and selected the haploid double mutants on SD - URA - HIS + GEN plates supplemented with 10 mM 3-Amino-1,2,4-triazole (3-AT), a competitive inhibitor of the *HIS5* gene product and thereby of leaky reporter expression (Daniel *et al.*, 2006).

Under these conditions, homozygous diploid *mdm38Δ* mutants failed to grow, thus confirming the inhibitory effect of 3-AT. Furthermore, we identified 32 additional synthetic lethal candidates. However, four of them did not grow because of impaired sporulation. In order to confirm that the lethal interactions of the remaining 28 double mutants were correct, random tetrad dissection was performed for all 28 strains. Surprisingly, in each case the haploid double mutants were viable. When these 28 haploid double mutants were grown on SD - URA - HIS + GEN medium containing or lacking 10 mM 3-AT, all double mutants were inviable on plates supplemented with 3-AT (data not shown), suggesting increased sensitivity to this chemical. Table 4 gives an overview of these 28 genes. Other double mutants were viable in presence of up to 100 mM 3-AT (data not shown). Thus, under these experimental conditions we could not identify any *mdm38Δ* synthetic lethal interactions.

5.7.2. Synthetic suppression screen

As a second approach based on SGA analysis, we aimed at identifying synthetic suppressors of the *mdm38Δ* strain. These are mutants that suppress the *mdm38Δ* mutation phenotype (Guarente, 1993). Screening for genetic suppressors has the potential to identify genes involved in pathways which need to be counteracted by mitochondrial K^+/H^+ exchange, like inwardly directed cation transporters.

To detect suppressor strains, all haploid double mutant strains obtained by the SGA approach were plated on YPG medium, incubated at 16, 28, and 35.5 °C, and screened for improved growth. In the first round, growth of 86 strains was judged to be improved by visual observation (data not shown). These strains were picked, plated in serial dilutions for a more precise evaluation of growth, and incubated under the same conditions as before. After this second round, 32 strains remained as suppressor candidates (data not shown). To confirm the suppression effect of the double mutation and to exclude a contamination with heterozygous diploid cells, random tetrad dissection of all 32 strains was performed and the resulting double mutants were spotted again on YPG medium. Only six double mutants remained with a

growth comparable to the wild-type, independently of the incubation temperature (Figure 30, *panel A and B*).

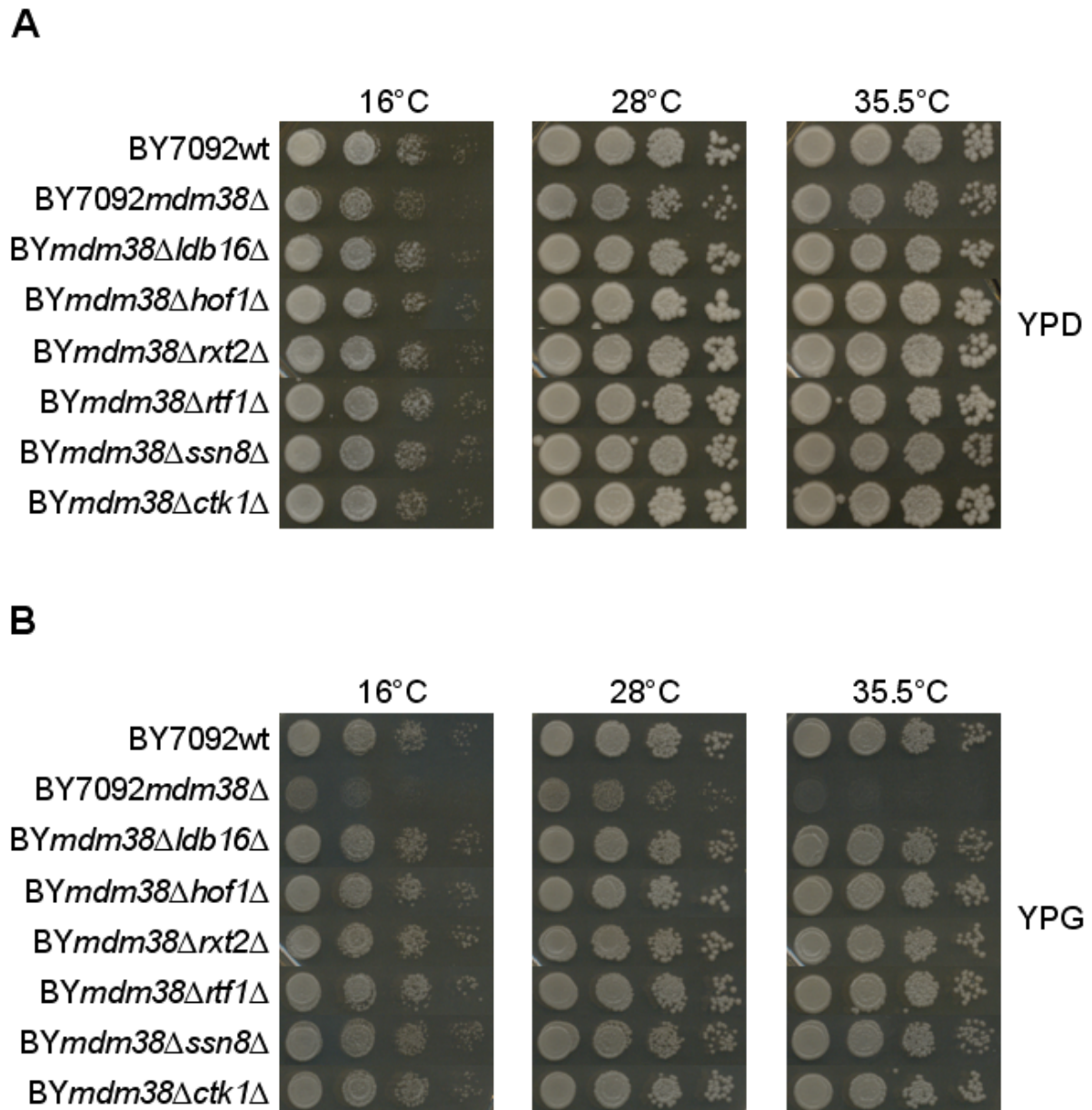


Figure 30: Synthetic suppression of the *mdm38Δ* respiratory growth defect

Ten-fold serial dilutions of wild-type strain BY7092 and mutant strains *mdm38Δ*, *mdm38Δldb16Δ*, *mdm38Δhof1Δ*, *mdm38Δrxt2Δ*, *mdm38Δrtf1Δ*, *mdm38Δssn8Δ*, and *mdm38Δctk1Δ* were incubated on YPD plates (*panel A*) at 16, 28, and 35.5°C for 4, 2, and 3 days, respectively. On YPG plates (*panel B*) cells were incubated at 16, 28, and 35.5°C for 6, 3, and 4 days, respectively.

Table 5 gives a description of the six genes suppressing the *mdm38Δ* respiratory growth defect when deleted in combination with the *mdm38Δ* strain. Surprisingly, three of those, *CTK1* (Hampsey & Kinzy, 2007; Rother & Strasser, 2007), *SSN8* (Balciunas & Ronne, 1995; Kuchin *et al.*, 1995), and *RTF1* (Mueller & Jaehning, 2002; Stolinski *et al.*, 1997), are involved in transcriptional regulation, either by modulation of RNA polymerase II directly or of associated factors.

Table 5: Synthetic suppression of the *mdm38Δ* mutant phenotype

List of the six genes suppressing the *mdm38Δ* respiratory growth defect when deleted in combination with the *mdm38Δ* strain. The right column gives a brief description of the gene's function according to the *Saccharomyces* Genome Database (SGD) (<http://genome-www.stanford.edu/Saccharomyces/>).

Systematic Name	Standard Name	Description
<i>YCL005W</i>	<i>LDB16</i>	Protein of unknown function; null mutants have decreased net negative cell surface charge; GFP-fusion protein expression is induced in response to the DNA-damaging agent MMS; native protein is detected in purified mitochondria
<i>YMR032W</i>	<i>HOF1</i>	Bud neck-localized, SH3 domain-containing protein required for cytokinesis; regulates actomyosin ring dynamics and septin localization; interacts with the formins, Bni1p and Bnr1p, and with Cyk3p, Vrp1p, and Bni5p
<i>YBR095C</i>	<i>RXT2</i>	Subunit of the histone deacetylase Rpd3L complex; possibly involved in cell fusion and invasive growth
<i>YGL244W</i>	<i>RTF1</i>	Subunit of the RNA polymerase II-associated Paf1 complex; directly or indirectly regulates DNA-binding properties of Spt15p and relative activities of different TATA elements; involved in telomere maintenance
<i>YNL025C</i>	<i>SSN8</i>	Cyclin-like component of the RNA polymerase II holoenzyme, involved in phosphorylation of the RNA polymerase II C-terminal domain; involved in glucose repression and telomere maintenance
<i>YKL139W</i>	<i>CTK1</i>	Catalytic (alpha) subunit of C-terminal domain kinase I (CTDK-I), which phosphorylates both RNA pol II subunit Rpo21p to affect transcription and pre-mRNA 3' end processing, and ribosomal protein Rps2p to increase translational fidelity

RXT2 is part of a histone deacetylase complex (Colina & Young, 2005) and involved in cell fusion (Entian *et al.*, 1999). In contrast, *HOF1* is involved in cell division and cytoskeletal organization (Lippincott & Li, 1998; Naqvi *et al.*, 2001) and *LDB16* encodes a protein of unknown function, detected in mitochondria and lipid particles (Reinders *et al.*, 2006; Wagner *et al.*, 2009).

We decided to focus on *LDB16*, *HOF1*, and *RXT2*, reasoning that the suppressor effect of *RTF1*, *SSN8*, and *CTK1* may be caused by secondary effects mediated by changes in transcription of their target genes.

5.7.3. Double mutant strains exhibit a restored mitochondrial network

We first compared the cellular growth of the synthetic suppressive double mutants and the respective single mutant strains. Cells were spotted in serial dilutions onto YPD and non-fermentable carbon sources to assess possible respiratory defects of the single deletion strains. Mutants lacking *HOF1* or *RXT2* showed slightly reduced growth on all media compared to their respective double mutant strains (Figure 31). In contrast, *ldb16Δ* and *mdm38Δldb16Δ* cells showed identical growth on all media, which was indistinguishable from the wild-type.

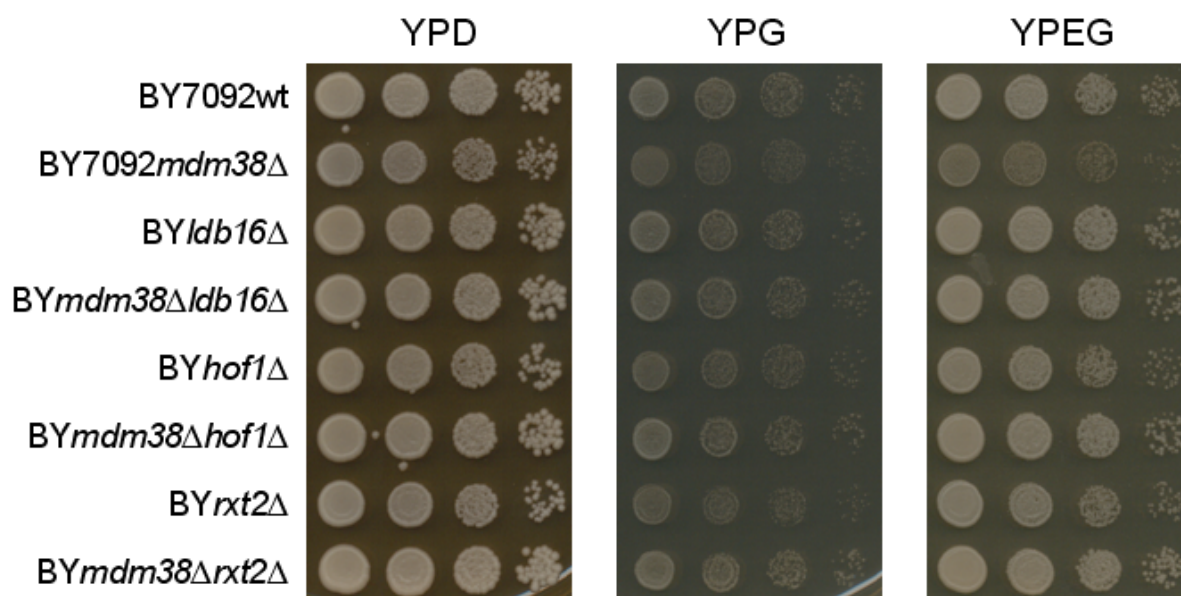


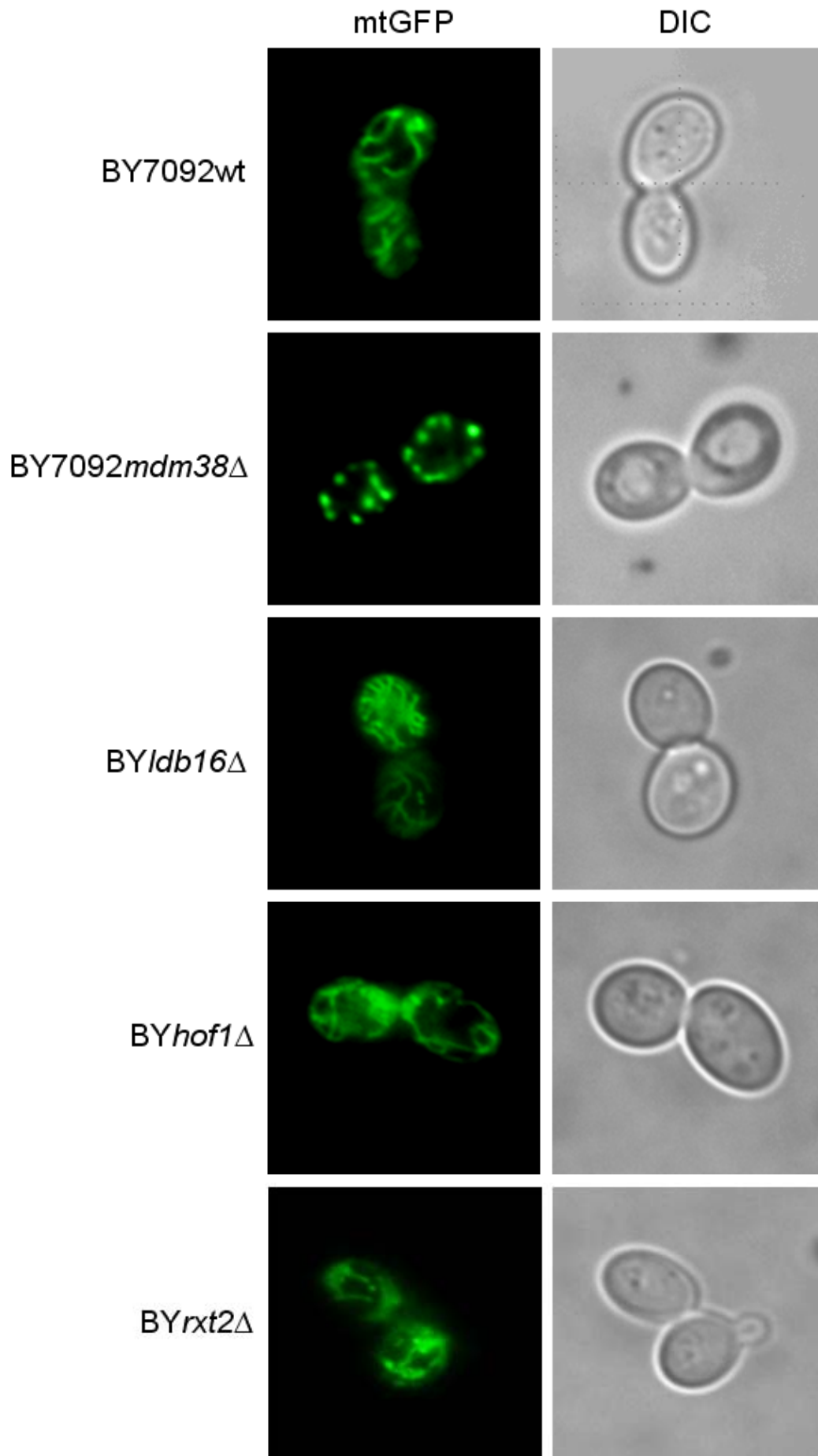
Figure 31: Comparison of growth phenotypes of synthetic suppressive single and double mutants
Ten-fold serial dilutions of wild-type strain BY7092 and mutant strains *mdm38Δ*, *ldb16Δ*, *mdm38Δldb16Δ*, *hof1Δ*, *mdm38Δhof1Δ*, *rxt2Δ*, and *mdm38Δrxt2Δ* were incubated at 28°C for two days on YPD plates and for three days on YPG and YPEG plates.

Next we assessed the mitochondrial morphology of the synthetic suppressors in single and double mutant strains under fluorescence microscopy of cells expressing a mitochondrial matrix-targeted GFP. Cells were cultivated in synthetic minimal medium containing galactose as a carbon source. First, the mitochondrial shape of the single mutant strains *ldb16* Δ , *hof1* Δ , and *rxt2* Δ was compared to BY7092 wild-type and *mdm38* Δ mutant cells.

As expected, wild-type cells exhibited a tubular and branched mitochondrial network, while *mdm38* Δ mitochondria appeared heavily fragmented (Figure 32A). Mitochondria of *ldb16* Δ cells were organized in a dense, highly branched network, whereas *hof1* Δ and *rxt2* Δ mitochondria formed elongated but somewhat disorganized and less branched networks (Figure 32A), likely correlating with the slight growth defect observed on non-fermentable carbon sources.

We subsequently investigated the mitochondrial shape of the double mutant strains *mdm38* Δ *ldb16* Δ , *mdm38* Δ *hof1* Δ , and *mdm38* Δ *rxt2* Δ . Strikingly, all three double mutant strains exhibited branched tubular mitochondrial networks, comparable to wild-type cells (Figure 32B). This suggests that deletion of *LDB16*, *HOF1*, or *RXT2* in combination with the *mdm38* Δ strain causes suppression of the respiratory growth deficiency by restoration of mitochondrial function and morphology by so far unknown mechanisms.

A



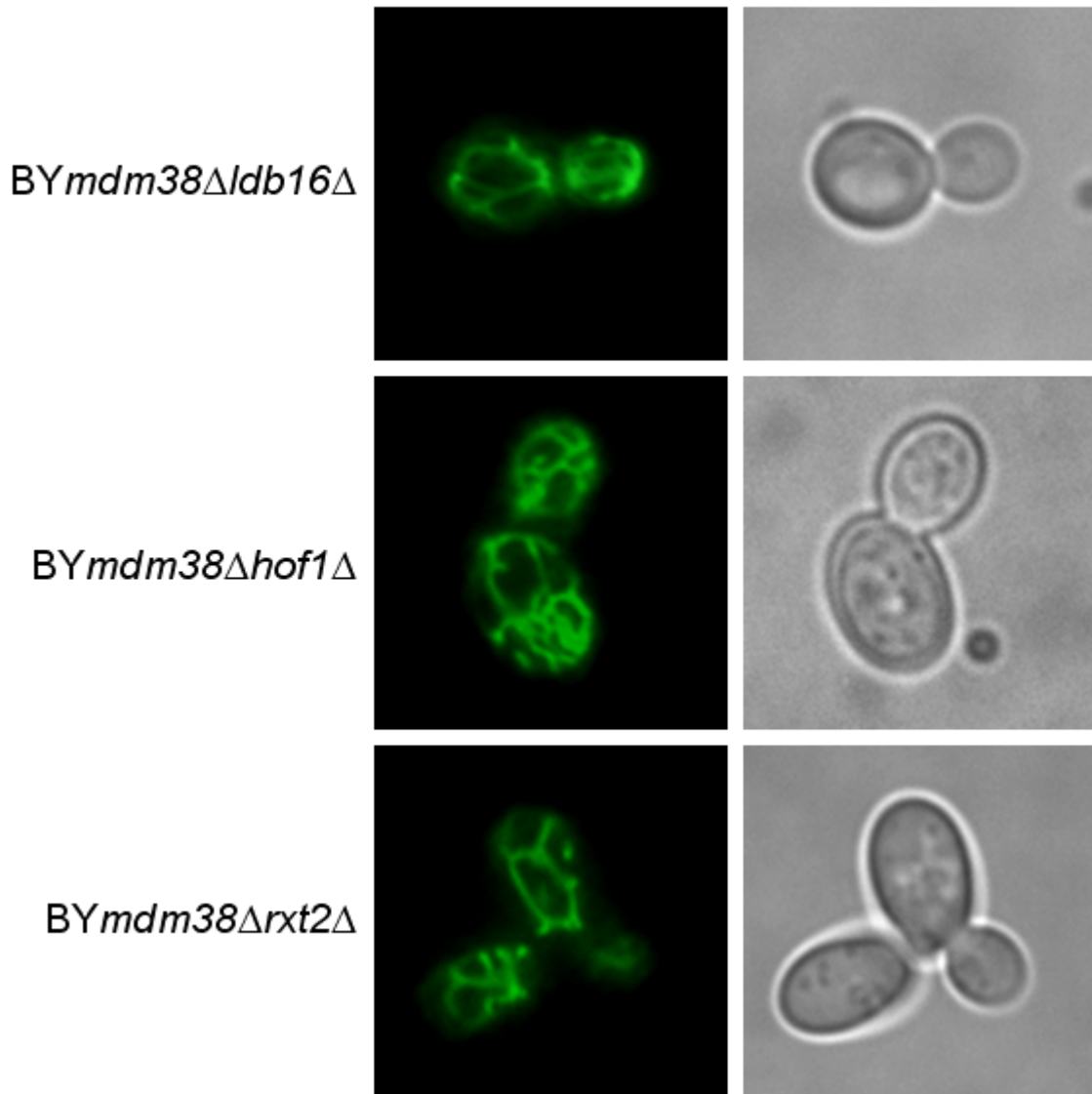
B

Figure 32: Mitochondrial morphology of synthetic suppressive single and double mutant strains Wild-type strain BY7092 and mutant strains $mdm38\Delta$, $ldb16\Delta$, $hof1\Delta$, $rxt2\Delta$ (panel A), $mdm38\Delta ldb16\Delta$, $mdm38\Delta hof1\Delta$, and $mdm38\Delta rxt2\Delta$ (panel B) were grown to logarithmic phase in synthetic minimal medium containing galactose as a carbon source. Mitochondrial morphology was visualized by expression of mitochondrial matrix-targeted GFP from plasmid pYX142-mtGFP (Westermann & Neupert, 2000). Shown are representative fluorescence microscopy images of live cells as well as respective DIC images.

6. Discussion

Mitochondria establish an inside negative membrane potential ($\Delta\psi$) which favors the uptake of cations across the inner membrane, including K^+ , the most abundant cellular cation. As postulated by Nobel Price winner Peter Mitchell (Mitchell, 1961; Mitchell, 1966) and well accepted since then (DiResta *et al.*, 1986; Dordick *et al.*, 1980; Froschauer *et al.*, 2005; Garlid *et al.*, 1986), mitochondria need a cation/proton antiporter system to counteract excess cation influx, thereby maintaining their integrity and the matrix ion and volume homeostasis. However, the molecular identity of the mitochondrial K^+/H^+ antiporter remained unknown until recently, when the yeast Mdm38p and its human homolog Letm1 have been identified as essential components thereof (Froschauer *et al.*, 2005; McQuibban *et al.*, 2010; Nowikovsky *et al.*, 2007; Zotova *et al.*, 2010). In the study presented here and in line with previous data on hLetm1 (Dimmer *et al.*, 2008; Hasegawa & van der Bliek, 2007; Tamai *et al.*, 2008), we found that Mdm38p is part of a high molecular weight protein complex of unknown composition (see (Zotova *et al.*, 2010) and Figure 10).

The fact that Mdm38p is a single membrane spanning protein and other exchangers contain up to twelve membrane spanning helices (Wakabayashi *et al.*, 2000), suggested that Mdm38p may act as an essential auxiliary protein of the unknown K^+/H^+ exchanger rather than forming the antiporter itself. By the use of affinity chromatography we aimed at pulling down the exchanger together with Mdm38p (see Figures 6 and 7). Data collected here showed that Mdm38p interacts with Ssc1p, an essential mitochondrial chaperone protein involved in protein import across the inner mitochondrial membrane and in protein folding in the mitochondrial matrix (Kang *et al.*, 1990; Liu *et al.*, 2001), and with Erg5p, a cytochrome P450 enzyme facilitating the penultimate step in ergosterol biosynthesis (Kelly *et al.*, 1995; Skaggs *et al.*, 1996). Furthermore, we analyzed the additive effects resulting from double deletion of *MDM38* and *ERG5* or *ERG6* on mitochondrial and vacuolar morphology, as well as on K^+/H^+ exchange activity.

Unexpectedly, by applying affinity chromatography we could not identify any obvious protein candidates with a role as a mitochondrial K^+/H^+ exchanger. These results strongly suggest that Mdm38p may be the exchanger *per se*. Although this would be the first case of a single membrane spanning antiporter, this possibility is supported by strong evidence for homo-oligomerization of Mdm38p (Zotova *et al.*, 2010).

In a second approach, a genome-wide synthetic genetic array analysis, we identified six synthetic suppressive interactions of the *mdm38Δ* mutant strain, characterized by restored respiratory growth and mitochondrial morphology of six double mutant strains. Functionally, these suppressor mutants are involved in different cellular processes, ranging from transcriptional regulation to cell fusion and cytoskeletal organization (Table 5). So far it is not clear if these mutations directly contribute to functional restoration of *mdm38Δ* mitochondria or if the suppression is caused by secondary effects. However, our findings represent the basis for uncovering new connections between these processes and mitochondrial cation homeostasis.

6.1. Interaction partners of Mdm38p

A previous study reported that the protein A-tagged Mdm38p interacted with a series of mitochondrial ribosomal proteins and its yeast homolog Mrs7p (Frazier *et al.*, 2006). Here we characterized Mrs7p as a multicopy suppressor of the *mdm38Δ* mutant strain (Zotova *et al.*, 2010). By use of Blue native electrophoresis and second dimension SDS-PAGE we showed that Mdm38p only hetero-oligomerized with TAP-tagged Mrs7p, whereas Mdm38p is able to homo-oligomerize (Zotova *et al.*, 2010). Since the bulky TAP tag reduced suppression efficiency of Mrs7p (see (Zotova *et al.*, 2010), Figure 11), this suggests that the observed interaction may represent a compensatory mechanism by which one protein supports the function of another. Alternatively, TAP-tagged Mrs7p may interact with Mdm38p, however causing less efficient function than self-interacting Mdm38p.

Furthermore, we showed that both Mdm38p and Mrs7p are part of high molecular weight complexes of similar size (see (Zotova *et al.*, 2010), Figures 9), but do not reside in the same complex. Accordingly, deletion of *MRS7* and also of a second strong suppressor, *YDL183C* (*MKRI*), did not influence the size of the Mdm38p complex as depicted by Blue native electrophoresis (data not shown), making direct interaction unlikely. Therefore, we investigated the molecular composition of the Mdm38p complex by affinity chromatography followed by mass spectrometry.

6.2. Ssc1p and Erg5p co-purify with Mdm38p

Intensive testing of various affinity tags resulted in the purification of the ~ 550 kDa Mdm38p complex, which was only possible by the use of the One-Strep tag, two tandemly arranged

Strep peptides specially designed for the purification of challenging protein complexes (Junttila *et al.*, 2005). Also Ni-NTA – Strep TAP of OSH-tagged Mdm38p allowed for recovery of the protein complex, although the predominant part of Mdm38p was detected in its putative dimeric conformation (Figure 23), likely caused by dissociation of the complex during purification. However, size exclusion chromatography showed that the majority of Mdm38p was organized into the high molecular weight complex (Figures 17 and 18), suggesting that this protein state represents the native conformation of Mdm38p *in vivo*.

Mass spectrometry analysis of proteins co-purified with OSH-tagged Mdm38p revealed physical association with two proteins, Ssc1p and Erg5p. Ssc1p (mtHsp70p) is an essential mitochondrial Hsp70 family ATPase, acting as a chaperone protein involved in protein import across the inner mitochondrial membrane and in protein folding in the mitochondrial matrix (Kang *et al.*, 1990; Liu *et al.*, 2001).

Ssc1p itself was shown to be important for correct mitochondrial morphology, as conditional inactivation of the protein caused aggregation of the mitochondrial network (Kawai *et al.*, 2001). Moreover, a genome-wide high throughput synthetic genetic array study revealed a negative genetic interaction of *SSC1* and *MDM38*, characterized by a more severe fitness defect of the double mutant strain compared to the expected additive effects of the combined single mutations (Costanzo *et al.*, 2010). However, although these findings support our results indicating a putative interaction of Ssc1p and Mdm38p, there is so far no evidence for a direct involvement of Ssc1p in mitochondrial ion homeostasis or K^+/H^+ exchange. Co-purification of Ssc1p with Mdm38p could therefore result from protein interaction during the import into and folding of Mdm38p inside mitochondria, without the necessity of involvement of both proteins in related processes and functions. This possibility is further supported by the finding that deletion of *MDM38* did not influence mitochondrial protein import (Frazier *et al.*, 2006). Nevertheless, direct measurement of K^+/H^+ exchange could be performed with mitochondria isolated from conditional *ssc1Δ* mutants, as deletion of *SSC1* is lethal.

The second identified interaction candidate Erg5p, a C-22 sterol desaturase which facilitates the penultimate step in ergosterol biosynthesis (Lees *et al.*, 1995), attracted our interest due to the following reasons: (i) ergosterol, which is the yeast counterpart of cholesterol in mammalian cells, plays an important role in membrane fluidity and permeability and membrane sterols were shown to influence the activity of cation transporters (Aguilera *et al.*, 2006; Benz & Cros, 1978; Deng *et al.*, 2009; Vemuri & Philipson, 1989) and membrane-bound enzymes, like the mitochondrial ATPase (Cobon & Haslam, 1973); (ii) enzymes involved in ergosterol synthesis were found to be associated with mitochondrial membranes

(Bailey & Parks, 1975; Zahedi *et al.*, 2006) and to be essential for maintenance of the mitochondrial morphology (Altmann & Westermann, 2005); and (iii) microarray experiments performed with the *mdm38* Δ mutant strain revealed upregulation of genes involved in the ergosterol synthesis pathway (Nowikovskiy K., unpublished data).

Interaction of Mdm38p with mitochondrial ribosomal proteins, as reported by Rehling and co-workers (Frazier *et al.*, 2006), was not observed in our hands. Human Letm1 was previously shown to interact with the AAA-ATPase Bcs1L, which influenced Letm1 complex assembly (Tamai *et al.*, 2008). Yeast encodes a homologous protein, Bcs1p, which is involved in the assembly of complex III of the mitochondrial respiratory chain (Conte *et al.*, 2010; Cruciat *et al.*, 1999). However, also Bcs1p was not co-purified with Mdm38p under our experimental conditions.

These discrepancies may either result from varying genetic backgrounds of the strains and different purification strategies used, or from diverse binding partners of Letm1 and Mdm38p in human and yeast, respectively.

6.3. Genetic interaction of *MDM38*, *ERG5*, and *ERG6*

To reveal possible genetic interactions of *MDM38*, *ERG5*, and *ERG6* we compared cellular growth of single and double mutant strains cultivated on fermentable (YPD) and non-fermentable (YPG, YPEG) media and under the influence of the potassium ionophore valinomycin (Figure 26), which specifically mediates potassium influx across the inner mitochondrial membrane (Kovac *et al.*, 1982a). Although Erg6p, a delta(24)-sterol C-methyltransferase converting zymosterol to fecosterol (Gaber *et al.*, 1989; Lees *et al.*, 1995), was not co-purified with Mdm38p, it was investigated since previous studies related its function with maintenance of mitochondrial morphology and cellular ion permeability (Dimmer *et al.*, 2002; Welihinda *et al.*, 1994).

Both double mutant strains, *mdm38* Δ *erg5* Δ and *mdm38* Δ *erg6* Δ , exhibited highly increased sensitivity to valinomycin compared to the single mutants. Moreover, on YPD or YPG, reduced fitness of the double mutants was observed as compared to single mutant strains, suggesting direct genetic interactions of Mdm38p, Erg5p, and Erg6p. Interestingly, *erg5* Δ mutant cells grew like wild-type cells. In contrast, *erg6* Δ cells exhibited a respiratory growth defect on non-fermentable media. Enzymes involved in the late steps of ergosterol biosynthesis were shown to be able to use improperly modified precursors as substrates and their disruption usually does not inhibit the ergosterol pathway (Daum *et al.*, 1998; Heese-

Peck *et al.*, 2002). The growth defect of *erg6Δ* mutants was therefore more likely caused by a role of Erg6p in an earlier step of the ergosterol biosynthesis than Erg5p, affecting more seriously the sterol composition and thus impairing mitochondrial function. Furthermore, *erg6Δ* cells exhibited an increased tolerance to valinomycin. Of note, *erg6Δ* mutants were also found to be hypersensitive to Na⁺ and Li⁺ (Welihinda *et al.*, 1994) and to various small lipophilic drugs (Emter *et al.*, 2002). As proposed by the authors, increased Na⁺ and Li⁺ uptake of *erg6Δ* cells may result from functionally altered cation transporters caused by a disturbed membrane sterol composition, as membrane sterols were shown to influence the activity of cation transporters (Benz & Cros, 1978; Deng *et al.*, 2009). Accordingly, Mdm38p would require Erg6p to function as a K⁺/H⁺ exchanger, to insert into the membrane, or to regulate the unknown exchanger. Alternatively, the unknown antiporter itself requires Erg6p to insert into the membrane or to exchange K⁺ against H⁺ and hence Mdm38p can hardly control the antiporter.

On the other hand, resistance to the lipophilic ionophore valinomycin cannot be completely explained. It has been shown previously that changes in the membrane sterol composition significantly influence the membrane response to ionophores (Kovac *et al.*, 1982a; Kovac *et al.*, 1982b). However, it is not clear how *erg6Δ* cells establish sensitivity to some lipophilic drugs and resistance to others. It is possible that the altered plasma membrane lipid composition either inhibits the cellular uptake of drugs larger than a certain molecular mass. Given that valinomycin is thought to specifically act on the mitochondrial inner membrane (Kovac *et al.*, 1982a), we may propose that the intercalation of the ionophore within the mitochondrial membrane is disturbed.

6.4. Disturbed mitochondrial and vacuolar morphology upon deletion of *MDM38*, *ERG5*, and *ERG6*

Based on the severe respiratory growth defect of *mdm38Δerg5Δ* and *mdm38Δerg6Δ* double mutant strains, we determined their mitochondrial and vacuolar morphology by fluorescence microscopy of cells expressing the mitochondrial matrix-targeted GFP and co-stained with the specific vacuole dye FM4-64.

Both single mutant strains, *erg5Δ* and *erg6Δ*, exhibited an intact mitochondrial reticulum but highly fragmented vacuoles when grown in galactose containing medium (Figure 27A). Similar vacuolar fragmentation was observed for both double mutant strains, although the multiple lobed vacuolar appearance was less pronounced in glucose medium (Figure 27B and

C), suggesting organellar morphology to be dependent on the provided carbon source. Vacuolar fragmentation in ergosterol mutants was already reported previously. Ergosterol was found to be important in the initial priming step of vacuolar fusion, thus disturbing this process when absent (Jones *et al.*, 2010; Kato & Wickner, 2001). Strikingly, mitochondria of *mdm38Δerg5Δ* and *mdm38Δerg6Δ* cells appeared completely fragmented irrespectively of the carbon source provided (Figure 27B and C), consistent with the reduced cellular viability caused by the disturbance of essential mitochondrial functions.

The organellar morphology of the *mdm38Δerg5Δ* and *mdm38Δerg6Δ* double mutant strains appeared similar to the triple mutant strain *mdm38Δmrs7Δ ydl183cΔ*. Triple mutant cells exhibited reduced viability, completely abolished K^+/H^+ exchange activity, and highly fragmented and colocalizing vacuoles and mitochondria, indicative of mitophagic degradation of dysfunctional mitochondria (Zotova *et al.*, 2010). Association of fragmented mitochondria and vacuoles was also observed in *mdm38Δerg5Δ* and *mdm38Δerg6Δ* cells (Figure 27B). However, although the organelles seemed to be in close contact, we never observed any overlapping fluorescence of the organellar markers, suggesting that mitophagy was blocked. Given the crucial role of ergosterol in fusion events for vacuoles, peroxisomes (Boukh-Viner *et al.*, 2005) or the plasma membrane during yeast mating (Jin *et al.*, 2008), it seems plausible that mitophagy was blocked in the double mutants, because engulfment and uptake of mitochondria would require membrane fusion of vacuoles.

6.5. Ergosterol and mitochondrial K^+/H^+ exchange

According to the observed physical and genetic interaction of Mdm38p with the ergosterol enzymes, we determined the K^+/H^+ exchange activity of the single and double mutant strains by KOAc-induced mitochondrial swelling.

Deletion of *MDM38* causes severely reduced mitochondrial swelling compared to the wild-type, indicative of impaired mitochondrial K^+/H^+ exchange (Figure 28 and (Nowikovsky *et al.*, 2004; Nowikovsky *et al.*, 2007)). Swelling of double mutant mitochondria of strains *mdm38Δerg5Δ* and *mdm38Δerg6Δ* was completely abolished, which is consistent with the synthetic phenotypic effects described above. Mitochondria of *erg5Δ* mutant cells exhibited wild-type swelling. In contrast, swelling of *erg6Δ* mitochondria was almost completely abolished. Absence of mitochondrial K^+/H^+ exchange leads to steadily increasing concentrations of matrix cations followed by an imbalance of osmotic pressure caused by subsequent water influx. Swelling of the mitochondria can be detected photometrically as a

reduced absorbance level. However, *erg6Δ* mitochondria were not swollen prior hypoosmotic KOAc treatment as detected by high initial light absorbance, and moreover, the mitochondrial reticulum of *erg6Δ* cells appeared intact under fluorescence microscopy (Figure 27A and 28A). These data are hard to reconcile with increased membrane fluidity suggested to be caused by ergosterol imbalance (Mukhopadhyay *et al.*, 2004; Sharma, 2006). Therefore we rather propose that reduced K^+/H^+ exchange activity seen in *erg6Δ* mitochondria is caused by an overload of matrix Mg^{2+} still remaining in isolated mitochondria, resulting from less or improper membrane insertion of the divalent cation ionophore A-23187. This hypothesis would be in line with the valinomycin resistance of *erg6Δ* cells and the reduced KOAc-induced mitochondrial swelling observed in absence of A-23187 (Nowikovskiy *et al.*, 2004). However, experimental evidence should be provided in future work.

Based on our results, the synthetic defects caused by double deletion of *MDM38* and *ERG5* or *ERG6* seem to be the consequence of several cellular alterations elicited by a disturbed membrane lipid composition. First, loss of membrane ergosterol was shown to increase cellular cation uptake in yeast (Welihinda *et al.*, 1994), suggesting that an altered membrane lipid composition causes an increased cytosolic cation concentration, followed by enhanced cation influx into cellular organelles. This may also explain the enhanced mitochondrial defect of the *mdm38Δerg5Δ* and *mdm38Δerg6Δ* double mutant strains. Second, ergosterol and cholesterol are not only needed for the regulation of membrane fusion and fluidity, but they also contribute to membrane organization by the formation of detergent-resistant plasma membrane domains called lipid rafts (Pike, 2009; Stradalova *et al.*, 2009), which were shown to be involved in cell signaling (Simons & Toomre, 2000) and endocytic protein turnover (Grossmann *et al.*, 2008; Walther *et al.*, 2006). Moreover, several cation transport proteins were found to be associated with lipid rafts, like the yeast plasma membrane Na^+/H^+ antiporter Nha1p (Dodelet-Devillers *et al.*, 2009; Mitsui *et al.*, 2009), and their function depends on the composition of their membrane lipid environment (Vemuri & Philipson, 1989). This raises the challenging question if changed membrane sterol contents directly affect mitochondrial ion homeostasis by modulating cation transporter activity. Interestingly, reduction of cholesterol in rat liver lysosomes caused increased fluidity and permeability of the membrane to potassium and protons, presumably provoked by the action of a lysosomal K^+/H^+ exchanger (Deng *et al.*, 2009). Furthermore, treatment of yeast cells with inhibitors of ergosterol synthesis caused increased K^+/H^+ exchange across the plasma membrane (Calahorra *et al.*, 2010). Finally, ergosterol biosynthesis itself appears to be linked to cation

homeostasis, as Erg6p was found to be inhibited by mitochondrial potassium accumulation (Bailey & Parks, 1975).

Taken together, our data represent the first direct correlation of mitochondrial K^+/H^+ exchange and membrane sterol composition for the maintenance of mitochondrial morphology, cation homeostasis, and cellular viability. However, it remains to be determined how ergosterol exactly affects Mdm38p and thereby mitochondrial function.

6.6. Synthetic genetic array analysis

We initially aimed at identifying synthetic lethal interactions of the *mdm38Δ* strain, thereby revealing genes involved in related functions or compensatory pathways of the mitochondrial K^+/H^+ exchange system.

Surprisingly, we failed to identify any synthetic lethal interactions of *mdm38Δ*. Synthetic lethality of the double mutant strains *mdm38Δcdc73Δ* and *mdm38Δchs1Δ*, as reported by two individual SGA screens (Lesage *et al.*, 2005; Tong *et al.*, 2004), was not observed in our assay. Recently, we found that the inner mitochondrial membrane proteins Mrs7p and Ydl183cp/Mkr1p restored K^+/H^+ exchange when overexpressed in *mdm38Δ* cells, but deletion of all three genes resulted only in synthetic sickness, not lethality (Zotova *et al.*, 2010). Together, this suggests an essential function of Mdm38p in K^+/H^+ exchange, apparently not completely compensated by functionally redundant proteins in its absence.

Subsequently, we investigated possible synthetic suppressive interactions of *mdm38Δ*, characterized by restored growth of double mutants due to deletion of genes involved in processes acting contrary to K^+/H^+ exchange, like cation import. We identified six double mutant strains exhibiting restored respiratory growth comparable to the wild-type (Figure 30 and 31). Three of those six genes deleted in the *mdm38Δ* background, *CTK1*, *SSN8*, and *RTF1*, were reported to be involved in transcriptional regulation (Table 5). Thus, synthetic suppression may be the secondary consequence of changed transcription of several unknown target genes. Therefore, we focused on the three residual genes (Table 5) which are of unknown function (*LDB16*), involved in cytokinesis (*HOF1*), and in histone modification and cell fusion (*RXT2*). By fluorescence microscopy we observed that the *mdm38Δldb16Δ*, *mdm38Δhof1Δ*, and *mdm38Δrxt2Δ* double mutant strains exhibited a restored branched mitochondrial reticulum (Figure 32B).

Currently, we can only hypothesize on the mechanisms underlying the suppressive effects exhibited by the double mutant strains. Based on cellular growth (Figure 31), suppression

observed for *mdm38Δldb16Δ* cells may result from a dominant effect of *LDB16* deletion, as growth of the double mutant strain was identical to the *ldb16Δ* single mutant. In contrast, suppression of *mdm38Δhof1Δ* and *mdm38Δrxt2Δ* may be the consequence of deletion of both genes, as the double mutants exhibited better growth than either single mutant. Cells deleted for *LDB16*, whose gene product was detected in lipid particles and mitochondria (Reinders *et al.*, 2006; Wagner *et al.*, 2009), were reported to be sensitive to Ni^{2+} (Bishop *et al.*, 2007), but so far there is no clear evidence that any of the genes found by SGA analysis is involved in cation transport. In our recent publication we characterized multicopy suppressors of the *mdm38Δ* strain. Two of those suppressors, the P_i carrier Pic2p and the Fe^{2+} carrier Mrs3p, were shown to be not directly involved in K^+/H^+ exchange but to increase the mitochondrial membrane potential ($\Delta\psi$), thereby possibly restoring mitochondrial morphology and respiratory growth of the *mdm38Δ* mutant (Zotova *et al.*, 2010). Hence, synthetic suppression of the double mutant strains may originate from similar indirect effects on mitochondrial $\Delta\psi$ or K^+ homeostasis, which will require further investigation for their revelation.

6.7. Is Mdm38p the mitochondrial K^+/H^+ exchanger?

According to previous studies and our own results, we established a working hypothesis based on the idea of Mdm38p functioning as an essential regulatory protein directly interacting with the so far unknown K^+/H^+ exchanger. To uncover the molecular identity of the antiporter, we performed affinity chromatography analyses of Mdm38p followed by mass spectrometry of co-purified proteins. Interestingly, we found the essential mitochondrial chaperon Ssc1p and the ergosterol biosynthetic enzyme Erg5p as interaction partners of Mdm38p, but failed to identify potential candidates serving as the K^+/H^+ exchanger.

This suggests two possible explanations. Either Mdm38p indeed is a regulatory component of the K^+/H^+ exchanger which was not identified due to dissociation from the protein complex during purification, or Mdm38p itself forms the exchanger, apparently by homo-oligomerization. Facing our presented data and extensive efforts to identify the antiporter, we tend to support the latter possibility although this would be in contrast to our initial consideration. However, based on SDS-PAGE migration of OSH-tagged Mdm38p (~ 80 kDa, Figure 24), which is slightly higher than its predicted molecular weight (~ 75 kDa), the Mdm38p complex (~ 550 kDa, Figure 23) may consist of a ‘core’ Mdm38p hexamer bound to its interaction partners, although size determination of protein complexes based on size exclusion chromatography and Blue native electrophoresis is not fully reliable.

A recent publication of Jiang *et al.* (Jiang *et al.*, 2009) reports that a genome-wide siRNA screen in *Drosophila* S2 cells identified Letm1 as the mitochondrial $\text{Ca}^{2+}/\text{H}^{+}$ exchanger. Knockdown of Letm1 caused decreased mitochondrial Ca^{2+} uptake and H^{+} efflux. Reconstitution of Letm1 in liposomes and uptake assays led the authors to the conclusion that Letm1 is an electrogenic mitochondrial $\text{Ca}^{2+}/\text{H}^{+}$ exchanger rather than the electroneutral $\text{K}^{+}/\text{H}^{+}$ exchanger.

These findings are very surprising, especially considering that the function of the $\text{Ca}^{2+}/\text{H}^{+}$ exchanger is to mediate Ca^{2+} efflux in order to avoid mitochondrial calcification (Gunter *et al.*, 2000; Mitchell, 1966). In yeast, *mdm38 Δ* mitochondria also exhibited reduced Ca^{2+} and Mg^{2+} influx, which was shown to be the cause of a decreased $\Delta\psi$ following absent $\text{K}^{+}/\text{H}^{+}$ exchange (Nowikovsky *et al.*, 2004). Finally, Jiang *et al.* reported that the Ca^{2+} fluxes mediated by Letm1 were Ruthenium Red sensitive. This is not in accord with the consensus that the $\text{Ca}^{2+}/\text{H}^{+}$ exchanger is insensitive to this inhibitor (Bernardi, 1999).

However, Letm1 was shown to restore yeast mitochondrial $\text{K}^{+}/\text{H}^{+}$ exchange as efficiently as the exogenous $\text{K}^{+}/\text{H}^{+}$ exchanger nigericin (Froschauer *et al.*, 2005; Nowikovsky *et al.*, 2004; Zotova *et al.*, 2010), suggesting a role of Letm1 in mitochondrial cation efflux. Interestingly, the mammalian mitochondrial $\text{K}^{+}/\text{H}^{+}$ exchanger, a ~ 82 kDa protein whose molecular identity still remains unknown, was functionally reconstituted into liposomes (Kakar *et al.*, 1989; Li *et al.*, 1990) and strikingly almost matches the molecular weight of Letm1 (~ 83 kDa).

These controversial results raise the question if Mdm38p and Letm1 are involved in different cation transport processes in yeast and higher eukaryotes, or if the observed effect on mitochondrial Ca^{2+} transport is the consequence of a disturbed K^{+} homeostasis. However, a coupled exchange of Ca^{2+} for K^{+} by the action of a mitochondrial $\text{Ca}^{2+}/\text{K}^{+}$ antiporter (Selwyn *et al.*, 1970) has already been ruled out, as Ca^{2+} influx into mitochondria was not found to be followed by K^{+} efflux (Puskin *et al.*, 1976).

In order to answer these challenging questions, we started to bacterially overexpress Letm1 for affinity purification, reconstitution into liposomes, and direct ion flux measurements (collaboration with Dr. Cesare Indiveri, University of Calabria, Italy). Thereby we hope to unravel possible $\text{K}^{+}/\text{H}^{+}$ exchange properties of Letm1 and, together with our results presented in this study, to contribute to a better understanding of the complex topic of cellular and organellar cation homeostasis.

7. Abbreviations

$\Delta\psi$	Mitochondrial membrane potential
Δp	Proton electrochemical gradient
ΔpH	pH gradient
$[K^+]_o$	Outside K^+ concentration
3-AT	3-Amino-1,2,4-triazole
ACAT	Acyl-CoA sterol acyl transferases
BCECF	2,7-bis(carboxyethyl)-5,6-carboxyfluorescein
CBP	Calmodulin binding peptide
DCCD	Dicyclohexylcarbodiimide
DIC	Differential interference contrast
DSS	Disuccinimidyl suberate
EMT	Epithelial-to-mesenchymal transition
ETC	Electron transport chain
FCCP	Carbonyl cyanide <i>p</i> -trifluoromethoxyphenylhydrazone
HAc	Acetic acid
HRP	Horse radish peroxidase
IMM	Inner mitochondrial membrane
IMS	Intermembrane space
KHE	K^+/H^+ exchanger
KOAc	Potassium acetate
mAU	Milliampere units
MET	Mesenchymal-to-epithelial transition
MS	Mass spectrometry
mtGFP	Mitochondrial matrix-targeted GFP
NaOAc	Sodium acetate
NHS	N-hydroxysuccinimide
Nig	Nigericin
Ni-NTA	Nickel-nitrilotriacetic acid
OMM	Outer mitochondrial membrane
OS	One-Strep
OSH	One-Strep-HIS

Abbreviations

PAP	Anti-protein A antibody
PBFI	Potassium-binding benzofuran isophthalate
SEC	Size exclusion chromatography
SGA	Synthetic genetic array
SGD	<i>Saccharomyces</i> Genome Database
SMP	Submitochondrial particles
TAP	Tandem affinity purification
TCA	Trichloroacetic acid
TEV	Tobacco Etch Virus
TX-100	Triton X-100
Val	Valinomycin
VDAC	Voltage-dependent anion channel
WHS	Wolf-Hirschhorn syndrome

8. References

- Abeliovich, H. & Klionsky, D. J. (2001).** Autophagy in yeast: mechanistic insights and physiological function. *Microbiol Mol Biol Rev* **65**, 463-479, table of contents.
- Aguilera, F., Peinado, R. A., Millan, C., Ortega, J. M. & Mauricio, J. C. (2006).** Relationship between ethanol tolerance, H⁺-ATPase activity and the lipid composition of the plasma membrane in different wine yeast strains. *International journal of food microbiology* **110**, 34-42.
- Alexander, C., Votruba, M., Pesch, U. E. & other authors (2000).** *OPA1*, encoding a dynamin-related GTPase, is mutated in autosomal dominant optic atrophy linked to chromosome 3q28. *Nature genetics* **26**, 211-215.
- Altmann, K. & Westermann, B. (2005).** Role of essential genes in mitochondrial morphogenesis in *Saccharomyces cerevisiae*. *Molecular biology of the cell* **16**, 5410-5417.
- Arino, J., Ramos, J. & Sychrova, H. (2010).** Alkali metal cation transport and homeostasis in yeasts. *Microbiol Mol Biol Rev* **74**, 95-120.
- Azzone, G. F., Massair, S. & Pozzan, T. (1976).** Mechanism of active shrinkage in mitochondria. II. Coupling between strong electrolyte fluxes. *Biochimica et biophysica acta* **423**, 27-41.
- Azzone, G. F., Bragadin, M., Pozzan, T. & Antone, P. D. (1977).** Proton electrochemical potential in steady state rat liver mitochondria. *Biochimica et biophysica acta* **459**, 96-109.
- Azzone, G. F., Bortolotto, F. & Zanotti, A. (1978).** Induction of electroneutral exchanges of H⁺ with K⁺ in rat liver mitochondria. *FEBS letters* **96**, 135-140.
- Bailey, R. B. & Parks, L. W. (1975).** Potassium translocation in yeast mitochondria and its relationship to ergosterol biosynthesis. *Journal of bacteriology* **122**, 606-609.
- Balciunas, D. & Ronne, H. (1995).** Three subunits of the RNA polymerase II mediator complex are involved in glucose repression. *Nucleic acids research* **23**, 4421-4425.
- Baloh, R. H., Schmidt, R. E., Pestronk, A. & Milbrandt, J. (2007).** Altered axonal mitochondrial transport in the pathogenesis of Charcot-Marie-Tooth disease from mitofusin 2 mutations. *J Neurosci* **27**, 422-430.
- Battaglino, R. A., Pham, L., Morse, L. R., Vokes, M., Sharma, A., Odgren, P. R., Yang, M., Sasaki, H. & Stashenko, P. (2008).** NHA-oc/NHA2: a mitochondrial cation-proton antiporter selectively expressed in osteoclasts. *Bone* **42**, 180-192.
- Bauerschmitt, H., Mick, D. U., Deckers, M., Vollmer, C., Funes, S., Kehrein, K., Ott, M., Rehling, P. & Herrmann, J. M. (2010).** Ribosome-binding proteins Mdm38 and Mba1 display overlapping functions for regulation of mitochondrial translation. *Molecular biology of the cell* **21**, 1937-1944.

- Beavis, A. D. & Garlid, K. D. (1990).** Evidence for the allosteric regulation of the mitochondrial K^+/H^+ antiporter by matrix protons. *The Journal of biological chemistry* **265**, 2538-2545.
- Benz, R. & Cros, D. (1978).** Influence of sterols on ion transport through lipid bilayer membranes. *Biochimica et biophysica acta* **506**, 265-280.
- Bereiter-Hahn, J. & Voth, M. (1994).** Dynamics of mitochondria in living cells: shape changes, dislocations, fusion, and fission of mitochondria. *Microscopy research and technique* **27**, 198-219.
- Bergemann, A. D., Cole, F. & Hirschhorn, K. (2005).** The etiology of Wolf-Hirschhorn syndrome. *Trends Genet* **21**, 188-195.
- Bernardi, P. (1999).** Mitochondrial transport of cations: channels, exchangers, and permeability transition. *Physiological reviews* **79**, 1127-1155.
- Biessels, G. & Gispen, W. H. (1996).** The calcium hypothesis of brain aging and neurodegenerative disorders: significance in diabetic neuropathy. *Life sciences* **59**, 379-387.
- Bishop, A. L., Rab, F. A., Sumner, E. R. & Avery, S. V. (2007).** Phenotypic heterogeneity can enhance rare-cell survival in 'stress-sensitive' yeast populations. *Molecular microbiology* **63**, 507-520.
- Bleazard, W., McCaffery, J. M., King, E. J., Bale, S., Mozdy, A., Tieu, Q., Nunnari, J. & Shaw, J. M. (1999).** The dynamin-related GTPase Dnm1 regulates mitochondrial fission in yeast. *Nature cell biology* **1**, 298-304.
- Blondin, G. A., Vail, W. J. & Green, D. E. (1969).** The mechanism of mitochondrial swelling. II. Pseudoenergized swelling in the presence of alkali metal salts. *Archives of biochemistry and biophysics* **129**, 158-172.
- Boone, C., Bussey, H. & Andrews, B. J. (2007).** Exploring genetic interactions and networks with yeast. *Nature reviews* **8**, 437-449.
- Boukh-Viner, T., Guo, T., Alexandrian, A. & other authors (2005).** Dynamic ergosterol- and ceramide-rich domains in the peroxisomal membrane serve as an organizing platform for peroxisome fusion. *The Journal of cell biology* **168**, 761-773.
- Bowers, K., Levi, B. P., Patel, F. I. & Stevens, T. H. (2000).** The sodium/proton exchanger Nhx1p is required for endosomal protein trafficking in the yeast *Saccharomyces cerevisiae*. *Molecular biology of the cell* **11**, 4277-4294.
- Brett, C. L., Wei, Y., Donowitz, M. & Rao, R. (2002).** Human $Na(+)/H(+)$ exchanger isoform 6 is found in recycling endosomes of cells, not in mitochondria. *Am J Physiol Cell Physiol* **282**, C1031-1041.
- Brett, C. L., Donowitz, M. & Rao, R. (2005a).** Evolutionary origins of eukaryotic sodium/proton exchangers. *Am J Physiol Cell Physiol* **288**, C223-239.

- Brett, C. L., Tukaye, D. N., Mukherjee, S. & Rao, R. (2005b).** The yeast endosomal Na⁺K⁺/H⁺ exchanger Nhx1 regulates cellular pH to control vesicle trafficking. *Molecular biology of the cell* **16**, 1396-1405.
- Brierley, G. P., Jurkowitz, M. S., Farooqui, T. & Jung, D. W. (1984).** K⁺/H⁺ antiport in heart mitochondria. *The Journal of biological chemistry* **259**, 14672-14678.
- Brierley, G. P., Davis, M. H., Cragoe, E. J., Jr. & Jung, D. W. (1989).** Kinetic properties of the Na⁺/H⁺ antiport of heart mitochondria. *Biochemistry* **28**, 4347-4354.
- Brierley, G. P., Panzeter, E. S. & Jung, D. W. (1991).** Regulation of mitochondrial K⁺/H⁺ antiport activity by hydrogen ions. *Archives of biochemistry and biophysics* **288**, 358-367.
- Brierley, G. P., Baysal, K. & Jung, D. W. (1994).** Cation transport systems in mitochondria: Na⁺ and K⁺ uniports and exchangers. *Journal of bioenergetics and biomembranes* **26**, 519-526.
- Burgess, D. L., Jones, J. M., Meisler, M. H. & Noebels, J. L. (1997).** Mutation of the Ca²⁺ channel beta subunit gene Cchb4 is associated with ataxia and seizures in the lethargic (lh) mouse. *Cell* **88**, 385-392.
- Butow, R. A. & Avadhani, N. G. (2004).** Mitochondrial signaling: the retrograde response. *Molecular cell* **14**, 1-15.
- Calahorra, M., Lozano, C., Sanchez, N. S. & Pena, A. (2010).** Ketoconazole and miconazole alter potassium homeostasis in *Saccharomyces cerevisiae*. *Biochimica et biophysica acta* **1808**, 433-445.
- Chan, D. C. (2006).** Mitochondrial fusion and fission in mammals. *Annual review of cell and developmental biology* **22**, 79-99.
- Chen, H. & Chan, D. C. (2009).** Mitochondrial dynamics--fusion, fission, movement, and mitophagy--in neurodegenerative diseases. *Human molecular genetics* **18**, R169-176.
- Cho, G. W., Shin, S. M., Kim, H. K., Ha, S. A., Kim, S., Yoon, J. H., Hur, S. Y., Kim, T. E. & Kim, J. W. (2007).** *HCCR-1*, a novel oncogene, encodes a mitochondrial outer membrane protein and suppresses the UVC-induced apoptosis. *BMC cell biology* **8**, 50.
- Cobon, G. S. & Haslam, J. M. (1973).** The effect of altered membrane sterol composition on the temperature dependence of yeast mitochondrial ATPase. *Biochemical and biophysical research communications* **52**, 320-326.
- Cockrell, R. S. (1973).** Energy-linked ion translocation in submitochondrial particles. 3. Transport of monovalent cations by submitochondrial particles. *The Journal of biological chemistry* **248**, 6828-6833.
- Colina, A. R. & Young, D. (2005).** Raf60, a novel component of the Rpd3 histone deacetylase complex required for Rpd3 activity in *Saccharomyces cerevisiae*. *The Journal of biological chemistry* **280**, 42552-42556.

- Conte, L., Trumpower, B. L. & Zara, V. (2010).** Bcs1p can rescue a large and productive cytochrome bc(1) complex assembly intermediate in the inner membrane of yeast mitochondria. *Biochimica et biophysica acta* **1813**, 91-101.
- Costanzo, M., Baryshnikova, A., Bellay, J. & other authors (2010).** The genetic landscape of a cell. *Science (New York, NY)* **327**, 425-431.
- Cruciat, C. M., Hell, K., Folsch, H., Neupert, W. & Stuart, R. A. (1999).** Bcs1p, an AAA-family member, is a chaperone for the assembly of the cytochrome bc(1) complex. *The EMBO journal* **18**, 5226-5233.
- Danial, N. N. & Korsmeyer, S. J. (2004).** Cell death: critical control points. *Cell* **116**, 205-219.
- Daniel, J. A., Yoo, J., Bettinger, B. T., Amberg, D. C. & Burke, D. J. (2006).** Eliminating gene conversion improves high-throughput genetics in *Saccharomyces cerevisiae*. *Genetics* **172**, 709-711.
- Daum, G., Lees, N. D., Bard, M. & Dickson, R. (1998).** Biochemistry, cell biology and molecular biology of lipids of *Saccharomyces cerevisiae*. *Yeast (Chichester, England)* **14**, 1471-1510.
- Deng, D., Jiang, N., Hao, S. J., Sun, H. & Zhang, G. J. (2009).** Loss of membrane cholesterol influences lysosomal permeability to potassium ions and protons. *Biochimica et biophysica acta* **1788**, 470-476.
- Dimmer, K. S., Fritz, S., Fuchs, F., Messerschmitt, M., Weinbach, N., Neupert, W. & Westermann, B. (2002).** Genetic basis of mitochondrial function and morphology in *Saccharomyces cerevisiae*. *Molecular biology of the cell* **13**, 847-853.
- Dimmer, K. S., Navoni, F., Casarin, A., Trevisson, E., Endeley, S., Winterpacht, A., Salvati, L. & Scorrano, L. (2008).** *LETM1*, deleted in Wolf-Hirschhorn syndrome is required for normal mitochondrial morphology and cellular viability. *Human molecular genetics* **17**, 201-214.
- DiResta, D. J., Kutschke, K. P., Hottois, M. D. & Garlid, K. D. (1986).** K^+ - H^+ exchange and volume homeostasis in brown adipose tissue mitochondria. *The American journal of physiology* **251**, R787-793.
- Dodelet-Devillers, A., Cayrol, R., van Horsen, J., Haqqani, A. S., de Vries, H. E., Engelhardt, B., Greenwood, J. & Prat, A. (2009).** Functions of lipid raft membrane microdomains at the blood-brain barrier. *Journal of molecular medicine (Berlin, Germany)* **87**, 765-774.
- Dordick, R. S., Brierley, G. P. & Garlid, K. D. (1980).** On the mechanism of A23187-induced potassium efflux in rat liver mitochondria. *The Journal of biological chemistry* **255**, 10299-10305.
- Douglas, M. G. & Cockrell, R. S. (1974).** Mitochondrial cation-hydrogen ion exchange. Sodium selective transport by mitochondria and submitochondrial particles. *The Journal of biological chemistry* **249**, 5464-5471.

- Duszynski, J. & Wojtczak, L. (1977).** Effect of Mg^{2+} depletion of mitochondria on their permeability to K^+ : the mechanism by which ionophore A23187 increases K^+ permeability. *Biochemical and biophysical research communications* **74**, 417-424.
- Egner, A., Jakobs, S. & Hell, S. W. (2002).** Fast 100-nm resolution three-dimensional microscope reveals structural plasticity of mitochondria in live yeast. *Proceedings of the National Academy of Sciences of the United States of America* **99**, 3370-3375.
- Emter, R., Heese-Peck, A. & Kralli, A. (2002).** *ERG6* and *PDR5* regulate small lipophilic drug accumulation in yeast cells via distinct mechanisms. *FEBS letters* **521**, 57-61.
- Endele, S., Fuhry, M., Pak, S. J., Zabel, B. U. & Winterpacht, A. (1999).** *LETM1*, a novel gene encoding a putative EF-hand Ca^{2+} -binding protein, flanks the Wolf-Hirschhorn syndrome (WHS) critical region and is deleted in most WHS patients. *Genomics* **60**, 218-225.
- Entian, K. D., Schuster, T., Hegemann, J. H. & other authors (1999).** Functional analysis of 150 deletion mutants in *Saccharomyces cerevisiae* by a systematic approach. *Mol Gen Genet* **262**, 683-702.
- Fafournoux, P., Noel, J. & Pouyssegur, J. (1994).** Evidence that Na^+/H^+ exchanger isoforms NHE1 and NHE3 exist as stable dimers in membranes with a high degree of specificity for homodimers. *The Journal of biological chemistry* **269**, 2589-2596.
- Frazier, A. E., Taylor, R. D., Mick, D. U., Warscheid, B., Stoepel, N., Meyer, H. E., Ryan, M. T., Guiard, B. & Rehling, P. (2006).** Mdm38 interacts with ribosomes and is a component of the mitochondrial protein export machinery. *The Journal of cell biology* **172**, 553-564.
- Froschauer, E., Nowikovsky, K. & Schweyen, R. J. (2005).** Electroneutral K^+/H^+ exchange in mitochondrial membrane vesicles involves *Yol027/Letm1* proteins. *Biochimica et biophysica acta* **1711**, 41-48.
- Fuster, D. G., Zhang, J., Shi, M., Bobulescu, I. A., Andersson, S. & Moe, O. W. (2008).** Characterization of the sodium/hydrogen exchanger NHA2. *J Am Soc Nephrol* **19**, 1547-1556.
- Gaber, R. F., Copple, D. M., Kennedy, B. K., Vidal, M. & Bard, M. (1989).** The yeast gene *ERG6* is required for normal membrane function but is not essential for biosynthesis of the cell-cycle-sparking sterol. *Molecular and cellular biology* **9**, 3447-3456.
- Garlid, K. D. (1980).** On the mechanism of regulation of the mitochondrial K^+/H^+ exchanger. *The Journal of biological chemistry* **255**, 11273-11279.
- Garlid, K. D., DiResta, D. J., Beavis, A. D. & Martin, W. H. (1986).** On the mechanism by which dicyclohexylcarbodiimide and quinine inhibit K^+ transport in rat liver mitochondria. *The Journal of biological chemistry* **261**, 1529-1535.
- Garlid, K. D., Shariat-Madar, Z., Nath, S. & Jezek, P. (1991).** Reconstitution and partial purification of the Na^+ -selective Na^+/H^+ antiporter of beef heart mitochondria. *The Journal of biological chemistry* **266**, 6518-6523.

- Garlid, K. D. & Paucek, P. (2003).** Mitochondrial potassium transport: the K(+) cycle. *Biochimica et biophysica acta* **1606**, 23-41.
- Gegg, M. E., Cooper, J. M., Chau, K. Y., Rojo, M., Schapira, A. H. & Taanman, J. W. (2010).** Mitofusin 1 and mitofusin 2 are ubiquitinated in a PINK1/parkin-dependent manner upon induction of mitophagy. *Human molecular genetics* **19**, 4861-4870.
- Geisler, S., Holmstrom, K. M., Treis, A., Skujat, D., Weber, S. S., Fiesel, F. C., Kahle, P. J. & Springer, W. (2010).** The PINK1/Parkin-mediated mitophagy is compromised by PD-associated mutations. *Autophagy* **6**, 871-878.
- Gietz, R. D. & Sugino, A. (1988).** New yeast-Escherichia coli shuttle vectors constructed with in vitro mutagenized yeast genes lacking six-base pair restriction sites. *Gene* **74**, 527-534.
- Goldman, S. J., Taylor, R., Zhang, Y. & Jin, S. (2010).** Autophagy and the degradation of mitochondria. *Mitochondrion* **10**, 309-315.
- Grossmann, G., Malinsky, J., Stahlschmidt, W., Loibl, M., Weig-Meckl, I., Frommer, W. B., Opekarova, M. & Tanner, W. (2008).** Plasma membrane microdomains regulate turnover of transport proteins in yeast. *The Journal of cell biology* **183**, 1075-1088.
- Guarente, L. (1993).** Synthetic enhancement in gene interaction: a genetic tool come of age. *Trends Genet* **9**, 362-366.
- Gueldener, U., Heinisch, J., Koehler, G. J., Voss, D. & Hegemann, J. H. (2002).** A second set of loxP marker cassettes for Cre-mediated multiple gene knockouts in budding yeast. *Nucleic acids research* **30**, e23.
- Gunter, T. E., Buntinas, L., Sparagna, G., Eliseev, R. & Gunter, K. (2000).** Mitochondrial calcium transport: mechanisms and functions. *Cell calcium* **28**, 285-296.
- Gutierrez, M. G., Master, S. S., Singh, S. B., Taylor, G. A., Colombo, M. I. & Deretic, V. (2004).** Autophagy is a defense mechanism inhibiting BCG and Mycobacterium tuberculosis survival in infected macrophages. *Cell* **119**, 753-766.
- Ha, S. A., Kim, H. K., Yoo, J. & other authors (2010).** Transdifferentiation-inducing *HCCR-1* oncogene. *BMC cell biology* **11**, 49.
- Hampsey, M. & Kinzy, T. G. (2007).** Synchronicity: policing multiple aspects of gene expression by Ctk1. *Genes & development* **21**, 1288-1291.
- Hasegawa, A. & van der Blik, A. M. (2007).** Inverse correlation between expression of the Wolfs Hirschhorn candidate gene *Letm1* and mitochondrial volume in *C. elegans* and in mammalian cells. *Human molecular genetics* **16**, 2061-2071.
- Heese-Peck, A., Pichler, H., Zanolari, B., Watanabe, R., Daum, G. & Riezman, H. (2002).** Multiple functions of sterols in yeast endocytosis. *Molecular biology of the cell* **13**, 2664-2680.

- Hisamitsu, T., Ben Ammar, Y., Nakamura, T. Y. & Wakabayashi, S. (2006).** Dimerization is crucial for the function of the Na⁺/H⁺ exchanger NHE1. *Biochemistry* **45**, 13346-13355.
- Hoffmann, E. K. & Dunham, P. B. (1995).** Membrane mechanisms and intracellular signalling in cell volume regulation. *International review of cytology* **161**, 173-262.
- Hoffmann, H. P. & Avers, C. J. (1973).** Mitochondrion of yeast: ultrastructural evidence for one giant, branched organelle per cell. *Science (New York, NY)* **181**, 749-751.
- Hofstetter, W., Siegrist, M., Simonin, A., Bonny, O. & Fuster, D. G. (2010).** Sodium/hydrogen exchanger NHA2 in osteoclasts: subcellular localization and role in vitro and in vivo. *Bone* **47**, 331-340.
- Huang, W. P. & Klionsky, D. J. (2002).** Autophagy in yeast: a review of the molecular machinery. *Cell structure and function* **27**, 409-420.
- Huh, W. K., Falvo, J. V., Gerke, L. C., Carroll, A. S., Howson, R. W., Weissman, J. S. & O'Shea, E. K. (2003).** Global analysis of protein localization in budding yeast. *Nature* **425**, 686-691.
- Jiang, D., Zhao, L. & Clapham, D. E. (2009).** Genome-wide RNAi screen identifies Letm1 as a mitochondrial Ca²⁺/H⁺ antiporter. *Science (New York, NY)* **326**, 144-147.
- Jin, H., McCaffery, J. M. & Grote, E. (2008).** Ergosterol promotes pheromone signaling and plasma membrane fusion in mating yeast. *The Journal of cell biology* **180**, 813-826.
- Jones, L., Tedrick, K., Baier, A., Logan, M. R. & Eitzen, G. (2010).** Cdc42p is activated during vacuole membrane fusion in a sterol-dependent subreaction of priming. *The Journal of biological chemistry* **285**, 4298-4306.
- Jung, D. W. & Brierley, G. P. (1999).** Matrix free Mg(2+) and the regulation of mitochondrial volume. *The American journal of physiology* **277**, C1194-1201.
- Junttila, M. R., Saarinen, S., Schmidt, T., Kast, J. & Westermarck, J. (2005).** Single-step Strep-tag purification for the isolation and identification of protein complexes from mammalian cells. *Proteomics* **5**, 1199-1203.
- Kakar, S. S., Mahdi, F., Li, X. Q. & Garlid, K. D. (1989).** Reconstitution of the mitochondrial non-selective Na⁺/H⁺ (K⁺/H⁺) antiporter into proteoliposomes. *The Journal of biological chemistry* **264**, 5846-5851.
- Kang, P. J., Ostermann, J., Shilling, J., Neupert, W., Craig, E. A. & Pfanner, N. (1990).** Requirement for hsp70 in the mitochondrial matrix for translocation and folding of precursor proteins. *Nature* **348**, 137-143.
- Kanki, T., Wang, K. & Klionsky, D. J. (2010).** A genomic screen for yeast mutants defective in mitophagy. *Autophagy* **6**, 278-280.

- Kanki, T., Wang, K., Cao, Y., Baba, M. & Klionsky, D. J. (2009).** Atg32 is a mitochondrial protein that confers selectivity during mitophagy. *Developmental cell* **17**, 98-109.
- Karbowski, M. & Youle, R. J. (2003).** Dynamics of mitochondrial morphology in healthy cells and during apoptosis. *Cell death and differentiation* **10**, 870-880.
- Kato, M. & Wickner, W. (2001).** Ergosterol is required for the Sec18/ATP-dependent priming step of homotypic vacuole fusion. *The EMBO journal* **20**, 4035-4040.
- Kawai, A., Nishikawa, S., Hirata, A. & Endo, T. (2001).** Loss of the mitochondrial Hsp70 functions causes aggregation of mitochondria in yeast cells. *Journal of cell science* **114**, 3565-3574.
- Kelly, S. L., Lamb, D. C., Corran, A. J., Baldwin, B. C., Parks, L. W. & Kelly, D. E. (1995).** Purification and reconstitution of activity of *Saccharomyces cerevisiae* P450 61, a sterol delta 22-desaturase. *FEBS letters* **377**, 217-220.
- Kinclova-Zimmermannova, O., Flegelova, H. & Sychrova, H. (2004).** Rice Na⁺/H⁺-antiporter Nhx1 partially complements the alkali-metal-cation sensitivity of yeast strains lacking three sodium transporters. *Folia microbiologica* **49**, 519-525.
- Kissova, I., Deffieu, M., Manon, S. & Camougrand, N. (2004).** Uth1p is involved in the autophagic degradation of mitochondria. *The Journal of biological chemistry* **279**, 39068-39074.
- Ko, J., Lee, Y. H., Hwang, S. Y. & other authors (2003).** Identification and differential expression of novel human cervical cancer oncogene *HCCR-2* in human cancers and its involvement in p53 stabilization. *Oncogene* **22**, 4679-4689.
- Ko, J., Shin, S. M., Oh, Y. M., Lee, Y. S., Ryoo, Z. Y., Lee, Y. H., Na, D. S. & Kim, J. W. (2004).** Transgenic mouse model for breast cancer: induction of breast cancer in novel oncogene *HCCR-2* transgenic mice. *Oncogene* **23**, 1950-1953.
- Kolisek, M., Zsurka, G., Samaj, J., Weghuber, J., Schweyen, R. J. & Schweigel, M. (2003).** Mrs2p is an essential component of the major electrophoretic Mg²⁺ influx system in mitochondria. *The EMBO journal* **22**, 1235-1244.
- Kovac, L., Bohmerova, E. & Butko, P. (1982a).** Ionophores and intact cells. I. Valinomycin and nigericin act preferentially on mitochondria and not on the plasma membrane of *Saccharomyces cerevisiae*. *Biochimica et biophysica acta* **721**, 341-348.
- Kovac, L., Poliachova, V. & Horvath, I. (1982b).** Ionophores and intact cells. II. Olefinin acts on mitochondria and induces disintegration of the mitochondrial genome in yeast *Saccharomyces cerevisiae*. *Biochimica et biophysica acta* **721**, 349-356.
- Kuchin, S., Yeghiayan, P. & Carlson, M. (1995).** Cyclin-dependent protein kinase and cyclin homologs *SSN3* and *SSN8* contribute to transcriptional control in yeast. *Proceedings of the National Academy of Sciences of the United States of America* **92**, 4006-4010.

- Kundu, M., Lindsten, T., Yang, C. Y., Wu, J., Zhao, F., Zhang, J., Selak, M. A., Ney, P. A. & Thompson, C. B. (2008).** Ulk1 plays a critical role in the autophagic clearance of mitochondria and ribosomes during reticulocyte maturation. *Blood* **112**, 1493-1502.
- Lathe, G. H. & Ruthven, C. R. (1955).** The separation of substances on the basis of their molecular weights, using columns of starch and water. *The Biochemical journal* **60**, xxxiv.
- Lee, J. Y., Nagano, Y., Taylor, J. P., Lim, K. L. & Yao, T. P. (2010).** Disease-causing mutations in parkin impair mitochondrial ubiquitination, aggregation, and HDAC6-dependent mitophagy. *The Journal of cell biology* **189**, 671-679.
- Lee, Y. J., Jeong, S. Y., Karbowski, M., Smith, C. L. & Youle, R. J. (2004).** Roles of the mammalian mitochondrial fission and fusion mediators Fis1, Drp1, and Opa1 in apoptosis. *Molecular biology of the cell* **15**, 5001-5011.
- Lees, N. D., Skaggs, B., Kirsch, D. R. & Bard, M. (1995).** Cloning of the late genes in the ergosterol biosynthetic pathway of *Saccharomyces cerevisiae*--a review. *Lipids* **30**, 221-226.
- Legros, F., Lombes, A., Frachon, P. & Rojo, M. (2002).** Mitochondrial fusion in human cells is efficient, requires the inner membrane potential, and is mediated by mitofusins. *Molecular biology of the cell* **13**, 4343-4354.
- Lehoux, S., Abe, J., Florian, J. A. & Berk, B. C. (2001).** 14-3-3 Binding to Na⁺/H⁺ exchanger isoform-1 is associated with serum-dependent activation of Na⁺/H⁺ exchange. *The Journal of biological chemistry* **276**, 15794-15800.
- Lemasters, J. J. (2005).** Selective mitochondrial autophagy, or mitophagy, as a targeted defense against oxidative stress, mitochondrial dysfunction, and aging. *Rejuvenation research* **8**, 3-5.
- Lesage, G., Shapiro, J., Specht, C. A., Sdicu, A. M., Menard, P., Hussein, S., Tong, A. H., Boone, C. & Bussey, H. (2005).** An interactional network of genes involved in chitin synthesis in *Saccharomyces cerevisiae*. *BMC genetics* **6**, 8.
- Li, X. Q., Hegazy, M. G., Mahdi, F., Jezek, P., Lane, R. D. & Garlid, K. D. (1990).** Purification of a reconstitutively active K⁺/H⁺ antiporter from rat liver mitochondria. *The Journal of biological chemistry* **265**, 15316-15322.
- Ligon, L. A. & Steward, O. (2000).** Role of microtubules and actin filaments in the movement of mitochondria in the axons and dendrites of cultured hippocampal neurons. *The Journal of comparative neurology* **427**, 351-361.
- Lim, D., Fedrizzi, L., Tartari, M., Zuccato, C., Cattaneo, E., Brini, M. & Carafoli, E. (2008).** Calcium homeostasis and mitochondrial dysfunction in striatal neurons of Huntington disease. *The Journal of biological chemistry* **283**, 5780-5789.
- Lippincott, J. & Li, R. (1998).** Dual function of Cyk2, a cdc15/PSTPIP family protein, in regulating actomyosin ring dynamics and septin distribution. *The Journal of cell biology* **143**, 1947-1960.

- Liu, Q., Krzewska, J., Liberek, K. & Craig, E. A. (2001).** Mitochondrial Hsp70 Ssc1: role in protein folding. *The Journal of biological chemistry* **276**, 6112-6118.
- Malka, F., Guillery, O., Cifuentes-Diaz, C., Guillou, E., Belenguer, P., Lombes, A. & Rojo, M. (2005).** Separate fusion of outer and inner mitochondrial membranes. *EMBO reports* **6**, 853-859.
- Mani, R., St Onge, R. P., Hartman, J. L. t., Giaever, G. & Roth, F. P. (2008).** Defining genetic interaction. *Proceedings of the National Academy of Sciences of the United States of America* **105**, 3461-3466.
- Martin, W. H., Beavis, A. D. & Garlid, K. D. (1984).** Identification of an 82,000-dalton protein responsible for K^+/H^+ antiport in rat liver mitochondria. *The Journal of biological chemistry* **259**, 2062-2065.
- McBride, H. M., Neuspiel, M. & Wasiak, S. (2006).** Mitochondria: more than just a powerhouse. *Curr Biol* **16**, R551-560.
- McQuibban, A. G., Joza, N., Megighian, A., Scorzeto, M., Zanini, D., Reipert, S., Richter, C., Schweyen, R. J. & Nowikovsky, K. (2010).** A *Drosophila* mutant of *LETMI*, a candidate gene for seizures in Wolf-Hirschhorn syndrome. *Human molecular genetics* **19**, 987-1000.
- Menze, M. A., Hutchinson, K., Laborde, S. M. & Hand, S. C. (2005).** Mitochondrial permeability transition in the crustacean *Artemia franciscana*: absence of a calcium-regulated pore in the face of profound calcium storage. *American journal of physiology* **289**, R68-76.
- Minton, A. P., Colclasure, G. C. & Parker, J. C. (1992).** Model for the role of macromolecular crowding in regulation of cellular volume. *Proceedings of the National Academy of Sciences of the United States of America* **89**, 10504-10506.
- Mitchell, P. (1961).** Coupling of phosphorylation to electron and hydrogen transfer by a chemi-osmotic type of mechanism. *Nature* **191**, 144-148.
- Mitchell, P. (1966).** Chemiosmotic coupling in oxidative and photosynthetic phosphorylation. *Biological reviews of the Cambridge Philosophical Society* **41**, 445-502.
- Mitchell, P. & Moyle, J. (1969).** Translocation of some anions cations and acids in rat liver mitochondria. *European journal of biochemistry / FEBS* **9**, 149-155.
- Mitsui, K., Yasui, H., Nakamura, N. & Kanazawa, H. (2005).** Oligomerization of the *Saccharomyces cerevisiae* Na^+/H^+ antiporter Nha1p: implications for its antiporter activity. *Biochimica et biophysica acta* **1720**, 125-136.
- Mitsui, K., Hatakeyama, K., Matsushita, M. & Kanazawa, H. (2009).** *Saccharomyces cerevisiae* Na^+/H^+ antiporter Nha1p associates with lipid rafts and requires sphingolipid for stable localization to the plasma membrane. *Journal of biochemistry* **145**, 709-720.
- Moreira, P. I., Siedlak, S. L., Wang, X. & other authors (2007).** Increased autophagic degradation of mitochondria in Alzheimer disease. *Autophagy* **3**, 614-615.

- Mueller, C. L. & Jaehning, J. A. (2002).** Ctr9, Rtf1, and Leo1 are components of the Paf1/RNA polymerase II complex. *Molecular and cellular biology* **22**, 1971-1980.
- Mukhopadhyay, K., Prasad, T., Saini, P., Pucadyil, T. J., Chattopadhyay, A. & Prasad, R. (2004).** Membrane sphingolipid-ergosterol interactions are important determinants of multidrug resistance in *Candida albicans*. *Antimicrobial agents and chemotherapy* **48**, 1778-1787.
- Nakashima, R. A., Dordick, R. S. & Garlid, K. D. (1982).** On the relative roles of Ca^{2+} and Mg^{2+} in regulating the endogenous K^+/H^+ exchanger of rat liver mitochondria. *The Journal of biological chemistry* **257**, 12540-12545.
- Nakashima, R. A. & Garlid, K. D. (1982).** Quinine inhibition of Na^+ and K^+ transport provides evidence for two cation/ H^+ exchangers in rat liver mitochondria. *The Journal of biological chemistry* **257**, 9252-9254.
- Nakatogawa, H., Suzuki, K., Kamada, Y. & Ohsumi, Y. (2009).** Dynamics and diversity in autophagy mechanisms: lessons from yeast. *Nat Rev Mol Cell Biol* **10**, 458-467.
- Naqvi, S. N., Feng, Q., Boulton, V. J., Zahn, R. & Munn, A. L. (2001).** Vrp1p functions in both actomyosin ring-dependent and Hof1p-dependent pathways of cytokinesis. *Traffic (Copenhagen, Denmark)* **2**, 189-201.
- Narendra, D. P., Jin, S. M., Tanaka, A., Suen, D. F., Gautier, C. A., Shen, J., Cookson, M. R. & Youle, R. J. (2010).** PINK1 is selectively stabilized on impaired mitochondria to activate Parkin. *PLoS biology* **8**, e1000298.
- Nass, R., Cunningham, K. W. & Rao, R. (1997).** Intracellular sequestration of sodium by a novel Na^+/H^+ exchanger in yeast is enhanced by mutations in the plasma membrane H^+ -ATPase. Insights into mechanisms of sodium tolerance. *The Journal of biological chemistry* **272**, 26145-26152.
- Nass, R. & Rao, R. (1998).** Novel localization of a Na^+/H^+ exchanger in a late endosomal compartment of yeast. Implications for vacuole biogenesis. *The Journal of biological chemistry* **273**, 21054-21060.
- Nikaido, H. & Rosenberg, E. Y. (1983).** Porin channels in *Escherichia coli*: studies with liposomes reconstituted from purified proteins. *Journal of bacteriology* **153**, 241-252.
- Novak, I., Kirkin, V., McEwan, D. G. & other authors (2009).** Nix is a selective autophagy receptor for mitochondrial clearance. *EMBO reports* **11**, 45-51.
- Novick, P., Osmond, B. C. & Botstein, D. (1989).** Suppressors of yeast actin mutations. *Genetics* **121**, 659-674.
- Nowikovsky, K., Froschauer, E. M., Zsurka, G., Samaj, J., Reipert, S., Kolisek, M., Wiesenberger, G. & Schweyen, R. J. (2004).** The *LETM1/YOL027* gene family encodes a factor of the mitochondrial K^+ homeostasis with a potential role in the Wolf-Hirschhorn syndrome. *The Journal of biological chemistry* **279**, 30307-30315.

- Nowikovsky, K., Reipert, S., Devenish, R. J. & Schweyen, R. J. (2007).** Mdm38 protein depletion causes loss of mitochondrial K^+/H^+ exchange activity, osmotic swelling and mitophagy. *Cell death and differentiation* **14**, 1647-1656.
- Numata, M., Petrecca, K., Lake, N. & Orlowski, J. (1998).** Identification of a mitochondrial Na^+/H^+ exchanger. *The Journal of biological chemistry* **273**, 6951-6959.
- Nunnari, J., Marshall, W. F., Straight, A., Murray, A., Sedat, J. W. & Walter, P. (1997).** Mitochondrial transmission during mating in *Saccharomyces cerevisiae* is determined by mitochondrial fusion and fission and the intramitochondrial segregation of mitochondrial DNA. *Molecular biology of the cell* **8**, 1233-1242.
- Ohgaki, R., Matsushita, M., Kanazawa, H., Ogihara, S., Hoekstra, D. & van Ijzendoorn, S. C. (2010).** The Na^+/H^+ exchanger NHE6 in the endosomal recycling system is involved in the development of apical bile canalicular surface domains in HepG2 cells. *Molecular biology of the cell* **21**, 1293-1304.
- Okamoto, K., Kondo-Okamoto, N. & Ohsumi, Y. (2009).** Mitochondria-anchored receptor Atg32 mediates degradation of mitochondria via selective autophagy. *Developmental cell* **17**, 87-97.
- Olichon, A., Baricault, L., Gas, N., Guillou, E., Valette, A., Belenguer, P. & Lenaers, G. (2003).** Loss of OPA1 perturbs the mitochondrial inner membrane structure and integrity, leading to cytochrome c release and apoptosis. *The Journal of biological chemistry* **278**, 7743-7746.
- Pang, T., Su, X., Wakabayashi, S. & Shigekawa, M. (2001).** Calcineurin homologous protein as an essential cofactor for Na^+/H^+ exchangers. *The Journal of biological chemistry* **276**, 17367-17372.
- Partridge, S. R., Foulger, D. & Errington, J. (1991).** The role of sigma F in prespore-specific transcription in *Bacillus subtilis*. *Molecular microbiology* **5**, 757-767.
- Perkins, D. N., Pappin, D. J., Creasy, D. M. & Cottrell, J. S. (1999).** Probability-based protein identification by searching sequence databases using mass spectrometry data. *Electrophoresis* **20**, 3551-3567.
- Piao, L., Li, Y., Kim, S. J. & other authors (2009).** Association of LETM1 and MRPL36 contributes to the regulation of mitochondrial ATP production and necrotic cell death. *Cancer research* **69**, 3397-3404.
- Pike, L. J. (2009).** The challenge of lipid rafts. *Journal of lipid research* **50 Suppl**, S323-328.
- Priault, M., Salin, B., Schaeffer, J., Vallette, F. M., di Rago, J. P. & Martinou, J. C. (2005).** Impairing the bioenergetic status and the biogenesis of mitochondria triggers mitophagy in yeast. *Cell death and differentiation* **12**, 1613-1621.
- Puig, O., Caspary, F., Rigaut, G., Rutz, B., Bouveret, E., Bragado-Nilsson, E., Wilm, M. & Seraphin, B. (2001).** The tandem affinity purification (TAP) method: a general procedure of protein complex purification. *Methods (San Diego, Calif)* **24**, 218-229.

- Puskin, J. S., Gunter, T. E., Gunter, K. K. & Russell, P. R. (1976).** Evidence for more than one Ca^{2+} transport mechanism in mitochondria. *Biochemistry* **15**, 3834-3842.
- Quintero, F. J., Blatt, M. R. & Pardo, J. M. (2000).** Functional conservation between yeast and plant endosomal $\text{Na}(+)/\text{H}(+)$ antiporters. *FEBS letters* **471**, 224-228.
- Reed, P. W. & Lardy, H. A. (1972).** A23187: a divalent cation ionophore. *The Journal of biological chemistry* **247**, 6970-6977.
- Reinders, J., Zahedi, R. P., Pfanner, N., Meisinger, C. & Sickmann, A. (2006).** Toward the complete yeast mitochondrial proteome: multidimensional separation techniques for mitochondrial proteomics. *Journal of proteome research* **5**, 1543-1554.
- Rigaut, G., Shevchenko, A., Rutz, B., Wilm, M., Mann, M. & Seraphin, B. (1999).** A generic protein purification method for protein complex characterization and proteome exploration. *Nature biotechnology* **17**, 1030-1032.
- Romagnoli, S., Cai, G., Faleri, C., Yokota, E., Shimmen, T. & Cresti, M. (2007).** Microtubule- and actin filament-dependent motors are distributed on pollen tube mitochondria and contribute differently to their movement. *Plant & cell physiology* **48**, 345-361.
- Rosenfeld, E. & Beauvoit, B. (2003).** Role of the non-respiratory pathways in the utilization of molecular oxygen by *Saccharomyces cerevisiae*. *Yeast (Chichester, England)* **20**, 1115-1144.
- Rother, S. & Strasser, K. (2007).** The RNA polymerase II CTD kinase Ctk1 functions in translation elongation. *Genes & development* **21**, 1409-1421.
- Santos, R. X., Correia, S. C., Wang, X., Perry, G., Smith, M. A., Moreira, P. I. & Zhu, X. (2010).** A synergistic dysfunction of mitochondrial fission/fusion dynamics and mitophagy in Alzheimer's disease. *J Alzheimers Dis* **20 Suppl 2**, S401-412.
- Schagger, H., Cramer, W. A. & von Jagow, G. (1994).** Analysis of molecular masses and oligomeric states of protein complexes by blue native electrophoresis and isolation of membrane protein complexes by two-dimensional native electrophoresis. *Analytical biochemistry* **217**, 220-230.
- Schagger, H. (2002).** Respiratory chain supercomplexes of mitochondria and bacteria. *Biochimica et biophysica acta* **1555**, 154-159.
- Schlickum, S., Moghekar, A., Simpson, J. C., Steglich, C., O'Brien, R. J., Winterpacht, A. & Ende, S. U. (2004).** *LETMI*, a gene deleted in Wolf-Hirschhorn syndrome, encodes an evolutionarily conserved mitochondrial protein. *Genomics* **83**, 254-261.
- Schwarten, M., Mohrluder, J., Ma, P. & other authors (2009).** Nix directly binds to GABARAP: a possible crosstalk between apoptosis and autophagy. *Autophagy* **5**, 690-698.
- Selwyn, M. J., Dawson, A. P. & Dunnett, S. J. (1970).** Calcium transport in mitochondria. *FEBS letters* **10**, 1-5.

- Sesaki, H. & Jensen, R. E. (1999).** Division versus fusion: Dnm1p and Fzo1p antagonistically regulate mitochondrial shape. *The Journal of cell biology* **147**, 699-706.
- Sharma, S. C. (2006).** Implications of sterol structure for membrane lipid composition, fluidity and phospholipid asymmetry in *Saccharomyces cerevisiae*. *FEMS yeast research* **6**, 1047-1051.
- Shi, G. Y., Jung, D. W., Garlid, K. D. & Brierley, G. P. (1980).** Induction of respiration-dependent net efflux of K⁺ from heart mitochondria by depletion of endogenous divalent cations. *The Journal of biological chemistry* **255**, 10306-10311.
- Shy, M. E. (2004).** Charcot-Marie-Tooth disease: an update. *Current opinion in neurology* **17**, 579-585.
- Simons, K. & Toomre, D. (2000).** Lipid rafts and signal transduction. *Nat Rev Mol Cell Biol* **1**, 31-39.
- Singh, I., Pass, R., Togay, S. O., Rodgers, J. W. & Hartman, J. L. t. (2009).** Stringent mating-type-regulated auxotrophy increases the accuracy of systematic genetic interaction screens with *Saccharomyces cerevisiae* mutant arrays. *Genetics* **181**, 289-300.
- Skaggs, B. A., Alexander, J. F., Pierson, C. A., Schweitzer, K. S., Chun, K. T., Koegel, C., Barbuch, R. & Bard, M. (1996).** Cloning and characterization of the *Saccharomyces cerevisiae* C-22 sterol desaturase gene, encoding a second cytochrome P-450 involved in ergosterol biosynthesis. *Gene* **169**, 105-109.
- Song, W., Chen, J., Petrilli, A. & other authors (2011).** Mutant huntingtin binds the mitochondrial fission GTPase dynamin-related protein-1 and increases its enzymatic activity. *Nature medicine*.
- Stolinski, L. A., Eisenmann, D. M. & Arndt, K. M. (1997).** Identification of *RTF1*, a novel gene important for TATA site selection by TATA box-binding protein in *Saccharomyces cerevisiae*. *Molecular and cellular biology* **17**, 4490-4500.
- Stradalova, V., Stahlschmidt, W., Grossmann, G., Blazikova, M., Rachel, R., Tanner, W. & Malinsky, J. (2009).** Furrow-like invaginations of the yeast plasma membrane correspond to membrane compartment of Can1. *Journal of cell science* **122**, 2887-2894.
- Szabadkai, G. & Duchen, M. R. (2008).** Mitochondria: the hub of cellular Ca²⁺ signaling. *Physiology (Bethesda, Md)* **23**, 84-94.
- Tal, R., Winter, G., Ecker, N., Klionsky, D. J. & Abeliovich, H. (2007).** Aup1p, a yeast mitochondrial protein phosphatase homolog, is required for efficient stationary phase mitophagy and cell survival. *The Journal of biological chemistry* **282**, 5617-5624.
- Tamai, S., Iida, H., Yokota, S., Sayano, T., Kiguchiya, S., Ishihara, N., Hayashi, J., Mihara, K. & Oka, T. (2008).** Characterization of the mitochondrial protein LETM1, which maintains the mitochondrial tubular shapes and interacts with the AAA-ATPase BCS1L. *Journal of cell science* **121**, 2588-2600.

- Tanaka, A., Cleland, M. M., Xu, S., Narendra, D. P., Suen, D. F., Karbowski, M. & Youle, R. J. (2010).** Proteasome and p97 mediate mitophagy and degradation of mitofusins induced by Parkin. *The Journal of cell biology* **191**, 1367-1380.
- Tolkovsky, A. M. (2009).** Mitophagy. *Biochimica et biophysica acta* **1793**, 1508-1515.
- Tong, A. H., Evangelista, M., Parsons, A. B. & other authors (2001).** Systematic genetic analysis with ordered arrays of yeast deletion mutants. *Science (New York, NY)* **294**, 2364-2368.
- Tong, A. H., Lesage, G., Bader, G. D. & other authors (2004).** Global mapping of the yeast genetic interaction network. *Science (New York, NY)* **303**, 808-813.
- Tong, A. H. & Boone, C. (2006).** Synthetic genetic array analysis in *Saccharomyces cerevisiae*. *Methods in molecular biology (Clifton, NJ)* **313**, 171-192.
- Twig, G., Elorza, A., Molina, A. J. & other authors (2008).** Fission and selective fusion govern mitochondrial segregation and elimination by autophagy. *The EMBO journal* **27**, 433-446.
- Ulery, T. L., Jang, S. H. & Jaehning, J. A. (1994).** Glucose repression of yeast mitochondrial transcription: kinetics of derepression and role of nuclear genes. *Molecular and cellular biology* **14**, 1160-1170.
- Vemuri, R. & Philipson, K. D. (1989).** Influence of sterols and phospholipids on sarcolemmal and sarcoplasmic reticular cation transporters. *The Journal of biological chemistry* **264**, 8680-8685.
- Visser, W., van Spronsen, E. A., Nanninga, N., Pronk, J. T., Gijs Kuenen, J. & van Dijken, J. P. (1995).** Effects of growth conditions on mitochondrial morphology in *Saccharomyces cerevisiae*. *Antonie van Leeuwenhoek* **67**, 243-253.
- Vives-Bauza, C., Zhou, C., Huang, Y. & other authors (2010).** PINK1-dependent recruitment of Parkin to mitochondria in mitophagy. *Proceedings of the National Academy of Sciences of the United States of America* **107**, 378-383.
- Wach, A., Brachat, A., Pohlmann, R. & Philippsen, P. (1994).** New heterologous modules for classical or PCR-based gene disruptions in *Saccharomyces cerevisiae*. *Yeast (Chichester, England)* **10**, 1793-1808.
- Wagner, A., Grillitsch, K., Leitner, E. & Daum, G. (2009).** Mobilization of steryl esters from lipid particles of the yeast *Saccharomyces cerevisiae*. *Biochimica et biophysica acta* **1791**, 118-124.
- Wakabayashi, S., Pang, T., Su, X. & Shigekawa, M. (2000).** A novel topology model of the human Na(+)/H(+) exchanger isoform 1. *The Journal of biological chemistry* **275**, 7942-7949.
- Waldherr, M., Ragnini, A., Jank, B., Teply, R., Wiesenberger, G. & Schweyen, R. J. (1993).** A multitude of suppressors of group II intron-splicing defects in yeast. *Current genetics* **24**, 301-306.

- Walther, T. C., Brickner, J. H., Aguilar, P. S., Bernales, S., Pantoja, C. & Walter, P. (2006).** Eisosomes mark static sites of endocytosis. *Nature* **439**, 998-1003.
- Weinman, E. J., Cunningham, R., Wade, J. B. & Shenolikar, S. (2005).** The role of NHERF-1 in the regulation of renal proximal tubule sodium-hydrogen exchanger 3 and sodium-dependent phosphate cotransporter 2a. *The Journal of physiology* **567**, 27-32.
- Welihinda, A. A., Trumbly, R. J., Garlid, K. D. & Beavis, A. D. (1993).** On the regulation of Na^+/H^+ and K^+/H^+ antiport in yeast mitochondria: evidence for the absence of an Na^+ -selective Na^+/H^+ antiporter. *Biochimica et biophysica acta* **1144**, 367-373.
- Welihinda, A. A., Beavis, A. D. & Trumbly, R. J. (1994).** Mutations in *LIS1 (ERG6)* gene confer increased sodium and lithium uptake in *Saccharomyces cerevisiae*. *Biochimica et biophysica acta* **1193**, 107-117.
- Westermann, B. & Neupert, W. (2000).** Mitochondria-targeted green fluorescent proteins: convenient tools for the study of organelle biogenesis in *Saccharomyces cerevisiae*. *Yeast (Chichester, England)* **16**, 1421-1427.
- Wiesenberger, G., Waldherr, M. & Schweyen, R. J. (1992).** The nuclear gene *MRS2* is essential for the excision of group II introns from yeast mitochondrial transcripts in vivo. *The Journal of biological chemistry* **267**, 6963-6969.
- Winzler, E. A., Shoemaker, D. D., Astromoff, A. & other authors (1999).** Functional characterization of the *S. cerevisiae* genome by gene deletion and parallel analysis. *Science (New York, NY)* **285**, 901-906.
- Xiang, M., Feng, M., Muend, S. & Rao, R. (2007).** A human Na^+/H^+ antiporter sharing evolutionary origins with bacterial NhaA may be a candidate gene for essential hypertension. *Proceedings of the National Academy of Sciences of the United States of America* **104**, 18677-18681.
- Yang, Z. & Klionsky, D. J. (2010).** Eaten alive: a history of macroautophagy. *Nature cell biology* **12**, 814-822.
- Yoon, Y. G., Haug, C. L. & Koob, M. D. (2007).** Interspecies mitochondrial fusion between mouse and human mitochondria is rapid and efficient. *Mitochondrion* **7**, 223-229.
- Youle, R. J. & Narendra, D. P. (2011).** Mechanisms of mitophagy. *Nat Rev Mol Cell Biol* **12**, 9-14.
- Yun, C. H., Tse, C. M., Nath, S. K., Levine, S. A., Brant, S. R. & Donowitz, M. (1995).** Mammalian Na^+/H^+ exchanger gene family: structure and function studies. *The American journal of physiology* **269**, G1-11.
- Zahedi, R. P., Sickmann, A., Boehm, A. M., Winkler, C., Zufall, N., Schonfisch, B., Guiard, B., Pfanner, N. & Meisinger, C. (2006).** Proteomic analysis of the yeast mitochondrial outer membrane reveals accumulation of a subclass of preproteins. *Molecular biology of the cell* **17**, 1436-1450.

Zeth, K. & Thein, M. (2010). Porins in prokaryotes and eukaryotes: common themes and variations. *The Biochemical journal* **431**, 13-22.

Zhang, J., Randall, M. S., Loyd, M. R., Dorsey, F. C., Kundu, M., Cleveland, J. L. & Ney, P. A. (2009). Mitochondrial clearance is regulated by Atg7-dependent and -independent mechanisms during reticulocyte maturation. *Blood* **114**, 157-164.

Zinser, E., Sperka-Gottlieb, C. D., Fasch, E. V., Kohlwein, S. D., Paltauf, F. & Daum, G. (1991). Phospholipid synthesis and lipid composition of subcellular membranes in the unicellular eukaryote *Saccharomyces cerevisiae*. *Journal of bacteriology* **173**, 2026-2034.

Zinser, E., Paltauf, F. & Daum, G. (1993). Sterol composition of yeast organelle membranes and subcellular distribution of enzymes involved in sterol metabolism. *Journal of bacteriology* **175**, 2853-2858.

Zinser, E. & Daum, G. (1995). Isolation and biochemical characterization of organelles from the yeast, *Saccharomyces cerevisiae*. *Yeast (Chichester, England)* **11**, 493-536.

Zollino, M., Lecce, R., Fischetto, R. & other authors (2003). Mapping the Wolf-Hirschhorn syndrome phenotype outside the currently accepted WHS critical region and defining a new critical region, WHSCR-2. *American journal of human genetics* **72**, 590-597.

Zotova, L., Aleschko, M., Sponder, G., Baumgartner, R., Reipert, S., Prinz, M., Schweyen, R. J. & Nowikovsky, K. (2010). Novel components of an active mitochondrial K(+)/H(+) exchange. *The Journal of biological chemistry* **285**, 14399-14414.

9. Acknowledgements

First of all, I would like to thank Prof. Rudolf Schweyen for the opportunity of working with him and the time in his lab, for sharing with us his enthusiasm and passion for science and for the chance to partake of his knowledge and insights into genetics, which already started in the early days of molecular biology.

I am indebted to Prof. Kristina Djinovic - Carugo for taking over my PhD supervision and for accepting me as a new group member in a very open-hearted and amicable way. I am grateful for her scientific input and straightforward ideas.

Furthermore, I also have to thank my PhD committee members Prof. Manuela Baccharini and Prof. Steffen Hering for their scientific advices and overall support.

Special thanks I owe to Karin Nowikovsky. Her outstanding support and patience throughout my thesis was a great asset. Whenever help was needed, she provided her scientific knowledge and some motivating words.

I must not forget the former MRS-group members Anton Graschopf, Elisabeth Froschauer – Neuhauser, Dagmar Hosiner, Tamás Henics, and of course Mirjana Iliev. Thank you very much for all the scientific discussions and input, the funny chats at lunch, the delicious salads and cakes, and for creating an enjoyable working atmosphere.

At this point, I have to thank Gerhard Sponder, the last MRS-group member besides me. I met Gerhard at the very beginning of my studies and our scientific ways through the last 10 years turned out to be the route to a close friendship. I wish him all the best for the future.

I am especially indebted to my parents Susanne und Hubert. Thank you for your selfless support and trust in me. This thesis is dedicated to you.

Above all, I want to thank my girlfriend Christine. I am grateful for her encouraging words and for showing me what is really important in life. Thank you for everything.

And finally, I would like to thank everyone who supported me during my studies and I did not mention so far.

10. Curriculum Vitae

Personal information

Name: Markus Aleschko
Date of birth: 11. 04. 1981
Place of birth: Klagenfurt, Carinthia
Nationality: Austria

Education

10. 2007 – 05. 2011 PhD thesis: '*The mitochondrial K^+/H^+ exchanger: identification and characterization of novel components*'
PhD fellowship (Initiativkolleg): Molecular drug targets
University of Vienna, Max F. Perutz Laboratories
Department of Microbiology, Immunobiology and Genetics
Supervisor: Prof. Rudolf Schweyen until 02. 2009 (deceased)
Current Supervisor: Prof. Kristina Djinovic - Carugo
06. 2007 - 10. 2007 Research associate
University of Vienna, Max F. Perutz Laboratories
Department of Microbiology, Immunobiology and Genetics
Supervisor: Prof. Rudolf Schweyen
04. 2006 - 05. 2007 Diploma thesis: '*Molecular and biochemical analysis of Ylr414p, a member of the claudin protein superfamily*'
University of Vienna, Max F. Perutz Laboratories
Department of Microbiology, Immunobiology and Genetics
Supervisor: Prof. Rudolf Schweyen
10. 2000 - 05. 2007 Studies in Microbiology and Genetics, University of Vienna
01. 2000 - 09. 2000 Basic military service

09. 1991 - 06. 1999 Grammar school, Stiftsgymnasium St. Paul / Lavanttal, Carinthia

09. 1987 - 07. 1991 Elementary school, VS Bleiburg, Carinthia

Publications

- 2011 *'Pun1p is a metal ion - inducible, calcineurin/Crz1p - regulated plasma membrane protein required for cell wall integrity'*
Hosiner D., Sponder G., Graschopf A., Reipert S., Schweyen R.J., Schüller C., and **Aleschko M.**
Biochim Biophys Acta. 2011 Jan 9. [Epub ahead of print]
- 2010 *'Novel components of an active mitochondrial K⁺/H⁺ exchange'*
Aleschko M., Zotova L., Sponder G., Baumgartner R., Reipert S., Prinz M., Schweyen R.J., and Nowikovsky K.
Journal of Biological Chemistry, 285(19):14399-414